

# Spin Excitations in Ultrathin Ferromagnets

## Habilitationsschrift

zur Erlangung des akademischen Grades

Dr. rer. net. habil.

vorgelegt der  
Naturwissenschaftlichen Fakultät II  
der Martin-Luther-Universität Halle-Wittenberg

von

**Herrn Dr. rer. nat. Khalil Zakeri Lori**  
geboren am 23.09.1979 in Sirjan, Iran

Gutachter:

1. Prof. Dr. Jürgen Kirschner, MPI für Mikrostrukturphysik, Germany
2. Prof. Dr. Stefan Blügel, Forschungszentrum Jülich, Germany
3. Prof. Dr. Julie B. Staunton, University of Warwick, United Kingdom

Halle (Saale), verteidigt am 20.10.2014, Probevorlesung am 10.11.2014



# Contents

<b>1</b>	<b>Introduction</b>	<b>1</b>
<b>2</b>	<b>Elementary spin excitations</b>	<b>5</b>
2.1	Spin excitations in an exchange coupled spin system . . . . .	5
2.1.1	Spin Hamiltonian . . . . .	5
2.1.2	The magnon dispersion relation . . . . .	8
2.2	Spin excitations in itinerant-electron ferromagnets . . . . .	10
2.2.1	Collective excitations . . . . .	10
2.2.2	Single particle Stoner excitations . . . . .	10
2.2.3	Single particle versus collective excitations . . . . .	12
2.2.4	Lifetime of spin excitations . . . . .	12
<b>3</b>	<b>Probing spin excitations</b>	<b>15</b>
3.1	Low-energy excitations . . . . .	15
3.1.1	Ferromagnetic resonance . . . . .	15
3.1.2	Brillouin light scattering . . . . .	17
3.1.3	Time-resolved spectroscopies . . . . .	17
3.2	High-energy excitations . . . . .	17
3.2.1	Neutron scattering . . . . .	17
3.2.2	Resonant inelastic x-ray scattering . . . . .	17
3.2.3	Spin polarized electron energy loss spectroscopy . . . . .	18
3.2.4	Spin polarized inelastic tunneling spectroscopy . . . . .	21
<b>4</b>	<b>Selected results</b>	<b>23</b>
4.1	Probing magnons by spin-polarized electrons . . . . .	23
4.2	Simultaneous probing of magnons and phonons . . . . .	25
4.3	Magnons in a ferromagnetic monolayer . . . . .	28
4.4	Atomic structure and magnon dispersion relation . . . . .	29
4.4.1	Coordination number . . . . .	29
4.4.2	Lattice relaxation . . . . .	30
4.4.3	Lattice modification . . . . .	31
4.5	The magnon lifetime . . . . .	33
4.6	Real space representation of magnons . . . . .	35
4.7	The effect of spin-orbit coupling on magnons . . . . .	37
4.7.1	Magnon Rashba effect . . . . .	38
4.7.2	The effect of spin-orbit coupling on the magnon lifetime . . . . .	39
4.8	Probing exchange interaction at the interface . . . . .	42
4.9	Magnons in thin films with perpendicular easy axis . . . . .	46

<b>5</b>	<b>Conclusions and outlook</b>	<b>51</b>
	<b>Bibliography</b>	<b>55</b>
<b>6</b>	<b>Original publications</b>	<b>67</b>
6.1	Probing Magnons by Spin-Polarized Electrons . . . . .	69
6.2	Surface Magnons Probed by Spin-Polarized Electron Energy Loss Spectroscopy . . . . .	87
6.3	Elementary Excitations at Magnetic Surfaces and Their Spin Dependence	95
6.4	Magnons in a Ferromagnetic Monolayer . . . . .	99
6.5	Nonmonotonic Thickness Dependence of Spin-wave Energy in Ultrathin Fe Films: Experiment and Theory . . . . .	103
6.6	Impact of Atomic Structure on the Magnon Dispersion Relation: A Comparison Between Fe(111)/Au/W(110) and Fe(110)/W(110) . . . . .	109
6.7	Relaxation Time of Terahertz Magnons Excited at Ferromagnetic Surfaces	115
6.8	Asymmetric Spin-Wave Dispersion on Fe(110): Direct Evidence of the Dzyaloshinskii-Moriya Interaction . . . . .	121
6.9	Magnon Lifetimes on the Fe(110) Surface: The Role of Spin-Orbit Coupling	125
6.10	Direct Probing of the Exchange Interaction at Buried Interfaces . . . . .	131
6.11	Magnons in Ultrathin Ferromagnetic Films with a Large Perpendicular Magnetic Anisotropy . . . . .	137

# 1 Introduction

One of the most profound and fundamental ideas in the quantum theory of condensed matter physics is the idea of “quasi-particles”. Usually, the behavior of a complex system is understood in terms of simple models of interacting or non-interacting quasi-particles. For instance, in a piece of metal, where a large number of electrons is placed in a small volume, the electrons become dressed by the presence of the other electrons in the system and form quasi-particles. Although they still obey the Fermi statistics, their interaction is rather weak. In addition to that the collective excitations of these highly interacting electrons can be regarded as bosonic quasi-particles called plasmons. Most of the properties of the system can be predicted by investigating the behavior of these quasi-particles.

Magnetism, as another fascinating phenomenon in nature, is also a many-body effect. Although the first scientific discussion on magnetism goes back to 600 BC, it is noticeable that still the research on magnetism is one of the pillars of condensed matter physics. In the quantum formalism, the collective modes of spin excitations in a magnetic solid are referred to as spin waves and their representative quasi-particles are called magnons. The word magnon is chosen in analogy to the quantized lattice vibrations, named phonons. Similar to phonons, plasmons and excitons, magnons are also Bosons. Magnons are essential for understanding many observed phenomena *e.g.* magnetic ordering, ultrafast magnetization processes, electrical and heat conductivity, current induced magnetization reversal and electron/spin dynamics. Recently, it is demonstrated that the coupling between electrons and high-energy magnons is a possible mechanism, which leads to superconductivity in high-temperature superconductors [1–3]. Besides these core fundamental aspects, magnons are of great importance for modern spintronics, since they are generated in tunneling magneto resistance (TMR) and spin transfer torque (STT) devices [4–6] and also in the read and write head of magnetic recording elements [7].

Magnons have entered the picture very early in the history of modern magnetism [8, 9], shortly after the time when Heisenberg explained the origin of the magnetic coupling [10], on the quantum mechanical bases. The concept of magnetic ordering at a finite temperature (known as Bloch law) has been explained by introducing new type of elementary excitations (magnons).

In the case of magnetic materials with localized moments, it is rather straightforward to imagine the magnons. For simplicity, imagine a ferromagnetic solid composed of magnetic atoms which are ferromagnetically coupled. In the ground state of the system, all the moments are aligned parallel. In the excited state of the system a wave-like motion of the atomic moments results in a propagating wave in the ferromagnetic solid. The magnons in antiferromagnets can also be imagined in analogy to the ones in ferromagnets. Since in *3d* ferromagnets like Fe, Co and Ni the magnetism is governed by conduction electrons, this description cannot provide a clear picture of the system.

Hence, a major controversy developed soon after introducing this new type of quasi-particles. The question of debate was: “Are there magnons in itinerant ferromagnets?”.

The answer of Stoner and Wohlfarth to this question was: No! In fact Stoner and Wohlfarth looked at the problem from a band-model view in which the properties of a ferromagnetic metal can be described by the single particle excitations (known as Stoner excitations) [11–13]. Within this picture, the exchange interaction in metals does not allow low energy magnons to exist. But the ferromagnetic resonance was already observed [14] and explained by a phenomenological approach [15, 16]. Van Krannendonk and Van Vleck had a different opinion. They pointed out that magnons may exist in metals [17, 18]. Based on a quantum theory, Herring and Kittel showed that magnons do exist in itinerant ferromagnets [19]. Magnons in antiferromagnets could be explained by a similar formalism [20]. The dispersion relation, which connects the magnons energy  $E$  (or eigenfrequency,  $\omega$ ) to their propagating wave vector  $q$ , in the small wave vector regime, is found to be  $E = \hbar\omega \propto q^2$  for ferromagnets and  $E = \hbar\omega \propto q$  for antiferromagnets. Dyson further used this formalism for a complete description of the thermodynamic properties of ferromagnets based on magnons and their interactions [21]. In addition to the description of the low temperature magnetic order, discussed by Bloch law, the scattering cross section of magnons was also addressed. He estimated a spin–spin mean free path being proportional to  $T^{-7/2}$ .

The experimental proof of the existence of magnons in ferromagnetic metals was first appeared when the neutron scattering technique was established. In fact the theory of Herring and Kittel was proven by the experiments performed on bulk crystals [22–31].

However, still it was not quite clear that how can the classical magnons, explained by phenomenology [15, 32–35], be understood from a microscopic point of view, *i.e.*, by looking at the electronic band structure. As it was pointed out by Stoner at the beginning of the development of the quantum theory of magnetism, the thermodynamic properties of a ferromagnetic metal, like magnetic phase transition and paramagnetic state above the Curie temperature, can be attributed to the single spin-flip particle interband transitions in the system.

Many authors tried to shed light on the relation between the so-called spin wave theory developed by Herring and Kittel [19] and the so-called collective electron theory by Stoner [11, 12] and Wohlfarth [13]. By starting from a single band ferromagnetic metal, Edwards [36, 37], Callaway [38, 39] and Sokoloff [40–42] have proposed a way of calculating the magnon energies in ferromagnetic metals. The theory was further developed for more realistic systems and could explain the magnon dispersion relation in itinerant electron ferromagnets [43–53]. In this description the magnons are treated similar to the excitons (electron-hole pairs) in which the electron and hole have opposite spins. The wave function of such an electron-hole pair is a linear superposition of electron and hole states (spin triplet particle hole excitations). This theory is now developed for calculating magnons in low-dimensional magnets [54–61].

Since low-dimensional magnets show novel properties, the concept of spin excitation in this class of materials is of great fundamental interest. For instance, according to the Mermin-Wagner theorem, an ideal two-dimensional spin system with an isotropic and short-range interaction cannot exhibit any long-range magnetic order at a finite temperature [62]. This theorem is even generalized for a lattice of spins which are coupled to itinerant interacting electrons in one- and two-dimension [63]. However,

---

in real two-dimensional spin systems, like ferromagnetic monolayers, small magnetic anisotropies or dipolar interactions are, in turn, sufficient to stabilize a long-range magnetic order [64–66]. It would be of great fundamental interest to probe the magnon dispersion relation in a real two-dimensional ferromagnetic system and to see how it changes with changing the system’s parameter such as temperature, number of atomic layers involved, chemical environment, etc. All these key experiments lie in the central understanding of the system’s behavior. When the wavelength of magnons approaches the nanometer scale, they are governed by the microscopic exchange interaction. In this case, the excitations are strongly confined in both time and space. Hence, they cannot be simply treated as in the case of classical magnons. This implies that a quantum mechanical description of the system is demanded. Moreover, since the translation symmetry in a ferromagnetic monolayer grown on a surface is broken, one would expect very interesting dimensionality effects, which are reflected in the properties of magnons. Hence, the experimental study of such excitations would provide a true microscopic view of the system.

Recently, the dream of measuring elementary spin excitations in low-dimensional spin systems has become a reality due to the development of spin-polarized spectroscopy methods such as high resolution spin-polarized electron energy loss spectroscopy and spin-polarized spin excitation spectroscopy.

In the course of this work, we have studied the elementary spin excitations in ultrathin ferromagnets. The full magnon spectrum measured on various systems allowed us to understand the properties of these systems in some details. The results have had also an impact on the development of the theory of spin excitations in low-dimensional solids. The thesis is organized as follows: the concept of spin excitations is discussed in **Chap. 2**. The important mechanisms which leads to magnon excitations are outlined in **Chap. 3**, where an introduction to the spin-polarized electron energy-loss technique, used to study the elementary spin excitations, is provided. The important properties of magnons such as their excitation energy, dispersion relation and lifetime probed in different systems will be discussed in detail in **Chap. 4**, where we present some of our selected results. The fundamental mechanisms involved in the excitation mechanism are presented in Sec. 4.1. The possibility of probing magnons and phonons simultaneously is discussed in Sec. 4.2. The results of spin excitations in an ideal model system *i. e.* a ferromagnetic monolayer are presented in Sec. 4.3. The impact of atomic structure on the magnon dispersion relation is discussed in Sec. 4.4. The results of magnon lifetime and their real space representation are presented in Secs. 4.5 and 4.6, respectively. The consequences of the relativistic spin–orbit coupling on the spin excitations and their properties are explained in Sec. 4.7. The possibility of using magnons for spectroscopy of buried interfaces will be discussed in Sec. 4.8. In Sec. 4.9 we show that a transversally spin-polarized beam can be used to excite the magnons in thin films with out-of-plane easy axis. **Chapter 5** summarizes the results and provides a perspective for future activities.





# 2 Elementary spin excitations

## 2.1 Spin excitations in an exchange coupled spin system

We start with the localized moment picture for describing a magnetic solid. In this description the local magnetic moments on each atomic sites are regarded as rigid entities (they are referred to as atomic spins). The next step is to introduce a mathematical way of treating such as system. Mathematically, the spin maybe considered as a vectorial object. This description might be useful for an intuitive thinking. However, it does not reflect its quantum mechanical origin. Therefore, in the course of this thesis we consider the spin as a quantum mechanical observable. Since it is an extra degree of freedom, it can be treated by the quantum mechanics algebra.

Similar to all quantum mechanical degrees of freedom, spin has discrete set of basis states, which are labelled by quantum numbers. The components of a spin should change sign under time reversal, since they are axial vectors. In the mathematical treatment of the spin Hamiltonian we use here, the term “spin” can be the representative of any given system *e.g.* a localized single electron’s (or hole’s) spin in a semiconductor, the overall spin of several *d*-electrons in transition metals or spin of a nuclei. As far as the spin Hamiltonian of these systems has the same form, the systems shall show the same behavior.

### 2.1.1 Spin Hamiltonian

In a very general case the Hamiltonian of a spin system including all the possible contributions can be written as:

$$\mathcal{H} = \mathcal{H}_B + \mathcal{H}_{An} + \mathcal{H}_{Ex} + \mathcal{H}_{DM} + \mathcal{H}_{Dip}. \quad (2.1)$$

$\mathcal{H}_B$  describes the coupling of the spins to an external magnetic field.  $\mathcal{H}_{An}$  describes the system in the presence of anisotropy. The last three contributions describe the spin–spin interactions in the system. They do not exists for the case of single spin.  $\mathcal{H}_{Ex}$  is the so-called symmetric exchange term,  $\mathcal{H}_{DM}$  is the antisymmetric exchange term and  $\mathcal{H}_{Dip}$  describes the long range dipolar interaction of the spins.

### Coupling of spin to an external magnetic field

An external magnetic field can couple to a spin in free space. The effect was first noticed by Zeeman. The quantum mechanical treatment of this effect is rather straightforward. Even with a simple quantum mechanical approach, starting from the Schrödinger equation and using canonical momentum one may derive all the desired quantities. A better

way would be starting from Dirac equation. In any case the spin Hamiltonian in the simplest form can be written as  $\mathcal{H}_B = -g\mu_B \mathbf{S} \cdot \mathbf{B}$ , where  $g$  is the  $g$ -factor,  $\mu_B$  is the Bohr magneton and  $\mathbf{B}$  denotes the magnetic flux density. For an array of non interacting spins the form of the Hamiltonian maybe written as:

$$\mathcal{H}_B = -\mathbf{B} \cdot \sum_i g_i \mu_B \mathbf{S}_i. \quad (2.2)$$

This Hamiltonian implies that the magnetic field defines a spacial direction in space. The effect of this term is to set the system into uniform precession of spin around  $\mathbf{B}$ . In a more general case where the microscopic spin-orbit coupling is important,  $g$  has to be replaced by the  $g$ -tensor. Discussion of this topic is out of the scope of the present writing. Further information may be found elsewhere [67].

Using a very simple and semi-classical approach one can show that the dynamics of a single spin in an external magnetic field can be written as the following form:

$$\frac{d\mathbf{S}}{dt} = -\gamma (\mathbf{S} \times \mathbf{B}), \quad (2.3)$$

where,  $\gamma = g\mu_B/\hbar$  is the so-called gyromagnetic ratio.

In fact, if the term introduced in Eq. (2.2) is the only term in the total Hamiltonian of the system, it brings the spin to a uniform precession around the magnetic field with the eigenfrequency  $\omega = \gamma B$ . Equation 2.3 is the basis of the classical descriptions of spin dynamics in the presence of a magnetic field. In Sec. 3.1.1 we will demonstrate the practical use of this equation in the case of uniform spin motion that is usually referred to as ferromagnetic resonance (FMR).

### Spins in the presence of magnetic anisotropy

The simplest way to imagine the effect of the anisotropy on the spin is to think about the coupling of the spin to the ‘‘anisotropy field’’. In fact, presence of the anisotropy in the spin system is in analogy to a field which breaks the symmetry of the system. The coupling is very similar to what we discussed for the case of coupling of spins to an external magnetic field. In the simplest case where the anisotropy is of uniaxial character, the Hamiltonian of the system can be written as:

$$\mathcal{H}_{An} = -\frac{1}{2}K (\mathbf{S} \cdot \hat{\mathbf{e}}_i)^2. \quad (2.4)$$

This Hamiltonian is basically the same as the one introduced by Ising [68] to explain the ferromagnetism of an atomic chain. Here  $K$  is the magnetic anisotropy constant and  $\hat{\mathbf{e}}$  denotes the spin easy axis. One may also consider the higher-order anisotropy terms. However, they become less important in terms of energy and can simply be neglected. For instance, if the system has a biaxial anisotropy the spin Hamiltonian will include terms with  $S^4$ .

## Symmetric exchange interaction

The simplest form of the spin Hamiltonian for interacting spins can be written as:

$$\mathcal{H}_{\text{Ex}} = - \sum_{i \neq j} J_{ij} \mathbf{S}_i \cdot \mathbf{S}_j, \quad (2.5)$$

where  $J_{ij}$  represents the exchange interaction between spins  $\mathbf{S}_i$  and  $\mathbf{S}_j$ . It is positive for the case that the spins are aligned parallel (ferromagnetic coupling) and it is negative where the spins are aligned antiparallel (antiferromagnetic coupling). This interaction is not restricted to the neighboring spins and can be extended beyond the nearest neighbors [9, 19, 21]. It is apparent that the Hamiltonian, given above, grants rotation symmetry.

In the Heisenberg spin Hamiltonian, shown in Eq. (2.5), the origin of the interaction is not explicitly discussed. In the case of electrons's spin the origin of this interaction lies on the overlap of the electrons' wavefunctions. In fact the exchange interaction is the consequence of the Coulomb interaction of electrons and Pauli exclusion principle. This term can be derived from the quantum mechanics, considering two interacting electrons with spin of 1/2 [10].

## Antisymmetric exchange interaction

In the discussion above, we only considered the most simplest part of a bilinear term of two interacting spins. However, in a more general case this term can be written in the form of  $\sum_{\sigma, \delta} C_{\sigma, \delta} S_{i, \sigma} S_{j, \delta}$ , where  $\sigma$  and  $\delta$  label Cartesian components of the coupling matrix  $C_{\sigma, \delta}$ . Any matrix can be decomposed into (i) a multiple of unit matrix, (ii) a traceless symmetric matrix and (iii) an antisymmetric matrix. The first term gives rise to the symmetric exchange interaction, presented in Eq. (2.5). The second term leads to any kind of anisotropic exchange term. The antisymmetric term can be written in the form of vector product of spins. We define the spin Hamiltonian of the antisymmetric exchange interaction, known as Dzyaloshinskii-Moriya interaction (DM) interaction, as:

$$\mathcal{H}_{\text{DM}} = - \sum_{i \neq j} \mathbf{D}_{ij} \cdot \mathbf{S}_i \times \mathbf{S}_j. \quad (2.6)$$

Here  $\mathbf{D}_{ij}$  is the so-called Dzyaloshinskii-Moriya vector. Note that there is also a possibility to have anisotropic exchange terms. This would simply mean that the coupling of spins along different axes are different ( $J_{ij,x} \neq J_{ij,y}$ ). Such situations usually happen when a cubic crystal is tetragonally distorted. For the case of ultrathin films grown on a substrate these situations are rather common due to the film epitaxy. Based on the symmetry arguments, we classify such kind of interactions as symmetric exchange interaction.

The symmetric Heisenberg exchange interaction favors a parallel (or antiparallel) alignment of spins while DM interaction favors a non-collinear spin structure. For a system of interacting electrons one can show that the antisymmetric DM interaction is a consequence of the spin-orbit coupling and absence of the inversion symmetry in the

system. The DM interaction vanishes for the systems with inversion symmetry. In the case of layered magnetic structures the presence of the surfaces or interfaces often breaks the inversion symmetry (in addition to fact that it breaks the translation symmetry) and therefore leads to the existence of the DM interaction. The spin Hamiltonian discussed in Eq. (2.6) has first been proposed in 1957 by Dzyaloshinskii based on symmetry arguments [69]. It has been shown at the same time by Moriya that, in principle, this interaction can be analytically derived by considering the relativistic spin-orbit correction in the Hamiltonian of the electronic system [70]. In the systems with large spin-orbit coupling and in the presence of broken inversion symmetry DM interaction can lead to very exotic ground states [71–75]. Recently, a correlated band theory of spin and orbital contributions to DM interaction is reported [76]. This theory allows one to calculate the components of the DM vector from first principles via the construction of a reliable tight-binding parametrization of the electronic Hamiltonian with the spin-orbit interaction included.

After a simple mathematical step one can show that this term leads to a linear term in the magnon dispersion relation for the limit of small wave vectors. We will come to this point in Sec. 4.7.

### Long-range dipolar interaction

In principle a spin can be coupled to the magnetic stray field created by the other spins located in longer distances. The term describing this long-range interaction would be similar to the term introduced in Eq. (2.2) in which  $\mathbf{B}$  is replaced by the magnetic field induced by the other spins. The dipolar interaction has the form:

$$\mathcal{H}_{\text{Dip}} = - \sum_{ij} \frac{(g\mu_B)^2}{r_{ij}^3} [\mathbf{S}_i \cdot \mathbf{S}_j - 3(\hat{\mathbf{r}}_{ij} \cdot \mathbf{S}_i)(\hat{\mathbf{r}}_{ij} \cdot \mathbf{S}_j)], \quad (2.7)$$

where  $\mathbf{r}_{ij}$  represents the location vector. This term is responsible for the demagnetizing field and ferromagnetic domains in ferromagnets.

### 2.1.2 The magnon dispersion relation

The magnon dispersion relation, which connects the energy (or eigenfrequency) to their wave vector, can be obtained by finding the eigenvalues of the spin Hamiltonian of the system. For simplicity, one may start with the classical dynamics introduced in Ref. [20]. Another approach is introduced in Refs. [9, 18, 21]. Since the dispersion relation derived based on this classical spin Hamiltonian do not describe the high energy magnons in itinerant ferromagnets, we do not discuss, in detail, how the equations are derived. Details may be found in textbooks or in Sec. 7.2.3 of [KhZ 6.1] and in Sec. 2 of [KhZ 6.2]. For a simple cubic structure and considering only the symmetric exchange interaction and only the nearest neighbor interactions, the dispersion relation can be simplified as:

$$\epsilon = \hbar\omega = 2nJS \left[ 1 - \frac{1}{n} \sum_{\mathbf{r}} \cos(\mathbf{q} \cdot \mathbf{r}) \right], \quad (2.8)$$

where  $n$  is the number of nearest neighbors,  $S$  is the magnitude of spin,  $J$  is the exchange coupling constant between the neighbors and  $\mathbf{r}$  represents the position vector of the respective neighbor.

It is relatively straightforward to imagine that the dimensionality aspects have a large impact on the dispersion relation. For instance, if the system consists of a few monolayers of a ferromagnetic material, different magnon modes are expected and each mode may have a different contribution to the dispersion relation. The lowest in energy magnon mode of the system is usually referred to as the “*acoustic mode*” of the system. In the absence of the relativistic effects, when the spin Hamiltonian of the system includes only the symmetric exchange interaction [Eq. (2.5)], this magnon mode shall satisfy the Goldstone theorem. This means that the energy of this mode shall be zero for  $q = 0$ . The higher energy magnon modes of the system are usually referred to as “*optical modes*”. These modes have a finite energy at  $q = 0$  even in the absence of the relativistic effects.

Since the dispersion relation is one of the main subjects of the present review we will discuss it in various places. No prediction concerning the magnon lifetime can be made by the Heisenberg spin Hamiltonian given in Eq. (2.1). Within this description, magnons shall live forever, which is not certainly true for the case of itinerant electron magnets.

One can show that for the limit of  $q \rightarrow 0$  Eq. (2.8) can be simplified to:

$$\epsilon = \hbar\omega = Dq^2 + \mathcal{O}(q^4), \quad (2.9)$$

where  $D = JSr$  is the so-called spin-wave stiffness constant.

Now let us consider only the DM term, introduced in Eq. (2.6). One can show that the dispersion relation of this term considering only the nearest neighbours interactions can be written as [77, 78]:

$$\epsilon_{DM} = c \sin^2 \theta \sum_{\mathbf{r}} (\mathbf{D}_1 \cdot \hat{\mathbf{e}}) \sin(\mathbf{q} \cdot \mathbf{r}). \quad (2.10)$$

Here  $c$  is the chirality rotation index (being +1 for right rotating sense and  $-1$  for the left rotating one),  $\theta$  denotes the relative angle between the neighbouring spins,  $\mathbf{D}_1$  is the DM vector of the nearest neighbors,  $\hat{\mathbf{e}}$  denotes the direction of the easy axis and  $\mathbf{r}$  represent the position vector of nearest neighbors. Equation (2.10) implies that only the components of the DM vector parallel to the easy axis contribute to the magnon energies. It is apparent that for the limit of  $q \rightarrow 0$  this term can be approximated by a term which is linear with respect to  $q$ .

For a ferromagnetic system in the presence of a large spin-orbit coupling and in the absence of the inversion symmetry both the symmetric exchange interaction and the antisymmetric DM interaction are active. In this case the resulting magnon dispersion

relation will include the term introduced in Eq. (2.8) and also the one introduced in Eq. (2.10). As a result the dispersion relation will be asymmetric with respect to  $q$ , meaning that  $\varepsilon(q) \neq \varepsilon(-q)$ . We will come to this point in Sec. 4.7.

## 2.2 Spin excitations in itinerant-electron ferromagnets

In literature, the elemental spin excitations are referred to as magnons. In many occasion the terms “magnons” and “spin waves” are interchanged. In our opinion, this is rather misleading, since the nature of spin excitations in itinerant ferromagnets is somewhat different than those in the ferromagnetic insulators. In itinerant electron ferromagnets the elementary spin excitations may be divided into collective and single particle excitations, which we will discuss them in Secs. 2.2.1 and 2.2.2, respectively.

In low-dimensional itinerant ferromagnets such as thin films grown on a nonmagnetic substrate the situation is even more complicated. First, the translation symmetry is broken and as a consequence, the momentum of the electronic states along the direction perpendicular to the surface of the film is not conserved anymore. Second, the electronic states of the ultrathin ferromagnetic film and the substrate may hybridize. Hence, the spectrum of the single particle excitations in momentum–energy space may be very much different than the bulk ferromagnets. This would imply that the magnon lifetime in ultrathin ferromagnets may also be substantially different than in the bulk.

We use the term magnon as an elementary quasi-particle which describes the elementary collective spin excitations in an itinerant electron ferromagnet.

### 2.2.1 Collective excitations

As discussed above, in a magnetically ordered solid of any form (ferromagnets, antiferromagnets, ferrimagnets, etc.) one may consider the quasi-particles of spin ordering in analog to the ones of crystal ordering (phonons). Although in itinerant ferromagnets the magnetism is caused by the itinerant electrons [79], one may consider that the electrons are partially localized on atomic sites. This allows one to associate a magnetic moment to each atomic site. The wave-like excitations of these magnetic moments (spins) that propagate through the lattice are of collective nature. Similar to other quasi-particles, the energy of spin waves’ representative quasi-particles is also quantized in units of  $\hbar\omega$ , where  $\omega$  represents the eigenfrequency of the quantized spin wave (magnon) with a given wave vector  $q$ . One may describe the magnons by a Heisenberg type of Hamiltonian as discussed in Sec. 2.1.1. In such a description, the interaction of spins is treated in the form of an effective interatomic exchange parameter which couples the moments. The dispersion relation may be derived by starting with a simple spin Hamiltonian in which the coupling constant is the effective interatomic exchange interaction. Although this description is not complete, it provides a simple description of the system. Such kinds of approaches are usually referred to as adiabatic methods.

### 2.2.2 Single particle Stoner excitations

Based on the band theory of magnetism, in a ferromagnetic solid the degeneracy of the electronic bands is lifted [80]. This degeneracy breaking originates from the electron-

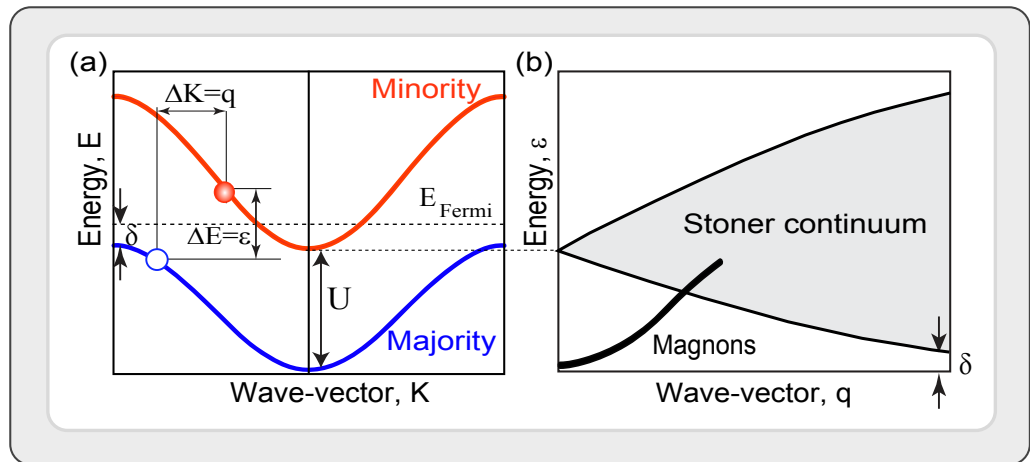


**Fig. 2.1:** (a) A schematic representation of Stoner excitations in an itinerant ferromagnet. A majority electron jumps from an occupied state below the Fermi-level to an unoccupied state above the Fermi-level, leaving a hole with majority spin behind. (b) Stoner density of states for a bulk metallic ferromagnet with a non-zero Stoner gap,  $\delta$ .

electron interactions in ferromagnets, which leads to a separation of the electronic bands for majority and minority electrons. The effect may be described as perturbations of a degenerate, paramagnetic band from which the energy degeneracy is lifted by the “exchange energy”. Generally, the exchange splitting depends on the spin and the wave vector of the electrons within the system. In the case that the Fermi-level lies between the bands derived from a single degenerate paramagnetic band, the lower energy (majority) states are occupied, while the higher energy (minority) states are unoccupied. This fact leads to a net spin polarization of the conduction electrons and can explain the magnetic state of the system. Now it is relatively easy to imagine that the spin-split bands across the Fermi-level can lead to the possibility of a unique single-particle excitation in the system. For instance an electron can jump from an occupied majority band and occupy a state in the minority band after undergoing a spin reversal. In such a case a hole of majority spin character will remain in the majority band. The resulting electron–hole pair which is usually referred to as “Stoner pair” carries a total angular momentum of  $1\hbar$ . Since it is created within the momentum–energy space, there is a wave vector and energy associated with that. The momentum (energy) of such a pair is the momentum (energy) difference of the electron and hole in the minority and majority bands, respectively [see Fig. 2.1 (a)]. Stoner excitations are spread over a large area of the Brillouin zone, see Figs. 2.1 (b). These excitations were first introduced by Stoner within the collective electron theory [11, 12] and later by Slater [81]. Van Kranendonk [18] has tried to connect this type of excitations to the collective modes of the itinerant ferromagnets.

The direct measurement of Stoner excitations was reported much later when the spin-polarized electron spectroscopy techniques were developed [82–85]. The substantial development of the theory of spin-polarized electron scattering which happened at the same time could help for a better understanding of the experiments [86–88]. One of

the key experiments was performed by Kirschner who used a spin-polarized beam and a spin-polarized detector to measure all the possible spin dependent features from a ferromagnetic surface [82]. The readers are referred to Ref. [89] for a review.

### 2.2.3 Single particle versus collective excitations

From a band view of magnetism the magnons may be considered as excitons (electron-hole pairs) in which the electron and hole have opposite spins. The wave function of a magnon is a linear superposition of the wave functions of electron and hole states in the system. Consequently, the coupling of magnons to Stoner excitations (single particle electron hole-pair excitations) is a mechanism which can lead to strong damping of magnons in itinerant electron systems. In simple words, consider that a magnon is excited at time zero. The precession of the spins take place in a metallic system, where all electrons sit in spin-polarized energy bands. The system has a continuous energy spectrum of spin triplet Stoner pairs. The collective mode may then decay by creating such single particle electron hole pairs. This is the main mechanism, which leads to the damping of magnons in itinerant electron ferromagnets and is usually referred to as Landau damping. Magnons in itinerant electron ferromagnets are strongly damped. Note that in ultrathin ferromagnets the location and the shape of the Stoner continuum depends also on the degree and the type of electronic hybridizations of the film and substrate. Hence, the situation can be rather complicated.

### 2.2.4 Lifetime of spin excitations

There are different mechanisms which determine the magnons' lifetime. Here we only briefly discuss the mechanism which is responsible for the lifetime of high wave vector magnons in itinerant ferromagnets. For high wave vector magnons, the lifetime is determined by the decay of the collective excitations into the single particle Stoner excitations and hence it depends strongly on the available Stoner states in the system. As discussed above in low-dimensional systems, such as magnetic monolayers, the Stoner continuum may be very much different than in the bulk ferromagnets and hence the lifetime of magnons in such systems is different than in the bulk. If the hybridization of the electronic states of the magnetic film with the ones of the substrate is such that a large number of Stoner states are created near the Fermi level, the lifetime of magnons will be very short. This means that the presence of the nonmagnetic substrate provides an addition decay channel of collective magnon modes into single particle Stoner excitations. In other words, the energy and the angular momentum of the spin system is transferred by the conduction electrons of the underlying substrate. However, this is not a general phenomenon and there are cases for which the substrate does not lead to additional Landau damping of magnons. This concept has been discussed in detail in Refs. [90, 91]. The key point to understand the underlying physics is the formation of the interfacial electronic complexes at the interface between the film and substrate. For example if the substrate features prominent surface states, these states can hybridize very efficiently with the states of the ferromagnetic film grown on top and form the interfacial electronic complexes. Due to the formation of the electronic complexes a large number of Stoner states can appear near the Fermi-level. In such



---

systems the magnons excited in the ferromagnetic film will decay rather quickly. We will come back to this point again when we discuss the magnon lifetime in ultrathin Co and Fe films (see Sec. 4.5). However, there are cases in which the formation of the electronic complexes is not favored. For these cases it is expected that the magnons in the ferromagnetic film live for a much longer time. It is important to point out that there are other sources for the damping of magnetic excitations. Even in the localized moment picture (Heisenberg ferromagnets) the high wave vector excitations are damped. This damping may be imagined as the dephasing of a certain magnon mode with a given  $q$  to all the other possible magnons with different wave vectors [92,93].

Finally, it is important to mention that the damping of magnons does not only involve the transfer of energy but also the transfer of angular momentum. The angular momentum stored in the spin system shall flow to other subsystems e.g. to the lattice. When the magnons decay to Stoner excitations, the angular momentum remains still in the spin system. The flow of both the energy and the angular momentum from the spin system ultimately ends up in the lattice. Consequently, the lattice experiences a torque. The transfer of the angular momentum from the spin system to the lattice requires a coupling mechanism which couples the spin to the lattice i.e. the spin-orbit coupling.

For  $q = 0$  the magnon lifetime is governed by spin-orbit coupling. In such cases the phenomenological damping parameter (known as Gilbert damping) shall explain the damping of the magnons in the system. In some cases, processes like two-magnon scattering may also be very important. Since here we mainly deal with high wave vector magnons, we do not discuss those kind of damping mechanisms further. A detailed explanation of those mechanisms and how to treat the damping of magnons with  $q = 0$  may be found in one of our previous works [94].



# 3 Probing spin excitations

In this chapter we shall briefly discuss the fundamental mechanisms which lead to magnon excitations in low-dimensional magnets. We will start with a brief outline of the schemes used for probing spin excitations. The methods are traditionally divided into two parts. Some are appropriate for probing low-energy excitations and some for high-energy ones.

## 3.1 Low-energy excitations

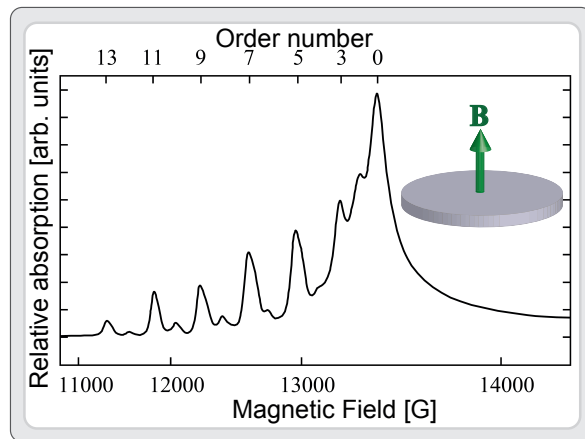
### 3.1.1 Ferromagnetic resonance

Basically, a spin system can be excited by applying a high frequency oscillatory magnetic field (with gigahertz frequency). The oscillatory magnetic field couples to the spins and since they are strongly coupled, one should see the dynamic response of the system. Such mechanisms are used for microwave excitation experiments e.g. ferromagnetic resonance (FMR). The frequency of the uniform precession (the magnon with  $q = 0$ ) is on the order of a few tens of gigahertz (energies on the order of micro-electron-volt). The dynamics of such processes is usually discussed using Eq. (2.3) including a phenomenological damping term [94].

In an FMR experiment the sample is placed in the microwaves field, and one observes resonant absorption of the microwaves as soon as the microwaves frequency matches the eigenfrequency of the uniform precession (the magnon mode with  $q = 0$ ). The magnetic field component of the microwaves is orthogonal to the applied static magnetic field. In metallic ferromagnets, the penetration of the microwaves field into the sample is not uniform. There is a so-called skin depth in which the microwaves field can penetrate. Generally, the skin depth depends on the microwaves frequency. At the resonance condition, the effective skin depth is only a few tens of nanometers. This leads to the fact that if the thickness of the sample is much larger than the skin depth, a nonuniform excitation will take place. The resulting FMR spectrum will contain not only the uniform precession (the magnon with  $q = 0$ ) but also the magnons with finite wave vectors (between 0 and  $10^{-2} \text{ \AA}^{-1}$ ). Since in the experiment one keeps the microwaves frequency constant, scans the static magnetic field and measures microwaves absorption, one observes more than a single absorption peak in the measured spectra.

In films of finite thickness, due to confinement effects the perpendicular component of the wave vector is quantized ( $q_z = n\pi/t$ , where  $t$  is the thickness of the film, and  $n$  denotes an integer number). Kittel showed that in such a situation one should see the so-called spin-wave resonance modes with odd numbers [95]. Due to the boundary conditions, the modes with even numbers are not allowed to be excited (because the spins are assumed to be pinned down at the boundaries of the sample due to the presence of the surface anisotropy). The mode with  $n = 0$  is the well-known uniform FMR mode

**Fig. 3.1:** Spin wave resonance modes of a 560 nm thick permalloy film measured by Seavey and Tannenwald [96]. In this experiment the static magnetic field was applied along the film normal as shown in the inset. Due to the boundary conditions only the odd resonance modes are expected to be excited [95]. Adopted from [96].



( $q = 0$ ), wherein all spins precess in phase. The higher order modes are the so-called spin wave resonance modes. Starting with the equation of motion introduced in Eq. (2.3) and replacing  $\mathbf{S}$  with the macro-spin i.e. the magnetization of the sample  $\mathbf{M}$ , one can show that in such a situation the dispersion relation of the modes for a ferromagnetic sample in the form of a disk and neglecting the in-plane magnetic anisotropy terms will be as following:

$$\omega = E/\hbar = \gamma (B_{res} + \mu_0 M_{eff} + Dq_z^2), \quad (3.1)$$

where  $B_{res}$  is the resonance field,  $M_{eff} = 2K_{\perp}/M - \mu_0 M$  denotes the effective out-of-plane anisotropy field ( $K_{\perp}$  is the out-of-plane uniaxial anisotropy and  $M$  is the saturation magnetization of the sample) and  $D$  is the spin wave stiffness constant. Equation (3.1) is valid when the applied magnetic field  $\mathbf{B}$  is applied perpendicular to the film surface, along the  $z$ -direction (see the measurement geometry in the inset of Fig. 3.1). For a detailed discussion on the ways that the resonance equations are derived by a classical dynamics the readers are referred to Refs. [33–35, 67, 95]. For the resonances  $q = n\pi/t$  ( $t$  is the film thickness and  $n$  is the mode number). Evidences of such spin wave resonance modes were first observed by Seavey and Tannenwald in a 560 nm thick permalloy film [96]. Figure 3.1 shows the spin wave resonance modes of the sample measured by Seavey and Tannenwald. The odd spin wave resonances are clearly visible. A plot of the resonance field versus  $n^2$  would lead to a direct determination of spin wave stiffness constant  $D$ .

The sensitivity of the technique is great. One can detect the signal of a nominal one atomic layer of a ferromagnet. It can also be intergraded into ultrahigh vacuum in order to measure the objects in the absence of any protecting layer [67, 97]. In addition, FMR is a powerful tool to investigate the damping mechanism of the uniform mode. The discussion of the damping mechanism is out of the scope of the present work and hence we will not discuss it further. We refer the reader to one of our seminal papers on this subject [94].

### 3.1.2 Brillouin light scattering

Magnons may be excited within inelastic scattering of light from the matter. This phenomenon is the basis of Brillouin light scattering (BLS) spectroscopy. The first observation of light scattering by magnons was observed by Fleury and co-workers [98] on  $\text{FeF}_2$  samples. In the conventional BLS experiments, a constant magnetic field is applied and the frequency shift of the light is measured after the scattering process [99].

The interaction mechanism is based on the modulation of the dielectric constant of the medium through the magneto-optical constants. The technique allows the investigation of magnons in low-dimensional magnetic structures [100]. The main restriction of the technique is that it only allows the measurement of low-energy (and low-wave-vector,  $q < 10^{-3} \text{ \AA}^{-1}$ ) magnons.

### 3.1.3 Time-resolved spectroscopies

Methods discussed above, allow probing the spin excitations in frequency domain. In addition to those conventional methods there are also methods which allow one to probe the excitations in time domain. In most of these experiments, the system is excited and the evolution of the spins is followed as a function of time. Depending on the excitation scheme, one may investigate a desired type of magnons. The excitation may be done by magnetic field pulses, microwaves or photons. A full description of those method is out of the scop of the present work. We do not aim to discuss them here, useful information may be found in [101].

## 3.2 High-energy excitations

### 3.2.1 Neutron scattering

Inelastic neutron scattering (INS) relies on the interaction of spin 1/2 of an incoming neutron interacting with an electron spin in the solid, via the magnetic dipole interaction, which allows for a simultaneous spin-flip of neutron and electron (a true spin-flip process). The scattered neutron then carries the information on the energy and momentum of elementary excitations left behind in the solid. The magnetic interaction between a neutron and an electron's spin that generates the spin-flip is local, but the excitation created in the scattering process can of course be delocalized being characterized by the wave vector  $\mathbf{q}$  and the energy  $\varepsilon$  transferred from the neutron to the magnetic quasi-particles in the system.

Since the interaction of neutrons with matter is relatively week, this technique does not allow probing magnons in low-dimensional magnets.

### 3.2.2 Resonant inelastic x-ray scattering

Similar to INS, one may imagine a magnetic scattering using x-ray photons. Since a photon carries an angular momentum of  $1\hbar$ , which can in principle be transferred to the spin-system, it can create elementary spin excitations. However, the direct interaction between the photon and the spin via the magnetic part of the electromagnetic field

is extremely small. This fact prohibits a simple experimental implementation of this idea. However, one may take the advantage of resonant process of photon absorption. In resonant inelastic x-ray scattering (RIXS) one scatters x-ray photons inelastically from the sample and measures the energy, momentum, and polarization change of the scattered photon. The changes in energy, momentum, and polarization of the photon are transferred to intrinsic excitations of the material under study. RIXS takes the advantage of resonant process in which the energy of the incident photon is chosen such that it coincides with, and hence resonates with, one of the atomic x-ray transitions of the system. The resonance can greatly enhance the inelastic scattering cross section, sometimes by many orders of magnitude, and offers a unique way to probe magnetic degrees of freedom on selective atomic sites in a crystal [102]. Since in RIXS process the core electrons are involved, one takes the advantage of large spin-orbit coupling of core electrons. In the so-called indirect RIXS process, an electron from a core level is promoted to a valance state by absorption of the x-ray photon. In the intermediate state the core-hole with a spin of  $1/2$  experiences a very strong spin-orbit coupling and if the core-hole orbital is of  $p$  character and thus has an angular momentum of  $1\hbar$ , the core-hole can exchange part of its angular momentum with its spin momentum, thereby flipping the spin of the core-hole. The promoted electron cannot anymore decay into this core-hole since it has not the right spin. The core hole can only be annihilated by an electron of opposite spin to the promoted electron. This fact leads to the creation of a magnon with a total angular momentum of  $1\hbar$ .

It has been proven that this technique can be applied to complex bulk samples, mainly magnetic oxides [102]. However, at the time of this writing we are unaware of any investigation on low-dimensional systems. Only very recently the magnons in superlattices of  $\text{La}_2\text{CuO}_4$  are reported [103].

### 3.2.3 Spin polarized electron energy loss spectroscopy

Spin polarized high resolution electron energy loss spectroscopy (SPHREELS or simply SPEELS) is based on the scattering of spin-polarized electrons from a magnetic surface, in which the elementary excitations are excited. It is often thought that the basic concepts of SPEELS are similar to the one of INS. In fact the fundamental basis of these two techniques are different. In SPEELS experiments the exchange mechanism plays an important role while in INS experiments the type of the interaction that is important is the dipolar interaction between the neutron magnetic moment with the magnetic moment of the unit cell.

In the following we will discuss how does the exchange mechanism during the scattering process lead to magnon excitations within the SPEELS experiments.

#### Spin-dependent electron scattering

Before we discuss the contributions to the inelastic scattering of the spin-polarized electrons, let us define the spin direction of the incoming and outgoing beam. It is defined with respect to the majority and minority spins of the sample (or with respect to the quantization axis, which is usually defined as the direction of the sample magnetization). When the spin of the electron is parallel to the majority electrons of the

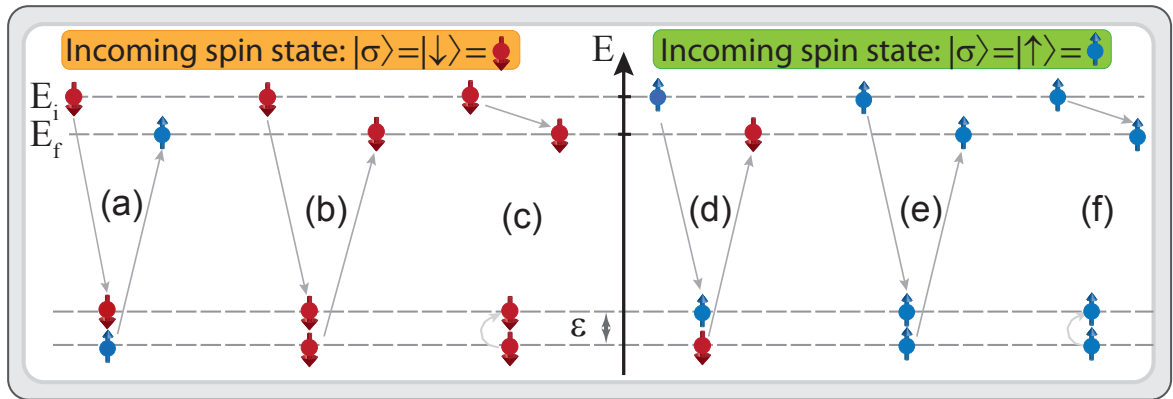


**Fig. 3.2:** A schematic representation of the possible processes taking place in the scattering of spin-polarized electrons from a magnetic surface. An electron with a given spin state  $|\sigma\rangle = |\downarrow\rangle$  (left) or  $|\sigma\rangle = |\uparrow\rangle$  (right) is incident to the sample. The spin state of the scattered electron can be either  $|\sigma\rangle = |\downarrow\rangle$  or  $|\uparrow\rangle$ . Processes marked as (a) and (d) are referred to as “flip” processes, since the spin state of the scattered electron is opposite to the one of the primary electron. Processes in which the spin of the scattered electron is the same as the one of the incoming electron are referred to as “non-flip” processes [(b), (c), (e) and (f)]. Processes (c) and (f) are usually referred to as direct processes whereas the other processes are referred to as exchange processes.

sample, it is called spin-up electron and when it is parallel to the minority electrons of the sample it is called spin-down electron. Generally, the inelastic scattering of spin-polarized electrons is a rather complicated topic. A complete description of the mechanisms involved in such processes is out of the scope of the present writing. An extended discussion can be found in Refs. [89, 104]. If an electron with a given spin is incident onto a ferromagnetic surface at a certain geometry, the outgoing electron has either the spin orientation parallel or antiparallel to the one of the incoming electron. Although in the former case an exchange of the electrons with the same spin is possible, in the latter case one can clearly talk about the exchange process. This means that the incident electron occupies an unoccupied state above the Fermi-level and another electron from an occupied state below the Fermi-level will be scattered out of the surface. The possible processes involved in the scattering of the spin-polarized electrons from a magnetic surface are schematically illustrated in Fig. 3.2 for incidence of spin-down ( $|\sigma\rangle = |\downarrow\rangle$ , left) and spin-up ( $|\sigma\rangle = |\uparrow\rangle$ , right) electrons. The processes in which the incident and scattered electrons have the same spin character are usually referred to as “non-flip” processes and the ones in which the spin of the scattered electron is opposite to the incident electron are called “flip” processes. It is essential to notice that no direct spin reversal is involved in the processes mentioned above. The underlying mechanism is the exchange process. The flip process mentioned above describes the process in which an incident electron with a given spin direction is exchanged with an electron from the sample with an opposite spin orientation (for an extended discussion see for example [105]).

### Experimental details

As mentioned above, SPEELS is based on the scattering of spin polarized electrons from a magnetic surface [82, 106–111]. Spin-polarized electrons are created by using spin-polarized photoemission from a GaAs photocathode. A circularly polarized laser beam is incident into the photocathode. According to the selection rules, the photoemitted electrons will have their spins either parallel or antiparallel to the incident direction of the laser beam, depending on the helicity of the incident photon. Since a normal GaAs has a total polarization of 50% (based on the spin dependent photoemission selection rules), usually a so-called strained semiconductor heterostructure is used for this purpose. Taking the advantage of hereroepitaxy one can grow a semiconductor heterostructure with a large lattice strain. The large strain would modify the band structure so that a large spin polarization (as large as 90 %) can be achieved [112]. The spin-polarized electrons are monochromatized to get a certain energy and are focused onto the sample surface. The spin of the incoming electrons is either parallel or

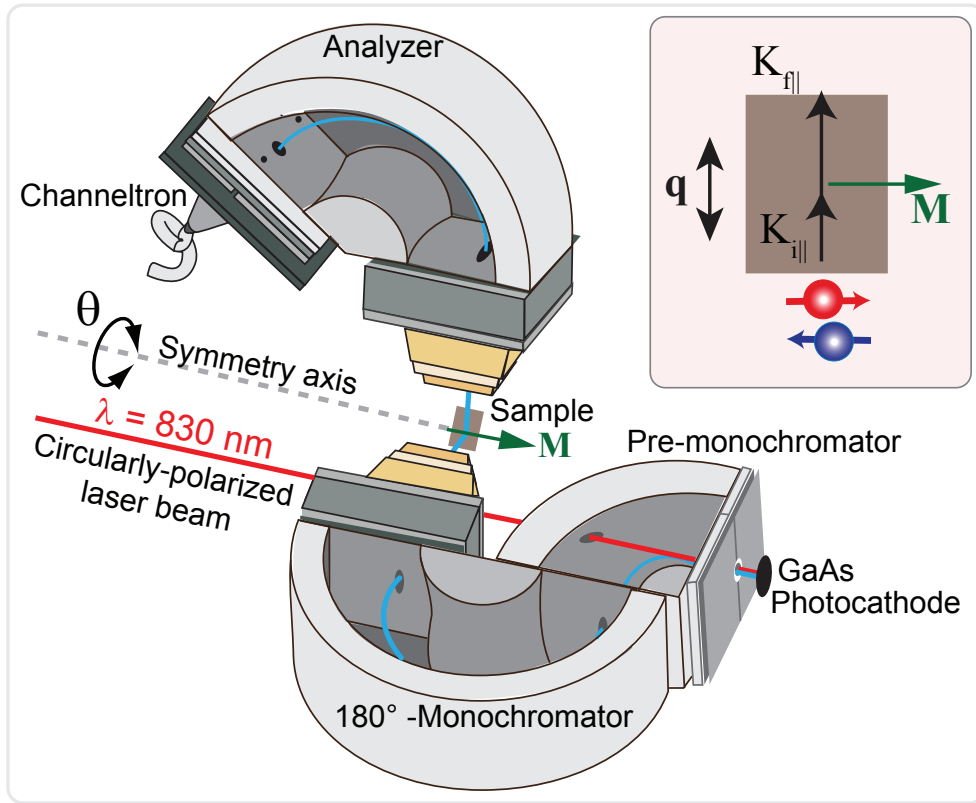
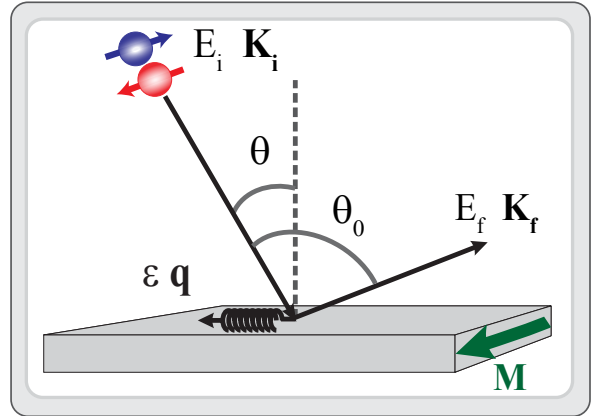


**Fig. 3.3:** A Schematic representation of the spectrometer used for this study. A spin polarized beam created by photoemission from a GaAs spin source is focused on the sample surface after passing through a pre- and an 180-monochromator. The scattered electrons are collected by a channeltron after energy analysis. Inset shows the propagation direction of magnons with respect to the parallel momentum of the incoming and outgoing electron beam and the sample magnetization.



**Fig. 3.4:** A schematic representation of the scattering geometry used in SPEELS experiments.

A monochromatic beam with a well-defined energy and momentum is scattered from the sample surface at a given geometry and the energy distribution of the scattered beam is measured for both spin orientations of the incoming beam.



antiparallel to the majority electrons of the sample. The former types of electrons are usually called as spin-down and the latter ones are called spin-up electrons. The scattered electrons are collected by a channeltron at a given scattering geometry and their energy is analyzed [110]. Note that no spin-resolved detection is involved in this experiment (see Fig. 3.3). The experiments are usually performed for both spin channels, simultaneously.

In Fig. 3.4, the scattering geometry is schematically sketched. If one assumes that the energy and momentum in initial and final states before and after scattering are  $E_i$ ,  $K_i$  and  $E_f$ ,  $K_f$ , respectively, the energy  $\epsilon = \hbar\omega$  and the wave vector  $q$  of the excitations can be given by the following expressions:

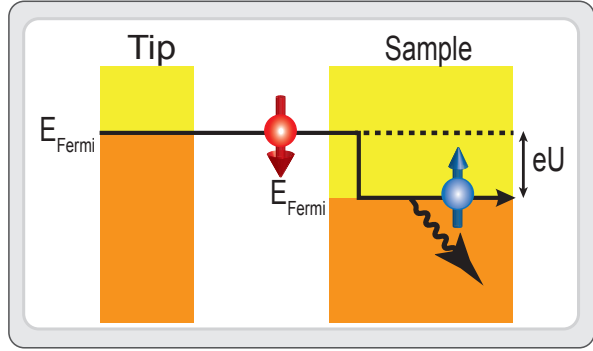
$$\epsilon = \hbar\omega = E_f - E_i; \quad q = -\Delta K_{\parallel} = K_i \sin \theta - K_f \sin(\theta_0 - \theta). \quad (3.2)$$

In addition to the conservation of energy and momentum, the total angular momentum has to also be conserved. Hence, magnon excitations are allowed only when minority electrons are incident. This implies that the magnon peak will appear only in the minority spin channel. Magnon excitations are forbidden when majority electrons are incident onto the sample surface.

### 3.2.4 Spin polarized inelastic tunneling spectroscopy

Magnons can also be excited within the tunneling process in scanning tunneling spectroscopy experiments [113–116]. Basically, the process is similar to the one in the SPEELS experiments. The tunneling electrons interact with the ones of the sample, and when they have enough kinetic energy to create an excitation, the tunneling current is enhanced. The excitation process leads to a step in the differential conductivity that is  $dI/dU$  and consequently a peak in  $d^2I/dU^2$ . The main difference here is that the excitation may happen in the forward and backward tunneling directions. This means that the peaks associated with the excitations shall be observed in both positive and negative bias voltages of the scanning tunneling microscope (STM) tip. The process which leads to creation of a magnon in the forward tunneling process is schematically sketched in the Fig. 3.5. If the tunneling electron is of minority character and during this process is exchanged with an electron of majority character, a magnon is created. In the backward tunneling (tunneling of electrons from the sample to the tip) if a majority

**Fig. 3.5:** The spin dependent tunneling process which leads to the excitation of a magnon in forward tunneling. The tunneling electron of minority character tunnels to the Fermi sea. If during this process it is exchanged with an electron of majority character, a magnon will be created.



electron of the sample is injected into the tip states a magnon is created.

Generally, the excitations seen in the tunneling spectra can be of magnetic or non-magnetic nature. By using a magnetic tip and changing the magnetization direction of the tip, one may confirm that the excitations are of magnetic origin. The main disadvantage of this technique is that the control of the tip magnetization is usually difficult. The tunneling current is almost perpendicular to the sample surface and the tunneling process takes place on a very small area (atomic length scales). This fact leads to creation of local excitations, which can be described as a superposition of the magnons with all different wave vectors. Unlike SPEELS, the technique cannot be used to excite magnons in a wave vector selective manner. However, when the magnons of different wave vectors are confined in a film or nanostructure, the standing waves are formed due to the confinement effects. Only then one would be able to assign different peaks observed in the tunneling spectra to those confined magnons and their wave vector to the corresponding quantized wave vector of the standing waves [113–116]. For investigation of magnons in ultrathin film, usually the tunneling spectra are recorded on films (or terraces) of different thicknesses. The observed peaks in the spectra are associated with the standing waves confined in the  $z$ -direction (perpendicular to the surface). In this case the wave vector is given by  $q_z = n\pi/t$ , where  $n = 0, 1, \dots$  is an integer number and  $t$  is the film thickness. The capability of measuring the magnetic excitations of adatoms and clusters on a surface is a unique possibility of this methods [116–120].

## 4 Selected results

In this chapter we present some of our selected results. The author realized that the basic concepts of the processes involved in the magnon excitations by spin-polarized electrons are not well-interpreted by many groups in various places, therefore, the basic concepts are first discussed. The nature of different types of excitations probed by electrons will be discussed in Secs. 4.1 and 4.2 in detail. The magnon dispersion relation and lifetime probed on different low-dimensional ferromagnets are addressed in Secs. 4.3, 4.4 and 4.5. The relativistic effects will be discussed in Sec. 4.7. A way of performing solid state spectroscopy of buried interfaces using magnons will be explained in Sec. 4.8. The possibility of using a transversally spin-polarized beam for probing magnons will be discussed in Sec. 4.9.

### 4.1 Probing magnons by spin-polarized electrons

This section is based on the original publications [KhZ 6.1] and [KhZ 6.2].

For studying the spin excitations in low-dimensional ferromagnets, initially an atomically clean sample has to be obtained. Such surfaces can be prepared by means of conventional thin film growth techniques under ultrahigh vacuum. Usually, prior to the SPEELS measurements the films are magnetically saturated by applying a magnetic field. The measurements are performed in the remnant state. As it is mentioned in Sec. 3.2.3, magnons carry a total angular momentum of  $1\hbar$ , therefore, they are created by minority electrons (see Fig. 4.1). Due to the thermal fluctuations, a spin system possess a large variety of magnons at a finite temperature. These are usually referred to as thermally excited magnons and are spread over a large momentum and energy space, depending on the temperature. The population of this class of magnons is given by Bose–Einstein statistics, which determines the statistical distribution of identical indistinguishable bosonic quasi-particles over the energy states in thermal equilibrium. In principle, the thermally excited magnons can be annihilated by majority electrons. A majority electron can be scattered to a minority one via the exchange scattering mechanism and hereby a magnon is annihilated (see Fig. 4.1). In this process, the energy of the electron in the final state is larger than the one in the initial state, and hence such a process can be observed in the energy gain region. The intensity of the peak associated with the magnon annihilation process depends on the population of the thermally excited magnons at the measurement temperature. The ratio of the intensity of the loss to the gain peak is given by a Boltzmann factor, which is about 0.17 for the magnons with an excitation energy of 46 meV at  $T = 300$  K. It is nearly zero for  $T = 10$  K. This means that at low temperatures the magnon annihilation process is expected to be suppressed and at high temperatures it is pronounced. Such a behavior is also expected for phonons that are also classified as bosons.

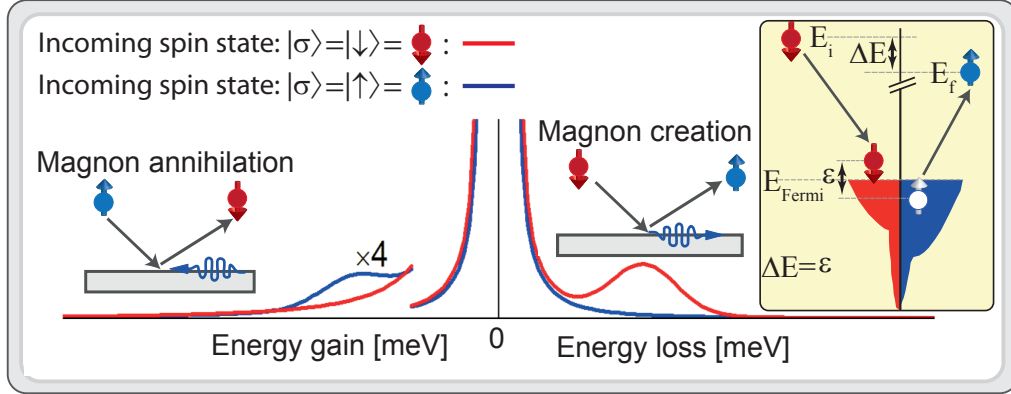


**Fig. 4.1:** A schematic representation of SPEELS spectra. The magnon excitation (creation) process takes place in the energy loss region when an incoming electron of minority spin state is scattered into an electron of majority spin state. The magnon annihilation process taking place in energy gain region is accomplished with incident electrons of majority spin state. Inset provides detailed information on the magnon excitation process. An electron of minority spin state occupies an empty state above the Fermi level and an electron of majority spin character leaves the sample from a state below the Fermi level.

At this point we would like to point out that in principle an electron beam with any polarization vector (or even an unpolarized beam) can be used to excite and probe magnons. However, the interpretation of data would not be as straightforward as the case where the beam polarization is parallel and antiparallel to the sample magnetization (the quantization axis). We will show in Sec. 4.9 how a transversally spin-polarized beam can be used to excite and probe magnons in an ultrathin film with out-of-plane easy axis.

An example of the experimental data is provided in Fig. 4.2 where the SPEELS spectra measured at different temperatures are presented. The spectra are recorded on a 2 monolayer (ML) thick Fe(110) film grown on W(110) at a wave vector of  $0.5 \text{ \AA}^{-1}$ . The magnon propagation direction in this particular experiment is along the [001]-direction of the Fe(110) surface ( $\bar{\Gamma}-\bar{H}$  direction of the surface Brillouin zone). For each case the spectra for spin-up ( $I_{\uparrow}$ ) and spin-down ( $I_{\downarrow}$ ) electrons are measured. In addition, the sum ( $I_{\downarrow} + I_{\uparrow}$ ), difference ( $I_{\downarrow} - I_{\uparrow}$ ), and asymmetry  $[(I_{\downarrow} - I_{\uparrow}) / (I_{\downarrow} + I_{\uparrow})]$  spectra are also presented. Let us first start with Fig. 4.2 (a). It is apparent that the spectra are dominated by presence of the quasi-elastic peak at  $E = 0 \text{ meV}$ . The magnon creation and annihilation peaks are located beside the quasi-elastic peak in the energy loss and gain region, respectively. These two processes are sketched schematically in the insets of Fig. 4.2. The asymmetry curve shows a change in the sign from negative to positive, when going from gain to loss region. The maxima (in the loss region) and the minima (in the gain region) are the places where the excitation and annihilation processes take place. If one neglects the spin-orbit coupling effects in the system the maxima and minima should be located at the same energies (one negative and the other positive). As it was mentioned earlier, at low temperature where the population of the thermally excited magnons is very low, the magnon annihilation peak supposed

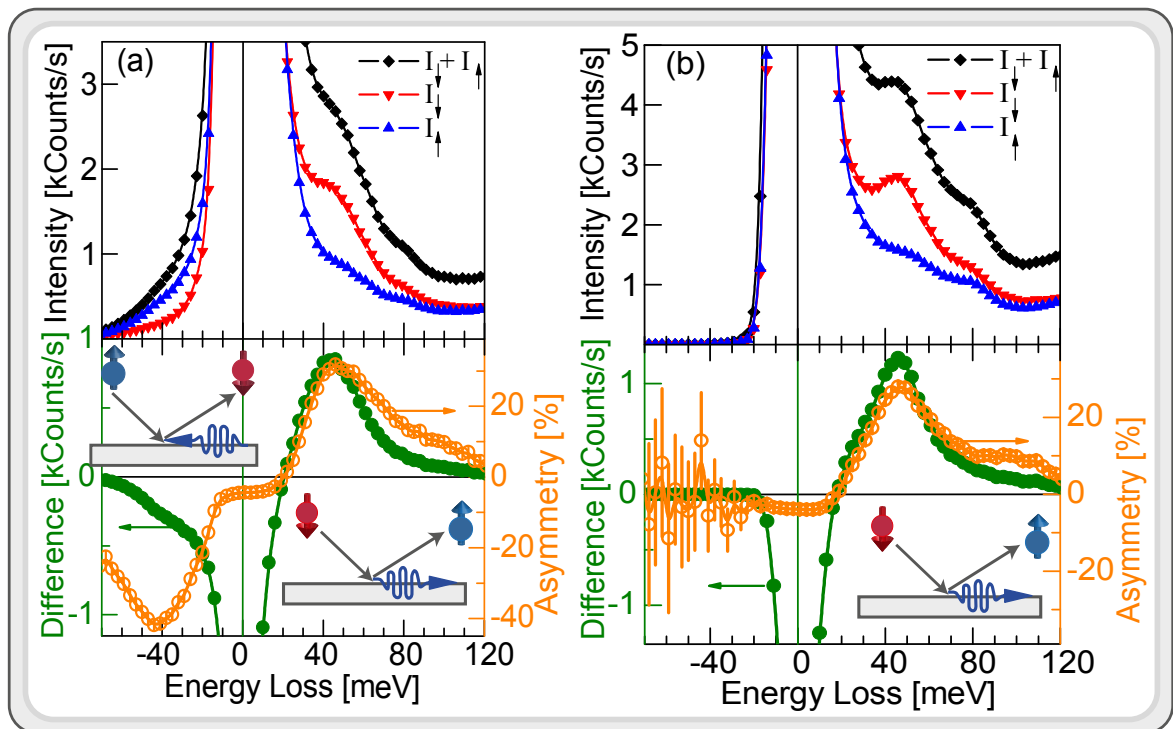


**Fig. 4.2:** SPEELS spectra measured at  $\Delta K_{\parallel} = 0.5 \text{ \AA}^{-1}$  on an ultrathin Fe(110) film on W(110) with a thickness of 2 ML at (a) 300 K and (b) 10 K. The upper panels show the spin up ( $I_{\uparrow}$ ), spin down ( $I_{\downarrow}$ ) and the sum ( $I_{\uparrow} + I_{\downarrow}$ ) spectra. The lower panels show the difference ( $I_{\downarrow} - I_{\uparrow}$ ) and asymmetry ( $(I_{\downarrow} - I_{\uparrow}) / (I_{\downarrow} + I_{\uparrow})$ ) spectra. The magnon creation and annihilation processes are schematically sketched in the insets. Taken from [KhZ 6.1].

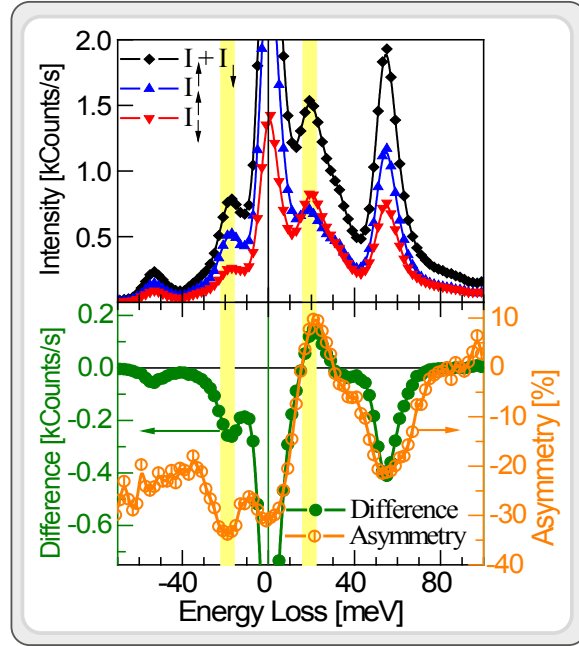
to be strongly suppressed. This fact can be clearly seen in Fig. 4.2 (b), where the measurements at 10 K, performed on the same sample, are presented. No trace of magnon annihilation could be detected neither in the difference nor in the asymmetry spectrum. In order to obtain the magnon dispersion relation, usually the spectra are recorded for different wave vectors [105, 121–126]. The desired wave vector is achieved by changing the scattering geometry.

## 4.2 Simultaneous probing of magnons and phonons

This section is based on the original publication [KhZ 6.3].

In principle, both magnons and phonons can be excited by electrons. Since both kinds of excitations may show very similar energies, it is rather difficult to distinguish between them experimentally. However, using the spin degree of freedom of spin-polarized electrons opens a possibility to separate magnons from phonons. As magnons carry a total angular momentum of  $1\hbar$ , they can only be excited by incidence of minority electrons. The time reversal process happens for incidence of majority electrons, which leads to the magnon annihilation. This fact would lead to a sign change in the asymmetry curve

**Fig. 4.3:** SPEELS spectra measured on the Fe(001)-O(1×1) surface at  $T = 300$  K and  $\Delta K_{\parallel} = 0.3 \text{ \AA}^{-1}$ . The upper panel shows the spin up ( $I_{\uparrow}$ ), spin down ( $I_{\downarrow}$ ) and the sum ( $I_{\uparrow} + I_{\downarrow}$ ) spectra. The lower panel shows the difference ( $I_{\downarrow} - I_{\uparrow}$ ) and asymmetry ( $(I_{\downarrow} - I_{\uparrow}) / (I_{\downarrow} + I_{\uparrow})$ ) spectra. The vertical yellow lines mark the position of the peaks resulting from the magnon excitation (energy loss) and annihilation (energy gain) processes. Taken from [KhZ 6.3].



in gain and loss regions [see the lower panel of Fig. 4.2 (a)]. In the case of phonons, the situation is different. Since phonons are spin-independent quasi-particles, they can be created and annihilated by incidence of electrons with any spin direction. We note that the process which leads to phonon creation can also be mediated by the exchange process (the exchange of the electrons with the same spin, see the discussion in Sec. 3.2.3). The particular dependence of magnon creation and annihilation on the spin of the incident electrons, as it is different from phonon excitations, is a fundamental feature, which can be used to distinguish between magnons and phonons in spin-polarized electron scattering experiments. The best way to identify the nature of an excited quasi-particle (magnon or phonon), is to compare the sign of asymmetry curve in loss and gain regions. An example is provided in Fig. 4.3, where the spectra of an oxygen passivated Fe(001), measured at  $T = 300$  K and  $\Delta K_{\parallel} = 0.3 \text{ \AA}^{-1}$ , are presented. The magnon and phonon excitations coincide within the same energy window. Interestingly, the intensity of all excitations depends on the spin orientation of the incoming beam. As it is discussed above, the identification of phonons and magnons can be done by looking at their different spin nature. The asymmetry of loss and gain regions of the peaks marked by the vertical yellow lines in Fig. 4.3 (at energies of  $\pm 19$  meV) is of opposite sign, and hence these peaks are associated with magnon excitations. Asymmetry of the other excitations has the same sign and almost identical magnitudes; therefore, they are caused by phonon excitations. It is interesting to mention that in the case of the O/Fe(001)- $p(1 \times 1)$  surface the asymmetry of phonon induced peaks is always negative. A complementary experiment showed that the asymmetry of the phonon peaks follows the one of the quasi-elastic peak. This fact implies that very likely the asymmetry of the phonon peaks has the same origin as the one of the elastic peak. The sign and magnitude of the asymmetry is expected to depend on the energy of the incident beam, excitation energy, and the scattering geometry. The asymmetry may even change the sign while changing the electron energy. The dispersion relation of

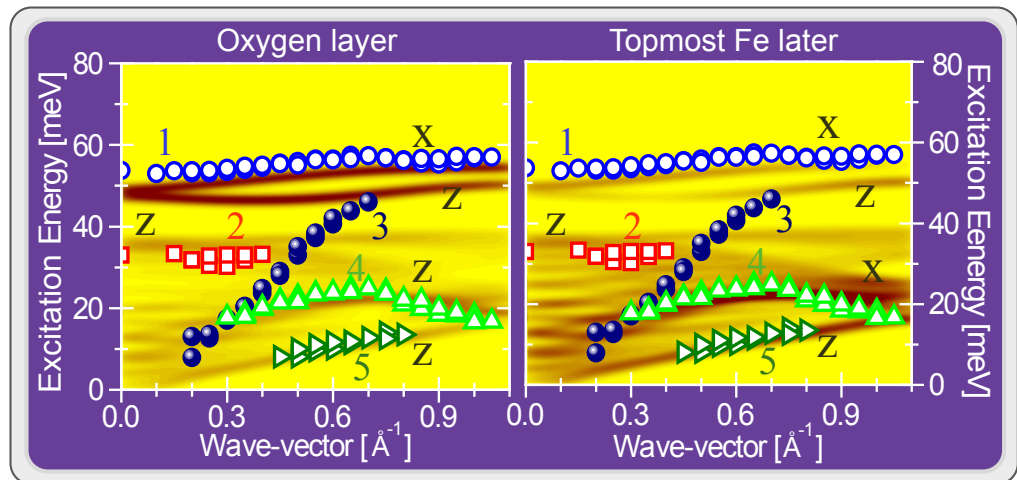


**Fig. 4.4:** Dispersion relation of all elementary excitations probed on the Fe(001)–O(1×1) surface. The color map represents the theoretically calculated phonon spectral density projected on the oxygen layer (left) and the topmost Fe layer (right). Open symbols denote the phonon branches numbered by 1, 2, 4 and 5; filled symbol denotes the magnon branch and is numbered by 3. Letters “x”, “y”, and “z” near each phonon band denote displacement directions of the corresponding phonon modes. Taken from [KhZ 6.3].

magnons and phonons could be measured simultaneously by varying the wave vector and the dispersion branches could be separated based on their different spin nature.

A careful fitting of the spectra using a superposition of Gaussian peaks revealed five excitation branches in both energy loss and energy gain regions. Figure 4.4 shows the dispersion relation of magnons and all different kinds of phonons measured on O/Fe(001)–p(1×1) surface. One clearly observes 4 different phonon modes and one magnon mode. Phonon branches are represented by open symbols, while the magnon branch is shown by filled symbols. Magnon branch disperses from 16 to about 40 meV as the wave vector increases from 0.2 to 0.7 Å<sup>-1</sup>. Magnon excitation peaks become very broad at high wave vectors. This broadening can be explained by a strong decay of magnons in itinerant electron systems. We will discuss this point in Sec. 4.5.

*ab initio* calculations in the framework of the direct calculations of the force matrix [127] can account for a more precise description of the observed phonon modes in the system. The results of the calculations are presented in Fig. 4.4. Based on the theoretical calculations, we classify the phonon modes as follows: the mode numerated as “5” with the lowest energy originates from the acoustical *z*-polarized transversal oscillations of atoms located at the topmost Fe and O layers. It is the so-called Rayleigh mode of the surface, which has been also observed in the He-atom scattering experiments [128]. The next phonon mode “4” shown in Fig. 4.4 with upward-oriented triangles is also localized in the two topmost layers. In the Fe layer mode “4” is a longitudinal acoustic phonon with *x* polarization, while in the oxygen layer it is transversal with *z* polarization. Phonon mode “2” spreading off the  $\bar{\Gamma}$  point at the energy of about 33 meV plotted by open squares in Fig. 4.4 is a *z*-polarized surface resonance of the

phonons of the Fe slab. Two high-energy branches at 50 meV are optical  $z$ -transversal and  $x$ -longitudinal phonons localized mostly on the oxygen sites. The agreement with experimental results for these excitations is not as perfect as in the other cases, but these modes can still be associated with the excitation branch “1”. The differences between the experiment and the theory might be due to the inharmonicity of oxygen vibrations, which couples the  $x$ - and  $z$ -polarized modes. The mode shown by filled symbols is a magnon mode. The theoretical calculations presented here do not account for magnons, and hence no magnon mode can be seen in the theoretical counterpart.

### 4.3 Magnons in a ferromagnetic monolayer

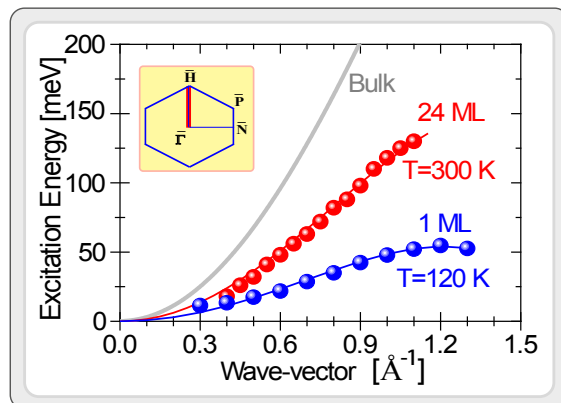
This section is based on the original publication [KhZ 6.4].

One of the most fundamental aspects in the field of spin excitations in low-dimensional magnets is the magnon spectrum in a real two-dimensional spin system *e.g.* a ferromagnetic monolayer grown on a non-magnetic substrate. Here, the fundamental questions are: if the magnons in real two-dimensional ferromagnets do exist, is it possible to see their signature of excitations in SPEELS spectra? How does the magnon dispersion relation look like in such a system?

We performed SPEELS experiments on a prototype ferromagnetic monolayer; one atomic layer Fe(110) grown on W(110). Since the Curie temperature of the Fe monolayer is below room temperature ( $T_c \simeq 223$  K [129]), the spectra are measured at 120 K (and also at 10 K, not shown here). We realized that in the Fe monolayer the magnon excitations occur at very low energies. In addition to that the spectra are very broad. The magnon dispersion relation measured over the whole Brillouin zone is presented in Fig. 4.5. For a better comparison the results of the surface mode of a thicker Fe film (with a thickness of 24 atomic layers) grown on the same substrate are also presented. Figure 4.5 which provides a direct comparison between the results of the monolayer Fe and the surface mode of Fe(110), reveals that the magnon energies in the Fe monolayer are very small. Experimental results on magnon dispersion relation measured at 10 K indicate that the magnon energies are slightly higher (about 10 meV) with respect to the ones measured at 120 K, which reflects the temperature effects on magnons.

As it is mentioned in Sec. 2.1.1 the nature of spin excitations in itinerant ferromagnets is rather complicated and the Heisenberg description of magnons would not lead to an

**Fig. 4.5:** The magnon dispersion relation of 1 ML Fe on W(110) measured at 120 K along the  $\bar{\Gamma}$ - $\bar{H}$  direction of the surface Brillouin zone (see the inset). The dispersion relation of the acoustic surface mode of a 24 ML thick sample is also shown. Data are taken from [KhZ 6.4]. The results are compared to the one of the bulk Fe [29].





appropriate description of the system. However, one may put the interaction in a form of an effective exchange coupling in order to estimate the strength of the coupling in the system. Taking this simple approach, one can derive an equation for the magnon dispersion relation as discussed in Sec. 2.1.2. Fitting the experimental results with the calculated magnon dispersion relation within that model, results in a very small effective exchange interaction ( $J_{\text{eff}}=11$  meV) and an effective magnetic anisotropy of  $K_{\text{eff}}= 2.3 \pm 1.3$  meV. These results are in reasonable agreement with the earlier theoretical [77] and experimental works obtained using static magnetic measurements [130]. Magnons in the Fe monolayer are even much softer than the acoustic surface mode of Fe(110). Fitting the experimental results with the well-known parabolic dispersion ( $E = Dq^2$ ) leads to a determination of the magnon stiffness constant,  $D$ . We found that  $D$  for the monolayer system is by a factor of 2.2 smaller than the one obtained for the Fe(110) surface ( $D_{\text{ML}}=74$  meVÅ<sup>2</sup> and  $D_{\text{surf.}}=160$  meVÅ<sup>2</sup>). It is only about one-fourth of the value measured for bulk Fe by INS [31, 131, 132]. A number of first principles calculations based on different approaches have predicted much larger energies for magnons in Fe monolayer [54–58, 77, 133, 134]. However, the theoretical results depend strongly on the parameters used for the calculations. The magnon softening in the Fe monolayer may have different origins. The first one might be the temperature effect. Since the experimental results are obtained at 120 K, which is half of the Curie temperature of the system, this may cause the softening of the magnons. The second origin might be the strong hybridization with the substrate and change in the electronic structure of the film caused by the W(110) substrate. The third origin might be the influence of the DM interaction, which we will show that is very important for the Fe films grown on W(110).

Our experimental data are well reproduced by a combining the first principles calculations with the so-called atomistic spin dynamics simulations [135]. This approach enables one to investigate the effect of temperature on the magnon properties. The authors could confirm that the temperature effects and the chemical relaxations, which influence the hybridization of the Fe film and W(110) lead to this magnon softening.

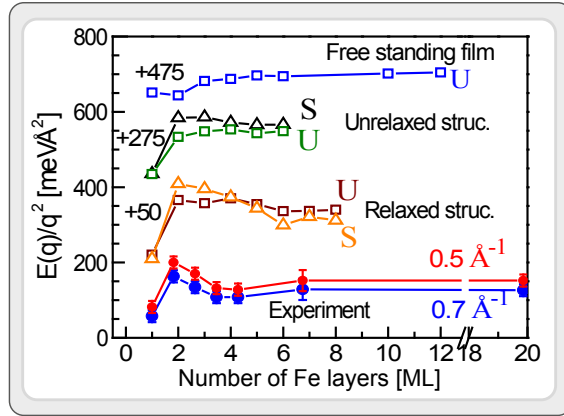
## 4.4 Atomic structure and magnon dispersion relation

This section is based on the original publications [KhZ 6.4], [KhZ 6.5] and [KhZ 6.6].

### 4.4.1 Coordination number

In order to investigate the dimensionality effects on magnons, we have investigated the magnon energy as a function of the film thickness for Fe(110) films on W(110). The results of such an investigation are summarized in Fig. 4.6. In order to have a better comparison of the energies, recorded for different wave vectors, the energies are normalized to the wave vector. It is apparent from Fig. 4.6 that the magnon energy increases by a factor of 2.2 while changing the film thickness from 1 to 2 atomic layers. To explain these results we use simple arguments based on an adiabatic approximation. We however note that in real itinerant ferromagnets the situation might be much more complicated. Consider one atomic layer of Fe pseudomorphically grown on W(110). In

**Fig. 4.6:** Normalized magnon energy as a function of the film thickness: experiment and theory. Letters U and S denote the uniform and surface modes, respectively. In the uniform (surface) mode the amplitude of the moments is assumed to be equal in all atomic layers (maximum in the surface layer). For all theoretical curves  $\Delta K_{\parallel}=0.5 \text{ \AA}^{-1}$ . Taken from [KhZ 6.5].



such a case the exchange coupling is confined in the plane of the film. Due to a lower coordination number one would expect lower magnon energies for the ferromagnetic monolayer with respect to a 2 ML film. The sudden increase of the magnon energy when changing the film thickness from 1 to 2 is the direct consequence of the increase of the coordination number. In the case of the 2 ML sample the Fe atoms sitting in different layers are also strongly coupled. The coupling of Fe atoms within each layer are referred to as *intralayer* coupling and the coupling of the atoms from different layers are referred to as *interlayer* coupling. Calculated effective coupling for a 2 ML sample shows that the nearest neighbor interlayer coupling is about 27 meV and the nearest neighbor intralayer coupling is about 20 meV (more information are provided in Sec. 4.4.3 and Fig. 4.8). For these calculations, it is assumed that the in-plane lattice constant of Fe is the same as underlying W(110) surface. The out-of-plane lattice constant is taken from the surface x-ray diffraction experiments [136]. If further increasing the film thickness do not change the film structure, one would expect the same magnon energy for a 3 ML film as it is predicted by the theory (see Fig. 4.6). However, it is known for Fe films on W(110) that the films start to relax when the thickness is larger than 2 ML. The lattice relaxations have a direct consequence on the magnon energies and is discussed in the next section.

#### 4.4.2 Lattice relaxation

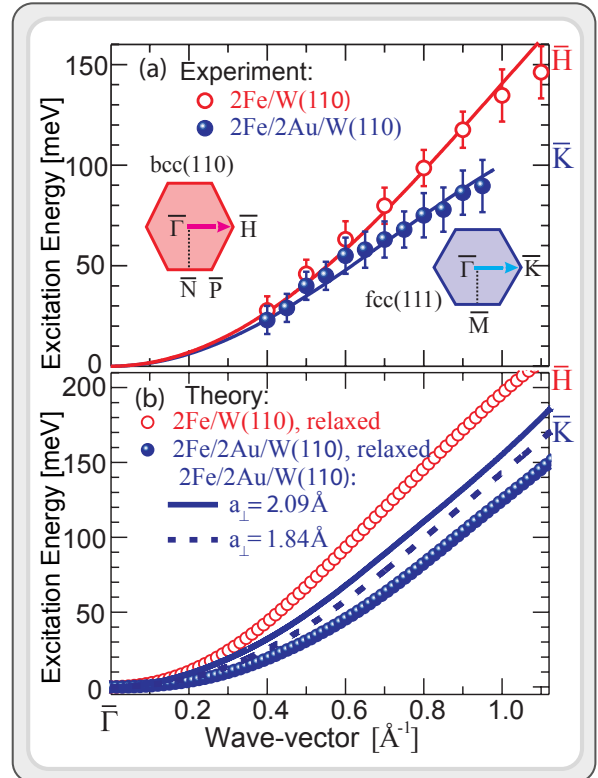
Taking into account the lattice relaxation one can explain the decrease of the magnon energy for the 3 ML sample. The magnon energy reaches an asymptotic value for films thicker than 5 ML where the structure is transferred into a bulk like film.

Another result of the calculation is that the mode seen in the experiment is mainly contributed from the surface layer. There are however cases in which the lowest magnon mode (usually referred to as acoustic mode) is mainly contributed from the interface layer. This unusual case happens when the effective exchange coupling in the interface layer is smaller than the one in the surface layer. We will come back to this point in Sec. 4.8.

### 4.4.3 Lattice modification

The modern methods of the fabrication of low-dimensional structures allow creating materials of given chemical content with different atomic structures. For instance by introducing a thin Au buffer between the Fe film and the W(110) substrate one can change the Fe surface structure from bcc-like stacking with (110) surface to fcc-like stacking with (111) surface orientation. In order to investigate the effect of the lattice modification on the magnon dispersion relation, the Fe film thickness has been kept unchanged (2 atomic layers) and just its structure is changed by introducing the Au buffer. The magnon dispersion relation measured for both Fe(110)/W(110) and Fe(111)/Au/W(110) is presented in Fig. 4.7 (a). The results indicate a large difference in the magnon dispersion relation of the two films. These changes could be understood on the bases of first principles adiabatic calculations. The change in the Fe lattice has a direct consequence on the magnetic exchange interaction in the film. Although the interlayer exchange constants increase when changing lattice structure from simple bcc stacking to the new (111)-close-packed structure, the intralayer exchange constants decrease. Since the intralayer coupling constants are counted more effectively, the dispersion relation of the Fe(111)/Au/W(110) system is lower in energy with respect to the one of the Fe(110)/W(110) system (number of nearest neighbors in the each layer are 4 while in the neighboring layer are 2). The comparison of the exchange constant for two systems, Fe/W(110) and Fe/Au/W(110), shows that the interlayer and intralayer coupling constants feature opposite trends [see Fig. 4.8 (a)–(c)]. As an example, the largest interlayer coupling constant  $J_{\perp}$  increases from 27 meV in Fe(110)/W(110) to 69 meV in Fe(111)/Au/W(110) whereas the largest intralayer coupling constant  $J_{\parallel}$  de-

**Fig. 4.7:** (a) The magnon dispersion relation measured on a 2 ML Fe film on 2 ML Au on W(110) and a 2 ML Fe film directly grown on W(110). The symbols represent the experimental results and the solid lines are the guide to the eyes. (b) Theoretical magnon dispersion relation for the same systems. The symbols represent the results of the calculations for the relaxed structure. The lines are the results for the Fe/Au/W(110) system calculated for different values of Fe interlayer spacing,  $a_{\perp}$ . Insets show the surface Brillouin zone. Taken from [KhZ 6.5].



creases from 20 to 14 meV for the interface layer and from 13 to 9 meV for the surface layer. The analysis shows that the softening of the magnons in Fe(111)/Au/W(110) is the consequence of the decreased intralayer exchange parameters that overcome the opposite trend of increasing the exchange parameters between the layers.

Calculations showed that increasing the interlayer distance in the Fe(110)/Au/W(110) structure leads to an expected decrease of the interlayer exchange parameters [see Fig. 4.8 (a)]. This is resulted from the decrease of the interlayer hybridization. At the same time an increase in the intralayer exchange parameters was observed [see Fig. 4.8 (b) and (c)]. Interestingly, this increase takes place for unchanged interatomic distances within the layers. This fact is a consequence of complex reconstruction of the electronic structure due to the increase of the interlayer distance. While changing the interlayer distance of Fe layers from 1.71 to 2.09 Å, the nearest neighbor intralayer coupling increases by a factor of 1.5 and 2.3 for the atoms in the interface and surface layer, respectively. In order to shed light onto the origin of this effect, one may carefully analyze the change in the density of states of different atomic orbitals. Figures 4.8 (d) and (e) show the spin-resolved DOS of 3d electrons calculated for different interlayer distances for Fe(110)/Au/W(110). The projected DOS of different orbitals are plotted separately. The 3d states responsible for the interlayer hybridization ( $d_{xz}$ ,  $d_{yz}$ , and

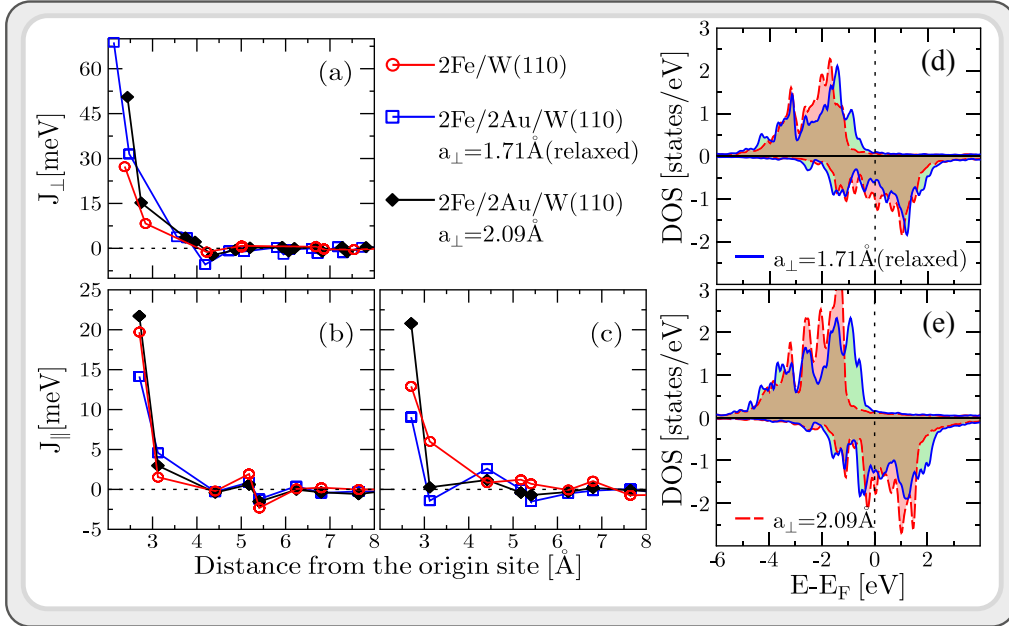


**Fig. 4.8:** Calculated site-resolved interlayer  $J_{\perp}$  (a) and intralayer  $J_{\parallel}$  exchange constants for the atoms located in the interface layer (b) and in the surface layer (c). Open and filled symbols represent the calculations for the relaxed and expanded structures, respectively. Spin-resolved DOS of 3d states in 2Fe/2Au/W(110), separated in a part with  $d_{xy}$  and  $d_{x^2-y^2}$  states (d) and a part corresponding to  $d_{xz}$ ,  $d_{yz}$  and  $d_{z^2}$  orbitals (e). The solid and dashed lines represent the results for relaxed and expanded structures, respectively. Taken from [KhZ 6.5].

$d_{z^2}$ ) appear substantially higher in energy than the states responsible for the intralayer hybridization ( $d_{x^2-y^2}$  and  $d_{xy}$ ). With increasing interlayer distance all states move to lower energies as a consequence of decreasing  $3d$  band width. However, this shift is more important for  $d_{xz}$ ,  $d_{yz}$ , and  $d_{z^2}$  states, since  $d_{x^2-y^2}$  and  $d_{xy}$  are located well below the Fermi level for the smallest value of the interlayer distance. Increasing the interlayer distance increases the spin-down density of  $3d$  states near the Fermi level. The appearance of a large number of states near the Fermi energy is an important factor in the enhancement of intralayer exchange interaction. These results clearly indicate that the magnetic properties of complex systems cannot be understood without careful microscopic study of the exchange interaction. In addition, the evolution of the electronic structures cannot be separated into features related to the interlayer and intralayer distances since the influences of both distances are strongly interconnected.

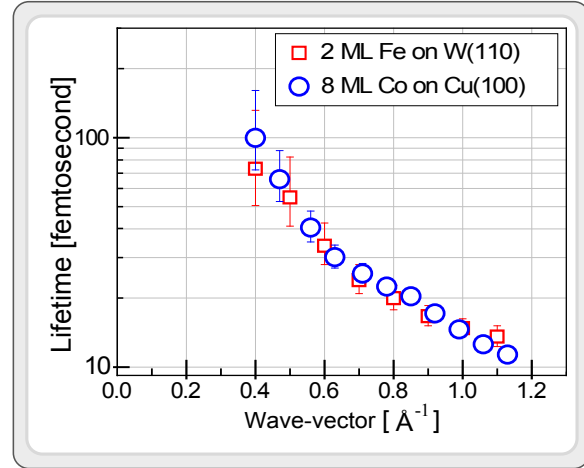
## 4.5 The magnon lifetime

This section is based on the original publication [KhZ 6.7].

As discussed in Chap. 1 one of the key properties of quasi-particles is their lifetime. In this section we shall present the results of magnon lifetime measured by SPEELS. These results would have a significant contribution to the understanding of the magnetic damping mechanism of terahertz magnons in ultrathin films and a possible tuning of the magnetic relaxation in ferromagnets. They may also offer a way of estimating the ultimate time scale of magnetic switching in low-dimensional ferromagnets.

The broadening of the magnon excitation peak provides a way of estimating the magnon lifetime. We first measure the SPEELS spectra for both spin orientations of the incoming beam polarization (parallel and antiparallel to the sample magnetization). Based on the measured spectra we obtain the difference spectra ( $I_{\text{Diff}} = I_{\downarrow} - I_{\uparrow}$ ). To extract the intrinsic linewidth, we fit the measured difference spectra by using a convolution of a Gaussian and a Lorentzian function, in which the Gaussian represents the instrumental broadening and the Lorentzian represents the intrinsic magnon signal. By fitting the experimental results, one realizes that the intrinsic linewidth of magnon excitations is typically from 20 up to a few hundreds of meV, which is usually larger than the instrumental broadening. As an example, a fit through the data measured on 2 ML Fe(110)/W(110) at  $\Delta K = 0.6 \text{ \AA}^{-1}$  shows that the intrinsic linewidth of the magnon is about  $42 \pm 7$  meV, while the instrumental broadening is about 20 meV. The large broadening of the loss spectrum indicates that magnons are strongly damped in time. The magnon lifetime can be obtained from the Fourier transform of the magnon signal. The Fourier transform of the Lorentzian in energy (or frequency) domain is an exponential decay in the time domain,  $\exp(-t\Gamma/2\hbar)$ , where  $\Gamma$  represents the intrinsic linewidth of the Lorentzian peak in energy and  $\hbar$  is the reduced Planck constant. We define the lifetime of a magnon as  $\tau = 2\hbar/\Gamma$ , a time in which the amplitude drops to its  $e^{-1}$  value. The magnon lifetime obtained using this approach is plotted in Fig. 4.9 for two systems; 2 ML Fe(110)/W(110) and 8 ML Co(100)/Cu(100). The lifetime depends strongly on the wave vector. It is about 100 fs at  $\Delta K_{\parallel} = 0.4 \text{ \AA}^{-1}$  and decreases to a value of about 10 fs for large wave vectors. Surprisingly, it is found that the lifetime for these two different systems are very similar in spite of the fact that the magnon energies

**Fig. 4.9:** The magnon lifetime as a function of the in-plane wave vector in a semi-logarithmic plot. The data are recorded for a 2 ML body-centered cubic Fe(110) film grown on W(110) (open squares) and an 8 ML face-centered cubic Co(100) film grown on Cu(100) (open circles). The Brillouin zone boundary for Fe/W(110) is at  $1.5 \text{ \AA}^{-1}$  while for Co/Cu(100) is at  $1.23 \text{ \AA}^{-1}$ . Taken from [KhZ 6.7].



are by a factor of two different.

Comparing to the spin relaxation of a single atom on the insulating substrate, whose relaxation time is about  $10^{-7}$  s [137], the lifetime of magnons in  $3d$  ferromagnetic films is almost  $10^7$  times shorter. Such a short lifetime of high-energy magnons is attributed to the strong damping due to the presence of the conduction electrons in the metal film and the substrate [56,57,90]. Since the high-energy magnons are a coherent superposition of the correlated electron hole pairs across the Fermi level, their damping may be regarded as the results of the strong decay of these collective magnons into the available Stoner states near the Fermi level. It has been shown that the Stoner excitations in the surface states play an important role in the decay effect [91,116,119]. If the ferromagnetic film is grown on a metallic substrate, due to the strong hybridization of the bands, there are lots of Stoner states available near the Fermi level, which can contribute to the damping mechanism. In other words, the strong decay effect may be imagined as the pumping of the spins of the magnetic film into the non-magnetic conductive substrate [57]. The similarity of the magnon lifetime in Fe and Co films, in spite of the fact that the magnon energy in the Co(100) film is almost twice of that in the Fe(110) film, may indicate that magnons can experience similar damping effects even though the electronic band structure of two systems are different. Besides the intrinsic damping effects due to the Stoner excitations, it has been proposed that the thermal effects may also play a role in the broadening of magnon peaks [138]. However, experiments performed on a 2 ML Fe film at different temperatures revealed that the temperature dependence of the intrinsic linewidth is negligible (see Fig. 4.2). As the Landau damping strongly depends on the available Stoner states near the Fermi level, the hybridization of the electronic bands of the ferromagnetic film with the ones of the substrate plays also an important role.

As the total magnetization of the sample is unchanged after creation and damping of a magnon, one cannot directly connect the magnon lifetime to the ultimate time scale of magnetization switching. However, this relaxation time can be directly compared to the time interval provided in excitation scheme. For instance, if the aim is to switch the magnetization of a nano-island using a spin-polarized current within a few femtoseconds, the terahertz magnons are governing this process. Hence, the time interval between two electrons has to be shorter than the lifetime of the magnons involved. Otherwise, the magnons do not contribute to this switching process and die out. The same analogy

applies to the other methods used to switch the magnetization.

Recently, a strong spin dependence of the decay rate of the image potential state has been observed in photoemission experiments and is attributed to the magnon generation and relaxation within a few tens of femtoseconds [139]. The observed decay rate is similar to the relaxation time of the magnons measured in our experiments.

## 4.6 Real space representation of magnons

This section is based on the original publication [KhZ 6.7].

For a real space representation of the magnons one may use a two-dimensional Fourier transformation of the magnons' distribution in the reciprocal space. If one measures the magnon intensity spectra for different wave vectors, a contour map can be constructed by plotting the difference spectra. Such data for a 2 ML Fe(110) film on W(110) are presented in Fig. 4.10 (a). If one assumes that the scattering geometry does not drastically influence the intensity distribution in far off-specular, one may estimate the spatial distribution of the magnon wave packets from the intensity profile presented in Fig. 4.10 (a). For simplicity we neglect the broadening in wave vectors due to the finite energy resolution. This is a rather good assumption, since the instrumental broadening is fairly small compared to the intrinsic linewidth. The spectral distribution as a function of the wave vector is fitted directly by a single Gaussian distribution. For example, the profile in Fig. 4.10 (c) shows a full width at half maximum (FWHM) of about  $0.32 \text{ \AA}^{-1}$ . After a Fourier transform, one obtains a Gaussian wave packet representing the magnon envelope function with an FWHM of about 2 nanometers. Now the magnon wave packet can be constructed from the experimental data. An example is presented in Fig. 4.10 (d), where the magnon wave packet for  $\Delta K = 0.7 \text{ \AA}^{-1}$  and  $E = 82 \text{ meV}$  is plotted. The wave packet is the product of three components: a moving Gaussian,  $\exp[-(x - v_g t)^2/2\sigma^2]$ , representing the motion of wave packet (the envelop function), an exponential decay factor  $\exp(-t/\tau)$  for the evolution of the amplitude in time, and finally a wave form,  $\cos(\Delta K_{\parallel} \cdot x - \omega t)$ , representing its wave nature ( $\omega = E/\hbar$  is the angular frequency of the wave). The velocity of the envelope function  $v_g$  is the group velocity of the wave packet, which is obtained from the slope of the dispersion relation,  $v_g = \partial\omega/\partial\Delta k_{\parallel}$ .  $\sigma$  and  $\tau$  are the natural broadening of the wave packet in space and lifetime, respectively, which are obtained from the Fourier transform of the intensity spectra in Fig. 4.10 (a).

To visualize the strong damping effects on terahertz magnons in ultrathin itinerant ferromagnets, we compare three states of magnons for 8 ML Co(100)/Cu(100) and 2 ML Fe(110)/W(110). State  $S_{\text{Fe}}$  represents the magnon wave packet in the Fe(110) film, and states  $S^1_{\text{Co}}$  and  $S^2_{\text{Co}}$  are the states in the Co(100) film.  $S_{\text{Fe}}$  and  $S^1_{\text{Co}}$  possess the same wave vector ( $\Delta K=0.8 \text{ \AA}^{-1}$ ), while  $S_{\text{Fe}}$  and  $S^2_{\text{Co}}$  have the same energy ( $E=100 \text{ meV}$ ). Figure 4.11 represents the evolution of the magnon wave packets for all three states mentioned above. The group velocity of the wave packets are about 26, 46 and 41 km/s for the  $S_{\text{Fe}}$ ,  $S^1_{\text{Co}}$  and  $S^2_{\text{Co}}$  states, respectively.

In a classic picture the amplitude of the waves in Fig. 4.11 can be regarded as the amplitude of the transverse component of spins projected along a certain direction on the surface *e.g.* the propagation direction of the wave. It may be also regarded as

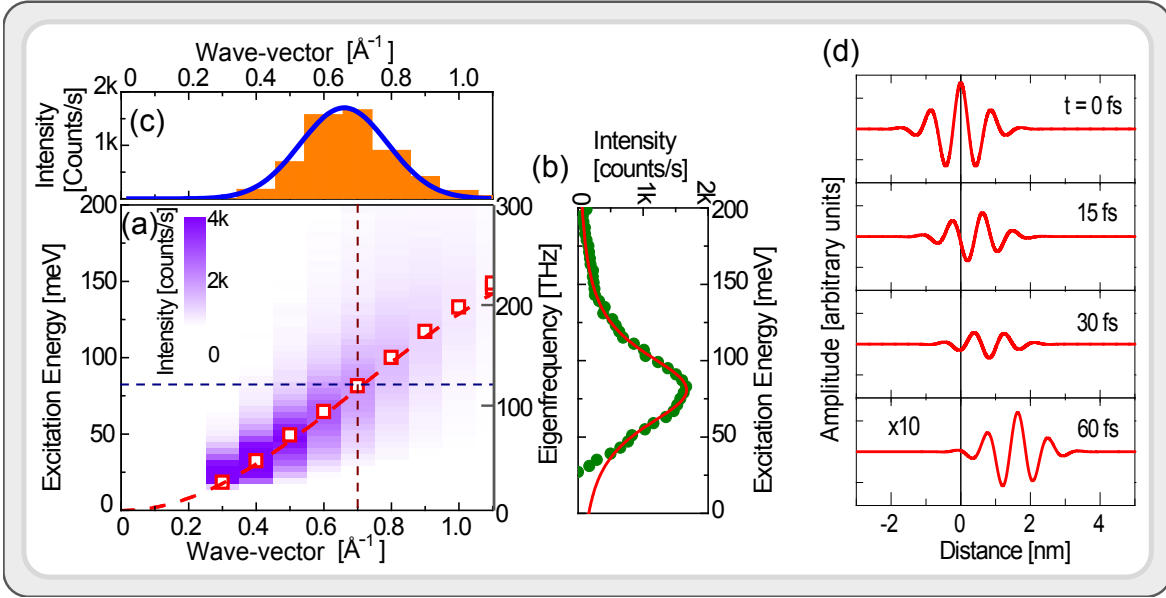
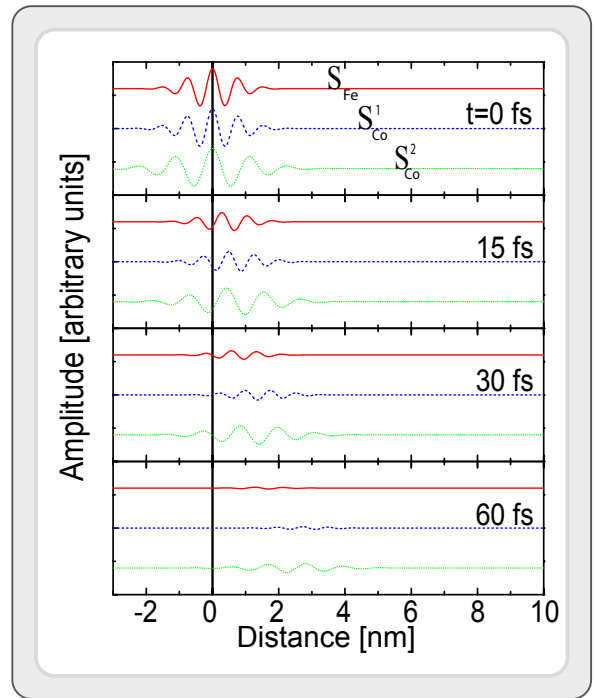


**Fig. 4.10:** (a) The difference spectra measured on a 2 ML Fe film on W(110), plotted as a contour map, for the wave vectors from 0 to 1 Å<sup>-1</sup>. The magnon peak in (b) is fitted by the convolution of a Gaussian and a Lorentzian function. The intrinsic linewidth of the peak is 55 meV. The intensity profile along the horizontal line at  $E \simeq 82$  meV in (c) is fitted by a Gaussian profile shown as a solid curve. (d) The magnon wave packet at  $\Delta K = 0.7$  Å<sup>-1</sup> and  $E = 82$  meV constructed from the experimental data. The amplitude may be regarded as the transverse component of a precessing spin projected to the wave propagation direction or the modulus of the magnon wave function. Taken from [KhZ 6.7]

the modulus of the magnon wave function. Figure 4.11 demonstrates that high wave vector magnons are strongly damped within a few tens of femtoseconds and confined in a few nanometers in both Fe and Co films. The wave packets only moved ahead by about 2–3 nm during their lifetime (much shorter than the spin diffusion length in 3d ferromagnets). For the states from the same system *i.e.*  $S_{\text{Co}}^1$  and  $S_{\text{Co}}^2$ , the one at higher wave vector ( $S_{\text{Co}}^1$ ) has a shorter lifetime than the one at lower wave vector ( $S_{\text{Co}}^2$ ). The wave packet of  $S_{\text{Co}}^1$  propagates a bit shorter than  $S_{\text{Co}}^2$ . Our results demonstrate that the decay of a magnon does strongly depend on its wave vector. Interestingly, for the states on different surfaces but with similar wave vectors *i.e.*,  $S_{\text{Fe}}$  and  $S_{\text{Co}}^1$ , it is noticed that although the  $S_{\text{Fe}}$  has a much lower energy, it possesses a similar lifetime and broadening of the wave packet as  $S_{\text{Co}}^1$ .  $S_{\text{Fe}}$  and  $S_{\text{Co}}^2$  have the same energy. The state at higher wave vector ( $S_{\text{Fe}}$ ) clearly shows shorter lifetime as compared to the low wave vector one ( $S_{\text{Co}}^2$ ). Regarding the propagation speed, both wave packets in the Co(100) film are much faster than the ones in the Fe(110) film as they experience a higher group velocity.



**Fig. 4.11:** Evolution of the magnons' wave packets for the states  $S_{\text{Fe}}$  ( $0.80 \text{ \AA}^{-1}$ , 95 meV) at the Fe surface,  $S_{\text{Co}}^1$  ( $0.81 \text{ \AA}^{-1}$ , 174 meV) and  $S_{\text{Co}}^2$  Co ( $0.55 \text{ \AA}^{-1}$ , 101 meV) at the Co surface. The amplitude may be regarded as the transverse component of a precessing spin projected to the wave propagation direction or the modulus of the magnon wave function. Taken from [KhZ 6.7].



## 4.7 The effect of spin–orbit coupling on magnons

This section is based on the original publications [KhZ 6.8] and [KhZ 6.9]

A key part of spintronics is concerned with effects, which are linked to the spin dependent phenomena [140]. In early 60's Rashba has proposed a formalism, which describes, nicely, the existence of a spin–split band structure in wurtzite crystals [141]. Later on, Bychkov and Rashba showed that such a spin splitting can also occur in quantum wells [142]. The physical explanation of this spin splitting phenomenon is rather straightforward: in a semiconductor quantum well, if the potential well is asymmetric, the electrons move in an effective electric field  $\mathbf{E}$  induced by the potential gradient of the quantum well. In the reference frame of the electron this electric field transforms into an effective magnetic field  $\mathbf{B}$  which causes a splitting in the energy levels of electrons with different spins. A similar effect is expected for the electrons in the absence of an inversion symmetry and in the presence of a large spin–orbit coupling [143]. A spin-split band structure has been observed on some metallic surfaces, where the inversion symmetry is broken [144] and could be explained in analogy to the conventional Rashba effect in semiconductor heterostructures [145–147]. The idea is further tailored to the surface alloys composed of heavy elements. The combination of strong spin–orbit interaction of the heavy elements with structural effects enhances the local potential gradients at the surface and thereby results in a large Rashba splitting [148]. The Rashba effect has been explored in detail in various systems and even some spintronic devices are proposed based on this effect [149–152].

Although for small wave vectors the magnons have a parabolic dispersion relation in ferromagnets (similar to the one of the free electrons), they are classified as bosonic quasi-particles (with a spin of  $1\hbar$ ), unlike the electrons. One of the most interesting phenomena is the effect of the relativistic spin–orbit coupling on magnons as bosonic

quasi-particles. Such an effect has not been explored in detail. We will discuss in Sec. 4.7.1 that the magnon dispersion relation in the presence of a large spin-orbit coupling and absence of inversion symmetry shows a splitting for different magnetization directions, similar to the electrons. Section 4.7.2 is dedicated to the effect of the spin-orbit coupling on the magnon lifetime.

### 4.7.1 Magnon Rashba effect

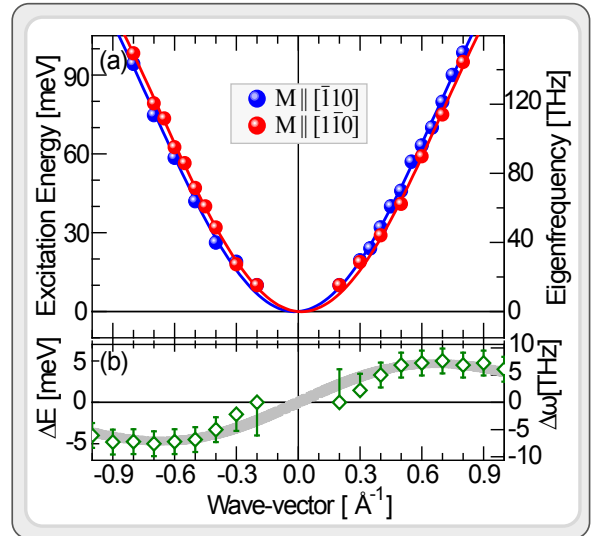
This section is based on the original publication [KhZ 6.8].

The magnon dispersion relation is measured along the  $\bar{\Gamma}$ - $\bar{H}$  direction of the surface Brillouin zone for a 2 ML Fe(110) film grown on W(110). The dispersion relation is obtained by measuring the SPEELS spectra at different wave vectors. The wave vectors were varied by changing the scattering geometries *i. e.* changing the angle between the incident beam and the surface normal [110, 125]. The measurements were performed for the magnetization parallel to the  $[\bar{1}10]$ - and  $[1\bar{1}0]$ -direction. The results of such measurements are summarized in Fig. 4.12, demonstrating that the magnon dispersion relation is split into two branches for magnetization along two opposite directions. The dispersion relation is antisymmetric, meaning that the magnon energies for positive wave vectors are equal to the ones with negative wave vectors and opposite magnetization direction and vice versa. In fact the presence of the relativistic spin-orbit coupling in the absence of time reversal and space inversion symmetry breaks the degeneracy of the surface magnons and leads to the splitting of the magnon band structure.

The asymmetric dispersion relation can be understood in terms of the antisymmetric Dzyaloshinskii-Moriya interaction, which is a consequence of the spin-orbit coupling [78, 153]. In such cases the Heisenberg spin Hamiltonian, including DM term (Eq. 2.6) may be used to obtain the components of the DM vectors. In order to reduce the fit parameters and since the magnetic anisotropy is usually orders of magnitude smaller than the exchange energy, the term representing the magnetic anisotropy (Eq. 2.4) may be neglected in the fitting procedure.

The solid lines in Fig. 4.12 are the fits based on Eq. (2.5) and including the term introduced in Eq. (2.6). The fit parameters are:  $J_1=7.5(5)$  meV,  $J_2=4.5(3)$  meV,  $|2D_1^x + \dot{D}_1^x|=0.9(3)$  meV and  $|D_2^x|=0.5(3)$  meV. The superscript  $x$  indicates the component of the DM vectors along the magnetization direction and the subscript 1(2) represents the nearest neighbor (next nearest neighbor) interaction.  $D_1^x$  ( $\dot{D}_1^x$ ) is the longitudinal component of the DM vector of the nearest neighbors in the same atomic plane (in the neighboring atomic plane). A detailed discussion concerning this effect can be found in Ref. [KhZ 6.8]. Very recently the values of the components of the DM vectors and the resulted energy asymmetry are calculated using *ab initio* DFT calculations and spin dynamics simulations, respectively [154]. The results are in well agreement with our experimental values. The splitting of the magnon band structure shown in Fig. 4.12 is very similar to the well-known Rashba effect observed for electrons in two-dimensional electron gas or at metal surfaces [145–147]. Since in this experiment we use an ultrathin film that is grown on a nonmagnetic substrate with a large spin-orbit coupling, due to the interaction with the substrate the inversion symmetry is broken. The system is very similar to a two-dimensional electron gas system (or electrons at the metal surfaces) in the presence of the spin-orbit coupling and absence of the space inversion symmetry.

**Fig. 4.12:** (a) The magnon dispersion relation measured on 2 ML Fe/W(110) for two different magnetization directions. (b) The energy splitting, defined as  $\Delta E(q) = E_{M\parallel[\bar{1}10]}(q) - E_{M\parallel[1\bar{1}0]}(q)$ , obtained from (a). The symbols represent the experimental results, while the solid lines represent the fits based on the extended Heisenberg spin Hamiltonian, including the DM term. Taken from [KhZ 6.9].



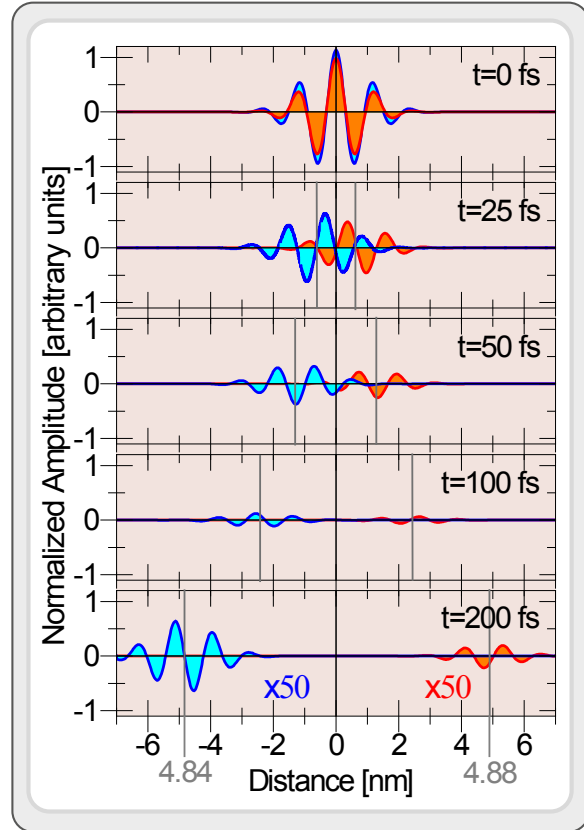
Here the lack of both the space inversion and the time-reversal symmetry leads to two branches for the dispersion curves. This makes a one to one analogy to the Rashba type spin splitting of the electronic band structure. Therefore the effect maybe called as “*magnon Rashba effect*” [155]. Note that in two-dimensional electron gas systems and at the normal metal surfaces the presence of the time-reversal symmetry requires two branches, one being the mirror image of the other. However, in ferromagnets, time-reversal symmetry is broken and there is one branch to the dispersion curve of each magnetization direction.

#### 4.7.2 The effect of spin–orbit coupling on the magnon lifetime

This section is based on the original publication [KhZ 6.9].

More importantly, we observed that the lifetime of the magnons is also influenced by spin–orbit coupling, in line with the recent theoretical calculations based on the multiband Hubbard model [155]. The surface magnons in this case are subjected to a large spin–orbit coupling coming mainly from the tungsten substrate. In a very naïve picture one may imagine the spin–orbit coupling as a magnetic field that is acting on the surface magnons. It tries to flip the spins and thereby causes an additional damping. A time reversal would just change the direction of the effective magnetic field, caused by spin–orbit coupling, and thereby would invert the asymmetry in the lifetime. This is exactly what we observe in our experiment. For high wave vector magnons the damping is mainly governed by dissipation into the Stoner states as discussed in Sec. 4.5. If the spin–orbit is large, it may cause additional damping in the system. The spin–orbit induced damping is a well known damping mechanism for small wave vector magnons, in particular in the case of the uniform FMR mode ( $q = 0$ ). As a simple model for the intrinsic FMR damping, one may imagine that the precession of the spin that is coupled to its orbital motion via the spin–orbit coupling. The orbital motion is perturbed by the lattice simultaneously and hence cannot anymore follow the same phase and it results in a damping. One would expect a similar mechanism here, which is superimposed to the Landau type of damping.

**Fig. 4.13:** A real time and space representation of the magnon wave packets with  $E = 46.5$  meV. The wave packets start to propagate at  $t = 0$  with the maximum amplitude at  $x = 0$ . The red wave packet propagates along the  $[001]$ -direction, and the blue one propagates along the  $[00\bar{1}]$ -direction. The vertical gray lines indicate the center of the mass of the wave packets. The difference in the wave packets which are propagating to the left and right is a direct consequence of the spin-orbit coupling. Taken from [KhZ 6.9].



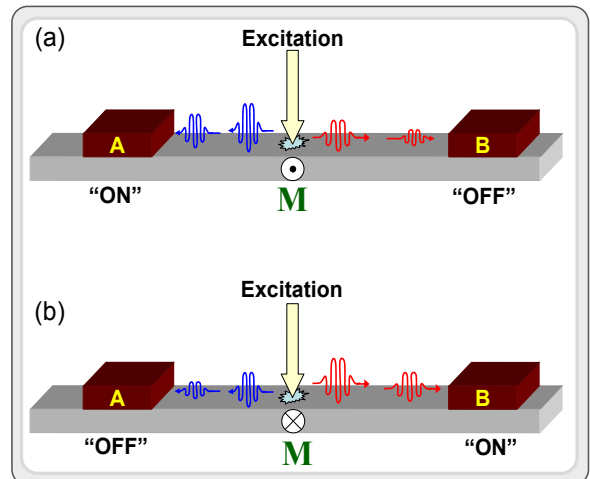
In order to obtain detailed, in depth, information on the magnons' lifetime and spatial distribution we attempt to provide a real space representation of magnons based on our experimental data. We use the procedure explained in Sec. 4.6. For that, the SPEELS spectra are measured at a fixed scattering geometry and with exactly the same parameters (like incidence energy, beam current and energy resolution) and only the sample magnetization is switched to opposite direction. The experiment is designed such that the magnons propagate in the mirror symmetry plane of the magnetization. Since the magnon intensity depends on the scattering's matrix elements, keeping the scattering geometry and experimental parameters unchanged, during the experiment, would avoid the effects caused by geometry on the electron scattering processes and thereby on the magnon intensity. Reversing the magnetization is equivalent to time inversion, therefore one can reverse the magnon propagation direction only by reversing the direction of the magnetization. This approach opens a possibility to measure the magnons with positive and negative wave vectors without changing the scattering geometry.

We directly attempt to provide a real time/space representation of magnons' wave packet. This is essential because only then we can clearly see the consequence of the differences in the lifetime amplitude, group and phase velocity on the behavior of the magnon wave packets. An example is given for the magnons with an excitation energy of  $E = 46.5$  meV. The distribution of magnon intensity in momentum space is obtained from the line profile at  $E = 46.5$  meV. Using the Fourier transform, one can have a direct access to the real space representation of the magnons. For the magnons with an energy of  $E = 46.5$  meV the wave vectors are  $+0.50 \text{ \AA}^{-1}$  and  $-0.52 \text{ \AA}^{-1}$ . The

corresponding wavelengths are about  $12.6 \text{ \AA}$  and  $12.1 \text{ \AA}$ , respectively. Note that in the absence of relativistic effects the absolute values of the wave vectors (wavelengths) for the positive and negative branches have to be exactly the same. The difference in the absolute value of the wave vectors (wavelengths) is a direct consequence of the spin-orbit coupling. The real time and space representation of the magnons is presented in Fig. 4.13. The magnon wave packet starts to propagate at  $t = 0$  with the maximum amplitude at  $x = 0$ . As it is mentioned in Sec. 4.5, the lifetime of the magnons in itinerant ferromagnets is usually very short. The values obtained at  $E = 46.5 \text{ meV}$  for positive and negative wave vectors are  $\tau_+ \approx 37 \pm 5 \text{ fs}$  and  $\tau_- \approx 45 \pm 5 \text{ fs}$ , respectively. The group velocity is obtained from the slope of the dispersion curve at the given energy ( $E = 46.5 \text{ meV}$ ) and wave vectors ( $q = +0.50 \text{ \AA}^{-1}$  and  $-0.52 \text{ \AA}^{-1}$ ). Since the dispersion relation is asymmetric, the group velocity is different for the magnons propagating along two opposite directions. For the ones that are propagating along the  $[001]$ -direction (the ones with  $q = +0.50 \text{ \AA}^{-1}$ )  $v_g = 24.4 \text{ km/s}$  and for the ones propagating along the  $[00\bar{1}]$ -direction (the ones with  $q = -0.52 \text{ \AA}^{-1}$ ) it is about  $v_g = -24.2 \text{ km/s}$ . The differences in the group velocity, lifetime and the amplitude lead to a different propagation behavior for the magnons along two opposite directions. Figure 4.13 demonstrates that after 200 fs the magnon's wave packet, which is propagating along the  $[001]$ -direction, propagates  $48.8 \text{ \AA}$  and is strongly damped but the one which is propagating along the  $[00\bar{1}]$ -direction propagates  $48.4 \text{ \AA}$ . Extrapolating of our results to  $q = 0$ , reveals that the uniform mode with zero wave vector possesses a finite group velocity of about  $v_g(q = 0) \approx 1 \text{ km/s}$ . The phase velocity can be obtained using the simple expression  $v_p = E/q$ , which results in  $v_p = 14.4 \text{ km/s}$  for the magnons with an energy of  $46.5 \text{ meV}$  and  $q = +0.50 \text{ \AA}^{-1}$ . It is about  $-13.4 \text{ km/s}$  for the magnons with an energy of  $46.5 \text{ meV}$  and  $q = -0.52 \text{ \AA}^{-1}$ . The phase velocity is smaller than the group velocity, meaning that the magnon wave packets disperse during the propagation.

The simplest device which may work based on these effects may be imagined as following: one excites the transversal surface magnons (the ones that are propagating perpendicular to the magnetization) on a magnetic surface. Simultaneously two wave packets will be generated and then will propagate to opposite directions (see Fig. 4.14). Let us assume that the magnetization is pointing outward as it is shown in Fig. 4.14

**Fig. 4.14:** A magnonic device based on the magnon Rashba effect. (a)  $\mathbf{M}$  is pointing outward. In this case a magnon signal can be detected by gate A and no magnon signal is detected by gate B (A:ON and B:OFF). (b)  $\mathbf{M}$  is pointing inward. In this case no magnon signal can be detected by gate A but a signal can be detected by gate B (A:OFF and B:ON). Taken from [KhZ 6.9].



(a). This implies that the wave packet which is propagating towards gate A possesses a larger amplitude and lifetime, while the one that is propagating towards gate B will die out quickly. When the magnon wave packet arrives at gate A, it can be detected. At the same time, no magnon signal can be detected by gate B. This state may be called as A:ON and B:OFF. The switching to the state A:OFF and B:ON can be realized just by reversing the magnetization of the ferromagnet [see Fig. 4.14 (b)].

Further applications are certainly possible. However, the magnonics is still in its infancy and a detailed knowledge of the effects associated with this phenomenon is required for realization of any device. Our results as a proof of principles demonstrate that such an effect fundamentally exists and if the physics is known one may think about further possibilities of application.

## 4.8 Probing exchange interaction at the interface

This section is based on the original publication [KhZ 6.10].

In principle, there are a few important differences between magnons excited in thin films (or layered structures) grown on a substrate compared to the ones in bulk crystals. In single-element bulk crystals all atoms are equivalent and contribute equally to different magnon modes (all magnon modes degenerate in energy). However, in thin films the atoms become inequivalent due to the absence of translational invariance in the direction orthogonal to the surface. Moreover, the atomic environment of the surface and interface atoms is substantially different from the one of the atoms located in the inner part of the film. The direct consequence of this fact is that different atomic layers possess different electronic and magnetic properties. In particular, the interatomic exchange parameters are layer-dependent. At the surface of the film the important factor influencing the properties of the film is the reduced atomic coordination. At the interface an additional strong influence comes from the hybridization of the electronic states of the atoms of the film with the ones of the substrate atoms. A natural consequence of the inequivalence of the atomic layers is a low-energy magnon mode which is formed due to the presence of the interface [57, 156]. Probing this mode would allow a direct way of probing magnetic exchange interaction at the interface.

To realize this idea, we have studied the exchange coupling constants at the interface of an epitaxial thin Fe(001) films with a thickness of 6 ML grown on Ir(001). The magnon dispersion relation is presented in Fig. 4.15 (a). The low excitation energy and decreasing intensity of this mode with increasing the thickness from 6 to 9 ML (specially close to the  $\bar{X}$ -point) without any substantial change in the energies indicate that this mode is mainly originated from the interface. Obviously, for a surface magnon mode we would expect a very different behavior, namely, no significant change in the magnon intensity while increasing the thickness [157, 158]. The definite proof of this hypothesis comes from our first-principles calculations. Two different sets of calculations are performed. The first set of calculations, accomplished with a self-consistent Green function method, yields the magnetic exchange parameters, magnon dispersion relation in an adiabatic approach and allows us to calculate the contribution of each atomic layer to the magnon modes. The second set of calculations, based on the linear response time dependent density functional theory, provides the information on the magnons lifetime.

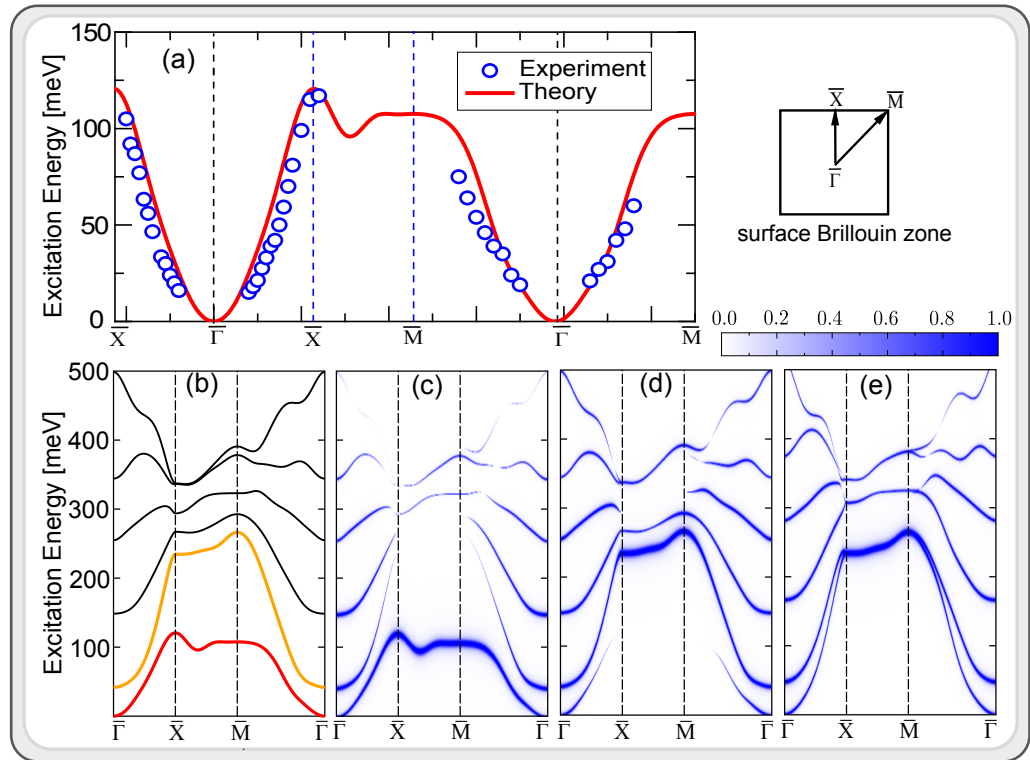


**Fig. 4.15:** The magnon dispersion relation of a 6 ML Fe film on Ir(001) measured along the main symmetry directions. (a) Experimental data plotted together with the low-energy mode of the theoretical calculations. (b) All the predicted magnon modes calculated using an adiabatic approach. (c) The susceptibility spectral function projected into the Fe layer next to Ir substrate (interface layer). (d) The susceptibility spectral function projected into the surface layer. (e) The susceptibility spectral function projected into the surface layer for a free standing Fe film consists of 6 layers. Taken from [KhZ 6.10].

The low-energy mode, which satisfies the Goldstone theorem  $E(q = 0) = 0$  calculated for 6 ML Fe on Ir(001) is shown in Fig. 4.15 (a) by the solid red line. The results of calculations agree very well with the experimental results. Moreover, the calculated atomic- or layer-resolved transverse magnetic susceptibility results in the spatial distribution of each magnon mode over the Brillouin zone and allows us to compare the contribution of each atomic layer to each magnon mode. Figure 4.15 (b) shows all magnon modes calculated using an adiabatic approach. The susceptibility spectral functions projected into the interface and surface layers are presented in Figs. 4.15 (c) and (d), respectively. In this representation the broadening of the lines indicates the contribution of the given layer to all magnon modes. For example in Fig. 4.15 (c) the broadening of the low-energy mode is much stronger than of the other modes meaning that a large contribution into this mode, comes from the Fe atoms located in the atomic layer next to the Ir(001) substrate. Figure 4.15 (d) shows the contribution of the surface layer to all magnon modes, indicating that the contribution of the surface

layer to the low-energy mode is small for magnon wave vectors larger than  $0.5 \text{ \AA}^{-1}$  and is zero near the zone boundaries (near  $\bar{X}$ - and  $\bar{M}$ -points). Since increasing magnon wave vector means larger angle  $\phi$  between neighboring atomic moments, the difference in the exchange parameters for different layers becomes increasingly more important leading to the localization of the magnons in the region of the smallest exchange parameters. At  $q = 0$  (Goldstone mode) all atomic layers contribute equally to the low-energy mode. The contribution of the interface layer to this mode becomes larger as the wave vector increases whereas the contributions from the other layers become smaller such that at the  $\bar{X}$  point only the contribution of the interface atomic layer remains [see Fig. 4.15 (c)]. Another way to illustrate that the low-energy mode is mainly contributed from the interface is to calculate the magnon spectrum of the free standing Fe(001) film. The results, presented in Fig. 4.15 (e), show that the dispersion relation of the low-energy mode changes strongly whereas the other modes are unaffected. For instance, the energy at  $\bar{X}$  is increased from 125 to 240 meV. Note that in this case the surface and interface layers are equivalent and hence the spectral weights of the two low-energy modes projected into the surface and interface layers are identical. A comparison between Fig. 4.15 (c), (d) and (e) manifest beautifully the effect of hybridization of the electronic states of the film with ones of the substrate on the magnon dispersion relation. It further illustrates how the degeneracy of the two low-energy magnon modes along the  $\bar{X}$ - $\bar{M}$  direction is broken and a mode with a lower energy is formed. This lowest-energy mode is mainly contributed from the atomic layer next to the substrate, where the exchange parameters are weaker.

By an independent experiment we have estimated the average spin-dependent inelastic mean free path of Co film being in the order of  $\lambda \simeq 4.5$  in the units of vertical layer spacing (being  $1.6 \text{ \AA}$ ). If one assumes that Fe films possess a similar spin-dependent mean free path one can estimate the expected intensity of the SPEELS spectra based on a simple kinematic model. As the rule of thumb one may take an exponential decay of the excitation probability with increasing deepness of the layer. Based on this assumption the overall contribution of all layers to each magnon mode can be calculated as  $A = \sum_{n=1}^6 A_n \exp(-l_{n,q}/\lambda)$ , where  $A_n$  is the contribution of  $n$ th layer to that particular magnon mode,  $n$  is the number of atomic layers counted from top and  $l_{n,q}$  is the path length of electrons inside the film (it depends on  $n$  and  $q$  or more precisely on the scattering geometry). The contribution of each layer to the low-energy mode resulted from the *ab initio* calculations is presented in Fig. 4.16 (a). The quantity  $A$  is calculated as a function of wave vector for the low-energy mode and is presented in Fig. 4.16 (b). It may be regarded as the expected intensity of the experimental difference spectra. Such a simple calculation reveals that the expected intensity close to the  $\bar{X}$  point is about 13% of the one for  $q=0.6 \text{ \AA}^{-1}$  in the middle of  $\bar{\Gamma}$ - $\bar{X}$  direction. This means that although at  $\bar{X}$  the main contribution to this mode is coming from the interface layer, it is still possible to be measured by SPEELS. At this point we would like to mention that in this simple kinematic model only the probability of probing interface magnons is calculated, there are other parameters which may influence the inelastic electrons scattering that are not considered in this simple model.

The localization of magnons at the Fe/Ir(001) interface can be understood on the basis of the analysis of exchange parameters. In principle, the reduction of the coordination number at surfaces/interfaces can lead to a magnon softening [157]. However, in many



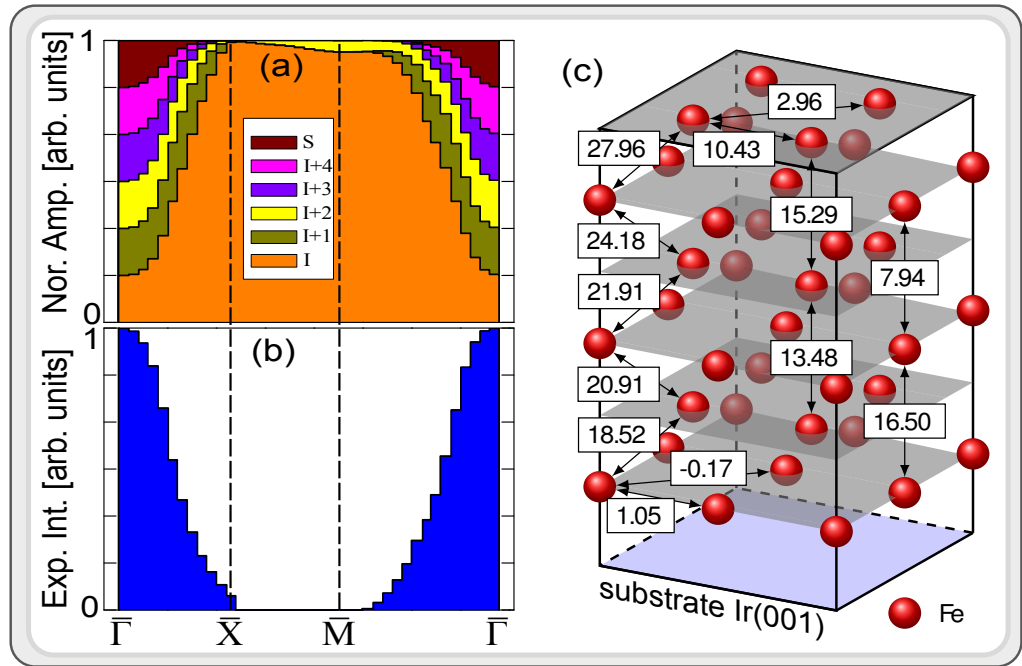


**Fig. 4.16:** (a) The contributions of each atomic layer to the low-energy magnon mode. (b) The expected intensity of this mode when an averaged spin-dependent mean free path of 4.5 (in the unit of vertical layer spacing) is taken into account. (c) The calculated interatomic exchange parameters. The values are given in meV. Taken from [KhZ 6.10].

systems the interface electronic properties are different from the surface ones. This fact leads to a significant difference in the exchange parameters at the surface and at the interface. Remarkably, at the Fe/Ir(001) interface the magnon softening induced by the interface hybridization is much more significant than that from the surface, which indicates a strong reduction of the intralayer exchange constants at the Fe/Ir(001) interface. Figure 4.16 (c) shows the exchange parameters in the Fe/Ir(001) system. For simplicity, only the relevant parameters are presented. While the interlayer coupling for both surface and interface layers is strongly ferromagnetic, the intralayer exchange parameters are relatively weak. In particular, the intralayer exchange parameters at the Fe/Ir interface have a strong tendency to be antiferromagnetic. Due to the strong ferromagnetic coupling between the layers, the ground state is still ferromagnetic.

Another aspect which is of prime importance is the damping mechanism of the high wave vector magnons which is governed by the decay of the collective magnons into single-particle Stoner excitations, as discussed in Sec. 4.5. As a result for each wave vector  $q$  only the lowest in energy magnon mode has a longer lifetime and can be unambiguously detected in the experiment. The contribution of all other magnon modes is drastically reduced because of their strong damping (short lifetime). In the final SPEELS response function the spatial localization of different magnon modes competes with their Landau damping. As discussed above the amplitude of the interface magnons in the upper layers is still significant whereas the damping of higher-energy magnons

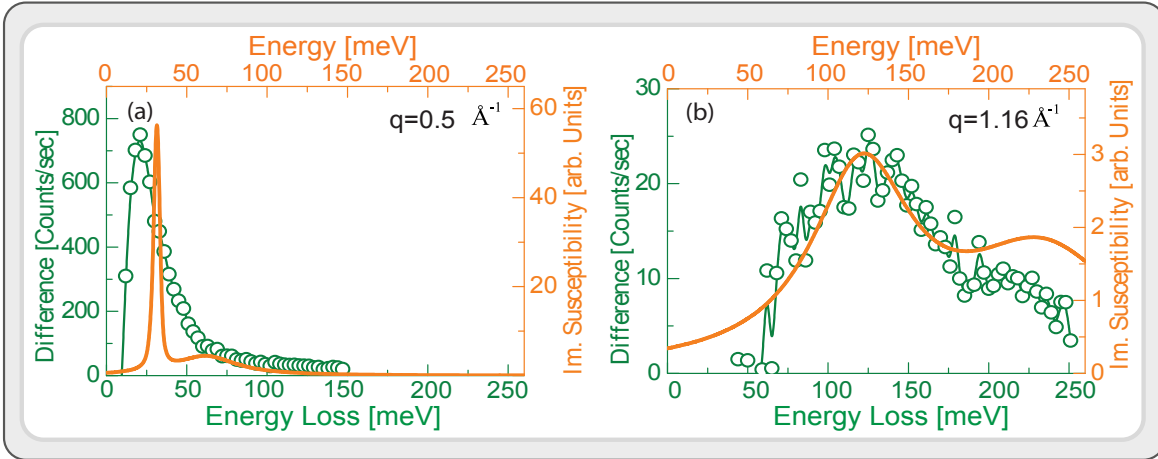


**Fig. 4.17:** A comparison between SPEELS difference spectra, recorded at (a)  $\Delta K_{\parallel} = 0.5 \text{ \AA}^{-1}$  and (b)  $\Delta K_{\parallel} = 1.16 \text{ \AA}^{-1}$ ,  $\bar{X}$ -point and the corresponding calculated imaginary part of the dynamical spin susceptibility. Taken from [KhZ 6.10].

is very strong. Although the spectral weight of interface mode is not as large as the surface mode, it has a much longer lifetime and hence dominates the spectra. Calculation of the dynamic transversal spin susceptibility considers on an equal footing both collective magnons and single-electron Stoner excitations and provides full account for the Landau damping of the magnons. These calculations are presented in Fig. 4.17 revealing a drastic Landau damping already of the second in energy magnon mode. Interestingly, a similar weak peak is obtained in the experimental spectra showing again a good correlation between experiment and theory even in such nontrivial features as observation of strongly damped magnons.

For further illustration of the capability of this method for probing the interface exchange interaction, we replaced the top five Fe atomic layers with three atomic layers of Co (keeping only one atomic layer of Fe at the interface). The measured magnon dispersion relation reveals a similar low-energy magnon mode meaning that this mode is mainly originated from the Fe atomic layer located at the interface (see [KhZ 6.10] for more details). The method illustrated above is also applicable to other ferromagnetic thin films grown on the other substrates. If the magnetic coupling at the interface is weaker than at the surface the low-energy magnon mode is mainly localized at the interface. Probing of this mode would lead to determination of exchange parameterless at the buried interface.

## 4.9 Magnons in thin films with perpendicular easy axis

This section is based on the original publication [KhZ 6.11].

Ultrathin films with large perpendicular magnetic anisotropy (PMA), have attracted much attention due to their interesting fundamental properties and also their promising technological applications in ultra-high density magnetic recording [159], magnetic

tunneling junctions and also spin-transfer torque devices [160, 161]. Many observed phenomena in the above mentioned devices are attributed to the emission or absorption of interface magnons while performing transport experiments. Certainly, the knowledge on terahertz magnons would have a large impact on the understanding of many observed phenomena in the transport experiments as well as the ultrafast spin dynamics in these materials. However, since the films with PMA possess an out-of-plane magnetic stray field, there has been a long-standing question concerning the possibility of probing magnons in these materials using SPEELS.

We have shown, for the first time, that magnons in PMA systems can be excited and probed by a transversally spin-polarized beam. Two kinds of ultrathin films were grown for this study, following the procedure reported in [162]: (a) an ultrathin  $\text{Fe}_{0.5}\text{Co}_{0.5}$  alloy film with a total thickness of 4 atomic layers (ML) prepared by co-deposition of Fe and Co at room temperature, (b) an ultrathin Fe/Co multilayer film composed of four alternating atomic layers of Co and Fe. In both cases the films grow epitaxially with the epitaxial relationship  $[100]_{\text{film}} \parallel [110]_{\text{substrate}}$  on Ir(001). Both systems exhibit an out-of-plane easy axis due to the large PMA, originating from the tetragonal distortion of the epitaxial layers [162, 163]. In the SPEELS measurements, the scattering plane was chosen to be parallel to the [110] direction of Ir(001) (the [010] direction of the films). The polarization vector of the beam  $\mathbf{P}$  is parallel (or antiparallel) to the  $[1\bar{1}0]$  direction of Ir(001). Different wave vectors were selected by changing the angle between incident and scattered beam *i. e.* by rotating the sample about the symmetry axis ( $[1\bar{1}0]$  direction of Ir(001)). In this configuration the effective beam polarization does not depend on the scattering geometry, since it is parallel to the symmetry axis [see Fig. 4.18 (a)]. SPEELS spectra were recorded for the spin polarization vector  $\mathbf{P}$  of the incident beam parallel and antiparallel to the  $[1\bar{1}0]$  direction of Ir(001) *i. e.* *perpendicular* to the quantization axis that is defined as the easy magnetization direction being normal to the sample plane (the [001] direction).

Figures 4.18 (b) and (c) show the  $I_+$  and  $I_-$  SPEELS spectra measured at a wave vector of  $1.1 \text{ \AA}^{-1}$  in a 4 ML  $\text{Fe}_{0.5}\text{Co}_{0.5}$  alloy film and a 4 ML Fe/Co multilayer film, respectively.  $I_+$  ( $I_-$ ) denotes the intensity of the scattered beam when  $\mathbf{P}$  is parallel (antiparallel) to the  $[1\bar{1}0]$  direction. In both systems, a pronounced peak appears in both  $I_+$  and  $I_-$  spectra with the same intensity and peak position. The peak intensity shows no dependence on the direction of  $\mathbf{P}$ , different than those recorded on ultrathin films with in-plane magnetization. This is due to the fact that unlike the previous experiments, where the beam polarization vector  $\mathbf{P}$  was parallel or antiparallel to the magnetization direction (quantization axis), in the present case it is perpendicular to that.

To answer the question: “How a transversally spin-polarized beam can excite the magnons?” let us assume a spin polarized beam with an arbitrary polarization vector  $\mathbf{P} = |\mathbf{P}|\mathbf{e}$ .  $\mathbf{e} = \sin \vartheta \cos \varphi \hat{i} + \sin \vartheta \sin \varphi \hat{j} + \cos \vartheta \hat{k}$  is the unit vector in space indicating the direction of the spin polarization vector [ $\vartheta$  and  $\varphi$  are the polar and azimuthal angles, respectively and are defined with respect to the quantization axis, see Fig. 4.18 (a)] and  $|\mathbf{P}|$  is the norm of the polarization vector. The polarization vector of a given spin polarized beam can be expressed in terms of Dirac spinors defining the spin-up and

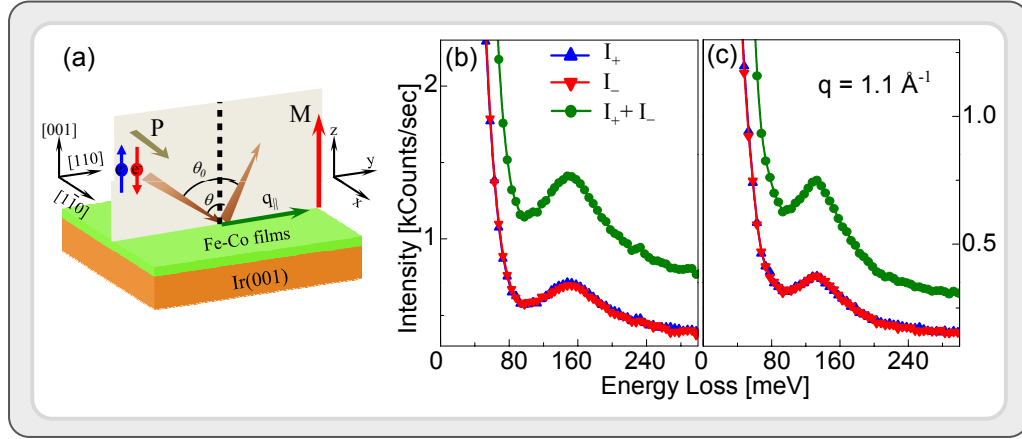


**Fig. 4.18:** (a) A schematic representation of the scattering geometry. All the crystallographic directions depicted here are the ones of Ir(001). SPEELS spectra recorded in a 4 ML Fe<sub>0.5</sub>Co<sub>0.5</sub> alloy film (b) and a 4 ML Fe/Co multilayer film (c) at a wave vector of  $\Delta K_{\parallel} = 1.1 \text{ \AA}^{-1}$ . The total spectrum is shown by  $I_{+} + I_{-}$ . Taken from [KhZ 6.11].

spin-down states [164]. This can be simply done by finding the eigenstates of:

$$(\boldsymbol{\sigma} \cdot \mathbf{e})\chi = \lambda\chi, \quad (4.1)$$

where  $\boldsymbol{\sigma}$  represents the Pauli spin matrices and  $\boldsymbol{\sigma} \cdot \mathbf{e}$  is the projection of spin operator in a polarization direction.  $\lambda$  and  $\chi$  represent the eigenvalue and the eigenstate of  $\boldsymbol{\sigma} \cdot \mathbf{e}$ , respectively.

The solution of Eq. (4.1) is:

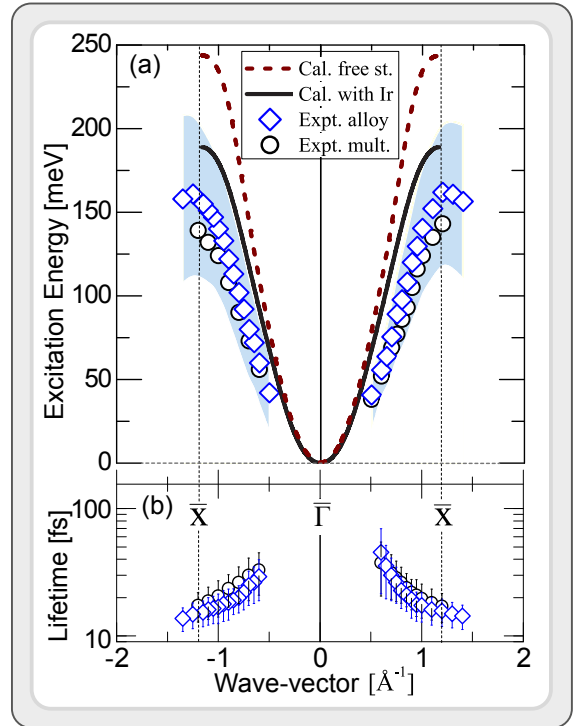
$$\chi = \begin{pmatrix} \cos \frac{\vartheta}{2} \\ \sin \frac{\vartheta}{2} e^{i\varphi} \end{pmatrix} \quad \text{for } \lambda = +1 \quad \text{and} \quad \chi = \begin{pmatrix} \sin \frac{\vartheta}{2} \\ -\cos \frac{\vartheta}{2} e^{i\varphi} \end{pmatrix} \quad \text{for } \lambda = -1. \quad (4.2)$$

For the case where  $\mathbf{P}$  is parallel or antiparallel to the magnetization (the quantization axis) one has  $\vartheta = 0, \varphi = 0$  [see Fig. 4.18 (a)] and hence Eq. (4.1) yields the expected eigenstate of  $\sigma_z$ ,  $\begin{pmatrix} 1 \\ 0 \end{pmatrix}$  or  $\begin{pmatrix} 0 \\ 1 \end{pmatrix}$ .

For the case where  $\mathbf{P}$  is parallel or antiparallel to the  $x$  direction and the magnetization (the quantization axis) is along the  $z$  direction one has  $\vartheta = \pi/2, \varphi = 0$  and hence Eq. (4.1) yields the eigenstate  $\chi = \frac{1}{\sqrt{2}} \begin{pmatrix} 1 \\ 0 \end{pmatrix} + \frac{1}{\sqrt{2}} \begin{pmatrix} 0 \\ 1 \end{pmatrix}$ , where,  $\begin{pmatrix} 1 \\ 0 \end{pmatrix}$  and  $\begin{pmatrix} 0 \\ 1 \end{pmatrix}$  are the Dirac spinors and can be regarded as majority and minority spin states of the sample, respectively. Note that in both examples the quantization axis is defined as the direction of the easy axis.

Now, it is rather straightforward to understand our experimental results. In the experiments, where  $\mathbf{P}$  is parallel or antiparallel to the quantization axis, the beam is composed of either majority or minority spins (assuming a polarization of 100%,  $|\mathbf{P}| = 1$ ). Since the magnons carry a total angular momentum of  $1\hbar$ , they can only

**Fig. 4.19:** (a) The magnon dispersion relation probed in a 4 ML  $\text{Fe}_{0.5}\text{Co}_{0.5}$  alloy film ( $\diamond$ ) and a 4 ML Fe/Co multilayer film ( $\circ$ ). The intrinsic linewidth of the spectra is depicted as the background color. The solid line represents the theoretical calculation for a 4 ML body-centered tetragonal film on Ir(001) composed of alternating layers of Co and Fe. The dashed line represents the results of the calculations for a free standing film. (b) The magnon lifetime as a function of the wave vector. Taken from [KhZ 6.11].



be excited by incident electrons of minority character via an exchange process. The magnon excitation is forbidden for incident electrons of majority character. Hence, one sees only the magnon excitation peak in minority spin spectra. In the present case where  $\mathbf{P}$  is perpendicular to the quantization axis, the beam can be regarded as a totally spin unpolarized beam equally composed of both majority and minority spins. Only the incident electrons of minority character are allowed to excite magnons (see Sec. 4.1). Since for both polarization directions (+ and -) the beam carries the same amount of majority and minority spins, one would expect exactly the same magnon peak intensity in  $I_+$  and  $I_-$  spectra.

The magnon dispersion relation measured on both  $\text{Fe}_{0.5}\text{Co}_{0.5}$  alloy and Fe/Co multilayer films is presented in Fig. 4.19 (a). At low wave vectors both systems possess almost identical magnon energies. Small differences in the magnon energies appear at high wave vectors. For the  $\text{Fe}_{0.5}\text{Co}_{0.5}$  alloy film the energy reaches a value of 160 meV at the  $\bar{X}$ -point whereas for the Fe/Co multilayer film the energy is about 140 meV. In both cases the magnon energies are much smaller than the one in bulk Fe and Co. They are even smaller than the one of 2 ML Fe(110)/W(110) and 8 ML Co(001)/Cu(001).

The results of first principles adiabatic calculations, are presented in Fig. 4.19 (a) showing a rather good agreement with the experimental data. To see the impact of the Ir(001) substrate on the magnon dispersion relation we performed calculations for a free standing film taking the interatomic distances the same as the film with substrate. The results, shown in Fig. 4.19 (a) as dashed line, indicate that the role of the substrate in determining the magnon energies is very important. The presence of the Ir(001) substrate reduces the magnon energies by 55 meV at the  $\bar{X}$  point. This fact is the consequence of the weakening of the interatomic exchange interaction and beautifully manifests the importance of electronic hybridization of the ultrathin film and

the substrate. Detailed information may be found in [KhZ 6.11]. Recent calculations of tetragonally distorted bulk FeCo compounds within the many-body perturbation theory predict a magnon softening [165]. Due to technical difficulties in those calculations the effects of the substrate, which seem to be important, could not be taken into consideration.

The background color in Fig. 4.19 (a) denotes the intrinsic linewidth of the magnon peaks as observed in the experiments. Since they are very similar in both systems we only show the results of the alloy film. The intrinsic linewidth increases from 40 to 100 meV when the wave vector increases from 0.5 to 1.2  $\text{\AA}^{-1}$ , similar to that of an 8 ML Co/Cu(100) and a 2 ML Fe/W(110). The magnon lifetime is obtained using the procedure explained in Sec. 4.5 and is presented in Fig. 4.19 (b). A large damping of magnons in the tetragonally distorted bulk FeCo compounds is also predicted theoretically [165].

These results demonstrate nicely that the high-energy magnons in ultrathin ferromagnetic films with an out-of-plane easy axis can be probed by a transversally spin-polarized beam. The excitation cross section is rather large so that a pronounced peak in the spectra can be observed. Since ultrathin films with PMA are of great fundamental and technological interest, these pioneering experiments would open a way towards investigation of magnon excitations in this class of materials by SPEELS and also by inelastic tunneling spectroscopy.

## 5 Conclusions and outlook

We have performed a comprehensive study of high-energy spin excitations in low-dimensional ferromagnets, mainly ultrathin ferromagnetic films grown on metallic substrates. The main mechanisms leading to the creation of magnons by spin-polarized electrons are outlined and explained based on our current understanding. The magnon excitation process is based on the exchange scattering mechanism. When a spin-polarized beam with a well-defined energy is scattered from the sample surface, magnons can only be excited (annihilated) if the incoming beam is of minority (majority) spin character. Since magnons possess a total angular momentum of  $1\hbar$ , the outgoing electron is of majority (minority) spin character. This fact leads to a peak in the energy loss (gain) region of the intensity spectra when minority (majority) electrons are incident. The scattering process itself is elastic and the observed energy loss (or gain) is due to the fact that the ejected electron stems from a lower (or higher) energy level of the excited solid. Such a process is purely mediated by exchange interaction that is of the Coulomb nature and no explicit spin-spin interaction is involved.

The technique provides also a way of measuring magnons and phonons simultaneously, without the need of any spin-resolved detection. Magnons can only be excited by incidence of minority electrons and annihilated by incidence of majority ones whereas, phonons can be excited and annihilated by incidence of electrons with any spin orientation. This fact would lead to a sign change in the asymmetry curve in the gain and loss regions where the magnons are excited. For the case of phonons, no change in the sign of the asymmetry curve is expected. This means that the magnons and phonons can be distinguished by comparing the sign of the asymmetry curves in loss and gain regions and there is no need of further spin resolved detection of the scattered electrons. We hope that these pioneering results will open a way towards probing the quasi-particles involved in lattice- and spin dynamics and their possible coupling, in particular, in the multifunctional complex hybrid and oxide materials as well as strongly correlated electron systems. This knowledge would be of substantial importance to investigate the possible coupling scenarios between different quasi-particles.

The magnon dispersion relation in various systems is probed and discussed in detail. The response of the magnon energies to the changes in the geometrical structure, number of atomic layers and rearrangement of atoms within the structure is investigated and explained in term of the complexity of the electronic structures of the ferromagnetic films and the substrate. It is demonstrated how the complexity of the electronic structure and the different contribution of orbitals to the hybridization and exchange interaction may lead to unusual behavior of the fundamental magnetic interactions in low-dimensional magnets. These results suggest a way of tailoring magnetic coupling in low-dimensional magnetic structures.

In addition, experimental results have had a very large impact on the development of the quantum theory of low-dimensional magnetism, in particular on the theory of spin

excitations in low-dimensional itinerant magnets.

The magnon lifetime and spatial distribution are studied. It is found that magnons in ultrathin Fe and Co films possess lifetimes ranging from tens to hundreds of femtoseconds depending on the wave vector. The analysis reveals that the magnons at the Fe(110) and Co(100) surfaces are strongly confined in time and space due to the large damping effects. Interestingly, the lifetime of both systems are very similar at a given wave vector in spite of the fact that the excitation energies in the Co(100) film are almost twice of that in the Fe(110) film. High-energy magnons propagate only a few nanometers within their lifetime. We hope that our results will inspire theoretical investigations for a better understanding of magnetic damping mechanism of terahertz magnons in low-dimensional magnets. This understanding would help us for a possibility of tuning of the magnetic relaxation in nanoscale ferromagnets. It may also offer a way of estimating the ultimate time scale of magnetic switching in nanostructures.

The first direct experimental evidence of the magnon Rashba effect is presented. It is demonstrated that the dispersion relation of the surface magnons in the presence of relativistic spin-orbit coupling and in the absence of time-reversal and inversion symmetry shows a splitting for different magnetization directions, similar to the electron dispersion relation at metal surfaces and in the presence of spin-orbit coupling. This discovery revised the conventional thinking in surface magnetism.

In a pioneering experiment, it is demonstrated that the lifetime, amplitude, group and phase velocity of the surface magnons propagating along two opposite (but equivalent) directions perpendicular to the magnetization are different meaning that magnons with the same energy propagate differently along two opposite directions. A new type of spintronic devices based on surface magnons is proposed. This discovery would open new routes towards possibilities of using surface magnons for information processing. Specially, in the devices made of ferromagnetic insulators, where the information cannot be carried by means of electrons and the role of magnons for carrying the information is essential.

It is illustrated that SPEELS may be used to probe the interface exchange parameters. If the magnetic coupling at the interface is weaker than at the surface, the low-energy magnon mode is mainly contributed from the interface layer. Probing of this magnon mode would lead to an unambiguous determination of the exchange coupling constants at the interface. Since the technique provides unique results on spin excitations, it has a large capability to be used for investigating the fundamental magnetic interactions in many systems.

Magnons in ultrathin films with out-of-plane easy axis are of particular fundamental interest. As a matter of fact, the pioneering SPEELS experiments on FeCo films with an out-of-plane easy axis have illustrated the capability of the method for investigation of such structures. The idea can be tailored to a large variety of ultrathin film systems, in which the magnetization is oriented perpendicular to the film.

Magnons in multilayer structures of alternating layers of ferromagnetic metals are also of fundamental interest. In this case one may observe different magnon modes associated with different layers in the structure. The preliminary experiments on this kind of systems are already started.

Magnons in an ultrathin antiferromagnetic film are also of great fundamental interest. In principle, one can investigate all the effects presented here in an antiferromagnetic



film. One candidate for such investigation is an ultrathin film of FeRh. It is expected that this material shows a ferromagnetic to antiferromagnetic phase transitions as a function of temperature and film thickness. It would be interesting to investigate the magnons in both ferromagnetic and antiferromagnetic phases and also observe the changes in the magnon spectrum across the transition temperature. The theoretical predictions of the magnons' behavior in each of these phases are appeared recently [166].

As it is proven, the technique allows probing both magnons and phonons, simultaneously. By choosing an appropriate system one may try to investigate and shed light onto the physics of magnon-phonon coupling in low-dimensional magnets.

The magnon lifetime needs to be investigated in more detail. It is believed that the main damping mechanism of high-energy magnons is their dissipation into single particle electron-hole pairs. In the case of low-dimensional ferromagnets in contact to metallic hosts, the angular momentum of magnons is transferred to the host via conduction electrons. It would be of great fundamental interest to prove this scenario. For that one needs to grow the ferromagnetic films on a(n) (semi-)insulating substrate and investigate the magnon lifetime for different thicknesses of the ferromagnetic film.



# Bibliography

- [1] I. I. Mazin, D. J. Singh, M. D. Johannes, and M. H. Du, “Unconventional Superconductivity with a Sign Reversal in the Order Parameter of  $\text{LaFeAsO}_{1-x}\text{F}_x$ ” *Phys. Rev. Lett.* **101** (2008) 057003.
- [2] I. I. Mazin and M. D. Johannes, “A key role for unusual spin dynamics in ferropnictides” *Nat. Phys.* **5** (2009) 141–145.
- [3] M. Le Tacon, G. Ghiringhelli, J. Chaloupka, M. M. Sala, V. Hinkov, M. W. Haverkort, M. Minola, M. Bakr, K. J. Zhou, S. Blanco-Canosa, C. Monney, Y. T. Song, G. L. Sun, C. T. Lin, G. M. De Luca, M. Salluzzo, G. Khaliullin, T. Schmitt, L. Braicovich, and B. Keimer, “Intense paramagnon excitations in a large family of high-temperature superconductors” *Nat. Phys.* **7** (2011) 725–730.
- [4] S. Zhang, P. M. Levy, A. C. Marley, and S. S. P. Parkin, “Quenching of Magnetoresistance by Hot Electrons in Magnetic Tunnel Junctions” *Phys. Rev. Lett.* **79** (1997) 3744–3747.
- [5] X.-F. Han, A. C. C. Yu, M. Oogane, J. Murai, T. Daibou, and T. Miyazaki, “Analyses of intrinsic magnetoelectric properties in spin-valve-type tunnel junctions with high magnetoresistance and low resistance” *Phys. Rev. B* **63** (2001) 224404.
- [6] P. M. Levy and A. Fert, “Spin Transfer in Magnetic Tunnel Junctions with Hot Electrons” *Phys. Rev. Lett.* **97** (2006) 097205.
- [7] V. Drewello, J. Schmalhorst, A. Thomas, and G. Reiss, “Evidence for strong magnon contribution to the TMR temperature dependence in MgO based tunnel junctions” *Phys. Rev. B* **77** (2008) 014440.
- [8] F. Bloch, “Zur Theorie des Ferromagnetismus” *Zeitschrift für Physik A Hadrons and Nuclei* **61** (1930) 206–219.
- [9] T. Holstein and H. Primakoff, “Field Dependence of the Intrinsic Domain Magnetization of a Ferromagnet” *Phys. Rev.* **58** (1940) 1098–1113.
- [10] W. Heisenberg, “Zur Theorie des Ferromagnetismus” *Zeitschrift für Physik A Hadrons and Nuclei* **49** (1928) 619–636.
- [11] E. C. Stoner, “Collective Electron Specific Heat and Spin Paramagnetism in Metals” *Proceedings of the Royal Society of London. Series A, Mathematical and Physical Sciences* **154** (1936) pp. 656–678.

- [12] E. C. Stoner, “Collective Electron Ferromagnetism” *Proceedings of the Royal Society of London. Series A, Mathematical and Physical Sciences* **165** (1938) pp. 372–414.
- [13] E. P. Wohlfarth, “The Theoretical and Experimental Status of the Collective Electron Theory of Ferromagnetism” *Rev. Mod. Phys.* **25** (1953) 211–219.
- [14] J. H. E. Griffiths, “Anomalous High-frequency Resistance of Ferromagnetic Metals” *Nature* **158** (1946) 670.
- [15] C. Kittel, “Interpretation of Anomalous Larmor Frequencies in Ferromagnetic Resonance Experiment” *Phys. Rev.* **71** (1947) 270–271.
- [16] C. Kittel, “On the Theory of Ferromagnetic Resonance Absorption” *Phys. Rev.* **73** (1948) 155–161.
- [17] J. H. Van Vleck, “Concerning the Theory of Ferromagnetic Resonance Absorption” *Phys. Rev.* **78** (1950) 266.
- [18] J. Van Kranendonk and J. H. Van Vleck, “Spin Waves” *Rev. Mod. Phys.* **30** (1958) 1–23.
- [19] C. Herring and C. Kittel, “On the Theory of Spin Waves in Ferromagnetic Media” *Phys. Rev.* **81** (1951) 869–880.
- [20] F. Keffer, H. Kaplan, and Y. Yafet, “Spin Waves in Ferromagnetic and Antiferromagnetic Materials” *American Journal of Physics* **21** (1953) 250–257.
- [21] F. J. Dyson, “General Theory of Spin-Wave Interactions” *Phys. Rev.* **102** (1956) 1217–1230.
- [22] R. N. Sinclair and B. N. Brockhouse, “Dispersion Relation for Spin Waves in a fcc Cobalt Alloy” *Phys. Rev.* **120** (1960) 1638.
- [23] R. A. Waldron, “What is ferromagnetic resonance?” *British Journal of Applied Physics* **11** (1960) 69.
- [24] G. Shirane, R. Nathans, O. Steinsvoll, H. A. Alperin, and S. J. Pickart, “Measurement of the Magnon Dispersion Relation of Iron” *Phys. Rev. Lett.* **15** (1965) 146.
- [25] G. Shirane, V. J. Minkiewicz, and R. Nathans, “Spin Waves in 3d Metals” *Journal of Applied Physics* **39** (1968) 383–390.
- [26] H. A. Mook, R. M. Nicklow, E. D. Thompson, and M. K. Wilkinson, “Spin-Wave Spectrum of Nickel Metal” *Journal of Applied Physics* **40** (1969) 1450–1451.
- [27] E. D. Thompson and H. A. Mook, “Energy Bands, Stoner Modes, and Spin Waves in Iron” *Journal of Applied Physics* **41** (1970) 1227–1228.
- [28] R. Lowde and C. Windsor, “On the magnetic excitations in nickel” *Advances in Physics* **19** (1970) 813–909.

- [29] H. A. Mook and R. M. Nicklow, “Neutron Scattering Investigation of the Magnetic Excitations in Iron” *Phys. Rev. B* **7** (1973) 336.
- [30] H. A. Mook and D. Tocchetti, “Neutron-Scattering Measurements of the Generalized Susceptibility  $\chi(q, E)$  for Ni” *Phys. Rev. Lett.* **43** (1979) 2029.
- [31] J. W. Lynn and H. A. Mook, “Temperature dependence of the dynamic susceptibility of nickel” *Phys. Rev. B* **23** (1981) 198–206.
- [32] R. W. Damon and J. R. Eshbach, “Magnetostatic modes of a ferromagnet slab” *Journal of Physics and Chemistry of Solids* **19** (1961) 308–320.
- [33] M. Sparks, “Ferromagnetic Resonance in Thin Films. I. Theory of Normal-Mode Frequencies” *Phys. Rev. B* **1** (1970) 3831–3856.
- [34] M. Sparks, “Ferromagnetic Resonance in Thin Films. II. Theory of Linewidths” *Phys. Rev. B* **1** (1970) 3856–3869.
- [35] M. Sparks, “Ferromagnetic Resonance in Thin Films. III. Theory of Mode Intensities” *Phys. Rev. B* **1** (1970) 3869–3880.
- [36] D. M. Edwards, “Spin Waves in Ferromagnetic Metals” *Proceedings of the Royal Society of London. Series A. Mathematical and Physical Sciences* **269** (1962) 338–351.
- [37] D. M. Edwards, “Spin Wave Energies in the Band Theory of Ferromagnetism” *Proceedings of the Royal Society of London. Series A, Mathematical and Physical Sciences* **300** (1967) 373–390.
- [38] J. Callaway, “Spin waves in ferromagnetic metals” *Physics Letters A* **27** (1968) 215 – 216.
- [39] J. Callaway, “Spin waves in metals” *International Journal of Quantum Chemistry* **2** (1968) 277–283.
- [40] J. B. Sokoloff, “Polar Spin Waves in Ferromagnetic Metals” *Phys. Rev.* **173** (1968) 617–630.
- [41] J. B. Sokoloff, “Theory of Inelastic Neutron Scattering in the Itinerant Model Antiferromagnetic Metals. I” *Phys. Rev.* **185** (1969) 770.
- [42] J. B. Sokoloff, “Theory of Neutron Scattering in the Itinerant Model of Antiferromagnetic Metals. II” *Phys. Rev.* **185** (1969) 783–791.
- [43] D. M. Edwards and J. A. Hertz, “Electron-magnon interactions in itinerant ferromagnetism. II. Strong ferromagnetism” *Journal of Physics F: Metal Physics* **3** (1973) 2191–2205.
- [44] D. M. Edwards and M. A. Rahman, “The transverse dynamical susceptibility of ferromagnets and antiferromagnets within the local exchange approximation” *Journal of Physics F: Metal Physics* **8** (1978) 1501.

- [45] J. F. Cooke, J. W. Lynn, and H. L. Davis, “Calculations of the dynamic susceptibility of nickel and iron” *Phys. Rev. B* **21** (1980) 4118–4131.
- [46] D. M. Edwards and R. B. Muniz, “Spin waves in ferromagnetic transition metals. I. General formalism and application to nickel and its alloys” *Journal of Physics F: Metal Physics* **15** (1985) 2339.
- [47] R. B. Muniz, J. F. Cooke, and D. M. Edwards, “Spin waves in ferromagnetic transition metals. II. Iron and its alloys” *Journal of Physics F: Metal Physics* **15** (1985) 2357.
- [48] H. Tang, M. Plihal, and D. Mills, “Theory of the spin dynamics of bulk Fe and ultrathin Fe films” *Journal of Magnetism and Magnetic Materials* **187** (1998) 23–46.
- [49] S. Y. Savrasov, “Linear Response Calculations of Spin Fluctuations” *Phys. Rev. Lett.* **81** (1998) 2570–2573.
- [50] J. Hong and D. L. Mills, “Spin excitations in ferromagnetic Ni: Electrons and neutrons as a probe” *Phys. Rev. B* **61** (2000) R858.
- [51] J. B. Staunton, J. Poulter, B. Ginatempo, E. Bruno, and D. D. Johnson, “Incommensurate and Commensurate Antiferromagnetic Spin Fluctuations in Cr and Cr Alloys from *Ab Initio* Dynamical Spin Susceptibility Calculations” *Phys. Rev. Lett.* **82** (1999) 3340–3343.
- [52] N. Karchev, “Magnonparamagnon effective theory of itinerant ferromagnets” *Journal of Physics: Condensed Matter* **15** (2003) 2797.
- [53] E. Şaşıoğlu, A. Schindlmayr, C. Friedrich, F. Freimuth, and S. Blügel, “Wannier-function approach to spin excitations in solids” *Phys. Rev. B* **81** (2010) 054434.
- [54] R. B. Muniz and D. L. Mills, “Theory of spin excitations in Fe(110) monolayers” *Phys. Rev. B* **66** (2002) 174417.
- [55] R. B. Muniz, A. T. Costa, and D. L. Mills, “Microscopic theory of spin waves in ultrathin ferromagnetic films: Fe on W(110)” *Journal of Physics: Condensed Matter* **15** (2003) S495.
- [56] A. T. Costa, R. B. Muniz, and D. L. Mills, “Theory of spin excitations in Fe(110) multilayers” *Phys. Rev. B* **68** (2003) 224435.
- [57] A. T. Costa, R. B. Muniz, and D. L. Mills, “Spin waves and their damping in itinerant ultrathin ferromagnets: Intermediate wave vectors” *Phys. Rev. B* **74** (2006) 214403.
- [58] R. Muniz, A. Costa, and D. Mills, “Spin Dynamics of Itinerant Electron Ferromagnetic Nanostructures” *IEEE Transactions on Magnetism*, **44** (2008) 1974–1977.

- [59] P. Buczek, A. Ernst, P. Bruno, and L. M. Sandratskii, “Energies and Lifetimes of Magnons in Complex Ferromagnets: A First-Principle Study of Heusler Alloys” *Phys. Rev. Lett.* **102** (2009) 247206.
- [60] S. Lounis, A. T. Costa, R. B. Muniz, and D. L. Mills, “Dynamical Magnetic Excitations of Nanostructures from First Principles” *Phys. Rev. Lett.* **105** (2010) 187205.
- [61] S. Lounis, A. T. Costa, R. B. Muniz, and D. L. Mills, “Theory of local dynamical magnetic susceptibilities from the Korringa-Kohn-Rostoker Green function method” *Phys. Rev. B* **83** (2011) 035109.
- [62] N. D. Mermin and H. Wagner, “Absence of Ferromagnetism or Antiferromagnetism in One- or Two-Dimensional Isotropic Heisenberg Models” *Phys. Rev. Lett.* **17** (1966) 1133.
- [63] D. Loss, F. L. Pedrocchi, and A. J. Leggett, “Absence of Spontaneous Magnetic Order of Lattice Spins Coupled to Itinerant Interacting Electrons in One and Two Dimensions” *Phys. Rev. Lett.* **107** (2011) 107201.
- [64] Y. Yafet, J. Kwo, and E. M. Gyorgy, “Dipole-dipole interactions and two-dimensional magnetism” *Phys. Rev. B* **33** (1986) 6519–6522.
- [65] M. Bander and D. L. Mills, “Ferromagnetism of ultrathin films” *Phys. Rev. B* **38** (1988) 12015–12018.
- [66] P. Bruno, “Spin-wave theory of two-dimensional ferromagnets in the presence of dipolar interactions and magnetocrystalline anisotropy” *Phys. Rev. B* **43** (1991) 6015–6021.
- [67] M. Farle, “Ferromagnetic resonance of ultrathin metallic layers” *Reports on Progress in Physics* **61** (1998) 755.
- [68] E. Ising, “Beitrag zur Theorie des Ferromagnetismus” *Zeitschrift für Physik A Hadrons and Nuclei* **31** (1925) 253–258.
- [69] I. E. Dzyaloshinskii, “Thermodynamic theory of “weak” ferromagnetism in antiferromagnetic substances” *Journal of Physics and Chemistry of Solids* **4** (1958) 241255.
- [70] T. Moriya, “Anisotropic Superexchange Interaction and Weak Ferromagnetism” *Phys. Rev.* **120** (1960) 91–98.
- [71] M. Bode, M. Heide, K. von Bergmann, P. Ferriani, S. Heinze, G. Bihlmayer, A. Kubetzka, O. Pietzsch, S. Blügel, and R. Wiesendanger, “Chiral magnetic order at surfaces driven by inversion asymmetry” *Nature* **447** (2007) 190–193.
- [72] M. Heide, G. Bihlmayer, and S. Blügel, “Dzyaloshinskii-Moriya interaction accounting for the orientation of magnetic domains in ultrathin films: Fe/W(110)” *Phys. Rev. B* **78** (2008) 140403.

- [73] P. Ferriani, K. von Bergmann, E. Y. Vedmedenko, S. Heinze, M. Bode, M. Heide, G. Bihlmayer, S. Blügel, and R. Wiesendanger, “Atomic-Scale Spin Spiral with a Unique Rotational Sense: Mn Monolayer on W(001)” *Phys. Rev. Lett.* **101** (2008) 027201.
- [74] M. Heide, G. Bihlmayer, and S. Blügel, “Describing Dzyaloshinskii–Moriya spirals from first principles” *Physica B: Condensed Matter* **404** (2009) 2678 – 2683.
- [75] C. D. Hu, “Relationship between ferroelectricity and Dzyaloshinskii–Moriya interaction in multiferroics and the effect of bond-bending” *Phys. Rev. B* **77** (2008) 174418.
- [76] M. I. Katsnelson, Y. O. Kvashnin, V. V. Mazurenko, and A. I. Lichtenstein, “Correlated band theory of spin and orbital contributions to Dzyaloshinskii–Moriya interactions” *Phys. Rev. B* **82** (2010) 100403.
- [77] L. Udvardi, L. Szunyogh, K. Palotas, and P. Weinberger, “First-principles relativistic study of spin waves in thin magnetic films” *Phys. Rev. B* **68** (2003) 104436.
- [78] L. Udvardi and L. Szunyogh, “Chiral Asymmetry of the Spin-Wave Spectra in Ultrathin Magnetic Films” *Phys. Rev. Lett.* **102** (2009) 207204.
- [79] T. Moriya and Y. Takahashi, “Itinerant Electron Magnetism” *Annual Review of Materials Science* **14** (1984) 1–25.
- [80] J. K. Kübler, *Theory of itinerant electron magnetism*, vol. 106 of *International series of monographs on physics*. Clarendon Press, Oxford, 2000.
- [81] J. C. Slater, “The Theory of Ferromagnetism: Lowest Energy Levels” *Phys. Rev.* **52** (1937) 198–214.
- [82] J. Kirschner, D. Rebenstorff, and H. Ibach, “High-Resolution Spin-Polarized Electron-Energy-Loss Spectroscopy and the Stoner Excitation Spectrum in Nickel” *Phys. Rev. Lett.* **53** (1984) 698–701.
- [83] H. Hopster, R. Raue, and R. Clauberg, “Spin-Flip Stoner Excitations in a Ferromagnet Observed by Inelastic Spin-Polarized Electron Scattering” *Phys. Rev. Lett.* **53** (1984) 695–697.
- [84] H. Hopster, “Direct observation of Stoner excitations in itinerant ferromagnets by spin-polarized inelastic electron scattering (invited; abstract)” *Journal of Applied Physics* **57** (1985) 3017–3017.
- [85] J. Kirschner, “Direct and Exchange Contributions in Inelastic Scattering of Spin-Polarized Electrons from Iron” *Phys. Rev. Lett.* **55** (1985) 973–976.
- [86] G. Vignale and K. S. Singwi, “Spin-flip electron-energy-loss spectroscopy in itinerant-electron ferromagnets: Collective modes versus Stoner excitations” *Phys. Rev. B* **32** (1985) 2824.



- [87] R. Saniz and S. P. Apell, “Model calculation of Stoner-excitation cross sections in spin-polarized crystals” *Phys. Rev. B* **48** (1993) 3206–3211.
- [88] M. P. Gokhale and D. L. Mills, “Spin excitations of a model itinerant ferromagnetic film: Spin waves, Stoner excitations, and spin-polarized electron-energy-loss spectroscopy” *Phys. Rev. B* **49** (1994) 3880–3893.
- [89] J. Kirschner, *Polarized electrons at surfaces*. Springer Tracts in Modern Physics. Springer-Verlag, 1985.
- [90] P. Buczek, A. Ernst, and L. M. Sandratskii, “Different dimensionality trends in the Landau damping of magnons in iron, cobalt, and nickel: Time-dependent density functional study” *Phys. Rev. B* **84** (2011) 174418.
- [91] P. Buczek, A. Ernst, and L. M. Sandratskii, “Interface Electronic Complexes and Landau Damping of Magnons in Ultrathin Magnets” *Phys. Rev. Lett.* **106** (2011) 157204.
- [92] J. S.-Y. Wang, “Energy Width of Ferromagnetic-Exchange Magnons in a Magnetic Field” *Phys. Rev. B* **6** (1972) 1908–1912.
- [93] V. V. Zolotarev, “Magnon Damping in the Heisenberg Ferromagnet” *Physica Status Solidi (b)* **64** (1974) K139–K141.
- [94] K. Zakeri, J. Lindner, I. Barsukov, R. Meckenstock, M. Farle, U. von Hörsten, H. Wende, W. Keune, J. Rucker, S. S. Kalarickal, K. Lenz, W. Kuch, K. Baberschke, and Z. Frait, “Spin dynamics in ferromagnets: Gilbert damping and two-magnon scattering” *Phys. Rev. B* **76** (2007) 104416.
- [95] C. Kittel, “Excitation of Spin Waves in a Ferromagnet by a Uniform rf Field” *Phys. Rev.* **110** (1958) 1295–1297.
- [96] M. H. Seavey and P. E. Tannenwald, “Direct Observation of Spin-Wave Resonance” *Phys. Rev. Lett.* **1** (1958) 168–169.
- [97] K. Zakeri, T. Kebe, J. Lindner, and M. Farle, “Magnetic anisotropy of Fe/GaAs(001) ultrathin films investigated by in situ ferromagnetic resonance” *Journal of Magnetism and Magnetic Materials* **299** (2006) L1 – L10.
- [98] P. A. Fleury, S. P. S. Porto, L. E. Cheesman, and H. J. Guggenheim, “Light Scattering by Spin Waves in FeF<sub>2</sub>” *Phys. Rev. Lett.* **17** (1966) 84–87.
- [99] B. Hillebrands, P. Baumgart, and G. Güntherodt, “Brillouin light scattering from spin waves in magnetic layers and multilayers” *Applied Physics A* **49** (1989) 589–598.
- [100] S. Demokritov, B. Hillebrands, and A. Slavin, “Brillouin light scattering studies of confined spin waves: linear and nonlinear confinement” *Physics Reports* **348** (2001) 441 – 489.

- [101] B. Hillebrands and K. Ounadjela, *Spin Dynamics in Confined Magnetic Structures II*. Topics in Applied Physics. Springer, 2003.
- [102] L. J. P. Ament, M. van Veenendaal, T. P. Devereaux, J. P. Hill, and J. van den Brink, “Resonant inelastic x-ray scattering studies of elementary excitations” *Rev. Mod. Phys.* **83** (2011) 705–767.
- [103] M. P. M. Dean, R. S. Springell, C. Monney, K. J. Zhou, J. Pereiro, I. Božović, B. Dalla Piazza, H. M. Rønnow, E. Morenzoni, J. Van Den Brink, T. Schmitt, and J. P. Hill, “Spin excitations in a single  $\text{La}_2\text{CuO}_4$  layer” *Nature Materials* **11** (2012) 850–854.
- [104] J. Kirschner, *Sources and detectors for polarized electrons*. Polarized Electrons in Surface Physics. World Scientific, 1985.
- [105] K. Zakeri and J. Kirschner, *Probing Magnons by Spin-Polarized Electrons*, vol. 125 of *Topics in Applied Physics Magnonics From Fundamentals to Applications*, ch. 7, pp. 84 – 99. Springer, Berlin, Heidelberg, 2013.
- [106] H. Ibach and D. Mills, *Electron Energy Loss Spectroscopy and Surface Vibrations*. Academic Press, New York, London, Paris, 1982.
- [107] H. Ibach, “Electron energy loss spectroscopy with resolution below 1 meV” *Journal of Electron Spectroscopy and Related Phenomena* **64–65** (1993) 819 – 823.
- [108] H. Hopster, “Spin-polarized electron energy loss spectroscopy” *Surface Review and Letters* **01** (1994) 89–96.
- [109] H. Ibach, M. Balden, and S. Lehwald, “Recent advances in electron energy loss spectroscopy of surface vibrations” *J. Chem. Soc., Faraday Trans.* **92** (1996) 4771–4774.
- [110] H. Ibach, D. Bruchmann, R. Vollmer, M. Etzkorn, P. S. A. Kumar, and J. Kirschner, “A novel spectrometer for spin-polarized electron energy-loss spectroscopy” *Review of Scientific Instruments* **74** (2003) 4089–4095.
- [111] H. Ibach, M. Etzkorn, and J. Kirschner, “Electron spectrometers for inelastic scattering from magnetic surface excitations” *Surface and Interface Analysis* **38** (2006) 1615–1617.
- [112] P. Drescher, H. Andresen, K. Aulenbacher, J. Bermuth, T. Dombo, H. Fischer, H. Euteneuer, N. Faleev, M. Galaktionov, D. von Harrach, *et al.*, “Photoemission of spin-polarized electrons from strained GaAsP” *Applied Physics A* **63** (1996) 203–206.
- [113] T. Balashov, A. F. Takács, W. Wulfhekel, and J. Kirschner, “Magnon Excitation with Spin-Polarized Scanning Tunneling Microscopy” *Phys. Rev. Lett.* **97** (2006) 187201.

- [114] T. Balashov, A. F. Takács, M. Däne, A. Ernst, P. Bruno, and W. Wulfhekel, “Inelastic electron-magnon interaction and spin transfer torque” *Phys. Rev. B* **78** (2008) 174404.
- [115] C. L. Gao, A. Ernst, G. Fischer, W. Hergert, P. Bruno, W. Wulfhekel, and J. Kirschner, “Spin Wave Dispersion on the Nanometer Scale” *Phys. Rev. Lett.* **101** (2008) 167201.
- [116] T. Balashov, T. Schuh, A. F. Takács, A. Ernst, S. Ostanin, J. Henk, I. Mertig, P. Bruno, T. Miyamachi, S. Suga, and W. Wulfhekel, “Magnetic Anisotropy and Magnetization Dynamics of Individual Atoms and Clusters of Fe and Co on Pt(111)” *Phys. Rev. Lett.* **102** (2009) 257203.
- [117] A. J. Heinrich, J. A. Gupta, C. P. Lutz, and D. M. Eigler, “Single-Atom Spin-Flip Spectroscopy” *Science* **306** (2004) 466–469.
- [118] S. Loth, C. P. Lutz, and A. J. Heinrich, “Spin-polarized spin excitation spectroscopy” *New Journal of Physics* **12** (2010) 125021.
- [119] A. A. Khajetoorians, S. Lounis, B. Chilian, A. T. Costa, L. Zhou, D. L. Mills, J. Wiebe, and R. Wiesendanger, “Itinerant Nature of Atom-Magnetization Excitation by Tunneling Electrons” *Phys. Rev. Lett.* **106** (2011) 037205.
- [120] T. Schuh, T. Balashov, T. Miyamachi, S.-Y. Wu, C.-C. Kuo, A. Ernst, J. Henk, and W. Wulfhekel, “Magnetic anisotropy and magnetic excitations in supported atoms” *Phys. Rev. B* **84** (2011) 104401.
- [121] R. Vollmer, M. Etzkorn, P. S. A. Kumar, H. Ibach, and J. Kirschner, “Spin-Polarized Electron Energy Loss Spectroscopy of High Energy, Large Wave Vector Spin Waves in Ultrathin fcc Co Films on Cu(001)” *Phys. Rev. Lett.* **91** (2003) 147201.
- [122] R. Vollmer, M. Etzkorn, P. S. A. Kumar, H. Ibach, and J. Kirschner, “Spin-wave excitation in ultrathin Co and Fe films on Cu(001) by spin-polarized electron energy loss spectroscopy (invited)” *Journal of Applied Physics* **95** (2004) 7435–7440.
- [123] R. Vollmer, M. Etzkorn, P. Kumar, H. Ibach, and J. Kirschner, “Spin-wave excitation observed by spin-polarized electron energy loss spectroscopy: a new method for the investigation of surface- and thin-film spin waves on the atomic scale” *Thin Solid Films* **464 - 465** (2004) 42–47.
- [124] R. Vollmer, M. Etzkorn, P. A. Kumar, H. Ibach, and J. Kirschner, “Spin-polarized electron energy loss spectroscopy: a method to measure magnon energies” *Journal of Magnetism and Magnetic Materials* **272 - 276** (2004) 2126–2130.
- [125] W. X. Tang, Y. Zhang, I. Tudosa, J. Prokop, M. Etzkorn, and J. Kirschner, “Large Wave Vector Spin Waves and Dispersion in Two Monolayer Fe on W(110)” *Phys. Rev. Lett.* **99** (2007) 087202.

- [126] K. Zakeri, Y. Zhang, J. Prokop, T. H. Chuang, W. X. Tang, and J. Kirschner, “Magnon excitations in ultrathin Fe layers: The influence of the Dzyaloshinskii-Moriya interaction” *Journal of Physics: Conference Series* **303** (2011) 012004.
- [127] K. Parlinski, Z. Q. Li, and Y. Kawazoe, “First-Principles Determination of the Soft Mode in Cubic  $\text{ZrO}_2$ ” *Phys. Rev. Lett.* **78** (1997) 4063–4066.
- [128] G. Fahsold, G. Knig, W. Theis, A. Lehmann, and K.-H. Rieder, “Epitaxial FeO films from ultrathin Fe on  $\text{MgO}(001)$  studied by He-atom scattering” *Applied Surface Science* **137** (1999) 224 – 235.
- [129] H. J. Elmers, “Ferromagnetic Monolayers” *International Journal of Modern Physics B* **09** (1995) 3115–3180.
- [130] M. Pratzner, H. J. Elmers, M. Bode, O. Pietzsch, A. Kubetzka, and R. Wiesendanger, “Atomic-Scale Magnetic Domain Walls in Quasi-One-Dimensional Fe Nanostripes” *Phys. Rev. Lett.* **87** (2001) 127201.
- [131] J. W. Lynn, “Temperature dependence of the magnetic excitations in iron” *Phys. Rev. B* **11** (1975) 2624–2637.
- [132] J. Lynn and H. Mook, “Nature of the magnetic excitations above  $T_c$  in Ni and Fe” *Journal of Magnetism and Magnetic Materials* **54–57** (1986) 1169–1170.
- [133] A. T. Costa, R. B. Muniz, J. X. Cao, R. Q. Wu, and D. L. Mills, “Magnetism of an Fe monolayer on  $\text{W}(110)$ ” *Phys. Rev. B* **78** (2008) 054439.
- [134] P. Buczek, A. Ernst, L. Sandratskii, and P. Bruno, “The energies and life times of magnons in bulk iron and one-monolayer Fe film” *Journal of Magnetism and Magnetic Materials* **322** (2010) 1396 – 1398.
- [135] A. Bergman, A. Taroni, L. Bergqvist, J. Hellsvik, B. Hjörvarsson, and O. Eriksson, “Magnon softening in a ferromagnetic monolayer: A first-principles spin dynamics study” *Phys. Rev. B* **81** (2010) 144416.
- [136] H. L. Meyerheim, D. Sander, R. Popescu, J. Kirschner, P. Steadman, and S. Ferrer, “Surface structure and stress in Fe monolayers on  $\text{W}(110)$ ” *Phys. Rev. B* **64** (2001) 045414.
- [137] S. Loth, M. Etzkorn, C. P. Lutz, D. M. Eigler, and A. J. Heinrich, “Measurement of Fast Electron Spin Relaxation Times with Atomic Resolution” *Science* **329** (2010) 1628–1630.
- [138] A. Taroni, A. Bergman, L. Bergqvist, J. Hellsvik, and O. Eriksson, “Suppression of Standing Spin Waves in Low-Dimensional Ferromagnets” *Phys. Rev. Lett.* **107** (2011) 037202.

- [139] A. B. Schmidt, M. Pickel, M. Donath, P. Buczek, A. Ernst, V. P. Zhukov, P. M. Echenique, L. M. Sandratskii, E. V. Chulkov, and M. Weinelt, “Ultrafast Magnon Generation in an Fe Film on Cu(100)” *Phys. Rev. Lett.* **105** (2010) 197401.
- [140] S. A. Wolf, D. D. Awschalom, R. A. Buhrman, J. M. Daughton, S. von Molnr, M. L. Roukes, A. Y. Chtchelkanova, and D. M. Treger, “Spintronics: A Spin-Based Electronics Vision for the Future” *Science* **294** (2001) 1488–1495.
- [141] E. Rashba, “Properties of semiconductors with an extremum loop. 1. Cyclotron and combinational resonance in a magnetic field perpendicular to the plane of the loop” *Sov. Phys. Solid State* **2** (1960) 1109–1122.
- [142] Y. A. Bychkov and E. I. Rashba, “Properties of a 2D electron gas with lifted spectral degeneracy” *JETP Letters* **39** (1984) 78.
- [143] R. Winkler, *Spin-Orbit Coupling Effects in 2D Electron and Hole Systems*. Springer, Berlin, 2003.
- [144] S. LaShell, B. A. McDougall, and E. Jensen, “Spin Splitting of an Au(111) Surface State Band Observed with Angle Resolved Photoelectron Spectroscopy” *Phys. Rev. Lett.* **77** (1996) 3419–3422.
- [145] J. Henk, A. Ernst, and P. Bruno, “Spin polarization of the  $L$ -gap surface states on Au(111)” *Phys. Rev. B* **68** (2003) 165416.
- [146] O. Krupin, G. Bihlmayer, K. Starke, S. Gorovikov, J. E. Prieto, K. Döbrich, S. Blügel, and G. Kaindl, “Rashba effect at magnetic metal surfaces” *Phys. Rev. B* **71** (2005) 201403.
- [147] G. Bihlmayer, Y. Koroteev, P. Echenique, E. Chulkov, and S. Blügel, “The Rashba-effect at metallic surfaces” *Surface Science* **600** (2006) 3888–3891.
- [148] C. Ast, J. Henk, A. Ernst, L. Moreschini, M. Falub, D. Pacilé, P. Bruno, K. Kern, and M. Grioni, “Giant Spin Splitting Through Surface Alloying” *Phys. Rev. Lett.* **98** (2007) 186807.
- [149] S. Datta and B. Das, “Electronic analog of the electro-optic modulator” *Applied Physics Letters* **56** (1990) 665–667.
- [150] T. Koga, J. Nitta, H. Takayanagi, and S. Datta, “Spin-Filter Device Based on the Rashba Effect Using a Nonmagnetic Resonant Tunneling Diode” *Phys. Rev. Lett.* **88** (2002) 126601.
- [151] H. C. Koo, J. H. Kwon, J. Eom, J. Chang, S. H. Han, and M. Johnson, “Control of Spin Precession in a Spin-Injected Field Effect Transistor” *Science* **325** (2009) 1515–1518.
- [152] M. I. Miron, G. Gaudin, S. Auffret, B. Rodmacq, A. Schuhl, S. Pizzini, and P. Vogel, J. and Gambardella, “Current-driven spin torque induced by the Rashba effect in a ferromagnetic metal layer” *Nature Materials* **9** (2010) .

- [153] K. Zakeri, Y. Zhang, J. Prokop, T.-H. Chuang, N. Sakr, W. X. Tang, and J. Kirschner, “Asymmetric Spin-Wave Dispersion on Fe(110): Direct Evidence of the Dzyaloshinskii-Moriya Interaction” *Phys. Rev. Lett.* **104** (2010) 137203.
- [154] L. Bergqvist, A. Taroni, A. Bergman, C. Etz, and O. Eriksson, “Atomistic spin dynamics of low-dimensional magnets” *Phys. Rev. B* **87** (2013) 144401.
- [155] A. T. Costa, R. B. Muniz, S. Lounis, A. B. Klautau, and D. L. Mills, “Spin-orbit coupling and spin waves in ultrathin ferromagnets: The spin-wave Rashba effect” *Phys. Rev. B* **82** (2010) 014428.
- [156] D. L. Mills, “Surface Corrections to the Specific Heat of Ferromagnetic Films” *Phys. Rev. B* **1** (1970) 264–274.
- [157] K. Zakeri, Y. Zhang, and J. Kirschner, “Surface magnons probed by spin-polarized electron energy loss spectroscopy” *Journal of Electron Spectroscopy and Related Phenomena* (2012) –.
- [158] Y. Zhang, P. Buczek, L. Sandratskii, W. X. Tang, J. Prokop, I. Tudosa, T. R. F. Peixoto, K. Zakeri, and J. Kirschner, “Nonmonotonic thickness dependence of spin wave energy in ultrathin Fe films: Experiment and theory” *Phys. Rev. B* **81** (2010) 094438.
- [159] D. Weller, A. Moser, L. Folks, M. E. Best, W. Lee, M. F. Toney, M. Schwickert, J.-U. Thiele, and M. F. Doerner, “High  $K_u$  materials approach to 100 Gbits/in” *IEEE Trans. Magn.* **36** (2000) 10.
- [160] L. Liu, C.-F. Pai, Y. Li, H. W. Tseng, D. C. Ralph, and R. A. Buhrman, “Spin-Torque Switching with the Giant Spin Hall Effect of Tantalum” *Science* **336** (2012) 555–558.
- [161] L. Liu, O. J. Lee, T. J. Gudmundsen, D. C. Ralph, and R. A. Buhrman, “Current-Induced Switching of Perpendicularly Magnetized Magnetic Layers Using Spin Torque from the Spin Hall Effect” *Phys. Rev. Lett.* **109** (2012) 096602.
- [162] F. Yildiz, M. Przybylski, X.-D. Ma, and J. Kirschner, “Strong perpendicular anisotropy in  $\text{Fe}_{1-x}\text{Co}_x$  alloy films epitaxially grown on mismatching Pd(001), Ir(001), and Rh(001) substrates” *Phys. Rev. B* **80** (2009) 064415.
- [163] T. Burkert, L. Nordström, O. Eriksson, and O. Heinonen, “Giant Magnetic Anisotropy in Tetragonal FeCo Alloys” *Phys. Rev. Lett.* **93** (2004) 027203.
- [164] J. Kesseler, *Polarized Electrons*. Springer, Berlin, 1985.
- [165] E. Şaşıoğlu, C. Friedrich, and S. Blügel, “Strong magnon softening in tetragonal FeCo compounds” *Phys. Rev. B* **87** (2013) 020410.
- [166] L. M. Sandratskii and P. Buczek, “Lifetimes and chirality of spin waves in antiferromagnetic and ferromagnetic FeRh from the perspective of time-dependent density functional theory” *Phys. Rev. B* **85** (2012) 020406.

## 6 Original publications

- 6.1 Kh. Zakeri and J. Kirschner.  
**Probing Magnons by Spin-Polarized Electrons**  
Magnonics, Eds. Sergej O. Demokritov and Andrei N. Slavin  
*Topics in Applied Physics, Vol. 125*, pp. 83–99 (2013), Springer Berlin Heidelberg.  
Reprinted with permission. Copyright 2013, Springer Science+Business Media.
- 6.2 Kh. Zakeri, Y. Zhang, and J. Kirschner.  
**Surface Magnons Probed by Spin-Polarized Electron Energy Loss Spectroscopy**  
*J. Electron. Spectrosc. Relat. Phenom.* **189**, 157 (2013).  
Reprinted with permission. Copyright 2013, Elsevier Science.
- 6.3 Y. Zhang, P. A. Ignatiev, J. Prokop, I. Tudosa, T. R. F. Peixoto, W. X. Tang, Kh. Zakeri, V. S. Stepanyuk, and J. Kirschner.  
**Elementary Excitations at Magnetic Surfaces and Their Spin Dependence**  
*Phys. Rev. Lett.* **106**, 127201 (2011).  
• [Highlighted by My science](#)  
• [Highlighted by Max-Planck research](#)  
Reprinted with permission. Copyright 2011, American Physical Society.
- 6.4 J. Prokop, W. X. Tang, Y. Zhang, I. Tudosa, T.R.F. Peixoto, Kh. Zakeri, and J. Kirschner.  
**Magnons in a Ferromagnetic Monolayer**  
*Phy. Rev. Lett.* **102**, 177206 (2009).  
Reprinted with permission. Copyright 2009, American Physical Society.
- 6.5 Y. Zhang, P. Buczek, L. Sandratskii, W. X. Tang, J. Prokop, I. Tudosa, T.R.F. Peixoto, Kh. Zakeri, and J. Kirschner.  
**Nonmonotonic Thickness Dependence of Spin-wave Energy in Ultrathin Fe Films: Experiment and Theory**  
*Phys. Rev. B* **81**, 094438 (2010).  
Reprinted with permission. Copyright 2010, American Physical Society.
- 6.6 T.-H. Chuang, Kh. Zakeri, A. Ernst, L. Sandratskii, P. Buczek, Y. Zhang, H. J. Qin, W. Adeagbo, W. Hergert, and J. Kirschner.  
**Impact of Atomic Structure on the Magnon Dispersion Relation: A Comparison Between Fe(111)/Au/W(110) and Fe(110)/W(110)**  
*Phys. Rev. Lett.* **109**, 207201 (2012).  
Reprinted with permission. Copyright 2012, American Physical Society.

- 6.7 Y. Zhang, T.-H. Chuang, Kh. Zakeri, and J. Kirschner.  
**Relaxation Time of Terahertz Magnons Excited at Ferromagnetic Surfaces**  
*Phys. Rev. Lett.* **109**, 087203 (2012).  
• Highlighted by [Terahertz technology](#)  
Reprinted with permission. Copyright 2012, American Physical Society.
- 6.8 Kh. Zakeri, Y. Zhang, J. Prokop, T.-H. Chuang, N. Sakr, W. X. Tang, and J. Kirschner.  
**Asymmetric Spin-Wave Dispersion on Fe(110): Direct Evidence of the Dzyaloshinskii–Moriya Interaction**  
*Phys. Rev. Lett.* **104**, 137203 (2010).  
Reprinted with permission. Copyright 2010, American Physical Society.
- 6.9 Kh. Zakeri, Y. Zhang, T.-H. Chuang, and J. Kirschner.  
**Magnon Lifetimes on the Fe(110) Surface: The Role of Spin–Orbit Coupling**  
*Phys. Rev. Lett.* **108**, 197205 (2012)  
• Selected for *Vir. J. Nan. Sci. & Tech.* Vol. **25**, Iss. 21  
• Selected for *Max-Planck Yearbook*  
Reprinted with permission. Copyright 2012, American Physical Society.
- 6.10 Kh. Zakeri, T.-H. Chuang, A. Ernst, L. M. Sandratskii, P. Buczek, H. J. Qin, Y. Zhang, and J. Kirschner.  
**Direct Probing of the Exchange Interaction at Buried Interfaces**  
*Nature Nanotechnology* **8**, 853 (2013).  
• Highlighted by [Nature New & Views](#)  
• Highlighted by [My science](#)  
• Highlighted by [Innovation reports](#)  
• Highlighted by [Max-Planck research](#)  
• Highlighted by [Pro-Physik](#)  
Reprinted with permission. Copyright 2013, Macmillan Publishers.
- 6.11 H. J. Qin, Kh. Zakeri, A. Ernst, T.-H. Chuang, Y.-J. Chen, Y. Meng, and J. Kirschner.  
**Magnons in Ultrathin Ferromagnetic Films with a Large Perpendicular Magnetic Anisotropy**  
*Phys. Rev. B* **88**, 020404(R) (2013)  
Reprinted with permission. Copyright 2013, American Physical Society.



## Chapter 7

# Probing Magnons by Spin-Polarized Electrons

K. Zakeri and J. Kirschner

**Abstract** High wave-vector magnon excitations in itinerant ferromagnets can be investigated by electron scattering experiments. In such an experiment, a spin-polarized beam with a well-defined energy is scattered from the sample surface and the energy distribution of the scattered electrons is measured. Since magnons possess a total angular momentum of  $1\hbar$ , they can only be excited (annihilated) by incidence of minority (majority) electrons. This fact leads to a peak in the energy loss (gain) region of the intensity spectra when minority (majority) electrons are incident. The scattering itself is elastic and the observed energy loss (or gain) is due to the fact that the ejected electron stems from a lower (or higher) energy level of the excited solid. Such a process is mediated by exchange interaction that is of a pure Coulomb nature and no explicit spin–spin interaction is involved.

We review the recent experimental attempts to probe and investigate the high wave-vector magnons in ultrathin ferromagnetic films by using spin-polarized electrons. Experimental results obtained by spin-polarized electron energy loss spectroscopy will be presented. The focus will be on the basic concepts and the nature of the different types of excitations probed by electrons. A possibility to distinguish between magnon- and phonon-excitations without the need of spin selective detection will be discussed.

### 7.1 Introduction

Low dimensional magnetic objects such as ultrathin magnetic films and nanostructures possess novel properties that have had a major impact on the innovation of the information and magneto-electronic technology [1]. Many static magnetic properties of this class of materials, which lead to their desired functionalities, are now well-known [2]. Since the speed of operation is important for faster information processing, nowadays the magneto-electronic technology pushes toward high speed operation. This fact implies that a better knowledge of the dynamic magnetic properties of magnetic thin films and nanostructures is required. Hence the processes

---

K. Zakeri (✉) · J. Kirschner  
Max-Planck-Institut für Mikrostrukturphysik, Weinberg 2, 06120 Halle, Germany  
e-mail: [zakeri@mpi-halle.de](mailto:zakeri@mpi-halle.de)

which are linked to spin excitations and ultrafast dynamics in solid are of great importance.

Besides its technological impact, spin dynamics in ferromagnets is of great fundamental interest because it lies in the central understanding of many physical phenomena. For instance, the temperature induced fluctuation of spins at low temperatures can be treated as collective spin excitations called spin waves. Spin waves are also important to understand the electron–electron interactions in high-temperature superconductors [3, 4]. Moreover, they are associated with the newly discovered phenomena like current-induced magnetization switching or current-induced domain wall motion [5–7].

The long wavelength spin wave excitations can be well-described using semi-classical models. However, when the wavelength of excitations approaches the nanometer scale, they are governed by the microscopic exchange interaction. In this case, the excitations are strongly confined in both time and space (their lifetime is mainly governed by the dissipation into the single particle excitations). Hence, they cannot be simply treated as in the case of classical spin waves. This implies that a quantum mechanical description of the system is demanded, and the experimental study of such excitations would provide a true microscopic view of the system.

This chapter is a review of the recent experimental results of high wave-vector magnon excitations by using spin-polarized electrons. The authors realized that the basic concepts of the processes involved in the magnon excitations by spin-polarized electrons are not well-interpreted by many groups in various places; therefore, the basic concepts are emphasized. The magnon dispersion relation and its differences in various systems will not be addressed in this chapter. The nature of the different type of excitations probed by electrons will be discussed in detail. Section 7.2 provides the basic information needed to follow this chapter. The magnetic excitations in ferromagnets are classified and explained in Sects. 7.2.1–7.2.3. The experimental tool, that is, spin polarized electron energy loss spectroscopy (SPEELS), used to investigate such excitations with a relatively high momentum and energy resolution is explained in Sect. 7.3. Moreover, the possibility of using scanning tunneling microscopy to study the surface excitations is briefly discussed. Section 7.4 will provide experimental results of high wave-vector magnon excitations in ultra-thin ferromagnetic films. A possibility to distinguish between magnon- and phonon-excitations without the need of spin selective detection is discussed in Sect. 7.4.2.

## 7.2 Basic Concepts

Ferromagnetism is characterized by a spontaneous magnetization without applying any external magnetic field. In a ferromagnetic solid, all magnetic moments are aligned parallel at  $T = 0$  K. It is caused by the direct exchange interaction of the electrons, which leads to a strong coupling of the spins to each other. The excited state of such a spin system can be described by creation of wavy like motions of the spins over the entire crystal called spin waves [8, 9]. The same picture can also be

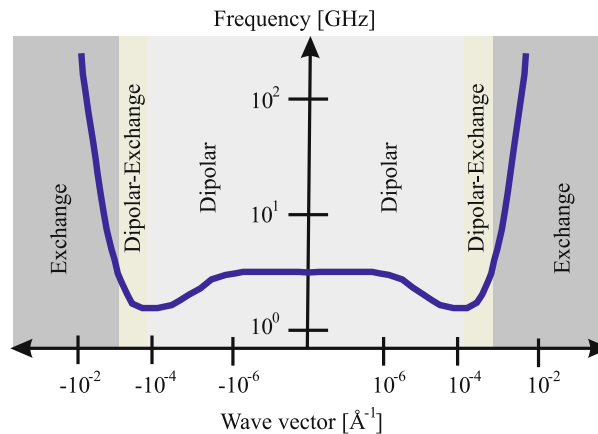


**Fig. 7.1** Different types of spin waves within the energy–momentum space. At the very low momentum values, the dominating magnetic energy is the long-range dipolar interaction, hence the spin waves are called dipolar spin waves. For the large momentum values, the dominating magnetic energy is the exchange energy, and thus it determines the energies of the spin waves. An intermediate regime is separating these two classes of spin waves [20]

applied to the antiferromagnets in which the atomic moments are aligned antiparallel at  $T = 0$  K. The spin waves in antiferromagnets can be understood in analogy to the ones in ferromagnets.

The classical picture mentioned above is only valid when the magnetic moments are localized. Since in  $3d$  ferromagnets the magnetism is governed by conduction electrons, this description cannot provide a clear picture of the system. In addition, another important question arises: How can the classical spin waves be understood from a microscopic point of view, i.e., by looking at the electronic band structure? This fact was pointed out by Stoner [10, 11] at the beginning of developing of the quantum theory of magnetism. In fact, a unique and satisfactory answer to this question is still missing. The elementary magnetic excitations in metallic ferromagnets can be classified as spin waves and Stoner excitations. Spin waves may be described similar to the excitons (electron–hole pairs). The wave function is a linear superposition of particle hole states (spin triplet particle hole excitations–Stoner excitations) [12]. In the following, we shall explain both excitations in detail.

### 7.2.1 Spin Waves

Spin waves are collective excitations of a spin system. They are well defined for the magnetic systems with localized moments, e.g., ferromagnetic insulators. In the itinerant ferromagnets, the low energy spin excitations can also be classified as spin waves. Spin waves may be described by Heisenberg Hamiltonian (see Sect. 7.2.3). In this description, the quantized spin waves are called magnons. The word “*magnon*” is chosen in analogy to the word “*phonon*”, which describes the quantized lattice vibrations. There is a large variety of magnons over the momentum and energy space. Spin waves caused by the coherent precession of the moments

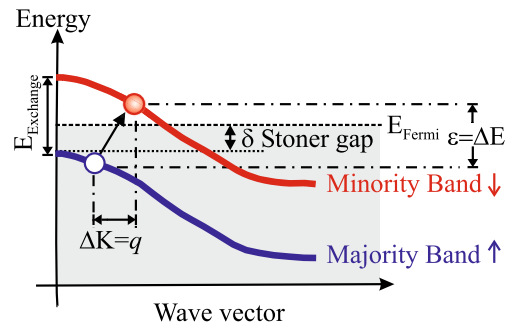


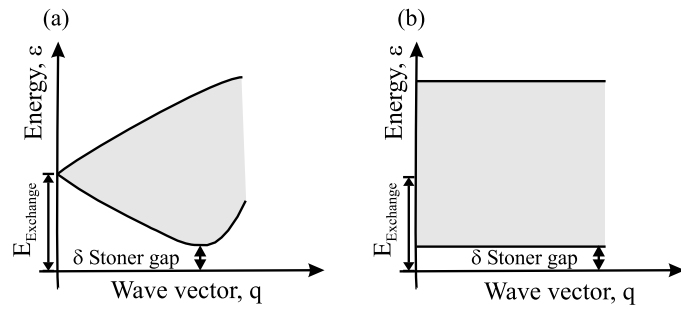
**Fig. 7.2** A schematic representation of Stoner excitations in an itinerant ferromagnet. A majority electron jumps from an occupied state below the Fermi-level to an unoccupied state above the Fermi-level, leaving a hole with majority spin behind

( $q = 0$ ) possess energies on the order of magnetic anisotropy energy of the system (few tens of micro-electron-volts) [13]. The lifetime of such spin waves reaches a value of a few tenths of a microsecond [14–17]. Figure 7.1 shows a schematic representation of different types of low-energy and low-wave-vector magnons. As the wave vector increases, the energy of spin waves increases. In the low wave-vector regime, where the magnetic anisotropy and long-range dipolar interactions are dominating, spin waves can be treated classically [18, 19]. At larger wave vectors (larger than  $10^{-3} \text{ \AA}^{-1}$ ) the exchange interaction becomes the dominating magnetic interaction and will determine the energy of spin waves.

### 7.2.2 Stoner Excitations

The electron–electron interactions in ferromagnets lead to a separation of the electronic bands for spin-up (majority) and spin-down (minority) electrons. In a simplified picture, this effect can be described as perturbations of a degenerate, paramagnetic band structure from which the energy degeneracy is lifted by the “*exchange splitting*”. The exchange splitting depends on the spin and the wave vector of the electrons within the system. If the Fermi-level lies between the bands derived from a single degenerate paramagnetic band, the lower energy (majority) states are occupied, while the higher energy (minority) states are unoccupied. This fact leads to a spin polarization of the conduction electrons and can explain the magnetic state of the system [11]. In such a case, the spin split bands across the Fermi-level would lead to the possibility of a unique single-particle excitation in the system. In principle, an electron can jump from an occupied majority band, undergo spin reversal, and occupy a state in the minority band. This process leads to a remaining hole of majority spin character in the majority band. The resulting electron–hole pairs (known as “*Stoner excitations*”) carry a total spin of  $1\hbar$  and a wave vector of  $q$ , which is the momentum difference of the electron and hole in the minority and majority bands, respectively. Stoner excitations are spread over the whole Brillouin zone (see Fig. 7.2).

**Fig. 7.3** Stoner density of states for a bulk (a) and an ultrathin (b) metallic ferromagnet with a non-zero Stoner gap  $\delta$



A schematic representation of the Stoner excitations is provided in Fig. 7.2. The bands are separated by the exchange splitting. The parameter  $\delta$ , known as Stoner gap, is defined as the energy between the highest occupied state below the Fermi-level and the Fermi-level,  $E_{\text{Fermi}}$ . Ferromagnets with non-zero  $\delta$  are usually called “*strong ferromagnets*” and the ones with  $\delta = 0$  are called “*weak ferromagnets*”). The energy,  $\varepsilon$ , and momentum,  $q$ , of the Stoner excitations are given by the energy and momentum difference of the electron and hole in the system, respectively. The distribution of the Stoner excitations in the momentum and energy space is usually called as Stoner density of states or Stoner states. It is given by the joint density of states for occupied and unoccupied states of appropriate spins with the momentum transfer  $\Delta K = q$ . In the case of bulk metallic ferromagnets, the conservation of the wave vector in three dimensions opens a gap for long-living-magnons with small energy and wave vector. This basically means that there are no Stoner states available for small  $q$  and  $\varepsilon$  ( $q \ll$  and  $\varepsilon < E_{\text{Exchange}}$ ). However, in the case of ultrathin metallic ferromagnets only the momentum parallel to the surface is conserved. This implies that the states should be projected into the energy axis meaning that there will be a very small gap left at  $q = 0$  (only the Stoner gap). Figure 7.3 represents the Stoner density of states for a strong ferromagnet with a non-zero Stoner gap  $\delta$ .

Stoner excitations describe a spin reversal in the system and are the elementary single-particle magnetic excitations in itinerant-electron ferromagnets. As it is mentioned above, at low energy and wave vector region, the configuration of the electronic bands does not allow single-particle Stoner excitations (see Fig. 7.3). In this case, the coherent superposition of “*virtual*” Stoner excitations of wave vector  $q$  can produce a collective magnetic excitation (or spin wave) of wave vector  $q$  at low energies. In regions of energy–momentum space where individual Stoner excitations are allowed, the spin wave and Stoner excitations are strongly coupled so that the excitations are heavily damped. In the case of two-dimensional ferromagnets (thin films and surfaces), the Stoner states cover the whole energy and momentum space [21–23]. It remains only a very tiny space for spin waves with very small energies ( $\varepsilon < \delta$ , see Fig. 7.3). Stoner excitations play a fundamental role in understanding of the excited states as well as the ground state of itinerant-electron ferromagnets. The band model of ferromagnets leads to the spin waves as the long-living excitations. However, in addition to spin waves, a spectrum of single particle Stoner excitation can also be obtained [24–34]. In principle, a proper theory must provide an account of both the spin waves and the Stoner excitations within a single framework. Espe-

cially at high wave vectors or at surfaces and ultrathin metallic ferromagnets, where both excitations overlap.

The representative elementary quasi-particles of both spin waves and Stoner excitations are the magnons. They carry an energy,  $\varepsilon$ , a momentum,  $q$ , and a total angular momentum of  $1\hbar$ .

### 7.2.3 Heisenberg Description of Magnons

The magnetically relevant part of the Hamiltonian for a ferromagnetic system in the absence of any external magnetic field is given by:

$$H = - \sum_{i \neq j} J_{ij} \mathbf{S}_i \cdot \mathbf{S}_j. \quad (7.1)$$

Here  $J_{ij}$  represents the exchange interaction between spins  $\mathbf{S}_i$  and  $\mathbf{S}_j$ . In the Heisenberg spin Hamiltonian given above, only the symmetric exchange interaction is taken into consideration. We note that in the presence of the magnetic anisotropy in the system, an additional term has to be added to (7.1). The term caused by magnetic anisotropy is directly proportional to the magnetic anisotropy energy of the system and basically acts as a Zeeman term which lifts the energy of the system up by a value of  $2K_{\text{eff}}S$ , where  $K_{\text{eff}}$  denotes the effective magnetic anisotropy energy and  $S$  is the magnitude of spins. Moreover, in the presence of the antisymmetric exchange interaction known as “*Dzyaloshinskii–Moriya interaction*”, an additional term which is proportional to the cross-product of the spins has to be added to the spin Hamiltonian [35, 36]. According to the formalism developed by Kittel [37], one can derive an expression for the magnon dispersion relation. In a classical picture, one may consider the exchange interaction as the source of a torque acting on each magnetic moment. By this consideration, the equation of motion reads as

$$\hbar \frac{d\mathbf{S}_i}{dt} = \tau_i = 2 \sum_j J_j (\mathbf{S}_i \times \mathbf{S}_j). \quad (7.2)$$

After a simple mathematical step, (7.2) can be written as

$$i\hbar \frac{dS_i^+}{dt} = 2JS \sum_j [S_i^+ - S_j^+], \quad (7.3)$$

where  $S^+ = S_x + iS_y$  is the raising operator. Usually, for surface magnons a wave form solution in the form of  $S_i^+ = A_i \exp[i(\mathbf{q} \cdot \mathbf{R}_i - \omega t)]$  is assumed.  $A_i$  is the amplitude of the magnon with the wave vector  $\mathbf{q}$  and angular frequency of  $\omega$  at position  $\mathbf{R}_i$ . The dot product between  $\mathbf{q}$  and  $\mathbf{R}_j$  implies that only the in-plane component of the wave vector is important here. Putting this solution into (7.3) results in the following expression:

$$\hbar\omega A_i = 2S \sum J_j \{A_i - A_j \exp[i\mathbf{q} \cdot (\mathbf{R}_j - \mathbf{R}_i)]\}. \quad (7.4)$$

Equation (7.4) is usually used to derive an equation for the magnon dispersion relation which connects the magnons' energy to their propagating wave vector. For an infinitely long cubic crystal and considering only the nearest neighbor interaction, the dispersion relation can be written as this simple form:

$$\varepsilon = \hbar\omega = 2nJS \left[ 1 - \frac{1}{n} \sum_{\delta} \cos(\mathbf{q} \cdot \mathbf{r}) \right], \quad (7.5)$$

where  $n$  is the number of nearest neighbors,  $J$  is the exchange coupling constant between the neighbors, and  $\mathbf{r}$  represents the position vector of the respective neighbor. Since the dispersion relation is not the main subject of the present chapter, we will not discuss it further. No prediction concerning the magnon lifetime can be made by the Heisenberg spin Hamiltonian given in (7.1). Within this description, magnons shall live forever, which is not certainly true for the case of itinerant electron ferromagnets. This classical picture even fails to describe the magnon dispersion relation in this class of materials [24–34, 38, 39].

#### 7.2.4 Spin Dependence of Electron Scattering

Generally, the inelastic scattering of electrons results from the so-called “dipolar” and “impact” scattering processes [40]. Dipolar scattering refers to the scattering of electrons by the electric dipolar field generated at the surface and may be described using the dielectric dipolar theory [40]. In such a description, detailed knowledge of the electrons and the sample surface is not needed. The dipolar scattering mainly happens for a scattering geometry very close to the specular geometry, where the angle of the incoming beam is the same as the one of the outgoing beam. In the case of off-specular geometries, the dominating process is the impact scattering. In contrast to the dipolar scattering, the inelastically scattered electrons are distributed over a large range of angles. The impact scattering is still poorly described by the theory due to lack of the detailed information about the interaction between the electrons and the sample surface [40].

As mentioned above, the inelastic scattering of spin-polarized electrons is a rather complicated process. The complete description of the processes involved in the scattering of spin-polarized electrons is out of the scope of the present chapter. More information may be found, for example, in Chap. 4 of [41] or in [42, 43]. Let us assume an ideal situation; one sends an electron with a given energy,  $E_i$ , and spin orientation (up  $\uparrow$  or down  $\downarrow$ ) onto a ferromagnetic surface at a certain geometry and performs a full energy and spin resolved detection of the scattered electron. Now the question would be: What are the possible scattering processes in such a situation? Figure 7.4 illustrates all the possible processes that may occur in an experiment where a primary electron with energy  $E_i$  and particular spin orientation

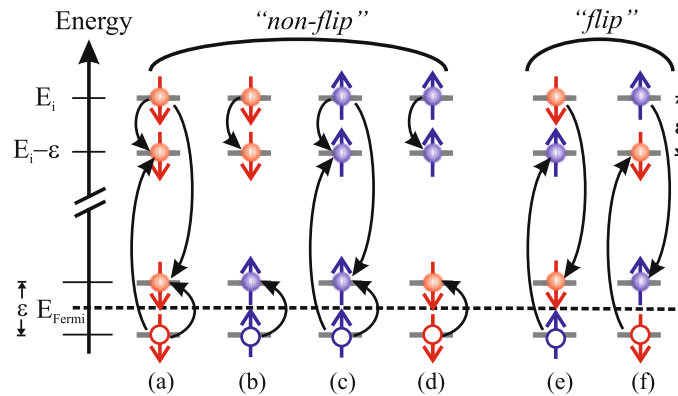


**Fig. 7.4** A schematic representation of the possible processes taking place in the scattering of spin-polarized electrons from a magnetic surface. Processes marked as (a), (b), (c), and (d) are referred to as “non-flip” processes, since the spin of the scattered electron is the same as the one of the primary electron. Processes in which the spin of the scattered electron is opposite to the one of the incoming electron are referred to as “flip” processes [(e) and (f)]

is launched onto a magnetic surface and an electron with energy  $E_i - \varepsilon$  is observed after scattering. During the scattering process, electrons in the sample are excited above the Fermi-level, and consequently holes are left in the system. The spin of the electron during the transition is conserved; therefore, only transitions from the states with the same spin orientation are allowed. A primary spin-down electron may experience two loss processes, each resulting in a scattered electron with the same spin orientation as the incident one (these processes will be referred to as “non-flip” processes). The incident spin-down electron either excites a minority electron from a state below the Fermi-level to a state above the Fermi-level, or it excites an electron of majority character to the same energy. Therefore, there are two “spin-down non-flip amplitudes”. These processes are marked as (a) and (b) in Fig. 7.4. The first one has an exchange contribution which partly cancels the direct amplitude. A primary spin-up electron may also experience two loss processes, each resulting in a scattered electron with the same spin orientation as the incident one (“non-flip” processes). The incident electron either excites a majority electron from a state below the Fermi-level to a state above the Fermi-level, or it excites an electron of minority character to the same energy. Therefore, there are two “spin-up non-flip amplitudes”. The corresponding processes are marked as (c) and (d) in Fig. 7.4. Again here the first one (process (c)) has an exchange contribution which partly cancels the direct amplitude. Note that the “non-flip intensities” result from the same spin system. A similar behavior is expected in an optical absorption experiment, e.g., photoemission, because the electric and magnetic fields involved are far too small to reverse the spin of an electron. The fact is that, disregarding exchange processes, electron energy loss spectroscopy and optical absorption are basically equivalent. Differences come into play by the possibility of electron exchange processes marked as (e) and (f) in Fig. 7.4. In the “spin-flip” process described by (e), the primary spin-down electron transfers its whole energy to a majority spin electron and occupies an empty state above the Fermi-level after the excitation. The excited



majority electron, coming from a state below the Fermi-level, emerges with an energy equal to the primary energy minus the energy of the electron–hole pair (Stoner excitation) around the Fermi-level. This process leads to creation of a magnon with the total angular momentum of  $1\hbar$  and energy  $\varepsilon$ . We will come to this point later in Sects. 7.3 and 7.4. The partial intensities for the “*spin-flip*” process with primary spin-up electron (process (f)) may be obtained analogously. The primary spin-up electron transfers its whole energy to a minority spin electron in a state below the Fermi-level and occupies an empty state above the Fermi-level after the excitation. The excited minority electron, coming from a state below the Fermi-level, leaves the sample with an energy equal to the primary energy minus the energy of the electron–hole pair around the Fermi-level. In addition to this process, there is another possibility (not shown in Fig. 7.4): the incoming spin-up electron excites an electron from a state above the Fermi-level and annihilates a hole in a state below the Fermi-level. The excited minority electron, coming from a state above the Fermi-level, leaves the sample with an energy equal to the primary energy plus the energy of the electron–hole pair around the Fermi-level. It looks like that the scattered electron has gained energy. The apparent energy gain is due to the fact that the electron stems from a higher energy level of the system (a state above the Fermi-level). Such a process would lead to annihilation of an available magnon with a total angular momentum of  $1\hbar$  and an energy of  $\varepsilon$  (see Sect. 7.4).

The relative rates of the processes mentioned in Fig. 7.4 for ferromagnetic surfaces have been measured first by Kirschner using a spin-polarized electron beam and a simultaneous spin-polarized detection [44]. It turned out that the “*flip*” rate of spin-down electrons is larger than the one of the spin-up electrons. This is mainly due to the fact that in normal ferromagnets there are more minority states available above the Fermi-level and consequently more majority electrons below the Fermi-level. This implies that the probability of having pairs of majority-hole and minority-electron is higher than the ones of minority-hole and majority-electron [44]. Interestingly, the experiment showed that the relative contributions of different rates depend on the wave vector of the excitations and could also be confirmed by other experiments [45–47].

At this point, we would like to emphasize that the processes referred to as “*flip*” processes above are due to the exchange scattering mechanism and there is no “*direct spin flip*” process involved via the scattering. The “*direct spin flip*” process can, in principle, happen under some circumstances. For instance, when electrons are scattered from a surface with a large spin-orbit coupling or when they experience a magnetic field, they may flip their spin via the well-known Larmor precession. However, these processes are very much slower than the exchange process and happen on the nano-/pico-second time-scale. The explanation of their physical origin is out of the scope of the present chapter (fruitful information may be found, for example, in [42, 43, 48, 49]). These processes are not relevant for the electron scattering from ferromagnetic surfaces with a small spin-orbit coupling. The electric and magnetic fields involved are far too small.

Since magnons carry a total angular momentum of  $1\hbar$ , they are created by minority electrons in an exchange scattering process [50]. The magnon creation process is mediated by the Coulomb interaction between the electrons and no explicit spin–spin interaction is involved. It takes place within a few tens of attoseconds.

### 7.3 Spin-Polarized Electron Energy Loss Spectroscopy

The spin-polarized electron energy loss spectroscopy (SPEELS) is based on the scattering of spin polarized electrons from a magnetic surface [51]. Spin polarized electrons are created by using spin-polarized photoemission from a GaAs photocathode. A circularly polarized laser beam is incident into the photocathode. According to the selection rules, the photo-emitted electrons will have their spins either parallel or antiparallel to the incident direction of the laser beam, depending on the helicity of the light. Since a normal GaAs has a total polarization of 50 % (based on the spin-dependent photoemission selection rules), usually a so-called strained semiconductor heterostructure is used for this purpose. Taking the advantage of hereroepitaxy one can grow a semiconductor heterostructure with a large lattice strain [52]. The large strain would modify the band structure so that a large spin polarization (as large as 90 %) can be achieved [52]. The spin-polarized electrons are monochromatized to get a certain energy and are focused onto the sample surface. The spin of the incoming electrons is either parallel or antiparallel to the majority electrons of the sample. The former type of electrons are usually called as spin up and the latter ones are called spin-down electrons. The scattered electrons are collected by a channeltron at a given scattering geometry and their energy is analyzed [51]. Note that no spin-resolved detection is involved in this experiment. The experiments are usually performed for both spin channels, simultaneously.

In Fig. 7.5, the scattering geometry is shown. If one assumes that the energy and momentum in initial and final states before and after scattering are  $E_i$ ,  $\mathbf{k}_i$  and  $E_f$ ,  $\mathbf{k}_f$ , respectively, the energy  $\varepsilon$  and the wave vector  $q$  of the excitations can be given by the following expressions:

$$\varepsilon = E_f - E_i; \quad q = -|\Delta\mathbf{k}_{\parallel}| = |\mathbf{k}_i| \sin\theta - |\mathbf{k}_f| \sin(\theta_0 - \theta). \quad (7.6)$$

In addition to the conservation of energy and momentum, the total angular momentum has to also be conserved. Hence magnon excitations are allowed only when minority electrons are incident. This implies that the magnon peak will appear only in the minority spin channel. Magnon excitations are forbidden when majority electrons are incident onto the sample surface. An example is given in Fig. 7.6, where typical SPEELS spectra measured on a Co film are shown. The peak in the minority spin channel ( $I_{\downarrow}$ ) is due to the long-living magnon excitations and the raising background is attributed to the single-particle electron–hole pair excitations [53].

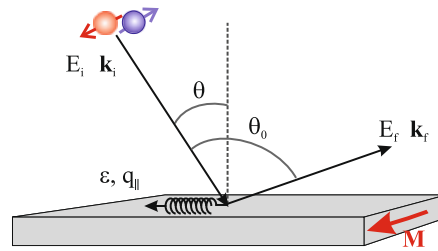


**Fig. 7.5** A schematic representation of the scattering geometry used in SPEELS experiments. A monochromatic beam with a well-defined energy and momentum is focused onto the sample surface and the energy distribution of the scattered beam is measured at a given geometry for both spin orientations

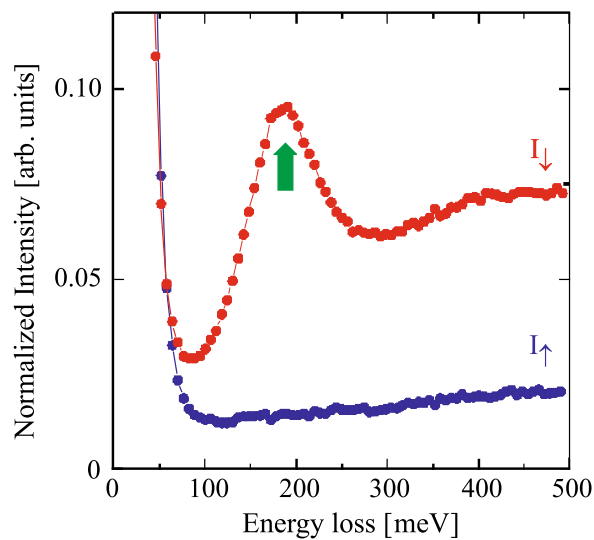


**Fig. 7.6** Typical SPEELS spectra recorded on an epitaxial Co(100) film, with a thickness of 8 ML, grown on Cu(100). The energy of incident beam and the in-plane wave vector transfer were about  $E_i = 6.7$  eV and  $|\Delta k_{\parallel}| = 0.87 \text{ \AA}^{-1}$ , respectively. The peak in the minority spin channel ( $I_{\downarrow}$ ) is due to the magnon excitations and the raising background is attributed to the single-particle electron-hole pair excitations [53]

In Sect. 7.4, it will be explained in detail how the magnons are created and annihilated in SPEELS experiments.

Magnons can also be excited within the tunneling process in scanning tunneling spectroscopy experiments [54–56]. Basically, the process is similar to the one in the SPEELS experiments. The tunneling electrons interact with the ones of the sample, and when they have enough kinetic energy to create an excitation, the tunneling current is enhanced. The excitation process leads to a step in the differential conductivity that is  $dI/dU$  and consequently a peak in  $d^2I/dU^2$ . The main difference here is that the excitation may happen in the forward and backward tunneling directions. The excitations can be of magnetic and non-magnetic nature. By using a magnetic tip and changing the magnetization direction of the tip, one may confirm that the excitations are of magnetic origin. The main disadvantage of this technique

is that the control of the tip magnetization is usually difficult. Due to the fact that the tunneling current is almost perpendicular to the sample surface, the technique is not capable of performing measurements at different wave vectors. Only when standing waves are formed due to confinement effects, one would be able to observe different magnon modes [54–56].

## 7.4 Recent Experimental Achievements

### 7.4.1 Magnon Excitations in Ferromagnetic Thin Films

For studying the surface magnons, initially an atomically clean surface has to be obtained. Such surfaces can be prepared by means of conventional thin film growth techniques under ultrahigh vacuum. Usually, prior to the SPEELS measurements the films are magnetically saturated by applying a magnetic field. The measurements are performed in the remnant state.

As it is mentioned in Sect. 7.2.4, magnons carry a total angular momentum of  $1\hbar$ , therefore, they are created by minority electrons. Due to the thermal fluctuations, a spin system possess a large variety of magnons at a finite temperature. These are usually referred to as “*thermally excited magnons*” and are spread over a large momentum and energy space, depending on the temperature. The population of this class of magnons is given by Bose–Einstein statistics, which determines the statistical distribution of identical indistinguishable bosonic quasi-particles over the energy states in thermal equilibrium [57]. In principle, the thermally excited magnons can be annihilated by majority electrons. A majority electron can be scattered to a minority one via the exchange scattering mechanism and hereby a magnon will be annihilated (see the inset of Fig. 7.7). In this process, the energy of the electron in the final state is larger than the one in the initial state, and hence such a process can be observed in the energy gain region. The intensity of the peak associated with the magnon annihilation process depends on the population of the thermally excited magnons at the measurement temperature. The magnon population is given by a Boltzmann factor, which is about 0.17 for the magnons with an excitation energy of 46 meV at  $T = 300$  K. It is nearly zero for  $T = 10$  K. This means that at low temperatures the magnon annihilation process is expected to be suppressed and at high temperatures it is pronounced. Here we would like to point out that such a behavior is also expected for phonons that are also classified as bosons. An example is provided in Fig. 7.7 where the SPEELS spectra measured at different temperatures are presented. The spectra are recorded on a 2 ML thick Fe(110) film grown on W(110) with a wave vector of  $0.5 \text{ \AA}^{-1}$ . The magnon propagation direction in this particular experiment is along the [001]-direction of the Fe(110) surface ( $\vec{\Gamma}-\vec{H}$ -direction of the surface Brillouin zone). For each case the spectra for spin-up ( $I_{\uparrow}$ ) and spin-down ( $I_{\downarrow}$ ) electrons are measured. In addition, the sum ( $I_{\downarrow} + I_{\uparrow}$ ), difference ( $I_{\downarrow} - I_{\uparrow}$ ), and asymmetry [ $(I_{\downarrow} - I_{\uparrow})/(I_{\downarrow} + I_{\uparrow})$ ] spectra are also presented. Let us first start with Fig. 7.7(a). It is apparent that the spectra are dominated by presence of the quasi-elastic peak at  $E = 0$  meV. The magnon creation and annihilation peaks are located

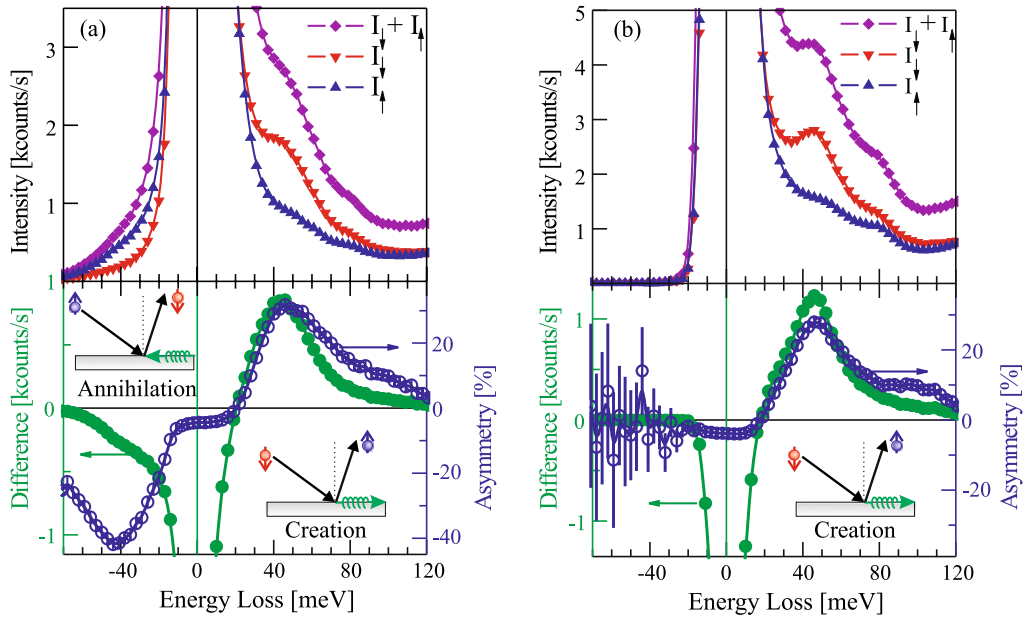


**Fig. 7.7** SPEELS spectra measured at  $|\Delta\mathbf{k}_{\parallel}| = 0.5 \text{ \AA}^{-1}$  on an ultrathin Fe(110)/W(110) film with a thickness of 2 ML at (a) 300 K and (b) 10 K. The *upper panels* show the spin up ( $I_{\uparrow}$ ), spin down ( $I_{\downarrow}$ ) and the sum ( $I_{\uparrow} + I_{\downarrow}$ ) spectra. The *lower panels* show the difference ( $I_{\downarrow} - I_{\uparrow}$ ) and asymmetry ( $\frac{I_{\downarrow} - I_{\uparrow}}{I_{\downarrow} + I_{\uparrow}}$ ) spectra. The magnon creation and annihilation processes are schematically sketched in the *insets*

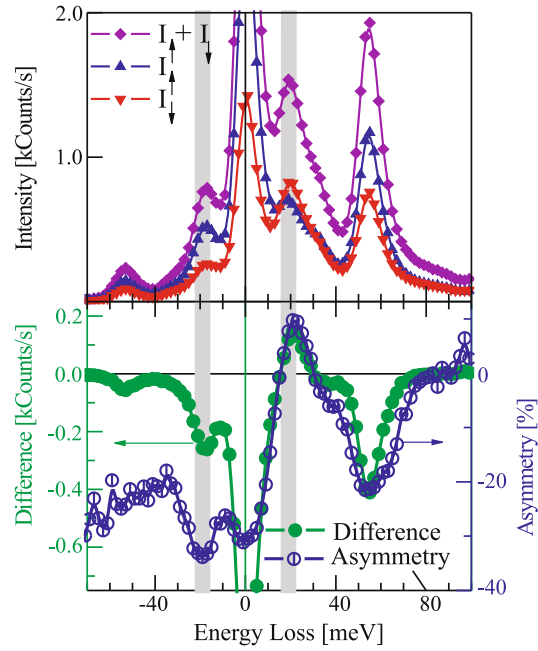
beside the elastic peak in the energy loss and gain region, respectively. These two processes are sketched schematically in the insets of Fig. 7.7. The asymmetry curve shows a change in the sign from negative to positive, when going from gain to loss region. The minima (in the gain region) and the maxima (in the loss region) are the places where the excitation and annihilation processes take place. If one neglects the spin-orbit coupling effects in the system the maxima and minima should be located at the same energies (one negative and the other positive). As it was mentioned earlier, at low temperature where the population of the thermally excited magnons is very low, the magnon annihilation peak supposed to be strongly suppressed. This fact can be clearly seen in Fig. 7.7(b), where the measurements at 10 K, performed on the same sample, are presented. No trace of magnon annihilation could be detected neither in difference nor in asymmetry spectrum.

In order to obtain the magnon dispersion relation, usually the spectra are recorded for different wave vectors [38, 39, 53, 58–61]. The desired wave vector is achieved by changing the scattering geometry, i.e., the angle between incident beam and the sample normal ( $\theta_i$ , see (7.6) and Fig. 7.5).

#### 7.4.2 Distinguishing Between Magnons and Phonons

In principle, both magnons and phonons can be excited by electrons. Since both kinds of excitations may show very similar energies, it is rather difficult to distin-

**Fig. 7.8** SPEELS spectra measured on the Fe(001)–O( $1 \times 1$ ) surface at 300 K and  $|\Delta \mathbf{k}_{\parallel}| = 0.3 \text{ \AA}^{-1}$ . The *upper panel* shows the spin up ( $I_{\uparrow}$ ), spin down ( $I_{\downarrow}$ ) and the sum ( $I_{\uparrow} + I_{\downarrow}$ ) spectra. The *lower panel* shows the difference ( $I_{\downarrow} - I_{\uparrow}$ ) and the asymmetry ( $\frac{I_{\downarrow} - I_{\uparrow}}{I_{\downarrow} + I_{\uparrow}}$ ) spectra. The *vertical gray lines* mark the position of the peaks resulting from the magnon excitation (energy loss) and annihilation (energy gain) processes



guish between them experimentally. However, using the spin degree of freedom of spin-polarized electrons opens a possibility to separate magnons from phonons. As magnons carry a total angular momentum of  $1 \hbar$ , they can only be excited by incidence of minority electrons. The time reversal process happens for incidence of majority electrons, which leads to the magnon annihilation. This fact would lead to a sign change in the asymmetry curve in gain and loss regions (see the lower panel of Fig. 7.7(a)). In the case of phonons, the situation is different. Since phonons are spin-independent quasi-particles, they can be created and annihilated by incidence of electrons with any spin direction. We note that the process which leads to phonon creation can also be mediated by the exchange process (the exchange of the electrons with the same spin, see Fig. 7.4). The particular dependence of magnon creation and annihilation on the spin of the incident electrons, as it is different from phonon excitations, is a fundamental feature, which can be used to distinguish between magnons and phonons in spin-polarized electron scattering experiments. The best way to identify the nature of an excited quasi-particle (magnon or phonon), is to compare the signs of asymmetry curves in loss and gain regions. An example is provided in Fig. 7.8, where the spectra of an oxygen passivated Fe(001), measured at  $T = 300$  K and  $|\Delta \mathbf{k}_{\parallel}| = 0.3 \text{ \AA}^{-1}$ , are presented. The magnon and phonon excitations coincide within the same energy window. Interestingly, the intensity of all excitations depends on the spin orientation of the incoming beam. In such a case, the fundamental question is: How can one distinguish between magnons and phonons? As it is discussed above, the identification of phonons and magnons can be done by looking at their different spin nature. Asymmetries of loss and gain spectra of the peaks marked by the vertical gray lines in Fig. 7.8 (at energies of  $\pm 19$  meV) are of opposite signs, and hence they are associated with magnon excitations. Asymmetry of the other excitations have the same sign and almost identical magnitudes; therefore, they are caused by phonon excitations.

It is interesting to mention that in the case of the Fe(001)–O(1 × 1) surface the asymmetries of phonon induced peaks are always negative. A complementary experiment showed that the asymmetry of the phonon peaks follows the one of the elastic peak. This fact implies that very likely the asymmetry of the phonon peaks has the same origin as the one of the elastic peak [62]. However, the details of the effect are expected to depend on many parameters like the energy of the incident beam, excitation energy, and the scattering geometry. Even, the sign of the spin asymmetry may change while changing the electron energy. Recently, the dispersion relation of magnons and phonons could be measured simultaneously by varying the wave vector and the dispersion branches could be separated based on their different spin nature [62].

## 7.5 Conclusion

We discussed the processes involved in high wave-vector magnon excitations in itinerant ferromagnets by using spin-polarized electron scattering experiments. Since magnons carry a total angular momentum of  $1\hbar$ , they can only be excited by incidence of minority electrons and annihilated by incidence of majority ones. The excitation process is commonly called as an inelastic electron scattering process. However, we think that the process itself is elastic and the observed energy loss (or gain) is due to the fact that the ejected electron stems from a lower (or higher) energy level of the excited solid. The process is extremely fast (taking place within a few tens of attoseconds). It is mediated by the exchange interaction, i.e., the Coulomb interaction between electrons and no explicit spin–spin interaction is needed to be taken into consideration.

A possibility to distinguish between magnon- and phonon-excitations based on their spin nature is discussed. Magnons can only be excited by incidence of minority electrons and annihilated by incidence of majority ones whereas, phonons can be excited and annihilated by incidence of electrons with any spin orientation. This fact would lead to a sign change in the asymmetry curve in the gain and loss regions where the magnons are excited. For the case of phonons, no change in the sign of the asymmetry curve is expected. This means that the magnons and phonons can be distinguished by comparing the sign of the symmetry curves in loss and gain regions and there is no need of further spin resolved detection of the scattered electrons.

**Acknowledgements** We thank all the present and former co-workers: H. Ibach, R. Vollmer, M. Etzkorn, P.S. Anil Kumar, W.-X. Tang, J. Prokop, I. Tudosa, Y. Zhang, T.R.F. Peixoto, and T.-H. Chuang who have contributed to the various experiments discussed here.

## References

1. S.A. Wolf, D.D. Awschalom, R.A. Buhrman, J.M. Daughton, S. von Molnar, M.L. Roukes, A.Y. Chtchelkanova, D.M. Treger, *Science* **294**, 1488 (2001)

2. C.A.F. Vaz, J.A.C. Bland, G. Lauhoff, Rep. Prog. Phys. **71**, 056501 (2008)
3. J.P. Carbotte, E. Schachinger, D.N. Basov, Nature **401**, 354 (1999)
4. T. Dahm, V. Hinkov, S.V. Borisenko, A.A. Kordyuk, V.B. Zabolotnyy, J. Fink, B. Büchner, D.J. Scalapino, W. Hanke, B. Keimer, Nat. Phys. **5**, 217 (2009)
5. K.-J. Lee, A. Deac, O. Redon, J.-P. Nozieres, B. Dieny, Nat. Matters **3**, 877 (2004)
6. D.-S. Han, S.-K. Kim, J.-Y. Lee, S.J. Hermsdoerfer, H. Schultheiss, B. Leven, B. Hillebrands, Appl. Phys. Lett. **94**, 112502 (2009)
7. Y. Le Maho, J.-V. Kim, G. Tatara, Phys. Rev. B **79**, 174404 (2009)
8. F. Bloch, Z. Phys. **61**, 206 (1930)
9. C. Herring, C. Kittel, Phys. Rev. **81**, 869 (1951)
10. E.C. Stoner, Proc. R. Soc. A **154**, 656 (1936)
11. E.C. Stoner, Proc. R. Soc. A **165**, 372 (1938)
12. D.M. Edwards, Proc. R. Soc. A **235**, 305 (1962)
13. M. Farle, Rep. Prog. Phys. **61**, 755 (1998)
14. C.E. Patton, C.H. Wilts, F.B. Humphrey, J. Appl. Phys. **38**, 1358 (1967)
15. C.E. Patton, Dynamic processes in magnetic thin films. Domain wall motion and ferromagnetic resonance, Ph.D. thesis, California Institute of Technology (1967)
16. D.L. Mills, S.M. Rezende, *Spin Dynamics in Confined Magnetic Structures II* (Springer, Berlin, 2003)
17. K. Zakeri, J. Lindner, I. Barsukov, R. Meckenstock, M. Farle, U. von Hörsten, H. Wende, W. Keune, J. Rocker, S.S. Kalarickal, K. Lenz, W. Kuch, K. Baberschke, Z. Frait, Phys. Rev. B **76**, 104416 (2007)
18. J.A.C. Bland, B. Heinrich, *Ultrathin Magnetic Structures III* (Springer, Berlin, 2005)
19. P.A. Grünberg, Surf. Sci. **18**, 1 (1985)
20. B. Hillebrands, K. Ounadiela (Eds), in *Spin Dynamics in Confined Magnetic Structures III*. Topics in Applied Physics, vol. 83 (Springer, Berlin, 2003)
21. J. Kirschner, D. Rebenstorff, H. Ibach, Phys. Rev. Lett. **53**, 698 (1984)
22. J. Kirschner, S. Suga, Surf. Sci. **178**, 327 (1986)
23. J. Kirschner, E. Langenbach, Solid State Commun. **66**, 761 (1988)
24. R.B. Muniz, D.L. Mills, Phys. Rev. B **66**, 174417 (2002)
25. R.B. Muniz, A.T. Costa, D.L. Mills, J. Phys., Condens. Matter **15**, S495 (2003)
26. A.T. Costa, R.B. Muniz, D.L. Mills, Phys. Rev. B **68**, 224435 (2003)
27. A.T. Costa, R.B. Muniz, D.L. Mills, Phys. Rev. B **74**, 214403 (2006)
28. R.B. Muniz, A.T. Costa, D.L. Mills, IEEE Trans. Magn. **44**, 1974 (2008)
29. A.T. Costa, R.B. Muniz, J.X. Cao, R.Q. Wu, D.L. Mills, Phys. Rev. B **78**, 054439 (2008)
30. E. Şaşıoğlu, A. Schindlmayr, C. Friedrich, F. Freimuth, S. Blügel, Phys. Rev. B **81**, 054434 (2010)
31. P. Buczek, A. Ernst, P. Bruno, L.M. Sandratskii, Phys. Rev. Lett. **102**, 247206 (2009)
32. P. Buczek, A. Ernst, L.M. Sandratskii, Phys. Rev. Lett. **105**, 097205 (2010)
33. P. Buczek, A. Ernst, P. Bruno, L.M. Sandratskii, J. Magn. Magn. Mater. **322**, 1396 (2010)
34. P. Buczek, A. Ernst, L.M. Sandratskii, Phys. Rev. Lett. **106**, 157204 (2011)
35. I.E. Dzyaloshinskii, Sov. Phys. JETP **5**, 1259 (1957)
36. T. Moriya, Phys. Rev. **120**, 91 (1960)
37. C. Kittel, *Introduction to Solid State Physics* (Wiley, New York, 1996)
38. W.X. Tang, Y. Zhang, I. Tudosa, J. Prokop, M. Etzkorn, J. Kirschner, Phys. Rev. Lett. **99**, 087202 (2007)
39. J. Prokop, W.X. Tang, Y. Zhang, I. Tudosa, T.R.F. Peixoto, K. Zakeri, J. Kirschner, Phys. Rev. Lett. **102**, 177206 (2009)
40. H. Ibach, D.L. Mills, *Electron Energy Loss Spectroscopy and Surface Vibrations* (Academic Press, New York, 1982)
41. J. Kessler, *Polarized Electrons* (Springer, Berlin, 1985)
42. J. Kirschner, *Polarized Electrons at Surfaces*. Springer Tracts in Modern Physics, vol. 106 (Springer, Heidelberg, 1985)



43. J. Kirschner, Inelastic electron scattering by ferromagnets, in *Polarized Electrons in Surface Physics*, ed. by R. Feder (World Scientific, Singapore, 1985)
44. J. Kirschner, Phys. Rev. Lett. **55**, 973 (1985)
45. R. Feder, J. Kirschner, Solid State Commun. **40**, 547 (1981)
46. D. Venus, J. Kirschner, Phys. Rev. B **37**, 2199 (1988)
47. M.S. Hammond, G. Fahsold, J. Kirschner, Phys. Rev. B **45**, 6131 (1992)
48. J. Kirschner, R. Feder, J.F. Wendelken, Phys. Rev. Lett. **47**, 614 (1981)
49. D. Venus, H.L. Johnston, Phys. Rev. B **50**, 15787 (1994)
50. M. Plihal, D.L. Mills, J. Kirschner, Phys. Rev. Lett. **82**, 2579 (1999)
51. H. Ibach, D. Bruchmann, R. Vollmer, M. Etzkorn, P.S.A. Kumar, J. Kirschner, Rev. Sci. Instrum. **74**, 4089 (2003)
52. P. Drescher et al., Appl. Phys. A **63**, 203 (1996)
53. R. Vollmer, M. Etzkorn, P.S. Anil Kumar, H. Ibach, J. Kirschner, Phys. Rev. Lett. **91**, 147201 (2003)
54. T. Balashov, A.F. Takacs, W. Wulfhekel, J. Kirschner, Phys. Rev. Lett. **97**, 187201 (2006)
55. C.L. Gao, A. Ernst, G. Fischer, W. Hergert, P. Bruno, W. Wulfhekel, J. Kirschner, Phys. Rev. Lett. **101**, 167201 (2008)
56. T. Balashov, A.F. Takacs, M. Däne, A. Ernst, P. Bruno, W. Wulfhekel, Phys. Rev. B **78**, 174404 (2008)
57. R. Kobu, M. Toda, N. Hashitsume, *Statistical Physics II Nonequilibrium Statistical Mechanics* (Springer, Heidelberg, 1992)
58. M. Etzkorn, P.S. Anil Kumar, W. Tang, Y. Zhang, J. Kirschner, Phys. Rev. B **72**, 184420 (2005)
59. M. Etzkorn, P.S. Anil Kumar, J. Kirschner, High-energy surface spin waves studied by spin-polarized electron energy loss spectroscopy, in *Handbook of Magnetism and Advanced Magnetic Materials*, ed. by H. Kronmüller, S. Parkin, Novel Techniques for Characterizing and Preparing Samples, vol. 3 (Wiley, New York, 2007)
60. Y. Zhang, P. Buczek, L.M. Sandratskii, W.X. Tang, J. Prokop, I. Tudosa, T.R.F. Peixoto, K. Zakeri, J. Kirschner, Phys. Rev. B **81**, 094438 (2010)
61. K. Zakeri, Y. Zhang, J. Prokop, T.-H. Chuang, N. Sakr, W.-X. Tang, J. Kirschner, Phys. Rev. Lett. **104**, 137203 (2010)
62. Y. Zhang, P.A. Ignatiev, J. Prokop, I. Tudosa, T.R.F. Peixoto, W.X. Tang, K. Zakeri, V.S. Stepanyuk, J. Kirschner, Phys. Rev. Lett. **106**, 127201 (2011)





Contents lists available at ScienceDirect

## Journal of Electron Spectroscopy and Related Phenomena

journal homepage: [www.elsevier.com/locate/elspec](http://www.elsevier.com/locate/elspec)

# Surface magnons probed by spin-polarized electron energy loss spectroscopy

Kh. Zakeri\*, Y. Zhang, J. Kirschner

Max-Planck-Institut für Mikrostrukturphysik, Weinberg 2, D-06120 Halle, Germany

### ARTICLE INFO

#### Article history:

Available online 26 June 2012

#### PACS:

75.30.Ds

75.50.Bb

75.70.Ak

#### Keywords:

Spin-polarized electron energy-loss spectroscopy  
 Surface magnetism  
 Spin waves  
 Magnons  
 Magnetic excitations

### ABSTRACT

Short-wavelength magnons at ferromagnetic surfaces can be probed by electrons. The unique property of electrons, i.e. having a very strong interaction with the surface together with the spin degree of freedom enables one to investigate the spin dependent quasi-particles, e.g. magnons at magnetic surfaces.

We review the experimental results of short-wavelength magnons probed at ferromagnetic Co(0001) and Fe(110) surfaces by spin-polarized electron energy-loss spectroscopy. The differences and similarities to their bulk counterpart are discussed in detail. Although in the case of Co(0001) surface magnons behave similar to the ones in bulk Co, in the case of Fe(110) they possess a smaller exchange stiffness meaning that the effective exchange coupling is smaller at the surface. In both cases, surface magnons have an extremely short lifetime being in the order of a few tens of femtosecond.

© 2012 Elsevier B.V. All rights reserved.

## 1. Introduction

Magnetism at surfaces and in ultrathin films has attracted a lot of attention because of exotic phenomena, which have not been observed in bulk materials [1–4]. Enhanced magnetic moment at the surface [3], perpendicular easy axis [4] and giant magnetoresistance effect [5,6] are all attributed to the presence of the surface and interface. The possibilities of using these new effects observed at the magnetic surfaces and interfaces in magneto-electronic technology have been extensively discussed and even some of the available devices in nowadays technology are based on these properties [7].

Magnetic excitations are well-established subjects in bulk magnetism. They are of crucial importance for understanding the microscopic origins of different observations in magnetism, e.g., the magnetic ordering phenomena at a finite temperature. From a fundamental physics point of view, a complete knowledge of magnetic excitations would lead to a better understanding of the physical phenomena related to the excited state of the system. In the case of low-dimensional magnetic objects or at surfaces, the magnetic excitations should, in principle, reflect the properties of these systems. This knowledge is essential to understand the theory of high-speed response of a magnetic material to different kinds

of excitations (for instance high frequency electromagnetic radiations). Moreover, it would allow a prediction of the role and the type of elementary excitations generated within the processes like spin-current induced magnetic switching [8,9]. From the application point of view this information would help us to design magnetic devices, which can be operated at high frequencies.

In a classical description, the wavy-like motions of the atomic magnetic moments, which are caused by the precession of the individual moments are called spin waves. Their representative quasi-particles are referred to as magnons. Long-wavelength (low-energy) excitations are usually treated classically using phenomenological approaches, e.g., using the so-called Landau–Lifshitz–Gilbert (LLG) equation of motion. The dominating magnetic interaction for this class of magnons is the magnetic dipolar interaction [10,11]. Although in various occasions it is shown that the LLG equation fails to describe the magnetic damping mechanisms in ferromagnets [12–15], however, it lies in the central explanation of long-wavelength spin waves, at least where processes like two-magnon scattering are not important. In contrary to this class of magnons the short-wavelength magnons are governed by magnetic exchange interaction and therefore their properties are entirely different than those of long-wavelength magnons.

In this paper we will provide the experimental results of short-wavelength magnon excitations probed by spin-polarized electron energy-loss spectroscopy (SPEELS) on different ferromagnetic surfaces. As examples we discuss the results of Co(0001) and Fe(110) films grown on W(110) surface. The results of magnon dispersion relation and the lifetime of surface magnons will be discussed.

\* Corresponding author. Tel.: +49 345 5582749; fax: +49 345 5511223.

E-mail address: [zakeri@mpi-halle.de](mailto:zakeri@mpi-halle.de) (Kh. Zakeri).URL: <http://www.mpi-halle.de/> (Kh. Zakeri).

Some comparison to the results of the bulk samples probed by inelastic neutron scattering (INS) measurements will be provided. The paper is organized as follows: In Section 2 we introduce the basic concepts needed to follow the paper. In Section 3, the experimental details concerning the sample preparation, characterization, and SPEELS measurements are provided. Section 4 is dedicated to the main experimental results followed by a discussion. A concluding remark is provided in Section 5.

## 2. Basic concepts

Spin waves governed by exchange interaction may be described by the classical Heisenberg Hamiltonian. In this description the representative quasi-particles of spin waves are referred to as magnons. The simplest form of Heisenberg spin Hamiltonian reads as:

$$H = - \sum_{i \neq j} J_{ij} \vec{S}_i \cdot \vec{S}_j. \quad (1)$$

Here  $J_{ij}$  denotes the isotropic exchange interaction between spins  $\vec{S}_i$  and  $\vec{S}_j$ . This Hamiltonian applies to a system of spins, which are coupled via an isotropic exchange interaction in the absence of any external magnetic field and magnetic anisotropy. In the systems with magnetic anisotropy, an additional term, which is proportional to the magnetic anisotropy energy of the system, should be added to Eq. (1). In the presence of the antisymmetric exchange interaction (usually referred to as Dzyaloshinskii–Moriya interaction [16,17]) an additional term, which is proportional to the vector product of the spins ( $\vec{S}_i \times \vec{S}_j$ ) may be added to the spin Hamiltonian [18].

In order to derive the equation of motion, in a semi-classical picture, one may consider the magnetic exchange interaction as the source of a torque acting on each magnetic moment. The equation of motion can be derived as:

$$\hbar \frac{d\vec{S}_i}{dt} = \vec{\tau}_i = 2 \sum_j J_{ij} (\vec{S}_i \times \vec{S}_j). \quad (2)$$

Writing the expansion of the cross product in terms of spin components leads to the following equations:

$$\hbar \frac{dS_i^x}{dt} = 2 \sum_j J_{ij} (S_j^y S_i^z - S_j^z S_i^y), \quad (3)$$

$$\hbar \frac{dS_i^y}{dt} = 2 \sum_j J_{ij} (S_j^z S_i^x - S_j^x S_i^z). \quad (4)$$

Now if one defines the rising operator as  $S^+ = S^x + iS^y$ , Eq. (2) can be simplified to:

$$i\hbar \frac{dS_i^+}{dt} = 2S \sum_j J_{ij} [S_i^+ - S_j^+], \quad (5)$$

where  $S \approx S^z$  denotes the magnitude of spin. By considering a wave form solution for the magnons ( $S_i^+ = A_i \exp[i(\vec{q} \cdot \vec{R}_i - \omega t)$ ],  $A_i$  denotes the amplitude of the magnon with the wave vector  $\vec{q}$  and angular frequency of  $\omega$  at position  $\vec{R}_i$ ) one can simply derive the following expression, which connects the magnons energy (eigenfrequency) to their wave vector:

$$\hbar\omega A_i = 2S \sum_j J_{ij} [A_i - A_j \exp[i\vec{q} \cdot (\vec{R}_j - \vec{R}_i)]]. \quad (6)$$

The above equation is usually used to derive the magnon dispersion relation for any system of interest. We will use it in Section 4 to calculate the dispersion relation of our systems. For an infinitely large crystal with simple cubic structure and considering only the

nearest neighbor interaction, the dispersion relation can be written as this simple form:

$$E = \hbar\omega = 2zJS \left[ 1 - \frac{1}{z} \sum_{\delta} \cos(\vec{q} \cdot \vec{a}_{\delta}) \right], \quad (7)$$

where  $z$  is the number of nearest neighbors,  $J=J_{ij}$  represents the exchange coupling constant between the neighbors and  $\vec{a}$  is the position vector of the respective neighbor. The Heisenberg Hamiltonian provides no information concerning the magnons' damping. The assumption is that the magnons live for an infinitely long time. In reality, the magnons possess a finite lifetime, which for the case of itinerant electron ferromagnets is quite short. We will provide some information on the magnon lifetimes at the Fe(1 1 0) surface in Section 4.2. The classical Heisenberg picture fails to describe the magnon dispersion relation in itinerant electron ferromagnets [19–31]. However, since it provides a simple way of understanding the magnon dispersion relation, we will use it for our data analysis in a comparative way.

In an itinerant ferromagnet the bands are spin-split across the Fermi-level, which can lead to a possibility of single-particle excitations called Stoner excitations. In fact, an electron of majority spin character can jump from an occupied majority band to an empty state in the minority band above the Fermi-level. A hole with majority spin character in the majority band will be left. The electron-hole pairs (Stoner pairs), generated within this process, possess a total spin of  $1\hbar$ . The energy and momentum of a Stoner pair is given by the momentum and energy difference of the electron and hole in the minority- and majority-band, respectively. The probability of having Stoner excitations depends on the band structure. In two-dimensional metallic ferromagnets, Stoner excitations are spread over the entire Brillouin zone and only a narrow area within the Stoner gap is left. They overlap with the collective excitations. It is shown that Stoner excitations lead to an energy renormalization of the high wave vector magnons, in addition to modifying their damping [28,29,32]. The excitations at very low energies (below the Stoner gap) will not be influenced by the Stoner continuum and may still be described in terms of spin waves.

## 3. Experimental details

For this study all the experiments were performed under ultra-high vacuum (UHV) condition with a base pressure better than  $3 \times 10^{-11}$  mbar. As with other surface sensitive methods, performing SPEELS experiments in UHV is essential to get rid of the effects induced by adsorbates.

### 3.1. Sample preparation

The samples were grown in situ in the form of ultrathin films by the molecular beam epitaxy technique. The structure and chemical properties were characterized using low-energy electron diffraction (LEED) and Auger electron spectroscopy (AES). The magnetic properties were studied by magneto-optical Kerr effect (MOKE). The magnon excitations were investigated using SPEELS. In the following section we will briefly introduce our SPEELS spectrometer. We also discuss and describe the basic physical processes involved in SPEELS experiments.

### 3.2. Spin-polarized electron energy-loss spectroscopy

SPEELS is a spectroscopy technique based on the scattering of spin-polarized electrons from a magnetic surface. In this technique a spin-polarized low-energy electron beam is incident onto the sample surface at a certain scattering geometry and the intensity of the scattered electrons is measured versus their energy loss. As

it is a spin polarized version of electron energy-loss spectroscopy (EELS), some basic principles are similar to the one of EELS experiments. The main advantage of SPEELS is that one has a direct access to control the spin of the incoming beam and thereby can distinguish the spin dependent and spin independent excitations at solid surfaces. This is essential for investigating magnon excitations. No spin selective detection is involved in this experiment. The energy of the incoming beam has usually been chosen to be in the order of a few electron-volts (3–10 eV). This is the range, where the magnons are observed as pronounced peaks in the energy-loss spectra [33].

It is often thought that the basic concepts of SPEELS are similar to the one of the inelastic neutron scattering (INS). In fact the fundamental basis of these two techniques are different. In SPEELS experiments the exchange mechanism plays an important role while in INS experiments the type of the interaction that is important is the dipolar interaction between the neutron magnetic moment with the magnetic field induced by magnons. In the following we will discuss how does the exchange mechanism during the scattering process lead to magnon excitations within the SPEELS experiments.

Before we discuss the contributions to the inelastic scattering of the spin-polarized electrons, let us define the spin direction of the incoming and outgoing beam. It is defined with respect to the majority and minority spins of the sample. When the spin of the electron is parallel to the majority electrons of the ferromagnetic surface, it is called spin-up electron  $\uparrow$  and when it is parallel to the minority electrons of the sample surface it is called spin-down electron  $\downarrow$ . Generally, the inelastic scattering of spin-polarized electrons is a rather complicated topic. A complete description of the mechanisms involved in such processes is out of the scope of the present paper. An extended discussion can be found in Ref. [34]. If an electron with a given spin ( $\uparrow$  or  $\downarrow$ ) is incident onto a ferromagnetic surface at a certain geometry, the outgoing electron has either the spin orientation parallel or anti-parallel to the one of the incoming electron. Although in the former case an exchange of the electrons with the same spins is possible, in the latter case one can clearly talk about the exchange process. This means that the incident electron occupies an unoccupied state above the Fermi-level and another electron from an occupied state below the Fermi-level will be scattered out of the surface. The corresponding processes are schematically illustrated in Fig. 1 for incident of spin-down (left) and spin-up (right) electrons. The processes in which the incident and scattered electrons have the same spin character are usually referred to as “non-flip” processes and the ones in which the spin of the scattered electron is opposite to the incident electron are called “flip” processes. It is essential to notice that no direct spin reversal is involved in the processes mentioned above. The underlying mechanism is the exchange process. The “flip” process mentioned above describes the fact that an incident electron with given spin direction is exchanged with an electron from the sample with an opposite spin orientation (for an extended discussion see for example [34–38]).

As discussed in Section 2 the total angular momentum of a magnon is  $1\hbar$ . If a spin-down electron is incident onto the surface, it excites a majority electron from a state below the Fermi-level and occupies an empty state above the Fermi-level. The excited majority electron will be scattered out of the sample. Such a process leads to excitation of a magnon with a total angular momentum of  $1\hbar$ . A magnon annihilation process may be imagined when a spin-up electron is incident onto the sample surface. However, during this process the outgoing electron would gain energy and hence this process would take place in the energy gain spectra. As such a process requires an available magnon, the intensity of the peak associated with this process is proportional to the number of the available magnons. In the thermodynamic steady state condition the number of magnons is given by the Bose–Einstein statistics,

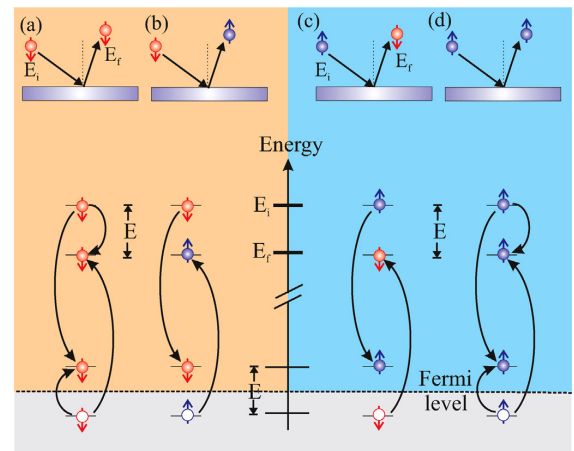


**Fig. 1.** A schematic representation of possible processes when a spin-down (a and b) or spin-up (c and d) electron is incident onto a magnetic surface. Since in processes shown as (a) and (d) the spin of the incident and scattered electron is the same we call these processes “non-flip” processes. Consequently processes (b) and (c) are called “flip” processes because the spin of the scattered electron is opposite to the one of the incident electron. Note that these processes are due to the exchange mechanism and no direct spin reversal process is involved here. The lower panel shows the corresponding excitation processes within the system. During such processes electrons from a state below the Fermi-level are excited and holes are created in the system. The incoming electron with energy  $E_i$  transfers its energy to an electron in a state below the Fermi-level and fills an unoccupied state. The excited electron leaves the sample from a state with energy  $E_f = E_i - E$ .

since they are bosons. In the processes mentioned above when an electron is excited from a state below the Fermi-level a hole is left in the system. The resulting electron and hole in the system are correlated and are considered as an electron–hole pair. The energy and momentum of the corresponding electron–hole pair (magnon) is the energy and momentum difference of the electron and hole.

We note that during the scattering, phonons can also be excited at the surface. Since the phonons are spin independent quasi-particles they can be excited by incidence of spin-down as well as spin-up electrons. The answer to this question: “how one can distinguish between magnons and phonons when the phonons also show a spin asymmetry?” is out of the scope of this paper. In principle, comparing the gain and loss features of each excitation should provide an access to its nature. A detailed discussion may be found in Ref. [39].

Fig. 2 shows a schematic view of the scattering processes within the SPEELS experiments. Since the energy and the parallel momentum of the electrons are conserved during the scattering process, the wave vector of the magnons can be selected by adjusting the scattering geometry (see Fig. 2). This fact enables one to probe the magnons in a wave vector selective manner. Assuming that the energy and momentum before and after scattering are  $E_i$ ,  $\vec{k}_i$  and  $E_f$ ,  $\vec{k}_f$ , respectively, the energy  $E$  and the in-plane component of the wave vector  $\vec{q}_{\parallel}$  of the excited magnons can be given by the following expressions:

$$E = E_f - E_i$$

$$|\vec{q}_{\parallel}| = |\Delta k_{\parallel}| = |\vec{k}_i| \sin \theta - |\vec{k}_f| \sin(\theta_0 - \theta). \quad (8)$$

Here,  $\theta$  ( $\theta_0$ ) is the angle between the incident beam and the surface normal (scattered beam).

The magnon dispersion relation can be obtained by performing the experiments at different wave vectors. The desired wave vector can be achieved by changing the angle between the incoming beam and the surface normal ( $\theta$ ) or the angle between the incoming beam

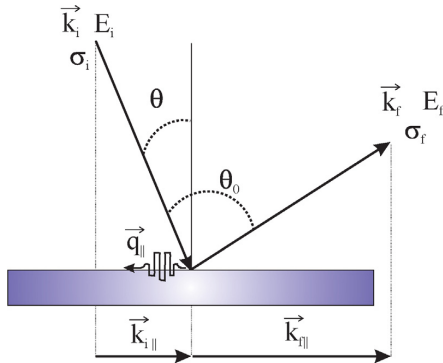


**Fig. 2.** A schematic representation of the scattering geometry in the SPEELS experiments. An electron beam with a given energy  $E_i$ , wave vector  $k_i$  and spin  $\sigma_i$  is scattered from the surface to an electron beam with energy  $E_f$ , wave vector  $k_f$  and spin  $\sigma_f$ . Since the energy and the in-plane wave vector is conserved within this process, the energy and the wave vector of the excited magnons (the in-plane component) is given by Eq. (8).

and the outgoing one ( $\theta_0$ ). In addition to the conservation of energy and parallel momentum, the total angular momentum has to also be conserved. Hence magnon excitations are allowed only when minority electrons are incident. This implies that the magnon peak will appear only in the minority spin channel. Magnon excitations are forbidden when majority electrons are incident onto the sample surface (see Fig. 3). We will come back to this point in Section 4.1.

#### 4. Results and discussion

##### 4.1. The magnon dispersion relation

Experimentally the properties of magnons like excitation energy (or eigenfrequency,  $\omega = E/\hbar$ , where  $E$  is the excitation energy), dispersion relation and the lifetime are obtained by recording the energy-loss spectra. An example is given in Fig. 3, where typical SPEELS spectra measured on a hexagonal close-packed (hcp) Co(0001) and a body-centered cubic (bcc) Fe(110) film recorded at a wave vector of  $0.7 \text{ \AA}^{-1}$  are presented. In the experiments one sequentially measures the spectra for both spin orientations of the incoming beam ( $I_{\uparrow}$  and  $I_{\downarrow}$ ). The peak in the minority spin channel ( $I_{\downarrow}$ ) is due to the magnon excitations. The peak intensity is usually

one or even two orders of magnitude smaller than the one of the elastic peak (the one at  $E_{\text{loss}} = 0$ ). The small satellites in the upper panel of Fig. 3(b) at energies of about 63 and 120 meV are due to the vibrational excitations of the adsorbed oxygen and hydrogen from the residual gases in the chamber. Since they appear in both spin channels and show a very weak energy dispersion, they can be clearly identified. The magnon peak shows a finite width that provides information about the typical lifetime of the magnons. A way to analyze the magnon peaks is taking the difference spectra that is  $I_{\downarrow} - I_{\uparrow}$  (see the lower panels of Fig. 3). We use the difference spectra for further data analysis.

For a thin film composed of a finite number of atomic layers, the Heisenberg model predicts  $n$  different modes, where  $n$  is the number of atomic layers. However, in the experiment irrespective of the number of atomic layers, only a single magnon peak was observed (the surface acoustic mode). The first reason may lie in the fact that in the case of the acoustic mode the moments precess in phase and hence the transverse components of spins are added to each other. Therefore this mode appears as a pronounced peak in the spectrum. The high-energy modes (the optical modes) are the results of the anti-phase precession of the spin moments. In such cases the transverse components of the spin moments may cancel out each other and hence no signal can be detected by SPEELS. The second reason might be the small excitation cross-section and the strong damping of the higher energy modes. The third reason might be due to the fact that the acoustic surface mode has the largest amplitude at the surface and the SPEELS technique is strongly surface sensitive.

In thin film systems monitoring the magnon excitation energy versus the film thickness would provide some information about the role of the surface structure and the interface effects on the magnons. Interestingly the measurements performed on ultrathin Co(0001) films on W(110) showed that the excitation energy slightly increases when the thickness of the Co layer increases [40]. The same behavior was observed for Co(001) films on Cu(001) [41]. The measurements performed on Fe(110) films with different thicknesses on W(110) revealed that the excitation energy shows an unusual thickness dependence [42]. Fig. 4 shows the excitation energy at a given wave vector ( $0.5 \text{ \AA}^{-1}$  or  $0.7 \text{ \AA}^{-1}$ ) versus the film thickness. The unusual thickness dependence of magnon energy could be understood in terms of lattice relaxation. Fe films grow pseudomorphically on W(110) from the initial stage of the growth up to a film thickness of about 2 monolayer (ML). As the third atomic layer is growing a network of dislocations start to form and the films start to relax towards the bulk structure [43–45]. This fact was confirmed by analysis of the LEED patterns recorded on the

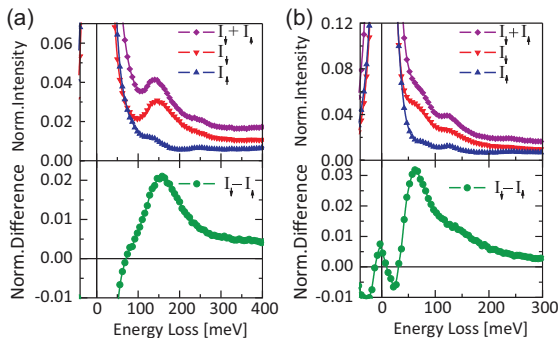


**Fig. 3.** Typical SPEELS spectra recorded at a wave vector of  $q_{\parallel} = 0.7(2) \text{ \AA}^{-1}$  on (a) an epitaxial Co(0001) film, with a thickness of 8 ML and (b) an epitaxial Fe(110) film with a thickness of 24 ML grown on W(110). The spectra are normalized to the total intensity of the quasi-elastic peak. The energy of incident beam was about  $E_i = 4 \text{ eV}$  for both cases. The peak in the minority spin channel ( $I_{\downarrow}$ ) is due to the magnon excitations. The difference spectra ( $I_{\downarrow} - I_{\uparrow}$ ) is shown in the lower panels.

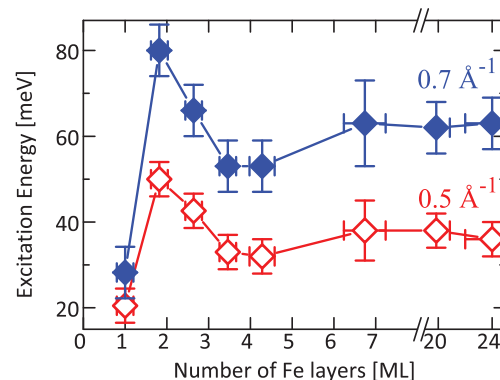


**Fig. 4.** Excitation energy at two different wave vectors ( $0.5 \text{ \AA}^{-1}$  and  $0.7 \text{ \AA}^{-1}$ ) versus the Fe film thickness in Fe(110)/W(110) structure [42]. The data of monolayer system are measured at 120 K and all other data are recorded at 300 K.

samples with different thicknesses. The small changes in the geometrical structure influence the electronic structure of the film and thereby changes the effective exchange interaction, which leads to a modification of the magnon energy (dispersion relation). This fact is confirmed by first-principles adiabatic spin dynamics calculations based on density-functional theory (DFT) [42]. Although within this approach the atomic magnetic moments are treated as rigid entities, which precess around the direction of the ferromagnetic ground state (similar to the Heisenberg model), the excitation energies are obtained by means of parameter-free DFT calculations. Within these calculations a mapping of the itinerant electron system onto a Heisenberg Hamiltonian is considered. The calculations performed within the framework of the itinerant electron theory also predicted that the magnon exchange stiffness ( $D = E/q^2$ , for  $q \ll \pi/a$ ) versus the number of Fe layers shall show a minimum at about 4 ML when the magnons are excited along the  $\bar{\Gamma} - \bar{H}$  direction of the surface Brillouin zone [20].

One of the important properties of magnons is the dispersion relation that connects the magnons' energy to their propagation wave vector. Since the main aim of the present paper is to discuss the surface magnons, we mainly discuss the results of magnon excitations in thicker films where the film thickness is large enough and the effects caused by the presence of the film/substrate interfaces are less important. Fig. 5 shows the surface magnon dispersion relation measured on a 24 ML Fe(1 1 0) film grown on W(1 1 0). The first attempt to understand the experimental data would be using the Heisenberg spin Hamiltonian discussed in Section 2. Starting with Eq. 6 and solving it for a system consisting of 24 slabs of Fe

in (1 1 0) structure results in 24 modes. The lowest mode is called the acoustic surface mode. The results of such a calculation are given in Fig. 5. For the first approximation we only consider the nearest neighbor coupling ( $J_{nn}$ ) and neglect the next nearest neighbor exchange interaction ( $J_{nns}$ ). In order to make a comparison to the bulk Fe, the value of  $J_{nn}S$  used for this calculation is obtained by fitting the available experimental data of the inelastic neutron scattering experiments measured by Lynn [46]. The fit to the experimental bulk dispersion results in a value of about  $J_{nn}S = 13.2$  meV (the fitting curve is shown by the solid red line in Fig. 5(a)). Taking this value and calculating the magnon dispersion relation for a slab consisting of 24 layers of Fe(1 1 0) results in the gray lines, presented in Fig. 5(a). As one can simply recognize from Fig. 5(a) the experimental magnon energies are smaller than the calculated acoustic surface mode of Fe(1 1 0) when the bulk exchange parameter is taken into account. If one tries to adopt the calculated dispersion relation to our experimental dispersion relation [see Fig. 5(b)] a value of about  $J_{nn}S = 9.8$  meV will be obtained. This implies that the effective exchange coupling at the surface is smaller than the one of bulk. In the next step one may also consider the next nearest neighbors. Again taking the experimental data of Lynn [46] for bulk dispersion and fitting the data with the next nearest neighbor Heisenberg model will result in  $J_{nn}S = 8.9$  meV and  $J_{nns}S = 0.6J_{nn}S$ . The results of such an analysis are presented in Fig. 5(c). The red solid curve is the bulk dispersion relation. The gray lines are the results of the Heisenberg model for 24 layers of Fe(1 1 0) in bcc structure, assuming the bulk exchange parameters. Fig. 5(c) indicates that the bulk parameters do not explain the surface magnon

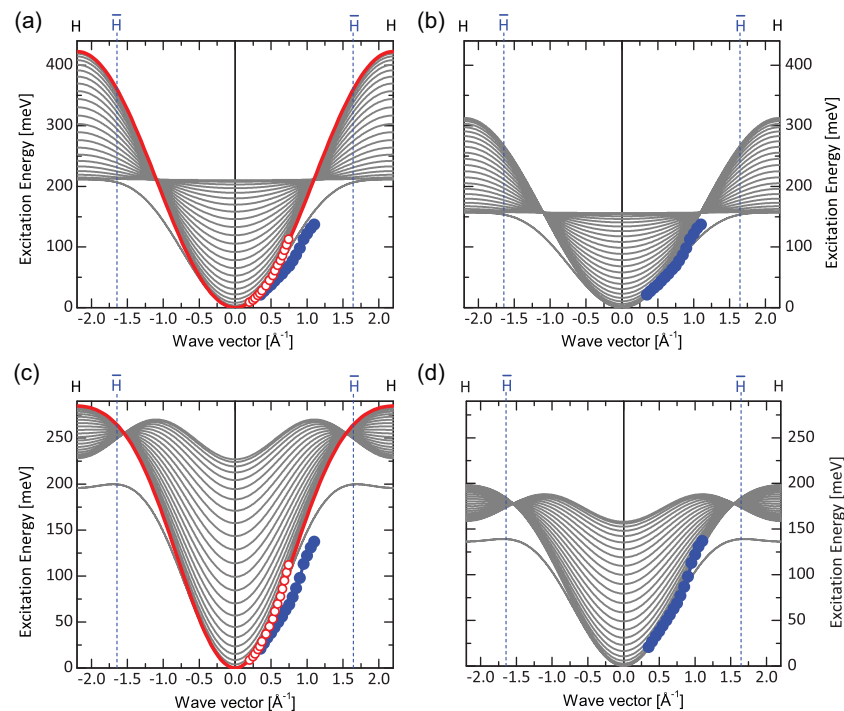


**Fig. 5.** The magnon dispersion relation. The experimental results of surface magnons measured by SPEELS are presented as solid circles. The results of bulk samples measured by inelastic neutron scattering by Lynn [46] are also plotted as open circles for a comparison. (a) The bulk dispersion relation is fitted to a nearest neighbor Heisenberg model (red solid line). The 24 ML film is modeled using the bulk value for  $J_{nn}S = 13.2$  meV (gray lines). (b) The nearest neighbor Heisenberg model is adopted to our results of surface magnon dispersion relation resulting in a value of  $J_{nn}S = 9.8$  meV. (c) The bulk dispersion relation is fitted to a next nearest neighbor Heisenberg model (red solid line). The 24 ML film is modeled using the bulk values [ $J_{nn}S = 8.9$  meV and  $J_{nns}S = 0.6J_{nn}S$  (gray lines)]. (d) The nearest neighbor Heisenberg model is adopted to the surface magnon dispersion relation resulting in values of  $J_{nn}S = 6.2$  meV and  $J_{nns}S = 0.6J_{nn}S$ .  $H$  and  $\bar{H}$  denote the bulk and surface Brillouin zone boundaries, respectively. (For interpretation of the references to color in the figure caption and in text, the reader is referred to the web version of the article.)

dispersion relation. A fit to our experimental data reveals that the effective exchange parameters at the surface are smaller than those of the bulk magnons [ $J_{nm}S = 6.2$  meV and  $J_{mnn}S = 0.6J_{nm}S$ , see Fig. 5(d)]. This means that the effective exchange parameter at the surface is smaller than in the bulk. A surface reduction of on-site exchange parameters is expected from a classical Heisenberg Hamiltonian [47,48]. This effect is explained in terms of a reduced coordination of surface atoms. However, ab initio electronic structure calculations has revealed that the interlayer exchange couplings derived from total-energy differences are enhanced at the surfaces over their bulk counterparts [47,48]. Interestingly, in the case of Co(0001) films on W(110) the measured surface magnon dispersion relation could be explained by using the bulk exchange parameter and taking the Heisenberg model [40,41]. In Co it is the nearest neighbor interaction that is important. The second nearest neighbor interaction is very small and can be neglected. It seems that in the case of Co the effective exchange coupling is not very sensitive to the small changes due to the surface effects. Again we would like to emphasize that such a comparison provides just a rough estimation of the effective exchange coupling of the system, since the Heisenberg picture is not an appropriate picture to describe the itinerant electron ferromagnets.

#### 4.2. The magnon lifetime

Another important result of our measurements is the estimation of the magnon lifetimes. The broadening of the spectra in energy (frequency) domain can be converted to lifetime. This can be done by a Fourier transformation of the magnon spectra. If one assumes a Lorentzian distribution for the peak in the difference spectra, the magnon lifetime can be simply calculated as following. The Fourier transform of a Lorentzian will be an exponential decay function. The lifetime of a magnon is defined as the time in which the amplitude of the magnon wave packet decays to  $e^{-1}$  of its original value at  $t=0$ . It is than given by this simple relation:

$$\tau = \frac{2\hbar}{\Delta E}, \quad (9)$$

where  $\tau$  is the magnon lifetime and  $\Delta E$  represents the intrinsic peak broadening in energy domain. In practice the measured difference spectra might be also affected by the experimental broadening. In order to consider this effect one may consider that the intensity profile is a convolution of a Lorentzian (describing the intrinsic broadening) and a Gaussian (caused by the experimental energy resolution) distribution. We observed in many cases that the experimental broadening has a small influence on the magnons, which have energies above 40 meV (the measured spectra can be fitted by a Lorentzian distribution). The typical values of the magnon lifetime for Fe films measured in our study is within the range of 10–100 fs (for the wave vector range of  $1.0$ – $0.4 \text{ \AA}^{-1}$ ). As an example, for the data shown in Fig. 3(b) the intrinsic broadening is about  $\Delta E \approx 54 \pm 10$  meV, which results in a lifetime of about  $\tau = 24 \pm 5$  fs.

#### 5. Conclusion

We presented the experimental results of short-wavelength magnon excitations at ferromagnetic surfaces probed by electrons in spin-polarized electron energy-loss spectroscopy. The strong interaction of the electrons with the ferromagnetic surface together with the spin degree of freedom enables one to investigate the surface magnons over the whole energy and momentum range up to the Brillouin zone boundary.

A comparison between Co(0001) and Fe(110) ultrathin films grown on W(110) shows that in contrast to the case of Co ultrathin films, the magnon energies of Fe films as a function of the film thickness show a minimum at about 4 ML, where the structural

relaxation takes place. This observation is attributed to the high sensitivity of the effective exchange interaction of the Fe films to the small changes in the structure.

The surface magnons of Fe(110) are softer than the one of Fe bulk meaning that the effective exchange parameter at the surface is smaller than the one in the bulk.

The high wave vector magnons possess very short lifetimes being of the order of few tens of femtoseconds. This means that the short-wavelength magnons are strongly confined in time as well as in space.

#### Acknowledgements

We acknowledge numerous discussions with the late D.L. Mills the grand pioneer of the theory of spin excitations in itinerant ferromagnets. We also acknowledge discussions with L.M. Sandratskii, A. Ernst, P. Buczek, L. Szunyogh, A.T. Costa and R.B. Muniz. We thank all the present and former co-workers: H. Ibach, R. Vollmer, M. Etzkorn, P.S. Anil Kumar, W.-X. Tang, J. Prokop, I. Tudosa, T.R.F. Peixoto and T.-H. Chuang who have contributed to some experiments discussed here.

#### References

- [1] S.A. Wolf, D.D. Awschalom, R.A. Buhrman, J.M. Daughton, S. von Molnar, M.L. Roukes, A.Y. Chtchelkanova, D.M. Treger, *Science* 294 (2001) 1488.
- [2] J.A.C. Bland, B. Heinrich, *Ultrathin Magnetic Structures. III: Fundamentals of Nanomagnetism*, Springer-Verlag, Berlin, Heidelberg, 2005.
- [3] A.J. Freeman, Ruqian Wu, *J. Magn. Magn. Mater.* 100 (1991) 497.
- [4] C.A.F. Vaz, J.A.C. Bland, G. Lauffhoff, *Rep. Prog. Phys.* 71 (2008) 056501.
- [5] M.N. Baibich, J.M. Broto, A. Fert, F. Nguyen Van Dau, F. Petroff, P. Etienne, G. Creuzet, A. Friederich, J. Chazelas, *Phys. Rev. Lett.* 61 (1988) 2472.
- [6] G. Binasch, P. Grünberg, F. Saurenbach, W. Zinn, *Phys. Rev. B* 39 (1989) 4828.
- [7] B. Heinrich, J.A.C. Bland, *Ultrathin Magnetic Structures. IV: Applications of Nanomagnetism*, Springer-Verlag, Berlin, Heidelberg, 2005.
- [8] J. Fernandez-Rossier, M. Braun, A.S. Núñez, A.H. MacDonald, *Phys. Rev. B* 69 (2004) 174412.
- [9] M. Elsen, O. Boulle, J.-M. George, H. Jaffres, R. Mattana, V. Cros, A. Fert, A. Lemaitre, R. Giraud, G. Faini, *Phys. Rev. B* 73 (2006) 035303.
- [10] B. Hillebrands, K. Ounadiela (Eds.), *Topics in Applied Physics*, vol. 83, Springer, Berlin, Heidelberg, New York, 2003.
- [11] D.L. Mills, S.M. Rezende, *Spin Dynamics in Confined Magnetic Structures. II*, Springer-Verlag, Berlin, Heidelberg, New York, 2003.
- [12] J. Lindner, K. Lenz, E. Kosubek, K. Baberschke, D. Spoddig, R. Meckenstock, J. Pelzl, Z. Frait, D.L. Mills, *Phys. Rev. B* 68 (2003) 060102.
- [13] K. Lenz, H. Wende, W. Kuch, K. Baberschke, K. Nagy, A. Jánossy, *Phys. Rev. B* 73 (2006) 144424.
- [14] Kh. Zakeri, J. Lindner, I. Barsukov, R. Meckenstock, M. Farle, U. von Hörsten, H. Wende, W. Keune, J. Rocker, S.S. Kalarickal, K. Lenz, W. Kuch, K. Baberschke, Z. Frait, *Phys. Rev. B* 76 (2007) 104416.
- [15] K. Baberschke, *Phys. Status Solidi B* 245 (2008) 174.
- [16] I.E. Dzyaloshinskii, *Sov. Phys. JETP* 5 (1957) 1259.
- [17] T. Moriya, *Phys. Rev.* 120 (1960) 91.
- [18] Kh. Zakeri, Y. Zhang, J. Prokop, T.-H. Chuang, N. Sakr, W.-X. Tang, J. Kirschner, *Phys. Rev. Lett.* 104 (2010) 137203.
- [19] R.B. Muniz, D.L. Mills, *Phys. Rev. B* 66 (2002) 174417.
- [20] R.B. Muniz, A.T. Costa, D.L. Mills, *J. Phys.: Condens. Matter* 15 (2003) S495.
- [21] A.T. Costa, R.B. Muniz, D.L. Mills, *Phys. Rev. B* 68 (2003) 224435.
- [22] A.T. Costa, R.B. Muniz, D.L. Mills, *Phys. Rev. B* 74 (2006) 214403.
- [23] R.B. Muniz, A.T. Costa, D.L. Mills, *IEEE Trans. Mag.* 44 (2008) 1974.
- [24] A.T. Costa, R.B. Muniz, J.X. Cao, R.Q. Wu, D.L. Mills, *Phys. Rev. B* 78 (2008) 054439.
- [25] E. Şaşıoğlu, A. Schindlmayr, C. Friedrich, F. Freimuth, S. Blügel, *Phys. Rev. B* 81 (2010) 054434.
- [26] P. Buczek, A. Ernst, P. Bruno, L.M. Sandratskii, *Phys. Rev. Lett.* 102 (2009) 247206.
- [27] P. Buczek, A. Ernst, L.M. Sandratskii, *Phys. Rev. Lett.* 105 (2010) 097205.
- [28] P. Buczek, A. Ernst, P. Bruno, L.M. Sandratskii, *J. Magn. Magn. Mater.* 322 (2010) 1396.
- [29] P. Buczek, A. Ernst, L.M. Sandratskii, *Phys. Rev. Lett.* 106 (2011) 157204.
- [30] W.X. Tang, Y. Zhang, I. Tudosa, J. Prokop, M. Etzkorn, J. Kirschner, *Phys. Rev. Lett.* 99 (2007) 087202.
- [31] J. Prokop, W.X. Tang, Y. Zhang, I. Tudosa, T.R.F. Peixoto, Kh. Zakeri, J. Kirschner, *Phys. Rev. Lett.* 102 (2009) 177206.
- [32] P. Buczek, A. Ernst, L.M. Sandratskii, *Phys. Rev. B* 84 (2011) 174418.
- [33] H. Ibach, D. Bruchmann, R. Vollmer, M. Etzkorn, P.S. Anil Kumar, J. Kirschner, *Rev. Sci. Instrum.* 74 (2003) 4089.



- [34] Kh. Zakeri, J. Kirschner, Probing Magnons by Spin-Polarized Electrons, in: S.O. Demokritov, A.N. Slavin (Eds.), *Topics in Applied Physics, Magnonics*, Springer-Verlag, Berlin, Heidelberg, 2012, [http://dx.doi.org/10.1007/978-3-642-30247-3\\_7](http://dx.doi.org/10.1007/978-3-642-30247-3_7).
- [35] J. Kessler, *Polarized Electrons*, Springer-Verlag, Berlin, Heidelberg, New York, Tokyo, 1985.
- [36] J. Kirschner, *Phys. Rev. Lett.* 55 (1985) 973.
- [37] J. Kirschner, *Springer Tracts in Modern Physics*, vol. 106, Springer, Heidelberg, 1985.
- [38] J. Kirschner, in: R. Feder (Ed.), *Polarized Electrons in Surface Physics*, World Scientific, Singapore, 1985.
- [39] Y. Zhang, P.A. Ignatiev, J. Prokop, I. Tudosa, T.R.F. Peixoto, W.X. Tang, Kh. Zakeri, V.S. Stepanyuk, J. Kirschner, *Phys. Rev. Lett.* 106 (2011) 127201.
- [40] M. Etzkorn, P.S. Anil Kumar, W. Tang, Y. Zhang, J. Kirschner, *Phys. Rev. B* 72 (2005) 184420.
- [41] M. Etzkorn, P.S. Anil Kumar, J. Kirschner, in: H. Kronmüller, S. Parkin (Eds.), *Handbook of Magnetism and Advanced Magnetic Materials*, vol. 3: *Novel Techniques for Characterizing and Preparing Samples*, Wiley & Sons, Ltd., 2007.
- [42] Y. Zhang, P. Buczek, L.M. Sandratskii, W.X. Tang, J. Prokop, I. Tudosa, T.R.F. Peixoto, Kh. Zakeri, J. Kirschner, *Phys. Rev. B* 81 (2010) 094438.
- [43] D. Sander, R. Skomski, C. Schmidhals, A. Enders, J. Kirschner, *Phys. Rev. Lett.* 77 (1996) 2566.
- [44] D. Sander, A. Enders, C. Schmidhals, D. Reuter, J. Kirschner, *Surf. Sci.* 402–404 (1998) 351.
- [45] H.J. Elmers, *Int. J. Mod. Phys. B* 9 (1995) 3115.
- [46] J.W. Lynn, *Phys. Rev. B* 11 (1974) 2624.
- [47] I. Turek, S. Blügel, G. Bihlmayer, P. Weinberger, *Czech. J. Phys.* 53 (2003) 81.
- [48] I. Turek, J. Kudrnovsky, V. Drchal, P. Bruno, *Philos. Mag.* 86 (2006) 1713.



## Elementary Excitations at Magnetic Surfaces and Their Spin Dependence

Y. Zhang,<sup>1,\*</sup> P. A. Ignatiev,<sup>1</sup> J. Prokop,<sup>1</sup> I. Tudosa,<sup>1</sup> T. R. F. Peixoto,<sup>1,2</sup> W. X. Tang,<sup>1,3</sup> Kh. Zakeri,<sup>1,†</sup>  
V. S. Stepanyuk,<sup>1,‡</sup> and J. Kirschner<sup>1</sup>

<sup>1</sup>Max-Planck-Institut für Mikrostrukturphysik, Weinberg 2, 06120 Halle, Germany

<sup>2</sup>Instituto de Física, Universidade de São Paulo, 05508-090, São Paulo, Brasil

<sup>3</sup>School of Physics, Monash University, Victoria 3800, Australia

(Received 27 October 2010; published 21 March 2011)

The elementary surface excitations are studied by spin-polarized electron energy loss spectroscopy on a prototype oxide surface [an oxygen passivated Fe(001)- $p(1 \times 1)$  surface], where the various excitations coexist. For the first time, the surface phonons and magnons are measured simultaneously and are distinguished based on their different spin nature. The dispersion relation of all excitations is probed over the entire Brillouin zone. The different phonon modes observed in our experiment are described by means of *ab initio* calculations.

DOI: 10.1103/PhysRevLett.106.127201

PACS numbers: 75.30.Ds, 63.20.D-, 63.20.kk, 75.47.Lx

It was realized at the very beginning of the development of the quantum theory of condensed matter that, although solids are composed of atoms, they cannot be described using atomic properties only. The reason lies in the collective phenomena that appears in solids. They should undoubtedly be taken into account when excitations are studied. Collective excitations in solids can be described by their representative quasiparticles. For instance, the collective modes of the lattice vibrations are well described by phonons. Phonons are characterized by their dispersion relation, which links the energies of the excitations to their propagating wave vectors. In magnetic solids there is another kind of collective excitation that originates from the precession of the atomic spins around their equilibrium position. Such excitations have a totally different nature and are called spin waves or magnons. Spin waves are also characterized by their dispersion relation and more importantly they carry a spin of  $1 \hbar$ . The above mentioned description of spin waves applies to the classical Heisenberg systems, where the spins are considered as localized moments. In itinerant ferromagnets, magnons can be also defined as electron-hole pair excitations, in which the spin orientation of the electron is opposite to the spin of the hole. From the energy point of view, phonons and magnons can have comparable energies and can coexist in a magnetic solid. The fundamental question in such a case is the following: How can one distinguish experimentally between these two different kinds of excitations, especially in low dimensional systems? The answer to this question is very important for deeper understanding of the lattice- and spin dynamics at surfaces and nano-objects.

In this Letter we report on the first simultaneous observation and unambiguous separations of phonons and magnons. Measurements are performed by means of a spin-polarized version of high resolution electron energy loss spectroscopy technique (SPEELS) [1–3]. We demonstrate that the spin degree of freedom of the incoming beam

can be used for clarifying the nature of different types of excitations observed at the surface despite the fact that phonons show a significant spin dependence in the scattering of electrons. As an example we show the results of a high quality oxygen passivated Fe(100) surface [4,5] [see Fig. 1(a)].

The inelastic scattering of low-energy electrons is usually considered as a superposition of the contributions from dipole and impact scattering. Originating from the Coulomb interaction between the incoming electrons and the dipolar electric field at the surface, dipole scattering does not reveal any asymmetry with respect to the spin orientation of incident electrons. In the impact scattering, the incident electrons interact with electrons of the solid and such an interaction can involve exchange processes, which is usually referred to as exchange scattering. Within the exchange scatterings, the incident electron may transfer its energy to another electron in the sample, and the latter one is thus scattered out of the surface. In specular geometry ( $\theta_i = \theta_f$ ), dipole scattering is usually a dominant process; however, at a magnetic surface the impact scattering can be rather pronounced and even comparable to the dipole scattering [6,7].

A schematic illustration of the scattering geometry in our SPEELS experiments is given in Fig. 1(b). In the experiment, an electron beam with energy  $E_i$  and spin  $\sigma_i$  is focused onto the sample surface. The angle- and energy-resolved intensity  $I(\theta_f, E_f)$  of backscattered electrons is recorded and analyzed. The energy conservation law provides a direct access to the energy  $\epsilon_{h\omega}$  of excitations, which can be obtained from  $\epsilon_{h\omega} = E_f - E_i$ , and zero energy is defined by the incident electron energy. A fraction of the backscattered electrons change their energy by  $\epsilon_{h\omega}$ , thus surface excitations can be observed as peaks in intensity spectrum centered exactly at excitation energies  $\epsilon_{h\omega}$ . An example of such spectra acquired for different spin directions of incident electrons at  $E_i = 4.1$  eV,  $\theta_i = 29.2^\circ$ ,

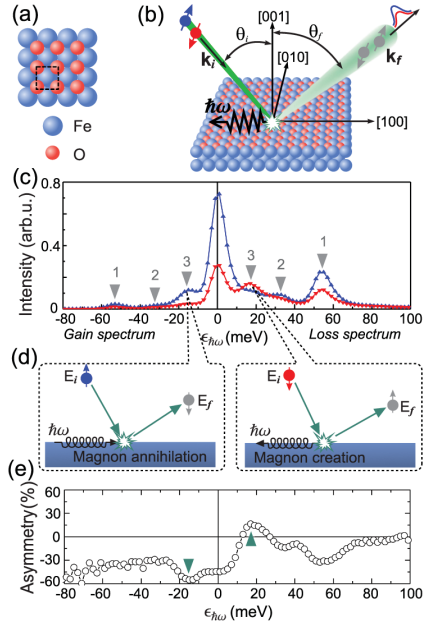


FIG. 1 (color). (a) Model of O/Fe(001)- $p(1 \times 1)$  surface. Surface  $p(1 \times 1)$  unit cell is marked with dashed black square. (b) Scheme of SPEELS experiments. Electron beam with energy  $E_i$ , momentum  $\mathbf{k}_i$ , spin  $\sigma_i$  (real polarization of  $70 \pm 10\%$ ) is aligned in the (010) plane with the angle  $\theta_i$  to the surface normal. The intensity of backscattered electrons at angle  $\theta_f$  is analyzed. The notched line represents an excited quasiparticle with energy  $\hbar\omega$  created due to inelastic scattering events. (c) SPEEL spectra of the O/Fe(001)- $p(1 \times 1)$  surface measured at  $\theta_i = 29.2^\circ$ ,  $\theta_f = 50.8^\circ$ . The blue and red curves are obtained with the spin of incident electrons parallel to that of the majority (spin-up) and minority (spin-down) electrons in the sample, respectively. The primary electron energy  $E_i$  is 4.1 eV. The twinned excitations marked by numbers are observed in loss and gain regions at room temperature. (d) Illustration of magnon creation and annihilation processes. Magnons can be created only by spin-down electrons, while they are annihilated only by spin-up electrons. (e) Asymmetry calculated using Eq. (1). Magnon excitations are marked by triangles.

$\theta_f = 50.8^\circ$  is given in Fig. 1(c). Spectra with positive and negative energies  $\epsilon_{\hbar\omega}$  are named as loss and gain spectra, respectively. This notation reflects the direction of the energy transfer during the scattering event. Excitation peaks in loss and gain spectra are “twinned” in a sense that electrons can both create certain quasiparticles losing energy  $\epsilon_{\hbar\omega}$ , and annihilate the thermally excited ones gaining energy  $\epsilon_{\hbar\omega}$ . The twinned loss and gain peaks are marked with the same numbers.

As a magnon excitation corresponds to a spin flip in the sample, if the incoming electron is of minority character with a spin of  $-1/2 \hbar$  then, according to total angular momentum conservation rule, the outgoing electron has to be of majority character with a spin of  $+1/2 \hbar$ , after the excitation of a magnon. It is worthwhile to emphasize that

the apparent “spin flip” between the spins of incident and outgoing electrons occurs due to an exchange of the incident electron with one of the sample electrons instead of a real spin reversal [8,9]. An incident electron with minority character occupies a state above the Fermi level, and an electron with majority character from a state slightly below the Fermi level is scattered out. The interaction is of a pure Coulomb nature. The process occurs within a few attoseconds and without any energy dissipation. The time reversal process happens for the incidence of majority electrons, i.e., the annihilation of a magnon. The creation and annihilation processes of magnons are sketched in Fig. 1(d). The magnon creation peak in the loss spectrum appears only when incident electrons are of minority character, while the magnon annihilation peak in the gain spectrum is only produced by majority electrons. Since phonons are spin-independent quasiparticles, they can be created and annihilated by incident electrons of both spin characters. This particular dependence of magnon creation and annihilation on the spin of incident electrons, as opposed to phonons, is a fundamental feature, which allows us to distinguish between magnons and phonons in SPEELS experiments.

To judge the type of the excitations on their spin-flip or non-spin-flip natures, the straightforward way is to know the spin orientations of the electrons before and after the scattering event. This might be realized by using a spin-polarized electron source and a spin detector after scattering [9]. However, such an experiment demands a rather high feeding current for the analysis of outgoing spins. One has to sacrifice the energy resolution to achieve enough beam intensity, which then loses the information concerning the low-energy excitations. In the present work we will show that, for low-energy excitations where the energy is comparable to the thermal energy, it is possible to discriminate phonons and magnons without further spin analysis of the backscattered electrons. The differentiation procedure based on the nature of the magnons and phonons is discussed below.

Quantitatively, the spin dependence of backscattered intensity can be characterized by the spin asymmetry defined as

$$A(\epsilon_{\hbar\omega}) = \frac{I_1(\epsilon_{\hbar\omega}) - I_1(\epsilon_{\hbar\omega})}{I_1(\epsilon_{\hbar\omega}) + I_1(\epsilon_{\hbar\omega})}, \quad (1)$$

where  $I_1(\epsilon_{\hbar\omega})$  and  $I_1(\epsilon_{\hbar\omega})$  are SPEEL spectra measured with spin-down and spin-up polarizations of incident electron beams, respectively. To reveal the nature of an excited quasiparticle, one has to compare the signs of spin asymmetries shown in Fig. 1(e) at energies of peaks in loss and gain spectra. Asymmetries of loss and gain spectra of excitation “3” at energies of  $-16$  and  $16$  meV are of opposite signs as it is marked with arrows in Fig. 1(e); therefore, peaks are associated with magnon excitations. Asymmetry of excitation “1” and “2” at  $\pm 53$  and  $\pm 33$  meV have the same sign and almost identical magnitudes; hence, these excitations are phonons [10].

Interestingly, in our case the asymmetries of phonon peaks are always negative. It is most likely related to the strong exchange scattering between the incoming electrons and the electrons at the sample surface. To clarify the origin of the spin asymmetries observed on phonons, we measured the spin-resolved intensities for elastically and inelastically ( $E_{\text{loss}} = 53$  meV) scattered electrons with respect to the incident electron energy (see the upper and lower panels of Fig. 2(a), respectively). It is clear that presented intensities are very similar, except for the fact that the intensity of the inelastically scattered electrons is 2 orders of magnitude smaller. It is known that the spin asymmetry of elastically scattered electrons has to be caused by the exchange scattering, as dipolar scattering does not involve the electron's spin. In this case the exchange scatterings only involve the electrons with the same spin orientation. Otherwise, it would lead to a change of energy (as the incident electron must come to an unoccupied state above the Fermi level, the one with the opposite spin leaves the system from a state below the Fermi level and this leads to an energy change). As it is demonstrated in Fig. 2(b), the asymmetry curves of the inelastic excitation at 53 meV are almost identical to those of the elastic peak in all scattering geometries. Therefore, it is highly possible that the physical origin of the observed large spin asymmetries for both the elastic and inelastic intensities are the same, mainly the exchange scattering of electrons with the same spin. Therefore, the similarity of the spin asymmetry for the elastic and inelastic scatterings strongly suggests that the inelastic peak at 53 meV is also of the non-spin-flip nature and the observed high asymmetry is due to the exchange of the electrons with the same spin

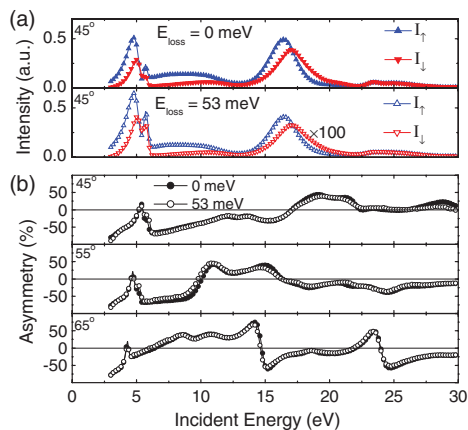


FIG. 2 (color). (a) Intensity of backscattered electrons as a function of the incident energy in the specular geometry recorded for elastically ( $E_{\text{loss}} = 0$  meV, upper panel) and inelastically ( $E_{\text{loss}} = 53$  meV, lower panel) scattered electrons. The incident angle is  $45^\circ$  and marked in the graphs. (b) The asymmetry curves for the elastically ( $\bullet$ ) and inelastically ( $\circ$ ) scattered electrons measured at specular geometry and the angles of  $\theta_i = \theta_f = 45^\circ, 55^\circ,$  and  $65^\circ$ .

character. The same arguments apply to the other phonon excitations.

The momentum conservation law provides a direct access to the quasiparticles momenta  $\mathbf{q}_{\parallel} = \mathbf{k}_i \sin\theta_i - \mathbf{k}_f \sin\theta_f$ . It is important to emphasize that this relation is valid only for momenta lying in the incident plane, and SPEELS does not probe excitations with momenta perpendicular to this plane. In our experiments, the incident plane of the electron beam is (010) plane and only surface excitations with nonzero  $x$ - and  $z$ - momenta lying at the  $\bar{\Gamma} - \bar{X}$  section of the reciprocal space are probed. To plot the entire excitations band structure we examined the back-scattered intensities of both loss and gain spectra. The intensity spectra recorded for different wave vectors are presented in Figs. 3(a) and 3(b). A careful fitting of the spectra with a superposition of Gaussian peaks revealed five excitation branches in both energy loss and energy gain spectra. Centers of the fitted peaks are marked in Figs. 3(c) and 3(d) with symbols. Phonon branches labeled 1, 2, 4, and 5 are represented by open symbols, while a magnon branch labeled 3 is plotted by filled symbols. The nature of those quasiparticles is clarified from the asymmetries of the gain and loss peaks as it is sketched in Figs. 1(c) and 1(d). Magnon branch clearly disperses from 16 to about 40 meV as the wave vector increases from 0.2 to 0.7  $\text{\AA}^{-1}$ . Magnon excitation peaks become much more broad at high wave vectors. This broadening can be explained by a strong decay of magnons in the itinerant electron system. In this case, the simple Heisenberg model cannot be applied to describe the spin wave dispersion in metal thin films, especially in the wave vector range that SPEELS measures [3,11].

To shed light on the origin of all the observed phonon modes we performed calculations of the harmonic phonons of the O/Fe(001)- $p(1 \times 1)$  surface by means of the direct calculations of the force matrix [12,13]. Surface was simulated with a slab built from 11 layers of bcc Fe stacked in the [001] direction. One side of the slab was covered by a layer of oxygen placed in hollow sites of Fe(001) and the whole system was relaxed. Hellmann-Feynman forces used to construct the force matrix were calculated from the first principles by means of the Vienna *ab initio* simulation package (VASP) [14]. The phonon band structure calculated with the help of the force matrix was projected on surface atoms of the system and on particular polarizations (or Cartesian directions) of oscillations. Figures 3(c) and 3(d) show the spectral densities of phonons projected on the oxygen and the topmost Fe atoms. Only phonons with  $x$ - and  $z$  polarization (displacement direction) lying in the incident (010) plane are taken into account in Figs. 3(c) and 3(d) because the SPEELS is sensitive exactly to these excitations due to the selection rules [15]. Based on the theoretical calculations, we conclude all the phonon excitations as follows: the phonon branch 5 with the lowest energy [right-oriented triangles in Figs. 3(c) and 3(d)] originates from the acoustical  $z$ -polarized transversal

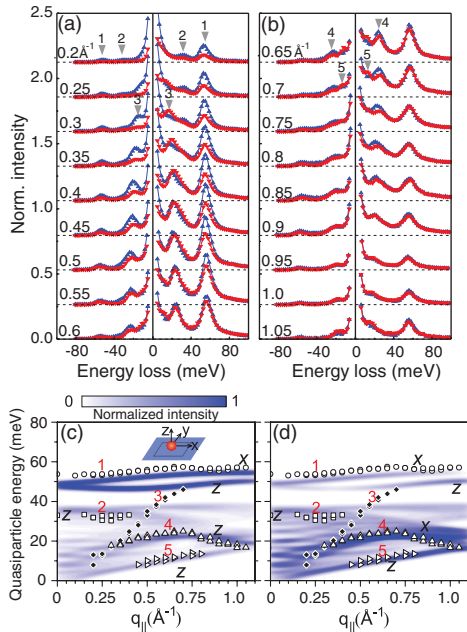


FIG. 3 (color). (a) and (b) SPEELS spectra measured on O/Fe(001)- $p(1 \times 1)$  with the spin of incident electrons parallel to that of the majority (blue curve) and minority (red curve) electrons. The corresponding in-plane wave vectors are marked in the graphs. The spectra have been shifted to have a clear view. Theoretically calculated phonon spectral density maps projected on (c) the oxygen layer and (d) the topmost Fe layer. Symbols represent the phonon and magnon peaks in the experimental data. Open symbols denote the phonon branches numbered by 1, 2, 4 and 5; filled symbol denotes the magnon branch and is numbered by 3. Letters “x”, “y”, and “z” near each of the pronounced phonon bands denote displacement directions of the corresponding phonons. The corresponding directions are illustrated in the inset of (c).

oscillations of the topmost Fe and O layers. It is the so-called Rayleigh wave of the O/Fe(001)- $p(1 \times 1)$  surface, which has been also observed in the He-atom scattering experiments [16]. The next phonon branch 4 shown in Figs. 3(c) and 3(d) with upward-oriented triangles is also localized in the two topmost layers. In the Fe layer branch 4 is a longitudinal acoustic phonon with  $x$  polarization, while in the O layer it is transversal with  $z$  polarization. Phonon branch 2 spreading off the  $\Gamma$  point at the energy of  $\approx 33$  meV plotted with squares in Figs. 3(c) and 3(d) is a  $z$ -polarized surface resonance of the phonons of the Fe slab. Two high-energy branches at  $\approx 50$  meV are optical  $z$ -transversal and  $x$ -longitudinal phonons localized mostly at the oxygen atoms. The agreement with experimental results for these excitations is not so sharp as in the above cases, but these phonons can still be associated with the excitation branch 1 at  $\approx 55$  meV plotted in Figs. 3(c) and 3(d) with circles. The differences between the experiment and the theory can be explained by the anharmonic

contribution to oxygen vibrations, which couples the  $x$ - and  $z$ -polarized phonon modes. Our theory has not revealed any traces of excitation branch 3, which indicates that it is not a phonon as was also confirmed by our experiments.

In summary, by presenting the example of the O/Fe(001)- $p(1 \times 1)$  surface, we have demonstrated the fundamental possibility to identify the spin-flip and non-spin-flip nature of different excited quasiparticles among the vast variety of loss and gain features observed in SPEELS. This ability is achieved by controlling the spin of incident electrons. The magnon and phonon are unambiguously distinguished based on their spin nature and their dispersion relation is measured over the whole Brillouin zone. Our *ab initio* calculations successfully described all the observed phonon branches. We hope that our results could open a way towards a better understanding of the quasiparticles involved in lattice- and spin dynamics and their possible coupling, in particular, in the multifunctional complex hybrid and oxide materials as well as strongly correlated electron systems.

The authors thank A. Winkelmann for many interesting discussions. T. R. F. P. gratefully acknowledges the support of CNPq-Brasil. The authors also acknowledge the valuable discussions with D. L. Mills and R. Q. Wu. The work was partly supported by SFB 762 of the Deutsche Forschungsgemeinschaft.

\*zhangyu@mpi-halle.de

†zakeri@mpi-halle.de

‡stepanyu@mpi-halle.de

- [1] H. Ibach *et al.*, *Rev. Sci. Instrum.* **74**, 4089 (2003).
- [2] R. Vollmer *et al.*, *Phys. Rev. Lett.* **91**, 147201 (2003).
- [3] W. X. Tang *et al.*, *Phys. Rev. Lett.* **99**, 087202 (2007).
- [4] A. Tange *et al.*, *Phys. Rev. B* **81**, 220404 (2010).
- [5] S. S. Parihar *et al.*, *Phys. Rev. B* **81**, 075428 (2010).
- [6] R. Feder, *Polarised Electrons in Surface Physics* (World Scientific, Singapore, 1985).
- [7] J. Kirschner, *Polarised Electrons at Surfaces* (Springer, Berlin/Heidelberg, 1985).
- [8] M. Plihal, D. L. Mills, and J. Kirschner, *Phys. Rev. Lett.* **82**, 2579 (1999).
- [9] J. Kirschner, *Phys. Rev. Lett.* **55**, 973 (1985).
- [10] J. P. Lu *et al.*, *Surf. Sci.* **215**, 348 (1989).
- [11] A. T. Costa, R. B. Muniz, and D. L. Mills, *Phys. Rev. B* **70**, 054406 (2004).
- [12] K. Parlinski, Z.-Q. Li, and Y. Kawazoe, *Phys. Rev. Lett.* **78**, 4063 (1997).
- [13] <http://jaist.dl.sourceforge.net/project/frophi/>
- [14] G. Kresse and J. Hafner, *Phys. Rev. B* **48**, 13 115 (1993); G. Kresse and J. Furthmüller, *Phys. Rev. B* **54**, 11 169 (1996). G. Kresse and J. Furthmüller, *Comput. Mater. Sci.* **6**, 15 (1996).
- [15] H. Ibach and D. L. Mills, *Electron Energy Loss Spectroscopy and Surface Vibrations* (Academic Press, New York, 1982).
- [16] G. Fahsold *et al.*, *Appl. Surf. Sci.* **137**, 224 (1999).

## Magnons in a Ferromagnetic Monolayer

J. Prokop,<sup>1</sup> W. X. Tang,<sup>1</sup> Y. Zhang,<sup>1</sup> I. Tudosa,<sup>1</sup> T. R. F. Peixoto,<sup>1,2</sup> Kh. Zakeri,<sup>1</sup> and J. Kirschner<sup>1</sup><sup>1</sup>Max-Planck-Institut für Mikrostrukturphysik, Weinberg 2, D-06120 Halle, Germany<sup>2</sup>Instituto de Física, Universidade de São Paulo, 05508-900, São Paulo, SP, Brazil

(Received 8 December 2008; published 30 April 2009)

We report the first observation of high wave vector magnon excitations in a ferromagnetic monolayer. Using spin-polarized electron energy loss spectroscopy, we observed the magnon dispersion in one atomic layer (ML) of Fe on W(110) at 120 K. The magnon energies are small in comparison to the bulk and surface Fe(110) excitations. We find an exchange parameter and magnetic anisotropy similar to that from static measurements. Our results are in sharp contrast to theoretical calculations, indicating that the present understanding of magnetism of the ML Fe requires considerable revision.

DOI: 10.1103/PhysRevLett.102.177206

PACS numbers: 75.30.Ds, 75.50.Bb, 75.70.Ak, 75.70.Rf

Quasiparticles play a fundamental role in nature. In magnetism, elemental magnetic collective excitations (magnons) are essential for explaining magnetic ordering [1,2] and electron and spin dynamics [3]. The magnons are of great importance also for modern spintronic devices [4–7]. Of particular interest are high wave vector excitations that are determined by exchange interaction, and occur on the scales of femtoseconds and nanometers [8–10]. However, the magnon excitations in a ferromagnetic monolayer (FML) have been never studied experimentally, even though the spin dynamics of FML belongs to one of the most fundamental problems of magnetism. The experimental techniques enabling magnon investigation either do not have the required monolayer sensitivity, as in inelastic neutron scattering (INS) [11], or probe only a small region of the momentum space close to the Brillouin zone center, as in Brillouin light scattering (BLS) [12,13], and ferromagnetic resonance (FMR) [14,15] experiments. Even inelastic scanning tunneling spectroscopy (ISTS), recently adopted to a magnon investigation in ultrathin films [16,17], cannot probe the surface states selectively due to a lack of in-plane momentum resolution.

The magnetic excitations in two-dimensional spin systems have been studied theoretically for many years [1,18–26]. According to the Mermin-Wagner theorem, a two-dimensional spin system with an isotropic and short-range interaction cannot exhibit any long-range magnetic order at finite temperatures [27]. However, arbitrarily small anisotropies or dipolar interactions are, in turn, sufficient to stabilize long-range magnetic order [18,28], and the FMLs reveal substantial Curie temperatures [29]. Yet, the experimental magnon spectrum in such spin systems is unknown.

In this Letter, we report the first observation of the high wave vector magnon excitations in the ferromagnetic Fe monolayer (ML). Using spin-polarized electron energy loss spectroscopy (SPEELS), we measured the magnon dispersion in pseudomorphic 1 ML Fe epitaxially grown on W(110). We find that the exchange and magnetic an-

isotropy constants are similar to that obtained from static measurements on vicinal W(110) [30]. We show that the magnons in the Fe ML are much softer than in the bulk Fe, and the surface Fe mode. Surprisingly, the measured magnon energies in 1 ML Fe are much smaller than theoretically predicted [22,25,26]. This discrepancy, related to the strong magnon softening, indicates that the present understanding of the magnetism of the ML Fe is not complete. Our results support the hypothesis that 1 ML Fe/W(110) may not be a simple ferromagnet, as usually assumed.

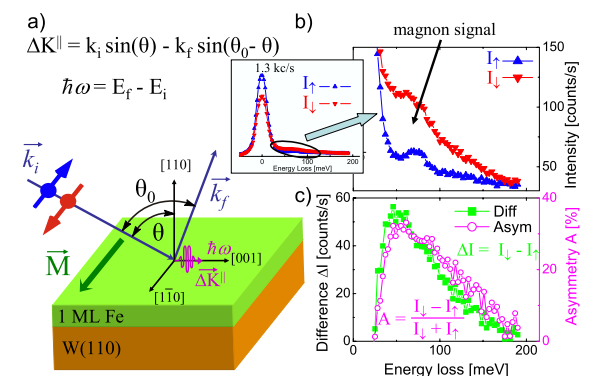


FIG. 1 (color online). (a) The geometry of our SPEELS experiment. A monochromatic spin-polarized electron beam with a polarization parallel or antiparallel to the sample magnetization ( $\vec{M}$ ) is scattered along the [001] direction from the Fe(110) monolayer in the remanent state. The degree of polarization  $P$ , in the present case, is  $0.7 \pm 0.1$ . The scattering angle is kept at  $\theta_0 = 80^\circ$ .  $k_i$  and  $k_f$  are the magnitudes of the wave vectors of the incident and scattered electrons, respectively. The inset shows the intensity  $I_1$  and  $I_2$  SPEELS spectra, as measured for 1 ML Fe/W(110) at 120 K, using electrons with energy  $E_i = 3.8$  eV at  $\Delta K^\parallel = 1.0 \text{ \AA}^{-1}$ . The energy resolution is  $\Delta E_i = 16$  meV. (b) The magnified spectra from the inset in (a). (c) The difference and asymmetry spectra clearly showing the magnon signal.

The 1 ML Fe on W(110) is a unique prototype system that has been intensively studied on both flat [29,31–34] and vicinal substrate surfaces [30,35,36]. Here, we used a flat W single crystal, prepared by cut at  $0^\circ \pm 0.1^\circ$  angle, with an average step width of 150 nm. We took advantage of the fact that the iron monolayer is thermodynamically stable even up to very high temperatures [32], which enables preparation of the homogenous Fe ML with good crystalline structure and morphology [29,36]. The experiments were performed in an ultrahigh vacuum (UHV) system with a base pressure of  $3 \times 10^{-11}$  mbar. Special care has been taken concerning the cleaning of the W crystal, which, initially performed under conditions proposed recently [37], has been improved by monitoring the thermal desorption spectra of CO. The iron layers were deposited onto a clean W(110) single crystal at room temperature (RT), and subsequently annealed at about 900 K. Prior to the SPEELS measurements, the sample was cooled down to 120 K. In order to assure that the MLs reproduce properties reported in the literature [29,31], LEED and MOKE measurements were performed after sample preparation. The pseudomorphic ML Fe is ferromagnetic below a Curie temperature of 223 K, and reveals an uniaxial magnetic anisotropy with an in-plane easy axis along the  $[1\bar{1}0]$  direction [31]. The SPEELS measurements were performed using a high performance spectrometer described elsewhere [38].

The geometry of the SPEELS experiment is shown in Fig. 1(a). The spin-polarized electrons are scattered from a magnetically ordered sample, and the electron energy loss spectra are measured as a function of the spin polarization of the electron beam, and of the electron momentum transfer. The surface magnons are excited in a spin dependent inelastic electron scattering process [8–10]. The conservation of angular momentum during the scattering forbids the magnon excitation for incoming electrons of the spin polarization antiparallel ( $I_\uparrow$ ) to the sample magnetization. Therefore, the magnon signal can be obtained by calculating the difference between the two spectra measured for the incident electrons with minority and majority spin directions.

The inset in Fig. 1(a) shows the intensity  $I_\uparrow$  and  $I_\downarrow$  SPEELS spectra obtained for 1 ML Fe/W(110) at 120 K. These spectra are magnified in Fig. 1(b). The difference ( $\Delta I = I_\downarrow - I_\uparrow$ ) and asymmetry [ $A = (I_\downarrow - I_\uparrow)/(I_\downarrow + I_\uparrow)$ ] spectra are shown in Fig. 1(c). The SPEELS spectra are dominated by a diffuse elastic peak at zero energy loss. However, there is a fine feature which arises from the shoulder of the elastic peak in the minority spectrum  $I_\downarrow$ , shown in Fig. 1(b), which is attributed to the magnon excitation [8–10]. In addition to the magnon feature, small peaks around 70 meV, originating from vibrational states of adsorbed oxygen, are observed in the SPEELS spectra [39,40]. Because of the high surface sensitivity of EELS [39], these vibrational peaks are easily visible, even for the

weakly contaminated Fe films [40]. It is interesting that the magnon feature does not appear as a sharp peak in the intensity spectra [9,10]. This observation can be partially explained by a strong damping of the magnons in ML Fe/W(110) leading to a severe broadening of the magnon peaks [20,22,25]. Note that the magnon signal can be clearly distinguished in the difference and asymmetry spectra. For this peak a relatively high asymmetry of 30% is observed (45% after corrections due to the incomplete polarization  $P$  of the electron beam). The magnon peaks measured at lower wave vectors are obstructed by the quasielastic peak, whose sign and nature are different from the magnon excitation [8].

Figure 2(a) shows a series of normalized difference spectra taken for different  $\Delta K^\parallel$  along the  $[001]$  direction. With an increase of the wave vector, we observe a decrease of the intensity and broadening of the magnon peaks [9,10]. By plotting the energy positions of the magnon peaks as a function of the wave vector, we obtain the dispersion relation, as shown in Fig. 2(b). Calculations performed in the frame of the itinerant electrons model predict magnon energies much higher (6 times) than those obtained experimentally [22,25]. Such a large discrepancy

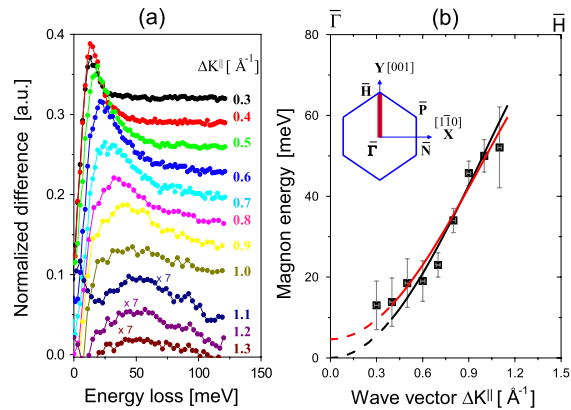


FIG. 2 (color online). (a) Series of normalized difference SPEELS  $\Delta I$  spectra measured for 1 ML Fe/W(110) at 120 K for different  $\Delta K^\parallel$  values, as denoted. The spectra are offset by 0.05 with respect to each other. Because of the low energy ( $E_i = 3.8$  eV) of the incident electrons, the parallel wave vector transfer is limited to the value of  $1.05 \text{ \AA}^{-1}$  (for  $\theta_0 = 80^\circ$ ). The higher wave vector excitations (above  $1.0 \text{ \AA}^{-1}$ ) are measured with a higher incident electron energy ( $E_i = 6.25$  eV) and a lower resolution ( $\Delta E = 18$  meV). (b) The magnon energy versus parallel wave vector transfer  $\Delta K^\parallel$ , as derived from the peak position in the difference SPEELS spectra observed in (a). Red (or gray) and black curves are fits to the dispersion obtained from the Heisenberg model with and without the anisotropy gap, respectively. The inset shows the 2D surface Brillouin zone of the bcc (110) surface with the states probed along the  $[001]$  direction.



cannot be explained only by the experimental uncertainties [25,41].

We now attempt to estimate the exchange parameter for the ML Fe using a solution of the Heisenberg Hamiltonian, where only the nearest neighbor interactions are taken into account. We consider the Heisenberg Hamiltonian:  $H = -(1/2)J\sum_{\langle i,j \rangle} S_i S_j - K_{\text{eff}} \sum_i (S_i \cdot \hat{n})^2$ , where  $J$  denotes the isotropic exchange coupling constant between spins  $S_i$  and  $S_j$ . Since our data suggest a gap in the magnon dispersion, as one may expect for a spin system with magnetic anisotropy [19,23–26], we add a term representing the effective magnetic anisotropy  $K_{\text{eff}}$ , with an easy axis along the unit vector  $\hat{n}$  (the  $[1\bar{1}0]$  direction). Assuming that we probe states along only the  $\bar{\Gamma} - \bar{H}$  ( $[001]$ ) direction, for the bcc(110) monolayer, one finds:  $\hbar\omega(\Delta K^{\parallel}) = 4JS[1 - \cos(\Delta K^{\parallel} a_0/2)] + 2K_{\text{eff}}S$ . Here,  $S$  is the magnitude of the spin per atom, and  $a_0 = 3.165 \text{ \AA}$  is the lattice constant of the pseudomorphic 1 ML Fe/W(110).  $JS$  and  $2K_{\text{eff}}S$  are treated as free parameters. The points measured above  $1.1 \text{ \AA}^{-1}$  showed very large errors and were omitted. Without the anisotropy, we find  $JS = 12.5 \pm 1 \text{ meV}$ . The best fit is obtained with  $JS = 11 \pm 1 \text{ meV}$  and  $2K_{\text{eff}}S = 4.6 \pm 2.5 \text{ meV}$ . The fits are shown in Fig. 2(b). The obtained value is in very good agreement with the  $JS^2$  value estimated from the static analysis of the magnetic domain wall in 1 ML Fe on vicinal W(110), where the  $JS^2$  ( $S = 1$ ) of  $14 \text{ meV}$  (at 14 K) is reported [30]. The value obtained here is also close to the  $J$  value ( $8.6 \text{ meV}$ ) derived from the two-dimensional Ising model [30]. The obtained anisotropy constant  $2K_{\text{eff}}S$  is similar to the effective anisotropy ( $4.2 \text{ meV/atom}$  at 14 K) reported in [30]. It is also in good agreement with the calculated values [25,26,42]. Our measurements of the ML dynamics provide exchange and anisotropy constants similar to that obtained from the static measurements.

Figure 3 shows the magnon dispersion for the bulk bcc Fe, and for the Fe/W(110) films of different Fe thicknesses: 1, 2, and 24 ML obtained by SPEELS [10]. Data for bulk Fe are represented by the black curve  $D(\text{bulk})\Delta K^{\parallel 2}(1 - \beta\Delta K^{\parallel 2})$ , with magnon stiffness coefficient  $D(\text{bulk}) \approx 280 \text{ meV \AA}^2$ , obtained from the neutron scattering measurements at RT [43]. The data for the double layer (DL) and 24 ML Fe films are measured at RT. The magnon dispersion for the 24 ML Fe/W(110) film is introduced because this sample enables a comparison between the dispersions of the bulk magnons and the surface modes on the Fe(110) surface [34]. The solid lines are guides to the eye obtained from a fit to the SPEELS data using the above formula with  $D(\text{DL}) = 180 \text{ meV \AA}^2$  and  $D(\text{surf}) = 160 \text{ meV \AA}^2$ . For the ML Fe at 120 K, we find  $D(\text{ML}) = 74 \pm 5 \text{ meV \AA}^2$ . In the following discussion we neglect  $\beta$  coefficients.

For the first time, we can directly compare the magnon dispersion for the Fe systems, where the number of the

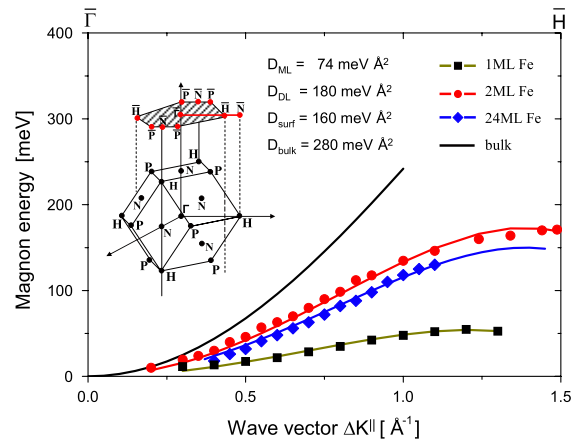


FIG. 3 (color online). Magnon dispersions for the different Fe systems. Black line denotes the parabolic magnon dispersion for the bcc Fe bulk  $D\Delta K^{\parallel 2}(1 - \beta\Delta K^{\parallel 2})$ , with  $D \approx 280 \text{ meV \AA}^2$ , compiled using the INS data [43]. The dispersions obtained by the SPEELS at RT for the 2 ML Fe/W(110), and for 24 ML Fe/W(110), are plotted using circles and diamonds, respectively. Squares indicate data for the 1 ML Fe/W(110) measured at 120 K. The solid lines are guides to the eye based on the same formula  $[D\Delta K^{\parallel 2}(1 - \beta\Delta K^{\parallel 2})]$ , with different  $D$  and  $\beta$ . The relation between the bulk Brillouin zone and the two-dimensional Brillouin zone of the (110) surface (shaded area) is shown in the inset.

nearest iron neighbors is systematically reduced, from 8 in bulk to 4 in the ML Fe. The bulk magnons have the highest energies, higher than the surface mode. The magnons in the ML are very soft. They reveal lower energy than the surface mode, and than the magnons in 2 ML Fe/W(110) film [10].

When comparing dispersions, however, it must be remembered that the bulk and surface Brillouin zones have different sizes (see inset in Fig. 3). In addition, the 1 and 2 ML Fe/W(110) films reveal lattice constants which are about 10% larger than in the bulk Fe [29]. Moreover, we have to take into account temperature effects. For the bulk Fe at 10 K,  $D(\text{bulk}) = 307 \pm 15 \text{ meV \AA}^2$  is measured [44]. The data for ML are measured at 120 K, i.e., at about  $0.5 T_c(\text{ML})$  of the ML's Curie temperature (223 K), and the DL Fe data are taken at RT, which corresponds to  $2/3$  of  $T_c(\text{DL})$  (450 K) [10,29]. Assuming that the  $D$  values follow the temperature dependence of the ML and DL Fe/W(110) magnetizations, i.e., they increase by about 30% at low temperature [29], we can estimate the  $D(\text{ML})$  and  $D(\text{DL})$  values in the ground state. We find  $D(\text{DL}) = 210 \text{ meV \AA}^2$  and  $D(\text{ML}) = 103 \text{ meV \AA}^2$ . Hence, the relative relation of the stiffness exchange coefficients  $D(\text{bulk}):D(\text{DL}):D(\text{ML})$  is about 3:2:1, respectively. Such strong softening of the magnons cannot be explained only by the reduction of the nearest neighbor number of the Fe atoms

derived from the Heisenberg model. One has to take into account modifications of the electronic structure of the Fe films, which, in the case of 1 ML Fe, are also related to the hybridization effects between Fe and W [22,25,26]. But even then, the predicted energies are still too large.

For the calculations of magnon energies, the ferromagnetic ground state of ML Fe/W(110) is usually anticipated [22,25]. However, recent calculations suggest a spin-spiral structure of the ML Fe/W(110) [45]. Chiral magnetic order induced by the strong Dzyaloshinskii—Moriya (DM) interaction has been observed in the antiferromagnetic ML Mn on W(110) [46]. One may expect that DM interaction should be present in the Fe monolayer as well [26,47], leading to a more exotic ground state of the ML Fe/W(110) with a net ferromagnetic moment [26]. In such a magnetically metastable spin system, the excitations of considerably lower energies are expected. The magnon softening in the ML Fe is in line with a pronounced softening of phonons [34]. A significant increase of the mean atomic displacement accompanied with the drop of the average force constant in the ML Fe/W(110) is reported [34]. For such a system, being close to stability limits, strong mutual phonon-magnon interactions cannot be excluded [48]. Alternatively, the considerable softening of magnons may also be due to the spin-charge coupling effects [49].

In conclusion, we have presented the magnon dispersion for 1 ML Fe on W(110) measured along the [001] direction at 120 K. We observed strong magnon softening in the ML Fe: The magnon energies in the ML are much smaller than those in the bulk Fe, and the Fe(110) surface. Our observations are in sharp contrast to the theoretical predictions. This fact is of fundamental importance for the understanding of the low dimensional magnetism with a large impact on a future theory.

We acknowledge numerous discussions with D. L. Mills, M. Bode, L. M. Sandratskii, P. Buczek, L. Szunyogh, and P. Weinberger. T. R. F. P. gratefully acknowledges the support of CNPq-Brazil.

- [1] F. Bloch, *Z. Phys.* **61**, 206 (1930).  
 [2] C. Herring and C. Kittel, *Phys. Rev.* **81**, 869 (1951).  
 [3] J. Schäfer *et al.*, *Phys. Rev. Lett.* **92**, 097205 (2004).  
 [4] J. A. Katine *et al.*, *Phys. Rev. Lett.* **84**, 3149 (2000).  
 [5] S. Petit *et al.*, *Phys. Rev. Lett.* **98**, 077203 (2007).  
 [6] J. C. Sankey *et al.*, *Nature Phys.* **4**, 67 (2008).  
 [7] H. Kubota *et al.*, *Nature Phys.* **4**, 37 (2008).  
 [8] M. Plihal, D. L. Mills, and J. Kirschner, *Phys. Rev. Lett.* **82**, 2579 (1999).  
 [9] R. Vollmer *et al.*, *Phys. Rev. Lett.* **91**, 147201 (2003).  
 [10] W. X. Tang *et al.*, *Phys. Rev. Lett.* **99**, 087202 (2007).  
 [11] M. R. Fitzsimmons *et al.*, *J. Magn. Magn. Mater.* **271**, 103 (2004).  
 [12] P. A. Grünberg, *Prog. Surf. Sci.* **18**, 1 (1985).  
 [13] B. Hillebrands, *Topics in Applied Physics* (Springer, Berlin, 2000), Vol. 75, p. 174.  
 [14] B. Heinrich, in *Ultrathin Magnetic Structures*, edited by B. Heinrich and J. A. C. Bland (Springer, Heidelberg, 1994), Vol. 2, p. 195.  
 [15] M. Farle, *Rep. Prog. Phys.* **61**, 755 (1998).  
 [16] T. Balashov *et al.*, *Phys. Rev. Lett.* **97**, 187201 (2006).  
 [17] C. L. Gao *et al.*, *Phys. Rev. Lett.* **101**, 167201 (2008).  
 [18] Y. Yafet, J. Kwo, and E. M. Gyorgy, *Phys. Rev. B* **33**, 6519 (1986).  
 [19] P. Bruno, *Phys. Rev. B* **43**, 6015 (1991).  
 [20] P. Kopietz and G. Castilla, *Phys. Rev. B* **43**, 11100 (1991).  
 [21] V. Kamberský, B. A. Ivanov, and E. V. Tartakovskaya, *Phys. Rev. B* **59**, 149 (1999).  
 [22] R. B. Muniz and D. L. Mills, *Phys. Rev. B* **66**, 174417 (2002).  
 [23] L. Udvardi *et al.*, *Phys. Rev. B* **68**, 104436 (2003).  
 [24] M. G. Pini, P. Politi, and R. L. Stamps, *Phys. Rev. B* **72**, 014454 (2005).  
 [25] A. T. Costa *et al.*, *Phys. Rev. B* **78**, 054439 (2008).  
 [26] L. Szunyogh *et al.* (private communication).  
 [27] N. D. Mermin and H. Wagner, *Phys. Rev. Lett.* **17**, 1133 (1966).  
 [28] M. Bander and D. L. Mills, *Phys. Rev. B* **38**, 12015 (1988).  
 [29] H. J. Elmers, *Int. J. Mod. Phys. B* **9**, 3115 (1995).  
 [30] M. Pratzner *et al.*, *Phys. Rev. Lett.* **87**, 127201 (2001); *Phys. Rev. B* **67**, 094416 (2003).  
 [31] M. Przybylski and U. Gradmann, *Phys. Rev. Lett.* **59**, 1152 (1987).  
 [32] U. Gradmann *et al.*, *Hyperfine Interact.* **57**, 1845 (1990).  
 [33] D. Sander *et al.*, *Phys. Rev. Lett.* **77**, 2566 (1996).  
 [34] S. Stankov *et al.*, *Phys. Rev. Lett.* **99**, 185501 (2007).  
 [35] H. J. Elmers, J. Hauschild, and U. Gradmann, *Phys. Rev. B* **54**, 15224 (1996).  
 [36] H. J. Elmers, J. Hauschild, and U. Gradmann, *J. Magn. Magn. Mater.* **221**, 219 (2000).  
 [37] M. Bode *et al.*, *Surf. Sci.* **601**, 3308 (2007).  
 [38] H. Ibach *et al.*, *Rev. Sci. Instrum.* **74**, 4089 (2003).  
 [39] H. Ibach and D. L. Mills, *Electron Energy Loss Spectroscopy and Surface Vibrations* (Academic Press, New York, 1982).  
 [40] R. Vollmer *et al.*, *Thin Solid Films* **464–465**, 42 (2004).  
 [41] Because the short wavelength magnons propagate within a few nanometers, the magnon scattering takes place mainly on flat ML terraces and contribution from the steps is negligible.  
 [42] T. Andersen and W. Hübner, *Phys. Rev. B* **74**, 184415 (2006).  
 [43] H. A. Mook and R. M. Nicklow, *Phys. Rev. B* **7**, 336 (1973).  
 [44] C.-K. Loong *et al.*, *J. Appl. Phys.* **55**, 1895 (1984).  
 [45] K. Nakamura *et al.*, *J. Appl. Phys.* **101**, 09G521 (2007).  
 [46] M. Bode *et al.*, *Nature (London)* **447**, 190 (2007).  
 [47] M. Heide *et al.*, *Phys. Rev. B* **78**, 140403(R) (2008).  
 [48] J. Łażewski *et al.*, *Phys. Rev. B* **76**, 205427 (2007).  
 [49] S. Pandey and A. Singh, *Phys. Rev. B* **78**, 014414 (2008).

## Nonmonotonic thickness dependence of spin wave energy in ultrathin Fe films: Experiment and theory

Y. Zhang (张雨),<sup>1</sup> P. Buczek,<sup>1</sup> L. Sandratskii,<sup>1</sup> W. X. Tang (唐文新),<sup>1,2,\*</sup> J. Prokop,<sup>1</sup> I. Tudosa,<sup>1</sup> T. R. F. Peixoto,<sup>1,3</sup> Kh. Zakeri,<sup>1</sup> and J. Kirschner<sup>1</sup>

<sup>1</sup>Max-Planck-Institut für Mikrostrukturphysik, Weinberg 2, 06120 Halle, Germany

<sup>2</sup>School of Physics, Monash University, Victoria 3800, Australia

<sup>3</sup>Instituto de Física, Universidade de São Paulo, São Paulo 05508-090, SP, Brazil

(Received 5 March 2010; published 31 March 2010)

High wave-vector spin waves in ultrathin Fe/W(110) films up to 20 monolayers (MLs) thick have been studied using spin-polarized electron energy-loss spectroscopy. An unusual nonmonotonous dependence of the spin wave energies on the film thickness is observed, featuring a pronounced maximum at 2 ML coverage. First-principles theoretical study reveals the origin of this behavior to be in the localization of the spin waves at the surface of the film, as well as in the properties of the interlayer exchange coupling influenced by the hybridization of the electron states of the film and substrate and by the strain.

DOI: 10.1103/PhysRevB.81.094438

PACS number(s): 75.30.Ds, 75.50.Bb, 75.70.Ak

### I. INTRODUCTION

Understanding of the elementary magnetic excitation such as spin waves (SWs) in ferromagnets, and the processes governing the spin dynamics on the atomic length ( $10^{-10}$  m) and femtosecond time scale ( $10^{-15}$  s), is one of the challenging topics in modern solid-state physics.<sup>1</sup> In particular, exploring high wave-vector SWs in low-dimensional magnets and their response to the reduced dimensionality, hybridization effects and strain, is essential to understand the intrinsic properties such as microscopic exchange interaction, magnetic ordering, and spin dynamics. Besides those core physical properties, high-energy SWs are also linked with phenomena such as fast magnetization reversal, polarized current induced magnetization switching, and domain-wall motion. This knowledge is crucial for designing faster and smaller spintronic devices.<sup>2</sup> Recent experiments indicate that the coupling between electrons and high-energy SWs is a possible coupling mechanism leading to high-temperature superconductivity.<sup>3,4</sup>

Bulk SWs can be studied by means of inelastic neutron scattering<sup>5,6</sup> but the method cannot be applied to ultrathin films because it lacks surface sensitivity. SWs in thin films and on the surface can be probed by ferromagnetic resonance and Brillouin light scattering<sup>1,7</sup> but those techniques are limited in a very small wave-vector region around the Brillouin-zone center. Recently, inelastic scanning tunneling spectroscopy<sup>8,9</sup> has been used to excite standing SWs in magnetic thin films but the method does not provide in-plane momentum resolution. Up to now, only the spin-polarized electron energy-loss spectroscopy (SPEELS) (Refs. 10–13) is capable of probing high-energy genuine surface SWs across the whole surface Brillouin zone. The applicability of SPEELS has been firmly established by mapping the SW dispersion relation in 1- and 2-monolayer (ML)-thick Fe/W(110) films.<sup>14,15</sup> Combined with first-principles theoretical approaches SPEELS can help to refine microscopic models of nanomagnets.<sup>16–18</sup>

In this work we present an experimental attempt to determine directly and systematically the properties of high-energy SWs in ferromagnetic Fe thin films of varying thickness. We discover that for the investigated in-plane momentum transfers  $\mathbf{q}$  between 0.5 and 0.7  $\text{\AA}^{-1}$  the energy of SWs,  $\omega_n(\mathbf{q})$ , is a nonmonotonous function of the thickness  $n$  (expressed in ML), with a distinct maximum for a 2-ML-thick film. An accompanying first-principles theoretical study of the SW excitations uses the clear experimental trend to choose between two complementary scenarios of polarized electron scattering. The theory suggests that the SWs excited in the experiment are localized at the surface of the film. Both the hybridization with substrate and the atomic relaxation of the Fe film are important for the nonmonotonous behavior of the SW energy.

This paper is structured as follows: In Sec. II we introduce the experiments on preparation, characterization, and SPEELS measurements of the Fe thin films on W(110). In Sec. III we present the experimental and theoretical results focusing the discussion on the nonmonotonous thickness dependence of the spin wave energies. The conclusions will be finally given in Sec. IV.

### II. EXPERIMENT

The experiments were performed in an ultrahigh vacuum chamber with a base pressure below  $5 \times 10^{-11}$  mbar. The ultrathin Fe films, with thickness between 1 and 20 ML were prepared by molecular-beam epitaxy at room temperature. After the deposition of Fe, the samples underwent a slight annealing in order to improve the structural quality.<sup>19</sup> The thickness uncertainty was well below 10%. Subsequently, the hysteresis loops of the films were recorded by the magneto-optic Kerr effect (MOKE) measurements in the longitudinal geometry. In the MOKE measurements the magnetic field was applied along the in-plane [110] direction.

The SPEEL spectra were measured in the magnetic remanent state using a high-performance SPEEL spectrometer.<sup>10–15</sup> The total-energy resolution was between

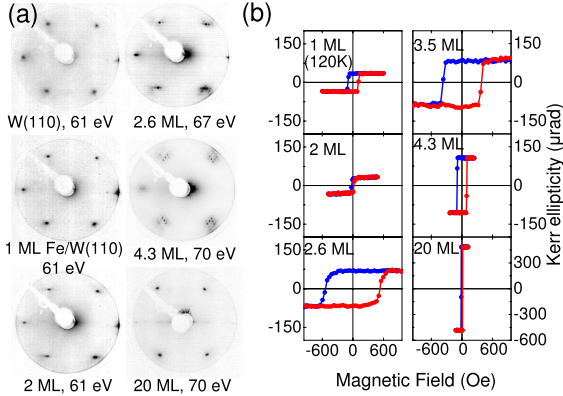
ZHANG *et al.*PHYSICAL REVIEW B **81**, 094438 (2010)

FIG. 1. (Color online) (a) LEED patterns for the clean W(110) substrate and the Fe thin films of different thicknesses on W(110). (b) The magnetic hysteresis loops measured by MOKE. The experiments are performed at room temperature except for the 1 ML Fe/W(110), which is measured at about 120 K.

20 and 30 meV. The degree of spin polarization  $P$  of the electron beam was  $0.65 \pm 0.08$ . Energy resolved detection of outgoing electrons allows the determination of energy and in-plane momentum loss caused by the excitation of surface SWs. The spin of the incident electrons can be parallel either to the minority (down,  $\downarrow$ ) or to the majority (up,  $\uparrow$ ) electrons of the ferromagnetic samples, and so two intensity spectra,  $I_{\downarrow}$  and  $I_{\uparrow}$ , are obtained for the scattered electrons. A SW can be created only by the incidence of minority electrons due to the conservation of the angular momentum.<sup>11</sup> The SW peak is found in the  $I_{\downarrow}$  spectrum or, more clearly, in the difference  $I_{\downarrow} - I_{\uparrow}$ .

### III. RESULTS AND DISCUSSION

The LEED patterns of the Fe films with different thicknesses are shown in Fig. 1(a). Sharp bcc (110)  $p(1 \times 1)$  spots were observed on 1 ML Fe/W(110), which indicate the pseudomorphic growth of the first Fe layer on the W(110) substrate. The dislocation lines and dislocation networks start to appear subsequently in 2 ML and a bit thicker Fe films as proved by the appearance of satellite spots. To have a dislocation-free Fe surface a 20 ML Fe film was prepared and the sharp LEED spots represent a well-defined bcc (110) surface. The magnetic hysteresis loops of the Fe thin films measured by MOKE are shown in Fig. 1(b). The MOKE results indicate that all the Fe thin films are ferromagnetic with the easy axis of magnetization along the in-plane  $[1\bar{1}0]$  direction. As the Curie temperature for 1 ML Fe/W(110) is about 220 K,<sup>20</sup> the MOKE and the later SPEELS measurements were performed at 120 K. The LEED and MOKE results show that the structural and magnetic properties of the Fe films are all consistent with the previous studies.<sup>21,22</sup>

Figure 2 shows typical SPEEL spectra measured on 2 ML Fe/W(110) with the wave-vector transfer of  $0.5 \text{ \AA}^{-1}$  along the in-plane  $[001]$  direction. Both the  $I_{\downarrow}$  and  $I_{\uparrow}$  spectra are

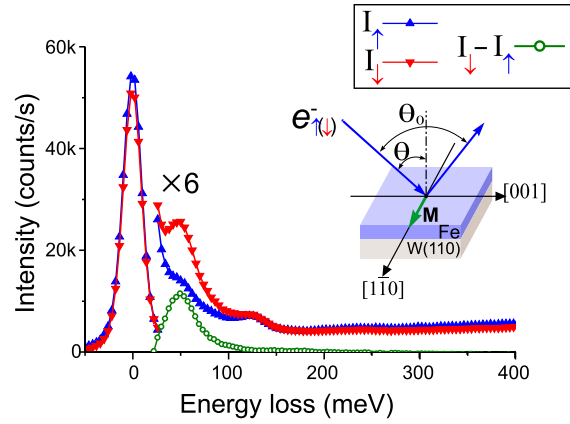


FIG. 2. (Color online) The SPEEL spectra measured with in-plane wave-vector transfer  $0.5 \text{ \AA}^{-1}$ . The up triangles ( $I_{\uparrow}$ ) and down triangles ( $I_{\downarrow}$ ) represent the intensity spectra of scattered electrons for the incidence of majority and minority electrons, respectively. The difference between the two spectra ( $I_{\downarrow} - I_{\uparrow}$ ) is shown as circles. The scattering geometry is schematically illustrated in the inset. The spin wave is probed with the wave vector along the  $[001]$  direction with the magnetization easy axis along the  $[1\bar{1}0]$  direction. The incident energy of electrons is about 4 eV.

dominated by the quasielastic peak located at 0 meV energy loss. Since only minority electrons can create SWs in the sample, the inelastic peak due to the SW excitations can be easily distinguished at about 50 meV, where the excitations only create a pronounced peak in the  $I_{\downarrow}$  spectrum. One may also notice another excitation located at about 120 meV. It is attributed to the vibrational excitations due to the adsorption of hydrogen atoms at surface.<sup>23</sup> Since vibrational excitations are mediated by the Coulomb interaction, they are of nonspin-flip nature, which are evidenced by the almost identical peaks in both  $I_{\downarrow}$  and  $I_{\uparrow}$  spectra. It is more convenient to identify the magnon peak in the difference spectrum defined as  $I_{\downarrow} - I_{\uparrow}$ , where the nonspin-flip excitations are almost canceled out. The scattering geometry is schematically illustrated in the inset. The in-plane momentum transfer is given by the scattering geometry  $q = k_f \sin(\Theta_0 - \Theta) - k_i$ , where  $k_i$  and  $k_f$  are, respectively, the magnitude of the wave vectors of the incident and scattered beams,  $\Theta_0$  is the angle between the incident beam and sample normal, and  $\Theta$  is the angle between the incident and outgoing beams. In this work,  $\Theta_0$  is kept at  $80^\circ$  for all the measurements.  $\Theta$  varies according to the desired surface wave-vector transfer.

Figure 3 presents SPEEL spectra measured for two in-plane momentum transfers  $0.5$  and  $0.7 \text{ \AA}^{-1}$ . A pronounced spin-dependent inelastic peak can be clearly seen at the energy loss about 40 meV, corresponding to the excitation of SWs. The SW energy changes nonmonotonously as the film thickness increases for both in-plane momentum transfers considered. SWs in 1 ML film have the lowest energy and experiences a sudden increase at 2 ML film. A local minimum is seen at about 4 ML and then the energy increases slightly in the thicker films. The asymptotic value of SWs energies is reached only at a relatively large coverage,

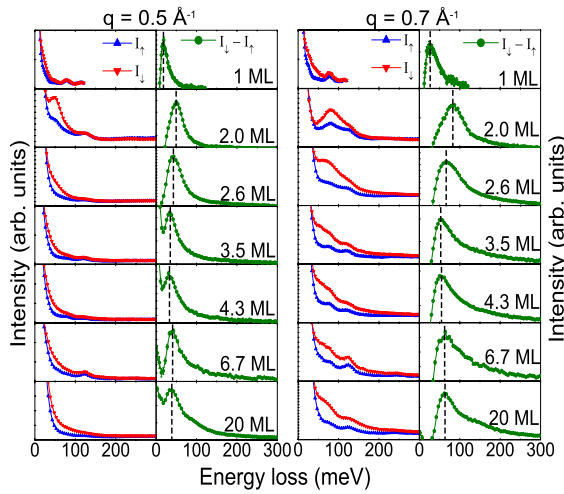


FIG. 3. (Color online) The SPEEL spectra,  $I_{\uparrow}$  and  $I_{\downarrow}$  measured for Fe films from 1 to 20 ML and the corresponding difference  $I_{\downarrow} - I_{\uparrow}$ . The wave-vector transfers are  $0.5 \text{ \AA}^{-1}$  (left) and  $0.7 \text{ \AA}^{-1}$  (right). The spectra for 1 ML are obtained at 120 K with incident energy of 3.8 eV. The other films are measured at room temperature using the incident energy of 4 eV. The energy resolution of the incident electron beam is about 20 meV.

around 7 ML. It should be noted that the Fe film thickness above 2 ML coverage is not uniform due to the statistical growth of Fe.<sup>11</sup> The spectrum contains excitations from patches of different thicknesses on the surface. Nevertheless, the tendency of the SW energies is clearly visible. For even higher wave vectors ( $>0.7 \text{ \AA}^{-1}$ ), the trend is still preserved, however, due to broadening of the spectrum, the change is not clearly discerned as in the lower wave-vector case.

No straightforward physical argument exists to explain the observed nonmonotonous behavior. In the case of Co/Cu(100) films the SPEELS measurements could be interpreted by means of a nearest-neighbor Heisenberg model with the exchange integral taken from the bulk.<sup>13</sup> A similar assumption for the Fe/W(110) system fails since it would result in  $\omega_n(\mathbf{q}) = \omega_{\text{bulk}}(\mathbf{q})(2n-1)/2n$ , i.e.,  $\omega_n(\mathbf{q})$  monotonously approaching the bulk value of SW energy from below.

To properly take into account the electronic structure of the film we performed first-principles adiabatic spin dynamics calculations based on density-functional theory (DFT). Within this approach the atomic magnetic moments are regarded as rigid entities precessing around the direction of the ground-state magnetization. The energies of the spin wave excitations are evaluated by means of parameter-free DFT calculations for the spiral magnetic structures with a given wave vector. This type of calculations allows also the mapping of the itinerant electron system onto a Heisenberg Hamiltonian<sup>17</sup> and determination of the effective parameters of interatomic exchange interactions. We assume that the ground state is collinear with the magnetization pointing along the  $z$  direction. The direction of an atomic moment  $i$  is determined by two angles, see Fig. 4, panel U. The polar angle  $\theta_i$  is the angle between the moment and the  $z$  axis and

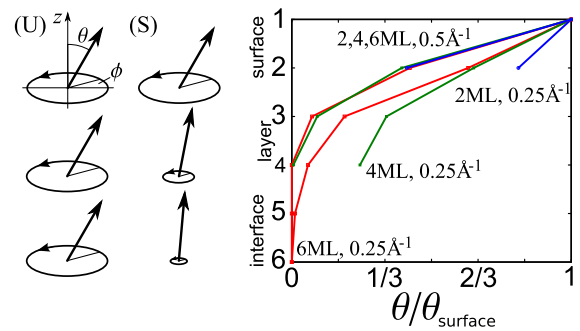


FIG. 4. (Color online) Angles  $\theta_i$  of the surface mode for several selected coverages and momentum transfers; the values are normalized to the deviation in the uppermost layer taken to be 30 in the calculations. Above  $0.5 \text{ \AA}^{-1}$  all curves follow roughly one universal  $\theta_i(\mathbf{q})$  dependence.

can be associated with the amplitude of a spin wave on a given atomic site. The azimuthal angle  $\phi_i$  determines the phase of the moment in its precessional motion and is determined by the momentum of the spin wave,  $\phi_i = \mathbf{q} \cdot \mathbf{s}_i$ , where  $\mathbf{s}_i$  stands for the position of the  $i$ th atomic site. We estimate the SW energy  $\omega(\mathbf{q})$  as the difference between the energy of the configuration of moments forming the SW,  $E(\{\theta_i\}, \mathbf{q})$ , and the ground-state energy  $E_0$

$$\omega(\mathbf{q}) = \frac{2}{\Delta M} (E(\{\theta_i\}, \mathbf{q}) - E_0), \quad (1)$$

where  $\Delta M = \sum_i (1 - \cos \theta_i) M_i$ ,  $M_i$  being the magnetic moment of the atom at site  $i$ . The normalization ensures that each SW changes the system magnetization by  $2\mu_B$ . We determine  $E(\{\theta_i\}, \mathbf{q})$  using the spin-spiral technique.<sup>24</sup> It allows to find  $\theta_i$ 's self-consistently: once a subset of angles is constrained to a specified value, the other angles are found ("relaxed") such that in the self-consistent state the spin-density matrices of the unrestricted sites are diagonal in the atomic coordinate systems.

The adiabatic spin dynamics neglects the presence of single-electron spin-flip excitations (Stoner excitations), therefore no prediction regarding the SWs' lifetimes can be made. However, the method provides a reliable account of the spin wave energies.<sup>25</sup>

The small penetration depth of electrons in SPEELS experiment raises an important question about the spatial localization of the magnetic excitations measured in this experiment. Two limits can be considered: (1) the incoming electron excites mainly the uppermost (surface) magnetic moments while the dynamics of the deeper layers arises as a secondary effect due to the exchange coupling with the top layers or (2) the magnetic moments of all layers are equally involved in the excitation process and the spin wave mode is uniform with respect to the depth of the film. The present understanding of SPEELS does not allow us to make an *a priori* choice between these two scenarios. We perform a comparative study of both limits and relate the results of the calculations to the experimental data, focusing, in particular, on the maximum of the spin wave energy for the 2 ML film.

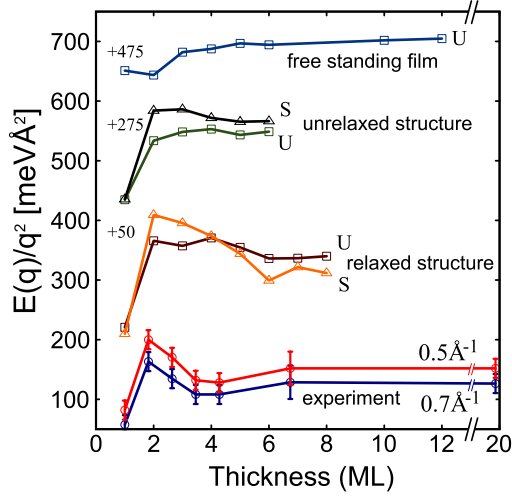
ZHANG *et al.*PHYSICAL REVIEW B **81**, 094438 (2010)

FIG. 5. (Color online) Energy of the SW modes (normalized to  $q^2$ ) as a function of the film thickness; experimental results are compared to the theoretical calculations. Selected curves are shifted upward for the sake of improved clarity. The mode with the amplitudes ( $\theta$  angles) of the moments forced to be equal in all film layers is marked with “U” ( $\square$ ) while the surface mode bears symbol “S” ( $\triangle$ ). All theoretical curves pertain to the momentum transfer of  $0.5 \text{ \AA}^{-1}$ .

The two limits are modeled as follows: in the uniform case the moments of all layers are restricted to deviate by the same angle  $\theta$ . To simulate the excitation localized at the surface, only the angle  $\theta$  of the moments of the surface layer is constrained whereas the directions of the moments of other layers are allowed to relax to self-consistent values.

We found that the relaxed magnetic configuration of the inner layers depends strongly on the wave vector of the SW. For  $\mathbf{q}=\mathbf{0}$  we obtained the expected result that the moments of all layers deviate by the same angle  $\theta$  as the constrained atomic moments of the surface layer, i.e., we obtained the collinear ferromagnetic structure rotated by the angle  $\theta$  with respect to the original ground-state configuration. The uniformly rotated spin structure has exactly the same energy as the original one, which follows the Goldstone theorem stating that the energy of the  $\mathbf{q}=\mathbf{0}$  SW must be zero in the absence of magnetic anisotropy, which we neglect. With increasing momentum transfer the deviation of the relaxed moments decreases with respect to the surface layer and with increasing depth of the layer, see Fig. 4. The degree of localization of the excitation also increases with decreasing the wavelength of the excitation.

First we performed calculations for the atomically unrelaxed films, characterized by the interlayer distances corresponding to the lattice parameter of bulk W. For both spin wave modes we get a strong increase in the excitation energy at the transition from 1 to 2 ML. For 1 ML film both modes are identical and have the same energy but for greater coverage they differ noticeably, Fig. 5. For the comparison with experiment it is important to note that the uniform mode does not have any maximum at 2 ML thickness. The energy

of this mode increases monotonously up to 4 ML and has a weak local minimum at 5 ML. On the other hand, the surface-type mode is much closer to the experimental behavior: the energies at 2 and 3 ML thicknesses are practically identical whereas they decrease noticeably starting from 4 ML. A possible reason for the less pronounced nonmonotonous behavior compared to experimental curves will be discussed below.

We now comment on the role of the substrate. We determined  $\omega_n(\mathbf{q})$  dependence of the uniform mode for the free standing films. As seen in Fig. 5, the curve has a qualitatively different character than for the supported film. The energies for 1 and 2 ML are almost identical. From 2 to 3 ML the energy increases strongly and for greater coverage reaches monotonously the asymptotic value. This reveals the importance of the nonmagnetic W(110) substrate for the magnetic properties of the Fe film. The hybridization of the Fe and W states strongly influences the electronic structure of the film and in turn the exchange parameters and SW dispersion relation.<sup>25</sup>

Returning to the supported films we took into account the atomic relaxations by using the interlayer distances determined experimentally.<sup>26,27</sup> Accounting for atomic relaxation results in a significant change in the SW energy in Fig. 3. The surface-type mode is now very similar to the curve obtained in the experiment, with a clear maximum at the 2 ML thickness.

The remarkable difference of energies for 1 and 2 ML films has its origin in the interlayer exchange coupling, necessarily absent in the single monolayer film. (The interlayer exchange is defined as  $J_{ll'}^0 \equiv \sum_s J_{ls|s'}$ , where the Heisenberg exchange integral  $J_{ls|s'}$  connects the moment  $s$  in the layer  $l$  with the moment  $s'$  in the layer  $l'$ .) The maximum of  $\omega_n(\mathbf{q})$  observed at  $n=2$  is the result of strong interlayer coupling  $J_{12}^0 = 86.5 \text{ meV}$  in this system. We found that this fact seems to be a general property of Fe/W(110) films that the interlayer coupling is increased by 10–25 % between the two upper layers compared to pairs of deeper layers. This observation applies equally to the structurally unrelaxed and relaxed films. In the case of 2 ML coverage and structurally relaxed film the increase is particularly strong. Somewhat surprisingly the intralayer exchange energy, at least for the wave vectors considered, changes rather weakly with the thickness and the interlayer distances, so the variations in SW energies are mainly determined by the changes in  $J_{ll'}^0$ . The latter quantity reaches its minimum for the relaxed film at 6 ML coverage. Additionally, we note that the energy is generally smaller in the case of the unrelaxed film, where  $J_{ll'}^0$  varies very weakly with the coverage reaching a value of around 61.0 meV for  $J_{12}^0$ .

Although the calculated dependence of the SW energy on the film thickness agrees with experiment the theoretical energies are higher than measured ones.<sup>28,29</sup> The unusual softening of the SW energies in Fe/W(110) films was noticed earlier and did not yet find its explanation. The account for Landau damping of the SW, because of the decay of the SW into Stoner excitations, can lead to the decrease in the SW energies, although the effect is not expected to be sufficient. Recently, it was shown that quantum corrections can lead to

the softening of the SW excitations.<sup>30</sup> These corrections are however strongly suppressed by the Hund's coupling. It remains an open question why the softening is observed for Fe films but is absent in the case of Co films.<sup>13,31</sup> This important issue should be the topic of separate study.

#### IV. SUMMARY

In summary, we report a combined experimental and theoretical investigation of the SW excitations in thin Fe films grown on W(110). The experimental excitation energy shows nonmonotonous behavior with respect to the film thickness with a distinct maximum for 2 ML film. The results of the

density-functional theory calculations suggest that the SWs excited in the SPEELS experiment have an amplitude decaying with the depth of the layer. We demonstrate that accounting for the hybridization with the substrate and the atomic relaxation in the film is crucial for the theoretical description of the experiment.

#### ACKNOWLEDGMENTS

The authors thank A. Winkelmann for many interesting discussions. T.R.F.P. gratefully acknowledges the support of CNPq, Brazil. The authors also acknowledge the valuable discussions with D. L. Mills and R. Q. Wu.

\*Corresponding author; wenxin.tang@sci.monash.edu.au

- <sup>1</sup>J. A. C. Bland and B. Heinrich, *Ultrathin Magnetic Structures: Fundamentals of Nanomagnetism* (Springer, New York, 2005).
- <sup>2</sup>I. Žutić, J. Fabian, and S. Das Sarma, *Rev. Mod. Phys.* **76**, 323 (2004).
- <sup>3</sup>D. J. Scalapino, *Phys. Rep.* **250**, 329 (1995).
- <sup>4</sup>A. Hofmann, X. Y. Cui, J. Schäfer, S. Meyer, P. Höpfner, C. Blumenstein, M. Paul, L. Patthey, E. Rotenberg, J. Bünemann, F. Gebhard, T. Ohm, W. Weber, and R. Claessen, *Phys. Rev. Lett.* **102**, 187204 (2009).
- <sup>5</sup>H. A. Mook and R. M. Nicklow, *Phys. Rev. B* **7**, 336 (1973).
- <sup>6</sup>T. G. Perring, A. D. Taylor, and G. L. Squires, *Physica B* **213-214**, 348 (1995).
- <sup>7</sup>B. Hillebrands, P. Baumgart, and G. Güntherodt, *Phys. Rev. B* **36**, 2450 (1987).
- <sup>8</sup>T. Balashov, A. F. Takács, W. Wulfhekel, and J. Kirschner, *Phys. Rev. Lett.* **97**, 187201 (2006).
- <sup>9</sup>C. L. Gao, A. Ernst, G. Fischer, W. Hergert, P. Bruno, W. Wulfhekel, and J. Kirschner, *Phys. Rev. Lett.* **101**, 167201 (2008).
- <sup>10</sup>H. Ibach, D. Bruchmann, R. Vollmer, M. Etzkorn, P. S. Anil Kumar, and J. Kirschner, *Rev. Sci. Instrum.* **74**, 4089 (2003).
- <sup>11</sup>M. Plihal, D. L. Mills, and J. Kirschner, *Phys. Rev. Lett.* **82**, 2579 (1999).
- <sup>12</sup>M. R. Vernoy and H. Hopster, *Phys. Rev. B* **68**, 132403 (2003).
- <sup>13</sup>R. Vollmer, M. Etzkorn, P. S. Anil Kumar, H. Ibach, and J. Kirschner, *Phys. Rev. Lett.* **91**, 147201 (2003).
- <sup>14</sup>W. X. Tang, Y. Zhang, I. Tudosa, J. Prokop, M. Etzkorn, and J. Kirschner, *Phys. Rev. Lett.* **99**, 087202 (2007).
- <sup>15</sup>J. Prokop, W. X. Tang, Y. Zhang, I. Tudosa, T. R. F. Peixoto, K. Zakeri, and J. Kirschner, *Phys. Rev. Lett.* **102**, 177206 (2009).
- <sup>16</sup>J. Hong and D. L. Mills, *Phys. Rev. B* **61**, R858 (2000).
- <sup>17</sup>S. V. Halilov, H. Eschrig, A. Y. Perlov, and P. M. Oppeneer, *Phys. Rev. B* **58**, 293 (1998).
- <sup>18</sup>A. T. Costa, R. B. Muniz, J. X. Cao, R. Q. Wu, and D. L. Mills, *Phys. Rev. B* **78**, 054439 (2008).
- <sup>19</sup>R. Popescu, H. L. Meyerheim, D. Sander, J. Kirschner, P. Steadman, O. Robach, and S. Ferrer, *Phys. Rev. B* **68**, 155421 (2003).
- <sup>20</sup>M. Przybylski and U. Gradmann, *Phys. Rev. Lett.* **59**, 1152 (1987).
- <sup>21</sup>X. Liu, M. M. Steiner, R. Sooryakumar, G. A. Prinz, R. F. C. Farrow, and G. Harp, *Phys. Rev. B* **53**, 12166 (1996).
- <sup>22</sup>K. Wagner, N. Weber, H. J. Elmers, and U. Gradmann, *J. Magn. Mater.* **167**, 21 (1997).
- <sup>23</sup>A. M. Baró and W. Erley, *Surf. Sci.* **112**, L759 (1981).
- <sup>24</sup>L. M. Sandratskii, *Adv. Phys.* **47**, 91 (1998).
- <sup>25</sup>P. Buczek, A. Ernst, L. Sandratskii, and P. Bruno, *J. Magn. Mater.* **322**, 1396 (2010).
- <sup>26</sup>H. L. Meyerheim, D. Sander, R. Popescu, J. Kirschner, P. Steadman, and S. Ferrer, *Phys. Rev. B* **64**, 045414 (2001).
- <sup>27</sup>D. Sander, R. Skomski, C. Schmidthals, A. Enders, and J. Kirschner, *Phys. Rev. Lett.* **77**, 2566 (1996).
- <sup>28</sup>Y. Zhang, Ph.D. thesis, Martin-Luther University, 2009.
- <sup>29</sup>L. Udvardi and L. Szunyogh, *Phys. Rev. Lett.* **102**, 207204 (2009).
- <sup>30</sup>S. Pandey and A. Singh, *Phys. Rev. B* **78**, 014414 (2008).
- <sup>31</sup>M. Etzkorn, P. S. Anil Kumar, W. Tang, Y. Zhang, and J. Kirschner, *Phys. Rev. B* **72**, 184420 (2005).





## Impact of Atomic Structure on the Magnon Dispersion Relation: A Comparison Between Fe(111)/Au/W(110) and Fe(110)/W(110)

T.-H. Chuang,<sup>1</sup> Kh. Zakeri,<sup>1,\*</sup> A. Ernst,<sup>1</sup> L. M. Sandratskii,<sup>1</sup> P. Buczek,<sup>1</sup> Y. Zhang,<sup>1</sup> H. J. Qin,<sup>1</sup> W. Adeagbo,<sup>2</sup> W. Hergert,<sup>2</sup> and J. Kirschner<sup>1</sup>

<sup>1</sup>Max-Planck-Institut für Mikrostrukturphysik, Weinberg 2, 06120 Halle, Germany

<sup>2</sup>Institut für Physik, Martin-Luther-Universität Halle-Wittenberg, Von-Seckendorff-Platz 1, 06120 Halle, Germany

(Received 2 August 2012; published 14 November 2012)

We present a combined experimental and theoretical study of the interplay between the atomic structure and the magnon excitations in low dimensional ferromagnets. Two monolayer thick Fe films on W(110) with and without a Au buffer layer are investigated. Our experiments show that adding the Au layer leads to a significant softening of the magnons. First-principles calculations confirm the experimental results revealing a strong dependency of exchange interactions on the atomic structure. It is observed that the *intralayer* exchange interactions increase with increasing distance between Fe layers. This unusual relationship is attributed to the complexity of the electronic structure and the contribution of different orbitals to the hybridization and exchange interaction. Our results suggest a way of tailoring magnetic excitations in low-dimensional magnetic structures.

DOI: 10.1103/PhysRevLett.109.207201

PACS numbers: 75.30.Ds, 75.50.Bb, 75.70.Ak, 75.70.Rf

One of the fascinating aspects in solid state physics is the magnetic response of a ferromagnet to the change of its atomic structure. Of particular interest is the response of the exchange interactions that determine both ground magnetic state and spin excitations. Since the excitations crucially influence the dynamic as well as thermodynamic properties of magnets, the interplay between atomic structure and exchange interactions is of great importance for the design of magnetic nanostructures with desired functionality.

Although the impact of the structural changes on the magnetic interactions has already been discussed theoretically for the case of bulk ferromagnets like Fe (see, for example, Refs. [1,2]), it has not been proven experimentally. The main reason for this is that in nature there exists only one stable Fe bulk phase, i.e., the body-centered cubic (bcc) phase.

The modern methods of the fabrication of low-dimensional structures open an inspiring possibility of creating materials of given chemical content with different atomic structures. Since the atomic structure influences essentially the properties of the system, this possibility strongly enhances the potential of designing materials with desired properties. A crucial step on this way is to understand the relation between the atomic structure and the electronic properties.

In this Letter, we report experimental and theoretical study of the magnon excitations in two Fe films of two monolayer (ML) thickness that differ in the atomic structure. On one hand, ultrathin Fe(110) films grow pseudomorphically on W(110) in bcc stacking [3,4]. On the other hand, by introducing an ultrathin Au buffer layer with the thickness of 2 ML, one can obtain an Fe(111) film with a close-packed structure [5,6].

Our measurements show a large difference in the magnon dispersion relation of the two films. Surprisingly, the *intralayer* exchange interaction increases when the

distance between Fe atomic layers increases. The response of the exchange interaction to the change of the atomic structure and interlayer distance is investigated in detail. Our first-principles calculations confirm the experimental results and provide a deeper insight into the microscopic origin of this effect.

All the experiments are performed under ultrahigh vacuum. Prior to the film deposition, the surface of the W(110) substrate was prepared using our standard cleaning procedure [7]. The Au and Fe films were grown by molecular beam epitaxy at 500 and 300 K, respectively. Tungsten has a bcc structure and the (110) surface is composed of rectangular unit cells. Since the gold crystal structure is face-centered cubic (fcc), the most similar surface to W(110) is the Au(111) surface. The Au ultrathin films grow in fcc(111) structure on W(110) as is verified by our low-energy electron diffraction (LEED) experiments. The LEED patterns recorded for a 2 ML Au film on W(110) indicate that Au does not grow in the same structure as W(110). The most probable structure is Au(111) with the epitaxial relationship  $\text{Au}_{\text{fcc}}[1\bar{1}0] \parallel \text{W}_{\text{bcc}}[001]$  known as the Nishiyama–Wassermann relationship. A similar observation is also reported by other groups [8,9].

The growth and the structure of the Fe films on the flat and vicinal Au(111) surfaces have been intensively investigated [10–12]. It has been shown by scanning tunneling microscopy that ultrathin Fe films grow pseudomorphically on Au(111) from the initial stage of growth up to a film thickness of about 2 ML. This is confirmed by our IV-LEED analysis. The evolution of the average interlayer distance with the number of Fe layers shows that for Fe thicknesses below 2 ML one sees a pseudomorphic growth of Fe on the Au(111) film. The films start to relax at thicknesses above 2 ML and finally, at an Fe thickness of

about 3.5 ML, the Fe film reaches the value of the layer spacing of the Fe bulk. A detailed analysis reveals that the LEED pattern is a slightly distorted hexagon. As the unit cell of Au possesses a threefold symmetry, this distortion results from the epitaxy of the Au(111) film on the W(110) surface. A similar observation is reported by Zdyb *et al.* [5,6].

Since for the Fe/Au/W(110) samples with the Fe film thickness above 2 ML, a structural transformation to the bcc structure occurs, we restrict our investigations to the samples composed of 2 ML Fe. The magnetic state of the samples was checked by means of the magneto-optical Kerr effect in longitudinal geometry with an external magnetic field applied along the W[110] direction (Fe[211] direction). The rectangular hysteresis loop shows a typical easy axis behavior (see the inset of Fig. 1).

The magnons are probed by means of spin polarized electron energy loss spectroscopy (SPEELS), which has opened a possibility to measure the magnons in such ultrathin structures [13–20]. The magnon dispersion relation is measured along the  $\bar{\Gamma}$ - $\bar{K}$  direction of the surface Brillouin zone. The SPEELS experiments are performed with an incident electron energy of 3.96 eV and a total energy resolution of about 14.9 meV. Figure 1 shows typical spin-down ( $I_{\downarrow}$ ) and spin-up ( $I_{\uparrow}$ ) SPEELS intensity spectra

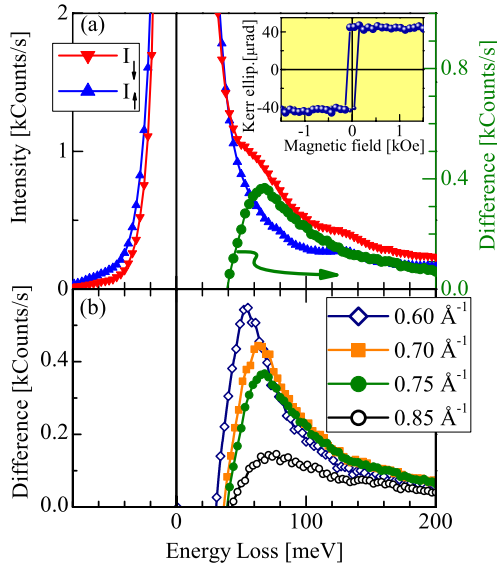


FIG. 1 (color online). (a) Typical spin polarized electron energy loss spectra recorded on 2 ML Fe/2 ML Au/W(110) at a wave-vector transfer of  $\Delta K_{\parallel} = 0.75 \text{ \AA}^{-1}$  and at room temperature. The difference spectrum ( $I_{\text{Diff.}} = I_{\downarrow} - I_{\uparrow}$ ) is shown as solid circles. Inset shows a typical hysteresis loop recorded in longitudinal geometry with an external magnetic field applied along the W[110]-direction (Fe[211]-direction). (b) Difference spectra measured at different wave-vector transfers from 0.6 to  $0.85 \text{ \AA}^{-1}$ .

recorded on 2ML Fe/2 ML Au/W(110) at room temperature and at a wave-vector transfer of  $\Delta K_{\parallel} = 0.75 \text{ \AA}^{-1}$ .  $I_{\downarrow}$  ( $I_{\uparrow}$ ) indicates the intensity of scattered electrons when incoming electrons have the spin polarization parallel (antiparallel) to the sample magnetization.  $\Delta K_{\parallel}$  is the wave-vector transfer parallel to the surface of the film. It is determined by the momenta of the incident and scattered electrons and the scattering geometry [21]. The peak at 68 meV in the minority channel,  $I_{\downarrow}$  (more clearly in the difference spectrum,  $I_{\text{Diff.}} = I_{\downarrow} - I_{\uparrow}$ ) is due to the magnon excitation. The magnon peak shows a clear dispersion with the variation of the wave-vector transfer [see Fig. 1(b)]. In Fig. 1(b), the difference spectra for various in-plane wave-vector transfers are shown.

By plotting the excitation energy versus the wave vector, one obtains the magnon dispersion relation, as shown by solid circles in Fig. 2(a). The open circles are experimental data obtained earlier on a 2 ML Fe film directly grown on W(110) [16]. Comparison of the experimental magnon

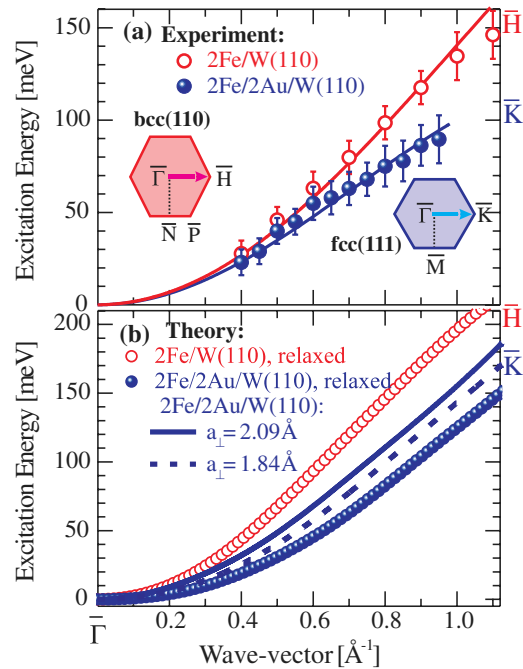


FIG. 2 (color online). (a) Experimental magnon dispersion relation measured on a 2 ML Fe on 2 ML Au on W(110) at room temperature. The results of a 2 ML Fe directly grown on W(110) are also shown [16]. The symbols represent the experimental results. The solid lines are the guide to the eyes. (b) Theoretical magnon dispersion relation of 2 ML Fe(111)/2 ML Au(111)/W(110) and 2 ML Fe(110)/W(110). The symbols represent the results of the calculation for the relaxed structure. The lines without symbols are the results for the Fe/Au/W(110) system calculated for different values of Fe interlayer spacing,  $a_{\perp}$ .

dispersions of the two systems reveals a strong softening of the magnon dispersion relation in the sample with a Au buffer. For instance, the softening at  $\Delta K_{\parallel} = 0.9 \text{ \AA}^{-1}$  reaches a value of 35 meV. This result demonstrates a way of tailoring magnetic excitations in low-dimensional structures by materials engineering.

Our next aim is to understand the microscopic nature of the observed effect on the basis of first-principles calculations. The calculations are performed within the generalized gradient approximation of the density functional theory [22]. The crystalline structure of Fe/W(110) was taken from the surface x-ray diffraction experiment [4], while the atomic positions in Fe/Au/W(110) were obtained using the VASP code, well known for providing accurate total energy and forces [23,24]. The structural information serves as an input for calculations of electronic and magnetic properties using a self-consistent Green function method, which is specially designed for layered semi-infinite systems [25]. The Heisenberg exchange parameters were determined employing the magnetic force theorem, likewise implemented within the Green function method [26].

The calculated magnon dispersion relation for both systems is presented in Fig. 2(b). The calculations are in good agreement with the experimental results, apart from the fact that they differ slightly in the absolute values of the energy. This means that the magnon softening is a consequence of adding the Au buffer. The analysis of the exchange parameters shows a strong anisotropy of exchange interaction for the systems we consider (see Fig. 3). The strongest interaction takes place between atoms of different layers. On the other hand, in the analysis of the magnon energies one should take into account that the number of the nearest neighbors within the layers is much larger than between the layers. In the following, the exchange interaction between atoms within the same atomic layer is referred to as *intralayer* interaction and the interaction between atoms from different layers is referred to as *interlayer* interaction.

The comparison of the exchange interactions for two systems, Fe/W(110) and Fe/Au/W(110), shows that the interlayer and intralayer interactions feature opposite trends. As an example, the largest interlayer interaction,  $J_{\perp}$ , increases from 27 meV in Fe/W(110) to 69 meV in Fe/Au/W(110) whereas the largest intralayer exchange interaction,  $J_{\parallel}$ , decreases from 20 to 14 meV for the interface layer and from 13 to 9 meV for the surface layer. The analysis shows that the softening of the magnons in Fe/Au/W(110) is the consequence of the decreased intralayer interactions that overcomes the opposite trend of increasing interactions between the layers.

The exchange parameters between Fe moments of the Fe/Au/W(110) system do not change significantly if we repeat the calculations for a free standing Fe film (keeping the atomic arrangement of the Fe/Au/W(110) system).

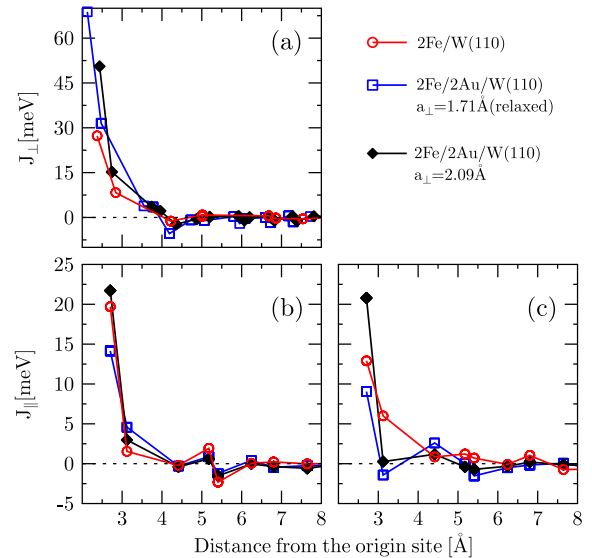


FIG. 3 (color online). Calculated site-resolved interlayer,  $J_{\perp}$ , (a) and intralayer,  $J_{\parallel}$ , (lower panels) exchange constants for the atoms located in the interface layer (b) and in the surface layer (c). Open and filled symbols represent the calculations for the relaxed and expanded structures, respectively.

Therefore, the role of the Au buffer is mostly reduced to the modification of the Fe atomic lattice. The change in the exchange parameters is the consequence of the change in the electronic structure caused by the modification of the Fe lattice.

In the epitaxial growth, the interatomic distance within the layers is determined by the atomic structure of the underlying lattice whereas the interlayer distance is governed by complex interplay of different interactions and can vary strongly from film to film. It is instructive to study the dependence of the exchange interactions and the magnon dispersion relation on the distance between Fe layers of the Fe/Au/W system. The prediction of the dependence of the effective interatomic exchange interactions on the interatomic distance is a difficult task because of a complex competition of various effects. On one hand, increasing distance between atoms leads to the narrowing of electron bands and increased atomic moments. On the other hand, it leads to a weaker overlap of the states of the atoms and produces the trend to decreasing interatomic exchange interaction [27].

Our calculations show that increasing the interlayer distance leads to an expected decrease of the interlayer exchange parameters. This results from the fact that a relatively small increase of the atomic moments is over-compensated by decreasing interlayer hybridization. Unexpectedly, at the same time we observe an increase in the energies of the acoustic magnons that become closer to the corresponding energies of the Fe/W(110) magnons.

Further analysis of the calculated exchange parameters shows that the origin of the increased magnon energies is in the strong increase of the intralayer exchange parameters. We emphasize that this increase takes place for unchanged interatomic distances within the layers. It is a consequence of complex reconstruction of the electronic structure due to the increase of the interlayer distance. Such a behavior cannot be understood without detailed first-principles calculation of the electronic structure. While changing the interlayer distance of Fe layers in Fe/Au/W(110) structure from 1.71 to 2.09 Å, the nearest neighbor intralayer coupling increases by a factor of 1.5 and 2.3 for the atoms in the interface and surface layer, respectively. This increase in the values of the intralayer exchange parameters is much larger than the increase of the atomic moments.

To understand the microscopic mechanism of the formation of effective interatomic exchange parameters, it is necessary to consider the consequence of the deviation of the atomic moments from the ground state directions. The larger the increase in the energy of the system following the deviation of the moments, the larger are the effective interatomic exchange parameters. The change in the total energy is a cumulative effect of the changes in the energies of individual electronic states. In a multiple-band real system the change in the electronic structure is complex and the reduction of the change in the total energy to a small number of “hot spots” in the electronic structure is usually not possible. Instead, we perform the analysis of the features of the density of states (DOS) that can contribute to the discussed effect. An important part of the response of the electronic systems to the deviation of the atomic moments is the hybridization of the spin-up and spin-down electron states of the collinear ground state of the system. The strength of the hybridization depends on the energy distance between hybridized states and on the overlap of their orbital wave functions. Since the hybridization leads to the formation of binding and antibinding states, the changes in the electronic energies strongly compensate each other if both binding and antibinding levels are occupied. However, if the hybridization involves the states lying close to the Fermi level, the compensation can be disturbed when certain unoccupied states become involved, since unoccupied states do not contribute to the total energy.

The analysis reveals important trends in the density of states. The 3d states responsible for the interlayer hybridization ( $d_{xz}$ ,  $d_{yz}$ , and  $d_{z^2}$ ) appear substantially higher in energy than the states responsible for the intralayer hybridization ( $d_{x^2-y^2}$  and  $d_{xy}$ ). Figure 4 shows the spin-resolved DOS of 3d electrons calculated for different interlayer distances. In order to see the contribution of different 3d-orbitals to the exchange interactions, their projected DOS are plotted in Figs. 4(c) and 4(d). With increasing interlayer distance all states move to lower energies as a

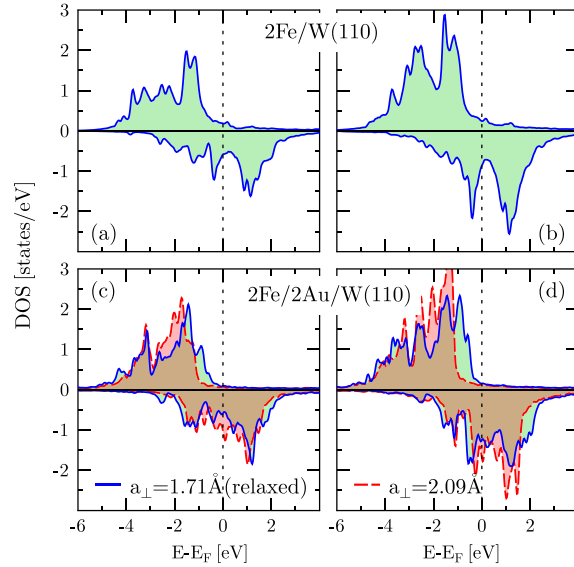


FIG. 4 (color online). Spin-resolved DOS of 3d states in 2Fe/W(110) (upper panels) and 2Fe/2Au/W(110) (lower panels) systems, separated in a part with  $d_{xy}$  and  $d_{x^2-y^2}$  states (a),(c) and a part corresponding to  $d_{xz}$ ,  $d_{yz}$  and  $d_{z^2}$  orbitals (b), (d). The solid and dashed lines represent the results for relaxed and expanded structures, respectively.

consequence of decreasing 3d band width. However, this shift is more important for  $d_{xz}$ ,  $d_{yz}$ , and  $d_{z^2}$  states, since  $d_{x^2-y^2}$  and  $d_{xy}$  are located well below the Fermi level for the minimal value of the interlayer distance. On the other hand, increasing the interlayer distance increases the spin-down density of 3d states on the Fermi level. The appearance of a large number of states near the Fermi energy makes the energy of the system sensitive to the deviation of the atomic moments and constitutes an important factor in the enhancement of intralayer exchange interactions. The discussion above indicates that the magnetic properties of complex systems cannot be understood without careful microscopic study of the exchange interactions. While the interlayer exchange parameters decreased as expected, the intralayer exchange parameters turned out to increase, upon increasing the interlayer distance, due to the reconstruction of the electronic structure. Clearly, the evolution of the electronic structure cannot be separated into features related to the interlayer and intralayer distances since the influences of both distances are strongly interconnected.

In summary, we have shown both experimentally and theoretically that the engineering of the atomic structure of low-dimensional magnets leads to a strong modification of the exchange interaction that provides a route to the design of the materials with desired magnetic properties. The analysis of the variation of the Heisenberg exchange parameters with the variation of the interlayer distances shows an unexpected effect of the strong increase of the

intralayer exchange interaction overcompensating the decrease of the interlayer exchange parameters. This behavior is not restricted to the systems studied here. It is expected also for ultrathin Fe films grown on other fcc surfaces. This demonstrates the necessity of the combined experimental-theoretical approach to the complex physical properties of the real materials and reveals strong potential of such studies for the design of new materials with desired properties.

Funding from the Deutsche Forschungsgemeinschaft is acknowledged by A.E. (DFG priority program SPP 1538 “Spin Caloric Transport”). The calculations were performed at the Rechenzentrum Garching of the Max Planck Society (Germany).

\*zakeri@mpi-halle.de

- [1] R. F. Sabiryanov and S. S. Jaswal, *Phys. Rev. Lett.* **83**, 2062 (1999).
- [2] S. Morán, C. Ederer, and M. Fähnle, *Phys. Rev. B* **67**, 012407 (2003).
- [3] H.-J. Elmers, *Int. J. Mod. Phys. B* **09**, 3115 (1995).
- [4] H. L. Meyerheim, D. Sander, R. Popescu, J. Kirschner, P. Steadman, and S. Ferrer, *Phys. Rev. B* **64**, 045414 (2001).
- [5] R. Zdyb and E. Bauer, *Phys. Rev. Lett.* **100**, 155704 (2008).
- [6] R. Zdyb, T. O. Mendes, A. Locatelli, M. A. Niño, and E. Bauer, *Phys. Rev. B* **80**, 184425 (2009).
- [7] K. Zakeri, T. Peixoto, Y. Zhang, J. Prokop, and J. Kirschner, *Surf. Sci.* **604**, L1 (2010).
- [8] H. Knoppe and E. Bauer, *Phys. Rev. B* **48**, 5621 (1993).
- [9] A. M. Shikin, O. Rader, G. V. Prudnikova, V. K. Adamchuk, and W. Gudat, *Phys. Rev. B* **65**, 075403 (2002).
- [10] P. Ohresser, N. B. Brookes, S. Padovani, F. Scheurer, and H. Bulou, *Phys. Rev. B* **64**, 104429 (2001).
- [11] H. Bulou, F. Scheurer, P. Ohresser, A. Barbier, S. Stanescu, and C. Quirós, *Phys. Rev. B* **69**, 155413 (2004).
- [12] T. Allmers and M. Donath, *New J. Phys.* **11**, 103049 (2009).
- [13] M. Plihal, D. L. Mills, and J. Kirschner, *Phys. Rev. Lett.* **82**, 2579 (1999).
- [14] H. Ibach, D. Bruchmann, R. Vollmer, M. Etzkorn, P. S. A. Kumar, and J. Kirschner, *Rev. Sci. Instrum.* **74**, 4089 (2003).
- [15] R. Vollmer, M. Etzkorn, P. S. Anil Kumar, H. Ibach, and J. Kirschner, *Phys. Rev. Lett.* **91**, 147201 (2003).
- [16] W. X. Tang, Y. Zhang, I. Tudosa, J. Prokop, M. Etzkorn, and J. Kirschner, *Phys. Rev. Lett.* **99**, 087202 (2007).
- [17] J. Prokop, W. X. Tang, Y. Zhang, I. Tudosa, T. R. F. Peixoto, K. Zakeri, and J. Kirschner, *Phys. Rev. Lett.* **102**, 177206 (2009).
- [18] Y. Zhang, P. Buczek, L. Sandratskii, W. X. Tang, J. Prokop, I. Tudosa, T. R. F. Peixoto, K. Zakeri, and J. Kirschner, *Phys. Rev. B* **81**, 094438 (2010).
- [19] K. Zakeri, Y. Zhang, J. Prokop, T.-H. Chuang, N. Sakr, W. X. Tang, and J. Kirschner, *Phys. Rev. Lett.* **104**, 137203 (2010).
- [20] H. Ibach, J. Rajeswari, and C. M. Schneider, *Rev. Sci. Instrum.* **82**, 123904 (2011).
- [21] M. Etzkorn, P. S. Anil Kumar, W. Tang, Y. Zhang, and J. Kirschner, *Phys. Rev. B* **72**, 184420 (2005).
- [22] J. P. Perdew, K. Burke, and M. Ernzerhof, *Phys. Rev. Lett.* **77**, 3865 (1996).
- [23] G. Kresse and J. Hafner, *Phys. Rev. B* **49**, 14 251 (1994).
- [24] G. Kresse and J. Furthmüller, *Phys. Rev. B* **54**, 11 169 (1996).
- [25] M. Lüders, A. Ernst, W. M. Temmerman, Z. Szotek, and P. J. Durham, *J. Phys. Condens. Matter* **13**, 8587 (2001).
- [26] A. I. Liechtenstein, M. I. Katsnelson, V. P. Antropov, and V. A. Gubanov, *J. Magn. Magn. Mater.* **67**, 65 (1987).
- [27] E. Sasioglu, L. M. Sandratskii, and P. Bruno, *Phys. Rev. B* **71**, 214412 (2005).



## Relaxation Time of Terahertz Magnons Excited at Ferromagnetic Surfaces

Y. Zhang (張雨),\* T.-H. Chuang (莊子弘), Kh. Zakeri,<sup>†</sup> and J. Kirschner

Max-Planck-Institut für Mikrostrukturphysik, Weinberg 2, 06120 Halle, Germany

(Received 13 March 2012; published 24 August 2012)

The temporal and spatial properties of terahertz magnons excited at ferromagnetic fcc Co(100) and bcc Fe(110) surfaces are investigated experimentally. The magnon lifetime is found to be a few tens of femtoseconds at low wave vectors, which reduces significantly as the wave vector approaches the Brillouin zone boundary. Surprisingly, the lifetime is very similar in both systems, in spite of the fact that the excitation energy in the Co(100) film is by a factor of two larger than in the Fe(110) film. The magnon wave packets propagate only a few nanometers within their lifetime. In addition to the fact that our results describe the damping mechanism in ultrafast time scales, they may provide a way to predict the ultimate time scale of magnetic switching in nanostructures.

DOI: 10.1103/PhysRevLett.109.087203

PACS numbers: 75.30.Ds, 75.70.Ak, 75.70.Rf, 75.78.Jp

Understanding the ultrafast spin dynamics on short length and time scales is essential for increasing the density, as well as the writing or reading speed of modern magnetic storage media. Thanks to advanced experimental techniques, our knowledge has greatly improved within the last few years [1–9]. It has been known for many years that the switching of a submicron magnet typically takes place within a range of few picoseconds up to some nanoseconds, depending on the applied external magnetic field [1]. The breakthrough of the ultimate time scale of magnetic switching (up to subpicoseconds) was reported when the ultrafast optical spectroscopy was developed such that it could allow the excitation and probing of the magnetic objects [2]. Later on it was demonstrated that femtosecond laser pulses can be applied to switch the magnetization [4–7]. This new time scale seems to be the ultimate time scale of magnetic switching up to now. Interestingly, recent experimental results of spin-polarized scanning tunneling microscopy revealed that the spin relaxation time of a single magnetic atom on an insulating substrate is in the order of a few hundreds of nanoseconds [9]. A connection between the ultrafast optical spectroscopy and the results of tunneling spectroscopy is still missing. The fact is that all the techniques mentioned above allow only the investigation of the magnetic excitations in real time or space. Moreover, it is not possible to select a particular excitation with a certain wave vector and eigenfrequency and follow its dynamics. Hence a wave vector selective excitation would provide a deeper knowledge on the processes involved in the magnetic switching on ultrafast time scales.

In this Letter, we present the experimental results on terahertz magnons probed at ferromagnetic surfaces. We compare the results of Fe(110) and Co(001) and provide a quantitative analysis of the magnon lifetime at different wave vectors. We will demonstrate how the magnons are confined in time and space. Moreover, we will provide a quantitative representation of the magnons in real space.

The results are obtained using spin-polarized electron energy loss spectroscopy (SPEELS) [10], a technique which has proven its unique capability in the study of high wave vector magnons [11–13]. The unique advantage of SPEELS is that one has a direct access to the wave vector and the energy of the excitations. In the SPEELS experiments, due to the angular momentum conservation during the scattering event, magnons can only be created by electrons of minority character. The magnon peaks thus only appear in the loss region of the  $I_1$  spectrum [14] (see the typical spectra in Fig. 1). The magnon excitations can be clearly identified by comparing the  $I_1$  and  $I_2$  spectra. The analysis of the peak position and broadening provides us information on the magnon excitation energy and lifetime, respectively [15].

We investigated the magnons in the ultrathin films of 8 monolayer (ML) fcc Co/Cu(001) and 2 ML bcc Fe/W(110). All experiments are performed at room temperature. Typical SPEELS spectra taken on 2 ML Fe/W(110) are presented in Fig. 1. As magnons can only be created by minority electrons, a magnon excitation peak appears in the  $I_1$  spectrum. The difference spectrum ( $I_1 - I_2$ ) is shown by the green curve. We note that non-magnetic excitations, such as phonons, usually show much lower spin asymmetry [13], and will be canceled out in the difference spectrum. As the difference spectrum offers all the necessary information, it is used for further data analysis to extract the properties of magnons. To change the in-plane wave vector transfer in the measurements, the sample is rotated about the magnetic easy axis, while the angle between the incident and outgoing beams is kept fixed at 80 degrees. The in-plane components of the magnon wave vectors can be simply expressed as  $\Delta k_{\parallel} = k_i[\sin(\theta_f) - \sin(\theta_i)]$ , where  $k_i$  represents the wave vector of incident electrons.  $\theta_i$  and  $\theta_f$  are the incident and outgoing angles, respectively. The resolution in wave vectors depends on the angular resolution of the spectrometer, which is typically about  $0.05 \text{ \AA}^{-1}$ .

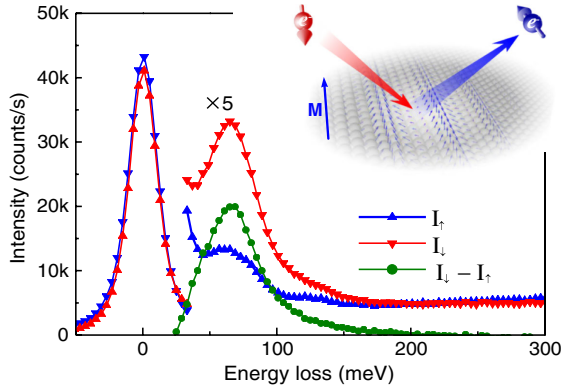


FIG. 1 (color online). Typical spectra recorded at an incident electron energy of 4 eV and a wave vector transfer of  $0.6 \text{ \AA}^{-1}$ . The red spectrum indicates the intensity of the scattered electrons for incidence of minority electrons  $I_l$ , and the blue one is for the incidence of majority electrons  $I_r$ . The green curve is the difference between the red and blue spectra ( $I_l - I_r$ ). The beam polarization was about 65%. The peak at about 65 meV in the red spectrum is attributed to the magnon excitations. The scattering geometry is schematically sketched in the inset.

To extract the intrinsic linewidth of the magnons, we fit the measured difference spectra by using a convolution of a Gaussian and a Lorentzian function, in which the Gaussian represents the instrumental broadening and the Lorentzian represents the intrinsic magnon signal. By fitting the experimental results, one realizes that the intrinsic linewidth of magnon excitations is typically from 20 up to a few hundreds of meV, which is usually larger than the instrumental broadening. As an example, a fit through the data shown in Fig. 1 shows that the intrinsic linewidth of the magnon is about  $42 \pm 7$  meV, while the instrumental broadening is about 20 meV. The large broadening of the loss spectrum indicates that magnons are strongly damped in time. The magnon lifetime can be obtained from the Fourier transform of the magnon signal. The Fourier transform of the Lorentzian in energy (or frequency) domain is an exponential decay in the time domain,  $\exp(-t\Gamma/2\hbar)$ , where  $\Gamma$  represents the intrinsic linewidth of the Lorentzian peak in energy and  $\hbar$  is the reduced Planck constant. We define the lifetime of a magnon as  $\tau = 2\hbar/\Gamma$ , a time in which the amplitude drops to its  $e^{-1}$  value. For the magnon measured on Fe(110) shown in Fig. 1, the lifetime is about  $31 \pm 5$  femtoseconds.

The magnon intensity spectra have been measured for different wave vectors. A contour map is constructed by plotting the difference spectra versus their wave vectors for 2 ML Fe/W(110) [see Fig. 2(a)]. Figures 2(b) and 2(c) show the intensity distributions at  $\Delta k_{\parallel} = 0.7 \text{ \AA}^{-1}$  and  $E = 82$  meV, respectively. If one assumes that the scattering geometry does not drastically influence the intensity in far off-specular [16], one may estimate the spatial

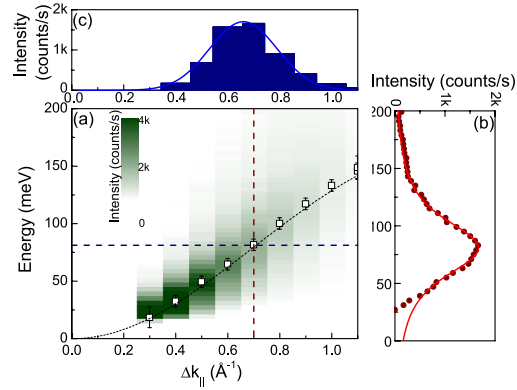


FIG. 2 (color online). (a) The difference spectra are plotted as a contour map for the wave vectors from 0 to  $1 \text{ \AA}^{-1}$ . The section profiles for a wave vector at  $0.7 \text{ \AA}^{-1}$  and energy at about 82 meV are shown in (b) and (c), respectively. The magnon peak in (b) is fitted by the convolution of a Gaussian and a Lorentzian function. The intrinsic linewidth of the peak is 55 meV. The intensity profile along the horizontal line at  $E = 82$  meV in (c) is fitted by a Gaussian profile shown as a solid curve.

distribution of the magnon wave packets from the intensity profile presented in Fig. 2(c). For simplicity we neglect the broadening in wave vectors due to the finite energy resolution. This is a rather good assumption, since the instrumental broadening is fairly small compared to the intrinsic linewidth. The spectral distribution as a function of the wave vector is fitted directly by a single Gaussian distribution. For example, the profile in Fig. 2(c) shows a full width at half maximum (FWHM) of about  $0.32 \text{ \AA}^{-1}$ . After a Fourier transform, we obtained a Gaussian wave packet representing the magnon envelope function with a FWHM of about 2 nanometers.

To visualize the strong damping effects on terahertz magnons in real time and space, we compared three states of magnons for 8 ML Co/Cu(001) and 2 ML Fe/W(110). Solid symbols labeled by  $S_{\text{Fe}}$ ,  $S_{\text{Co}}^1$ , and  $S_{\text{Co}}^2$  mark the centers of these states in Fig. 3(a). State  $S_{\text{Fe}}$  represents the magnon packet in the Fe(110) film, and states  $S_{\text{Co}}^1$  and  $S_{\text{Co}}^2$  are states in the Co(100) film.  $S_{\text{Fe}}$  and  $S_{\text{Co}}^1$  possess the same wave vector ( $\Delta k_{\parallel} = 0.8 \text{ \AA}^{-1}$ ), while  $S_{\text{Fe}}$  and  $S_{\text{Co}}^2$  have the same energy ( $E = 100$  meV), as indicated by the dashed lines. Figure 3(b) represents the evolution of the magnon wave packets for the states  $S_{\text{Fe}}$ ,  $S_{\text{Co}}^1$ , and  $S_{\text{Co}}^2$  indicated above. Each wave packet in Fig. 3(b) is the product of three components: A moving Gaussian,  $\exp[-(x - vt)^2/2\sigma^2]$ , representing the motion of wave packet (the envelop function), an exponential decay factor  $\exp(-t/\tau)$  for the evolution of the amplitude in time, and finally a wave form,  $\cos(\Delta k_{\parallel}x - \omega t)$ , representing its wavy nature ( $\omega = E/\hbar$  is the angular frequency of the wave). The velocity of the envelope function,  $v$ , is the group velocity of the wave packet, which is obtained



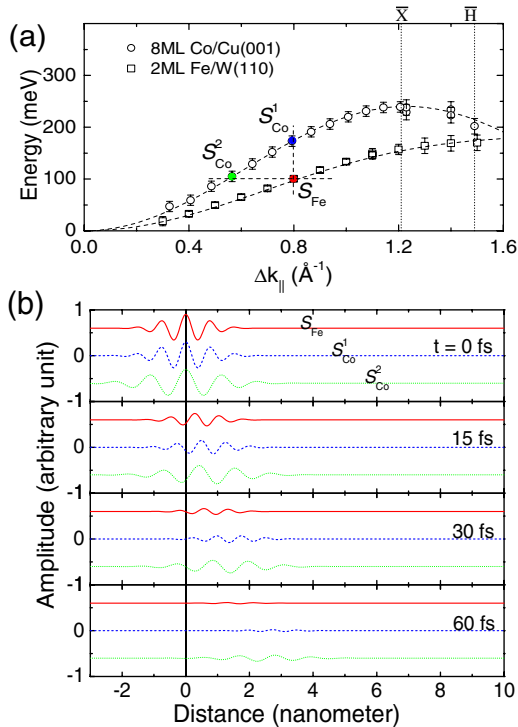


FIG. 3 (color online). (a) Magnon dispersion relation in 8 ML Co/Cu(001) (open circles) and 2 ML Fe/W(110) (open squares). Solid symbols mark the center of three states for Fe and Co surfaces, which are named as  $S_{\text{Fe}}$ ,  $S_{\text{Co}}^1$ , and  $S_{\text{Co}}^2$  respectively.  $S_{\text{Fe}}$  and  $S_{\text{Co}}^1$  are at nearly the same wave vectors  $0.8 \text{ \AA}^{-1}$ ,  $S_{\text{Fe}}$  and  $S_{\text{Co}}^2$  are at almost the same energy 100 meV. The dotted lines at about 1.21 and 1.49 mark the surface Brillouin zone boundaries of Co(001) and Fe(110) surfaces. (b) The plot of the evolution of wave packets for the states  $S_{\text{Fe}}$  ( $0.80 \text{ \AA}^{-1}$ , 95 meV) at Fe surface,  $S_{\text{Co}}^1$  ( $0.81 \text{ \AA}^{-1}$ , 174 meV) and  $S_{\text{Co}}^2$  ( $0.55 \text{ \AA}^{-1}$ , 101 meV) at Co surface. The amplitude may be regarded as the transverse component of a precessing spin projected to the wave propagation directions or the modulus of the magnon wave function.

from the slope of the dispersion curves,  $v = \partial\omega/\partial\Delta k_{\parallel}$ . They are about 26, 46, and 41 km/s for the  $S_{\text{Fe}}$ ,  $S_{\text{Co}}^1$ , and  $S_{\text{Co}}^2$  states, respectively.  $\sigma$  and  $\tau$  are the natural broadening of the wave packet in space and lifetime, respectively, which are obtained from the Fourier transform of the intensity spectra in Fig. 2.

In a classic picture the wave forms in Fig. 3(b) can be regarded as the amplitude of the transverse component of spins projected along a certain direction on the surface e.g., the propagation direction of the wave. It may be also regarded as the modulus of the magnon wave function. Figure 3(b) demonstrates that magnons are strongly damped within a few tens of femtoseconds and confined in a few nanometers for both Fe and Co for high wave vectors. The wave packets only moved ahead by about 2–3 nm during their lifetime (much shorter than the spin

diffusion length in the 3d ferromagnets). For the states from the same system i.e.,  $S_{\text{Co}}^1$  and  $S_{\text{Co}}^2$ , the state at a higher wave vector ( $S_{\text{Co}}^1$ ) has a shorter lifetime than the one at a lower wave vector ( $S_{\text{Co}}^2$ ). The wave packet of  $S_{\text{Co}}^1$  propagates a bit shorter than  $S_{\text{Co}}^2$ . Our results demonstrate that the decay of a magnon does strongly depend on its wave vector. Interestingly, for the states on different surfaces but with similar wave vectors, i.e.,  $S_{\text{Fe}}$  and  $S_{\text{Co}}^1$ , it is noticed that although the  $S_{\text{Fe}}$  has a much lower energy, it possesses a similar lifetime and broadening of the wave packet as  $S_{\text{Co}}^1$ .  $S_{\text{Fe}}$  and  $S_{\text{Co}}^2$  have the same energy. The state at a higher wave vector ( $S_{\text{Fe}}$ ) clearly shows a shorter lifetime as compared to the low wave vector one ( $S_{\text{Co}}^2$ ). Regarding the propagation speed, both wave packets in the Co(100) film are much faster than the ones in the Fe(110) film [see Fig. 3(b)].

The intrinsic linewidth and the corresponding lifetime of magnons versus wave vector are shown in Fig. 4 for 8 ML Co/Cu(001) and 2 ML Fe/W(110). The intrinsic linewidth of the magnon signal shows a clear dependence on the wave vector. As a result, the lifetime of magnons at the surface of 2 ML Fe/W(110) ranges from tens to hundreds of femtoseconds. Comparing to the spin relaxation of a single atom on the insulating substrate, whose relaxation time is about  $10^{-7}$  s [9], the lifetime of magnons at a metal surface is almost  $10^7$  times shorter. Such a short lifetime of terahertz magnons is attributed to the strong damping due to the presence of the conduction electrons in the metal film and the substrate [17–19]. Since the terahertz magnons are a coherent superposition of the correlated electron hole pairs across the Fermi level, their damping may be regarded as the result of the strong decay of these collective magnons into the available Stoner states near the Fermi level. It has been shown that the Stoner excitations in the surface states play an important role in the decay effect

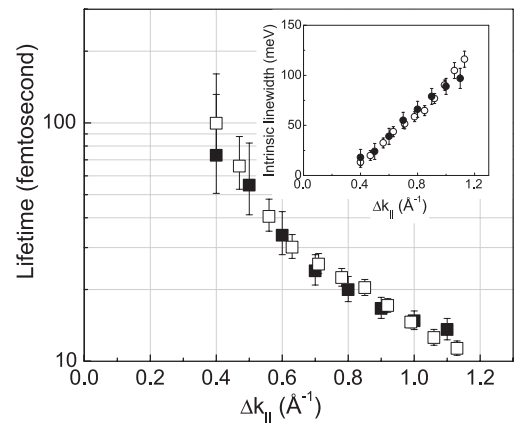


FIG. 4. The magnon lifetime as a function of the in-plane wave vector measured for 2 ML Fe/W(110) (solid symbols) and 8 ML Co/Cu(001) (open symbols). Inset shows the intrinsic linewidth of the magnon peaks.

[19–21]. If the ferromagnetic film is grown on a metallic substrate, due to the strong hybridization of the bands, there are lots of Stoner states available near the Fermi level, which can contribute to the damping mechanism. In other words, the strong decay effect may be imagined as the pumping of the spins of the magnetic film into the nonmagnetic conductive substrate [18]. It is worth pointing out that the lifetimes of both systems are very similar at the same wave vectors in spite of the fact that the magnon energy in the Co(100) film is almost twice of that in the Fe(110) film. Besides the intrinsic damping effects due to the Stoner excitations, it has been proposed that the thermal effects may also play a role in the broadening of magnon peaks [22]. However, experiments performed on a 2 ML Fe film at different temperatures revealed that the temperature dependence of the intrinsic linewidth is negligible.

The strong damping observed in our experiments is governed by the decay of collective type of magnons, to the single particle Stoner excitations (usually referred to as Landau damping [19]). It strongly depends on the available Stoner states near the Fermi level; hence, the hybridization of the electronic bands of the ferromagnetic film with the ones of the substrate plays an important role [19]. As the total magnetization of the sample is unchanged after creation and damping of a magnon, one cannot directly connect the magnon lifetime to the ultimate time scale of magnetization switching. However, this relaxation time can be directly compared to the time interval provided in the excitation scheme. For instance, if the aim is to switch the magnetization of a nanoisland using a spin-polarized current within a few femtoseconds, the terahertz magnons are governing this process. Hence, the time interval between two electrons has to be shorter than the lifetime of the magnons involved. Otherwise, the magnons do not contribute to this switching process and die out. The same analogy applies to the other methods used to switch the magnetization. If terahertz magnons are generated within the process, one would expect the response of the system in such timescales. Since the timescale in optical experiments is similar to what we predict as the typical lifetime of the terahertz magnons, we think that the terahertz magnons are also important in the laser induced demagnetization processes.

The strong spin dependence of the decay rate of the image potential state observed in photoemission experiments is attributed to the magnon generation and relaxation within a few tens of femtoseconds [23]. Our results are the direct experimental proof of this hypothesis.

In summary, the magnon lifetime and spatial distribution in 8 ML fcc Co(001) and 2 ML bcc Fe(110) are studied. The magnons on both surfaces possess lifetimes ranging from tens to hundreds of femtoseconds depending on the wave vector. Our analysis reveals that the magnons at the Fe(110) and Co(100) surfaces are strongly confined in time and space due to the damping effects. Interestingly,

the lifetime of both systems are very close at a given wave vector in spite of the fact that the excitation energy in the Co(100) film is almost twice of that in the Fe(110) film. Terahertz magnons propagate only a few nanometers within their lifetime. Our results shall have a significant contribution to the understanding of the magnetic damping mechanism of terahertz magnons at surfaces and a possible tuning of the magnetic relaxation in nanoscale ferromagnets. They may also offer a way of estimating the ultimate time scale of magnetic switching in nanostructures.

We acknowledge the fruitful discussions with P. Buczek and L. M. Sandraskii. We thank W.-X. Tang, J. Prokop and M. Etzkorn for their contribution to some experiments.

\*zhangyu@mpi-halle.de

†zakeri@mpi-halle.de

- [1] *Spin Dynamics in Confined Magnetic Structures II*, edited by B. Hillebrands and K. Ounadjela (Springer, Heidelberg, 2003).
- [2] E. Beaurepaire, J.-C. Merle, A. Daunois, and J.-Y. Bigot, *Phys. Rev. Lett.* **76**, 4250 (1996).
- [3] I. Tudosa, C. Stamm, A. B. Kashuba, F. King, H. C. Siegmann, J. Stöhr, G. Ju, B. Lu, and D. Weller, *Nature (London)* **428**, 831 (2004).
- [4] C. D. Stanciu, F. Hansteen, A. V. Kimel, A. Kirilyuk, A. Tsukamoto, A. Itoh, and Th. Rasing, *Phys. Rev. Lett.* **99**, 047601 (2007).
- [5] U. Bovensiepen, *J. Phys. Condens. Matter* **19**, 083201 (2007).
- [6] B. Koopmans, G. Malinowski, F. Dalla Longa, D. Steiauf, M. Fähnle, T. Roth, M. Cinchetti, and M. Aeschlimann, *Nature Mater.* **9**, 259 (2010).
- [7] A. Kirilyuk, A. V. Kimel, and T. Rasing, *Rev. Mod. Phys.* **82**, 2731 (2010).
- [8] M. Fähnle and C. Illg, *J. Phys. Condens. Matter* **23**, 493201 (2011).
- [9] S. Loth, M. Etzkorn, C. P. Lutz, D. M. Eigler, and A. J. Heinrich, *Science* **329**, 1628 (2010).
- [10] H. Ibach, D. Bruchmann, R. Vollmer, M. Etzkorn, P. S. Anil Kumar, and J. Kirschner, *Rev. Sci. Instrum.* **74**, 4089 (2003).
- [11] R. Vollmer, M. Etzkorn, P. S. Anil Kumar, H. Ibach, and J. Kirschner, *Phys. Rev. Lett.* **91**, 147201 (2003).
- [12] W. X. Tang, Y. Zhang, I. Tudosa, J. Prokop, M. Etzkorn, and J. Kirschner, *Phys. Rev. Lett.* **99**, 087202 (2007).
- [13] Y. Zhang, P. A. Ignatiev, J. Prokop, I. Tudosa, T. R. F. Peixoto, W. X. Tang, Kh. Zakeri, V. S. Stepanyuk, and J. Kirschner, *Phys. Rev. Lett.* **106**, 127201 (2011).
- [14] M. Plihal, D. L. Mills, and J. Kirschner, *Phys. Rev. Lett.* **82**, 2579 (1999).
- [15] M. Etzkorn, P. S. Anil Kumar, and J. Kirschner, *Handbook of Magnetism and Advanced Magnetic Materials* (John Wiley & Sons, New York, 2007) Vol. 3, p. 1658.
- [16] H. Ibach and D. L. Mills, *Electron Energy Loss Spectroscopy and Surface Vibrations* (Academic Press, New York, 1982).

- [17] A. T. Costa, R. B. Muniz, and D. L. Mills, *Phys. Rev. B* **68**, 224435 (2003).
- [18] A. T. Costa, R. B. Muniz, and D. L. Mills, *Phys. Rev. B* **74**, 214403 (2006).
- [19] P. Buczek, A. Ernst, and L. M. Sandratskii, *Phys. Rev. Lett.* **106**, 157204 (2011).
- [20] T. Balashov, T. Schuh, A. F. Takács, A. Ernst, S. Ostanin, J. Henk, I. Mertig, P. Bruno, T. Miyamachi, S. Suga, and W. Wulfhekel, *Phys. Rev. Lett.* **102**, 257203 (2009).
- [21] A. A. Khajetoorians, S. Lounis, B. Chilian, A. T. Costa, L. Zhou, D. L. Mills, J. Wiebe, and R. Wiesendanger, *Phys. Rev. Lett.* **106**, 037205 (2011).
- [22] A. Taroni, A. Bergman, L. Bergqvist, J. Hellsvik, and O. Eriksson, *Phys. Rev. Lett.* **107**, 037202 (2011).
- [23] A. B. Schmidt, M. Pickel, M. Donath, P. Buczek, A. Ernst, V. P. Zhukov, P. M. Echenique, L. M. Sandratskii, E. V. Chulkov, and M. Weinelt, *Phys. Rev. Lett.* **105**, 197401 (2010).



## Asymmetric Spin-Wave Dispersion on Fe(110): Direct Evidence of the Dzyaloshinskii-Moriya Interaction

Kh. Zakeri,<sup>1,\*</sup> Y. Zhang,<sup>1</sup> J. Prokop,<sup>1</sup> T.-H. Chuang,<sup>1</sup> N. Sakr,<sup>1</sup> W. X. Tang,<sup>1,2</sup> and J. Kirschner<sup>1</sup>

<sup>1</sup>Max-Planck-Institut für Mikrostrukturphysik, Weinberg 2, 06120 Halle, Germany

<sup>2</sup>School of Physics, Monash University, Victoria 3800, Australia

(Received 20 January 2010; published 30 March 2010)

The influence of the Dzyaloshinskii-Moriya interaction on the spin-wave dispersion in an Fe double layer grown on W(110) is measured for the first time. It is demonstrated that the Dzyaloshinskii-Moriya interaction breaks the degeneracy of spin waves and leads to an asymmetric spin-wave dispersion relation. An extended Heisenberg spin Hamiltonian is employed to obtain the longitudinal component of the Dzyaloshinskii-Moriya vectors from the experimentally measured energy asymmetry.

DOI: 10.1103/PhysRevLett.104.137203

PACS numbers: 75.30.Ds, 75.50.Bb, 75.70.Ak, 75.70.Rf

In 1957, Dzyaloshinskii proposed an antisymmetric exchange interaction, based on symmetry arguments, to explain the weak ferromagnetism observed in some oxide materials, e.g.,  $\alpha$ -Fe<sub>2</sub>O<sub>3</sub> (Hematite) [1]. Only three years later it was shown by Moriya that, in principle, this interaction can be analytically derived by considering the relativistic spin-orbit correction in the Hamiltonian [2]. The antisymmetric exchange interaction, Dzyaloshinskii-Moriya (DM) interaction, became very important to understand many physical properties of different systems, i.e., spin glasses [3], cuprates [4], molecular magnets [5,6], and multiferroics [7,8].

In nanomagnetism, where the surface effects are noticeable, the spin-orbit coupling is one of the most important intrinsic magnetic perturbations, which creates novel phenomena. Recently, it has been shown that a strong spin-orbit coupling in the presence of the broken inversion symmetry at the surface leads to the DM interaction, which stabilizes a noncollinear spin structure for a Mn monolayer on W(110) [9] and W(100) [10] surfaces.

An ultrathin Fe film grown on W(110) is another system that is believed to show the DM interaction [11–13]. Magnetic excitations in this quasi-two-dimensional spin system have been studied theoretically for many years [14–21]. In the description of the collective magnetic excitations, only the symmetric exchange interaction was considered and the DM interaction has been neglected. In such systems, where DM interaction is relatively large, it should, in principle, change the intrinsic properties of the spin waves (SWs). Only very recently, the influence of the DM interaction on the spin-wave dispersion has been predicted to give rise to an asymmetric spin-wave dispersion in an Fe monolayer on W(110) [22]. However, the effect of the DM interaction on the spin-wave dispersion in low-dimensional systems has never been measured experimentally.

In this Letter we report the first experimental evidence of the influence of DM interaction on the spin-wave dispersion in a double-layer Fe. We show that in the presence of

the DM interaction the spin-wave dispersion is asymmetric. By measuring the highly resolved spin-polarized electron energy loss (SPEEL) spectra in both energy loss and gain regimes and by reversing the magnetization of the film, we measure the DM interaction driven asymmetry in the spin-wave dispersion of Fe double-layer grown on W(110). By using an extended Heisenberg spin Hamiltonian, the energy asymmetry is modeled giving rise to a quantitative determination of the longitudinal components of DM vectors.

The iron layer was deposited onto a clean W(110) single crystal at room temperature (RT). Special care has been taken concerning the cleaning of the W crystal as described elsewhere [23]. Prior to the spin-polarized electron energy loss spectroscopy (SPEELS) measurements, the structural, chemical, and magnetic properties were checked by means of low energy electron diffraction, Auger electron spectroscopy, and magneto-optical Kerr effect measurements. The Fe films reveal the expected structural and magnetic properties well known from literature [24–26]. The SPEELS measurements were performed using our high performance spectrometer with an energy resolution well below 20 meV and a beam polarization of about  $70 \pm 10\%$  [27].

A schematic representation of the scattering geometry is given in the inset of Fig. 1(a). A well-defined monochromatized spin-polarized electron beam is scattered from the sample and the electron energy loss and gain spectra are measured as a function of the in-plane momentum transfer ( $\Delta K^{\parallel}$ ) for both spin orientations of the incoming electron beam (up  $\uparrow$  and down  $\downarrow$ ). The surface SWs are excited in a virtual spin-flip scattering process [28–31]. The conservation of the angular momentum during the scattering prohibits SW excitations for incoming electrons with a spin polarization antiparallel to the sample magnetization ( $I_f$ ). Hence, only electrons having minority spin character ( $I_f$ ) can create SWs. The electrons with majority spin character ( $I_f$ ) can, in principle, annihilate the thermally excited SWs while gaining energy. These facts lead to a peak in the

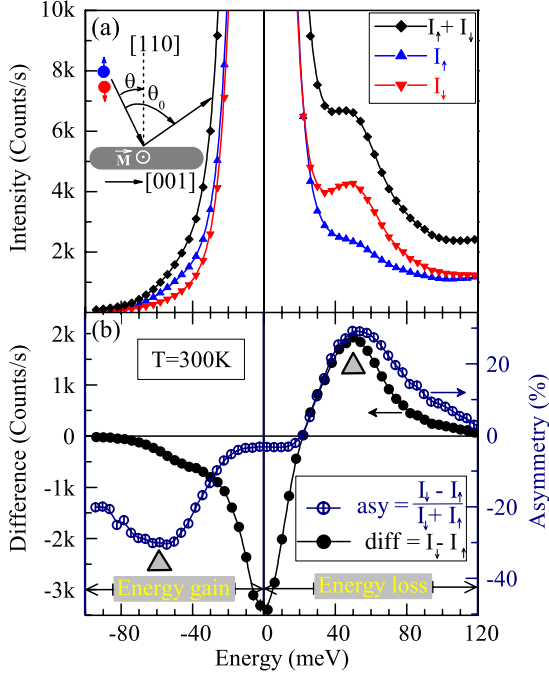


FIG. 1 (color online). (a) SPEEL spectra measured on a 2 ML Fe film epitaxially grown on W(110). The incoming electron beam had an energy of  $E_0 = 4$  eV. The inset shows the geometry of our SPEELS experiment. The spin-polarized electron beam is scattered along the [001] direction of the Fe(110) surface in the magnetic remanent state. The scattering angle is kept at  $\theta_0 = 80^\circ$ . By changing the incident angle  $\theta$ , the in-plane wave-vector transfer parallel to the surface,  $\Delta K^\parallel$ , can be adjusted [ $\Delta K^\parallel = k_f \sin(\theta_0 - \theta) - k_i \sin(\theta)$ , where  $k_i$  and  $k_f$  are the initial and final momentums of the electrons, respectively]. For this experiment it was chosen to be  $\Delta K^\parallel = 0.5 \text{ \AA}^{-1}$ . (b) The difference and asymmetry spectra. The big triangles show the peak position due to the SW creation and annihilation taking place in energy loss and gain, respectively.

minority spin channel in the energy loss region and a peak in the majority spin channel in the energy gain region (this is in analogy to the Stokes and anti-Stokes peaks in a Raman or Brillouin light scattering experiment). Figure 1(a) shows a typical SPEEL spectra measured at  $\Delta K^\parallel = 0.5 \text{ \AA}^{-1}$  on a 2 ML Fe film. The amplitude of the peak due to the SW annihilation (in the energy gain region) is much smaller than the one caused by the SW creation. This is due to the fact that the probability of having thermally excited SWs in the system is given by the Boltzmann factor, which is about 0.01–0.1 at RT. This gives rise to a large peak in the energy loss region and a small dip in the energy gain region of the difference spectra. However, both features can be seen clearly in the asymmetry curves, where the  $\text{asy} = \frac{I_\downarrow - I_\uparrow}{I_\downarrow + I_\uparrow}$  is plotted as a function of energy for both loss and gain regions. In Fig. 1(b), the difference and asymmetry curves are pre-

sented. The big triangles mark the peak positions due to the spin-wave creation and annihilation processes.

In the absence of the DM interaction the spin-wave dispersion has to be symmetric with respect to the energy axis, meaning that measuring the SW spectra for negative wave-vector transfers has to result in the same excitation energy as the one measured at positive wave-vector transfers:  $\Delta E = E(\Delta K^\parallel) - E(-\Delta K^\parallel) = 0$ .

Figure 2 shows a series of difference and asymmetry curves measured on a 2 ML Fe film on W(110) at RT. The full symbols are the results of measurements when the magnetization is pointing along the  $[\bar{1}10]$  direction. One clearly sees that for  $\Delta K^\parallel = 0.5 \text{ \AA}^{-1}$  the SW creation peak (energy loss) is at higher energies, whereas the SW annihilation peak (energy gain) is at lower ones (it can be seen better in the asymmetry curves). The situation is totally reversed for negative wave-vector transfers, i.e.,  $\Delta K^\parallel = -0.5 \text{ \AA}^{-1}$ ; the SW annihilation peak is at higher energies and SW creation peak is at lower energies now. If this

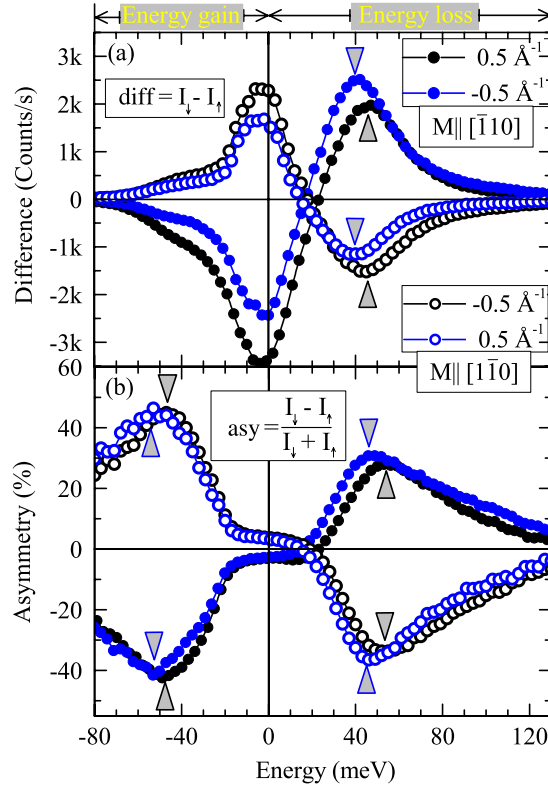


FIG. 2 (color online). (a) Series of difference,  $\text{diff} = I_\downarrow - I_\uparrow$ , and (b) asymmetry,  $\text{asy} = \frac{I_\downarrow - I_\uparrow}{I_\downarrow + I_\uparrow}$ , SPEEL spectra measured for  $\Delta K^\parallel = \pm 0.5 \text{ \AA}^{-1}$  on a 2 ML Fe at RT. The filled symbols are for  $\mathbf{M} \parallel [\bar{1}10]$  and the open ones are for  $\mathbf{M} \parallel [1\bar{1}0]$ . The spectra are recorded at a beam energy of  $E_0 = 4.163$  eV with an energy resolution of 19 meV. The big triangles mark the peak positions of SW creations and annihilations, taking place at energy loss and gain, respectively.

effect is caused by an uncertainty in the wave-vector transfer, due to the stray fields induced bending of the electron beam in two different experiments, one would expect the same effect in the gain and loss regions (increase or decrease in both energies). The reversed phenomenon in energy gain and loss regions indicates that this effect cannot be due to a slightly different electron trajectory in two different experiments. Another argument which clarifies that this is an intrinsic property of the system comes from measuring the same spectra for opposite magnetization directions. In magnetism, reversing the sample magnetization is equivalent to time inversion (in our experiment it basically means that the beam source and the detector are interchanged). The data for magnetization along the  $[1\bar{1}0]$  direction are shown by open symbols in Fig. 2. In the case of reversed magnetization the SW excitation peak for  $\Delta K_{\parallel} = -0.5 \text{ \AA}^{-1}$  is at higher energies with respect to the one for  $\Delta K_{\parallel} = 0.5 \text{ \AA}^{-1}$ . This clearly indicates that having a slightly different energy for the SWs propagating along the  $[001]$  direction with respect to the ones propagating along the  $[00\bar{1}]$  direction is an intrinsic property of the SWs in this particular system. Based on the spin-wave theory the symmetric exchange interaction cannot lead to any degeneracy breaking of the spin waves. One may think about the presence of the dipolar interaction that is responsible for the unidirectional Damon-Eshbach surface modes [32]. In this case the energy difference should be about 0.1 meV, which is much smaller than values observed in our experiment. Finally, we conclude that the presence of DM interaction breaks the degeneracy of the SW energies and leads to different energies for a given  $\Delta K_{\parallel}$ . Therefore, the assumption  $\Delta E(\Delta K_{\parallel}) = \Delta E(-\Delta K_{\parallel})$  is not valid here anymore.

It is worth mentioning that measurements on a 20 ML thick sample showed also an energy asymmetry. The values of the energy asymmetry in this case are smaller than the ones measured for the double layer. This observation reveals two facts: (i) since SPEELS is only sensitive to the topmost layer(s), this effect is more likely a surface effect and is preserved up to even 20 ML thick films; (ii) this effect has nothing to do with the stray fields caused by the sample, because the stray fields strength is proportional to the film thickness. If this effect was caused by stray fields, one would expect a larger effect for the thicker films.

The energy asymmetry,  $\Delta E = E(\Delta K_{\parallel}) - E(-\Delta K_{\parallel})$ , induced by DM interaction varies with the in-plane wave-vector transfer. In Fig. 3(a) the energy asymmetry is plotted as a function of the in-plane wave-vector transfer,  $\Delta K_{\parallel}$ . Our data show that  $\Delta E$  has a distinct maximum at  $\pm 0.5 < \Delta K_{\parallel} < \pm 1$ .

Now, we attempt to estimate the amplitude of the DM vectors from our experimental data. By starting with a simple classical description of the SWs, the modified Heisenberg Hamiltonian in the presence of the DM interaction can be written as  $H = \sum_{i \neq j} J_{ij} \mathbf{S}_i \cdot \mathbf{S}_j - K_{\text{eff}} \sum_i (\mathbf{S}_i \cdot \hat{\boldsymbol{\epsilon}})^2 + \sum_{i \neq j} \mathbf{D}_{ij} \cdot \mathbf{S}_i \times \mathbf{S}_j$ . Here the first term is the symmet-

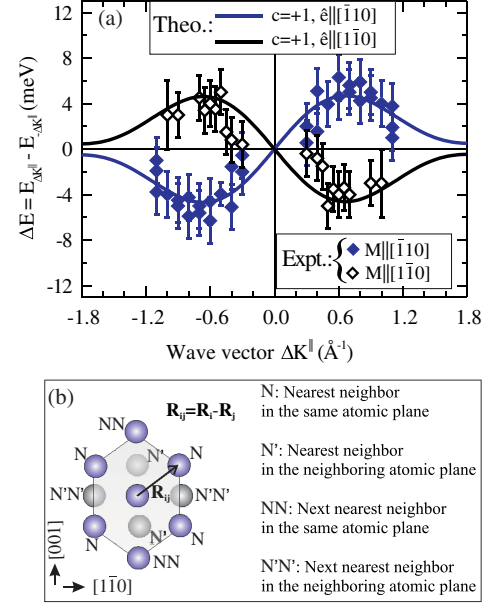


FIG. 3 (color online). (a) The energy asymmetry as a function of wave-vector transfer. The symbols are the measured values for two different magnetization directions and the solid curves are the fits using Eq. (2) for  $c = +1$  and different magnetization directions. The error bars represent both the statistical and systematic uncertainties. (b) Real space representation of a 2 ML Fe slab.

ric exchange interaction ( $J_{ij}$  is the exchange coupling constant between spins  $\mathbf{S}_i$  and  $\mathbf{S}_j$ ), the second term is the magnetic anisotropy energy (MAE) term ( $K_{\text{eff}}$  is the effective MAE constant with an easy axis along  $\hat{\boldsymbol{\epsilon}}$ ), and the last term is the DM interaction term ( $\mathbf{D}_{ij}$  are the DM vectors). The last term is the only one, which leads to an asymmetric dispersion relation. Using the same notation as in Ref. [22], the asymmetry in the SW energies,  $\Delta E = E_{\text{DM}}(\mathbf{q}) - E_{\text{DM}}(-\mathbf{q})$ , reads

$$\Delta E = 2c \sin^2 \theta \sum_{i \neq j} (\mathbf{D}_{ij} \cdot \hat{\boldsymbol{\epsilon}}) \sin[\mathbf{q} \cdot (\mathbf{R}_i - \mathbf{R}_j)], \quad (1)$$

where  $\mathbf{q}$  is the wave vector of the SWs (in our case SWs are propagating along the  $[001]$  direction, therefore  $|\mathbf{q}| = \Delta K_{\parallel}$ ),  $c = \pm 1$  is the chirality rotation index (being +1 for right rotating sense and -1 for the left rotating one),  $\hat{\boldsymbol{\epsilon}}$  is the unit vector of the magnetization  $\mathbf{M}$ ,  $\theta$  is the relative angle between moments and  $\hat{\boldsymbol{\epsilon}}$ , and  $\mathbf{R}_i(\mathbf{R}_j)$  is the position vector of site  $i(j)$ . For a double-layer slab Eq. (1) can be simplified to

$$\Delta E = \pm 4c \left[ (2D_1^x + \check{D}_1^x) \sin\left(\frac{\Delta K_{\parallel} a}{2}\right) + D_2^x \sin(\Delta K_{\parallel} a) \right]. \quad (2)$$

Here the  $\pm$  sign stands for different magnetization directions,  $a$  is the interatomic distance being  $3.16 \text{ \AA}$ , and

$D_i^x = \sin^2\theta \mathbf{D}_i \cdot \hat{e}$  ( $\dot{D}_i^x = \sin^2\theta \dot{\mathbf{D}}_i \cdot \hat{e}$ ) is the longitudinal component of the DM vector of the  $i$ th neighbors in the same atomic plane (in the neighboring atomic plane), see Fig. 3(b). The maximum  $|\Delta E|$  observed in our experiments, taking place at  $\pm 0.5 < \Delta K^{\parallel} < \pm 1$ , is in line with the fact that Eq. (2) has also a local extremum at  $\pm \pi/2a \approx \pm 0.5 < \Delta K^{\parallel} < \pm \pi/a \approx \pm 1$ . By fitting the experimental data with Eq. (2) for different magnetization directions ( $\hat{e} \parallel [1\bar{1}0]$ - and  $\hat{e} \parallel [\bar{1}10]$  direction) one finds  $|2D_1^x + \dot{D}_1^x| = 0.9(3)$  meV and  $|D_2^x| = 0.5(3)$  meV. Note that the fits are performed for  $c = +1$  meaning that the spin spiral structure, which is formed by DM interaction, has right rotating sense, in agreement with the recent experimental results obtained by spin-polarized scanning tunneling microscopy [13].

This is the first direct experimental determination of the DM vector components on each individual atomic site. The measured values are smaller than the theoretically predicted values for an Fe monolayer [22]. However, those calculations were done for the monolayer Fe without considering the temperature effects, whereas our experimental results are obtained for the double layer at RT by employing a simple model. This discrepancy might also be due to the fact that in the calculations the electron-magnon and phonon-magnon coupling are not considered.

In summary, we showed that the DM interaction lifts the degeneracy of the SWs and leads to an asymmetric spin-wave dispersion relation. The DM interaction induced energy asymmetry of SW energies is measured for an Fe double layer grown on W(110) using SPEELS. It is shown that the DM interaction is preserved even up to RT. An extended Heisenberg spin Hamiltonian is used to obtain the component of the DM vectors from the experimentally measured energy asymmetry. Our results, which reveal the importance of the antisymmetric exchange interaction, provide a new insight into the spin dynamics in magnetic nanostructures and would contribute to a better understanding of magnetism on the nanoscale.

The authors appreciate the fruitful discussions with D. L. Mills and L. Szunyogh.

\*Corresponding author.

zakeri@mpi-halle.de

- [1] I. E. Dzyaloshinskii, Sov. Phys. JETP **5**, 1259 (1957).
- [2] T. Moriya, Phys. Rev. **120**, 91 (1960).
- [3] A. Fert and P. M. Levy, Phys. Rev. Lett. **44**, 1538 (1980).
- [4] D. Coffey, T. M. Rice, and F. C. Zhang, Phys. Rev. B **44**, 10112 (1991).
- [5] J. Z. Zhao, X. Q. Wang, T. Xiang, Z. B. Su, and L. Yu, Phys. Rev. Lett. **90**, 207204 (2003).
- [6] H. De Raedt, S. Miyashita, K. Michielsen, and M. Machida, Phys. Rev. B **70**, 064401 (2004).
- [7] I. A. Sergienko and E. Dagotto, Phys. Rev. B **73**, 094434 (2006).
- [8] C. D. Hu, Phys. Rev. B **77**, 174418 (2008).
- [9] M. Bode, M. Heide, K. von Bergmann, P. Ferriani, S. Heinze, G. Bihlmayer, A. Kubetzka, O. Pietzsch, S. Blügel, and R. Wiesendanger, Nature (London) **447**, 190 (2007).
- [10] P. Ferriani, K. von Bergmann, E. Y. Vedmedenko, S. Heinze, M. Bode, M. Heide, G. Bihlmayer, S. Blügel, and R. Wiesendanger, Phys. Rev. Lett. **101**, 027201 (2008).
- [11] E. Y. Vedmedenko, L. Udvardi, P. Weinberger, and R. Wiesendanger, Phys. Rev. B **75**, 104431 (2007).
- [12] M. Heide, G. Bihlmayer, and S. Blügel, Phys. Rev. B **78**, 140403(R) (2008); Physica (Amsterdam) **404B**, 2678 (2009).
- [13] S. Meckler, N. Mikuszeit, A. Pressler, E. Y. Vedmedenko, O. Pietzsch, and R. Wiesendanger, Phys. Rev. Lett. **103**, 157201 (2009).
- [14] F. Bloch, Z. Phys. **61**, 206 (1930).
- [15] Y. Yafet, J. Kwo, and E. M. Gyorgy, Phys. Rev. B **33**, 6519 (1986).
- [16] P. Bruno, Phys. Rev. B **43**, 6015 (1991).
- [17] V. Kamberský, B. A. Ivanov, and E. V. Tartakovskaya, Phys. Rev. B **59**, 149 (1999).
- [18] R. B. Muniz and D. L. Mills, Phys. Rev. B **66**, 174417 (2002).
- [19] L. Udvardi, L. Szunyogh, K. Palotás, and P. Weinberger, Phys. Rev. B **68**, 104436 (2003).
- [20] M. G. Pini, P. Politi, and R. L. Stamps, Phys. Rev. B **72**, 014454 (2005).
- [21] A. T. Costa, R. B. Muniz, J. X. Cao, R. Q. Wu, and D. L. Mills, Phys. Rev. B **78**, 054439 (2008).
- [22] L. Udvardi and L. Szunyogh, Phys. Rev. Lett. **102**, 207204 (2009).
- [23] Kh. Zakeri, T. R. F. Peixoto, Y. Zhang, J. Prokop, and J. Kirschner, Surf. Sci. **604**, L1 (2010).
- [24] H. J. Elmers, Int. J. Mod. Phys. B **9**, 3115 (1995).
- [25] D. Sander, A. Enders, C. Schmidhals, J. Kirschner, H. L. Johnston, C. S. Arnold, and D. Venus, J. Appl. Phys. **81**, 4702 (1997); D. Sander, R. Skomski, A. Enders, C. Schmidhals, D. Reuter, and J. Kirschner, J. Phys. D **31**, 663 (1998); C. Schmidhals, D. Sander, A. Enders, and J. Kirschner, Surf. Sci. **417**, 361 (1998).
- [26] H. J. Elmers, J. Hauschild, and U. Gradmann, J. Magn. Magn. Mater. **221**, 219 (2000).
- [27] H. Ibach, D. Bruchmann, R. Vollmer, M. Etzkorn, P. S. Anil Kumar, and J. Kirschner, Rev. Sci. Instrum. **74**, 4089 (2003).
- [28] M. Plihal, D. L. Mills, and J. Kirschner, Phys. Rev. Lett. **82**, 2579 (1999).
- [29] R. Vollmer, M. Etzkorn, P. S. Anil Kumar, H. Ibach, and J. Kirschner, Phys. Rev. Lett. **91**, 147201 (2003).
- [30] W. X. Tang, Y. Zhang, I. Tudosa, J. Prokop, M. Etzkorn, and J. Kirschner, Phys. Rev. Lett. **99**, 087202 (2007).
- [31] J. Prokop, W. X. Tang, Y. Zhang, I. Tudosa, T. R. F. Peixoto, Kh. Zakeri, and J. Kirschner, Phys. Rev. Lett. **102**, 177206 (2009).
- [32] P. A. Grünberg, Prog. Surf. Sci. **18**, 1 (1985).



## Magnon Lifetimes on the Fe(110) Surface: The Role of Spin-Orbit Coupling

Kh. Zakeri,\* Y. Zhang, T.-H. Chuang, and J. Kirschner

*Max-Planck-Institut für Mikrostrukturphysik, Weinberg 2, 06120 Halle, Germany*

(Received 16 January 2012; published 9 May 2012)

We provide direct experimental evidence which demonstrates that, in the presence of a large spin-orbit coupling, the lifetime, amplitude, group, and phase velocity of the magnons propagating along two opposite (but crystallographically equivalent) directions perpendicular to the magnetization are different. A real time and space representation reveals that magnons with the same energy (eigenfrequency) propagate differently along two opposite directions. Our findings can inspire ideas for designing new spintronic devices.

DOI: 10.1103/PhysRevLett.108.197205

PACS numbers: 75.30.Ds, 75.50.Bb, 75.70.Ak, 75.70.Rf

A key part of spintronics is concerned with effects, which are linked to the spin-dependent phenomena [1]. In 1960, Rashba proposed a formalism which nicely describes the existence of a spin-split band structure in wurtzite crystals [2]. Later on, Bychkov and Rashba showed that such a spin splitting can also occur in quantum wells [3]. The physical explanation of this spin splitting phenomenon is rather straightforward: in a semiconductor quantum well, if the potential well is asymmetric, the electrons move in an effective electric field,  $\mathbf{E}$ , induced by the potential gradient of the quantum well. In the reference frame of the electron, this electric field transforms into an effective magnetic field,  $\mathbf{B}$  [4], which causes a splitting in the energy levels of electrons with different spins. A similar effect is expected for the electrons in the absence of an inversion symmetry and in the presence of a large spin-orbit coupling [5]. A spin-split band structure has been observed on some metallic surfaces, where the inversion symmetry is broken [6] and could be explained in analogy to the conventional Rashba effect in semiconductor heterostructures [7–9]. The idea is further tailored to the surface alloys composed of heavy elements. The combination of strong spin-orbit interaction of the heavy elements with structural effects enhances the local potential gradients at the surface and thereby results in a large Rashba splitting [10]. The Rashba effect has been explored in detail in various systems, and even some spintronic devices are proposed based on this effect [11–14].

Magnons describe the collective and single particle excitations of a spin system. Although for small wave vectors they have a parabolic dispersion relation in ferromagnets (similar to the one of the free electrons), they are classified as bosonic quasiparticles (with a spin of  $1\hbar$ ), unlike the electrons. One of the most interesting phenomena is the effect of the relativistic spin-orbit coupling on magnons as bosonic quasiparticles. Such an effect has not been explored in detail. Only recently, we have shown that the presence of the spin-orbit coupling in a spin system with broken inversion symmetry leads to an asymmetric magnon dispersion relation via the antisymmetric exchange

interaction, known as Dzyaloshinskii-Moriya interaction (DMI) [15]. In principle, the spin-orbit coupling in the presence of the broken inversion symmetry may also influence the magnon lifetime and amplitude.

In this Letter, we will show that a large spin-orbit coupling in the presence of the broken space inversion symmetry does not only break the degeneracy of the magnon energy but also influences the magnon lifetime and amplitude (modulus). By probing the surface magnons along a direction lying exactly in the mirror symmetry plane of the film magnetization, we demonstrate that (i) in addition to the magnon energy, the magnon lifetime and amplitude are substantially affected by the presence of the spin-orbit coupling, and (ii) a careful analysis of the magnon spectra in real time and space reveals that the magnons with the same energy (eigenfrequency) but opposite propagation direction propagate differently in the presence of the spin-orbit coupling. Moreover, we will comment on the role of temperature on the observed effects within the temperature range of 10–300 K.

The magnon dispersion relation is measured along the  $\bar{\Gamma}$ - $\bar{H}$  direction of the surface Brillouin zone for a two-atomic-layer thick Fe film grown on W(110) at room temperature using spin-polarized electron energy loss spectroscopy (SPEELS) [16]. A two-atomic-layer thick Fe film on W(110) is ferromagnetic, with a Curie temperature far above room temperature [17]. It shows a strong uniaxial magnetic anisotropy with an easy axis along the  $\langle\bar{1}10\rangle$  direction [17]. The dispersion relation is obtained by measuring the SPEEL spectra at different wave vectors [16,18]. The measurements were performed for the magnetization parallel to the  $[\bar{1}10]$  and  $[1\bar{1}0]$  directions. The results of such measurements are summarized in Fig. 1, demonstrating that the magnon dispersion relation is split into two branches for magnetization along two opposite directions. The dispersion relation is antisymmetric, meaning that the magnon energies for positive wave vectors are equal to the ones with negative wave vectors and opposite magnetization direction (or vice versa). In fact, the presence of the relativistic spin-orbit coupling in the absence of

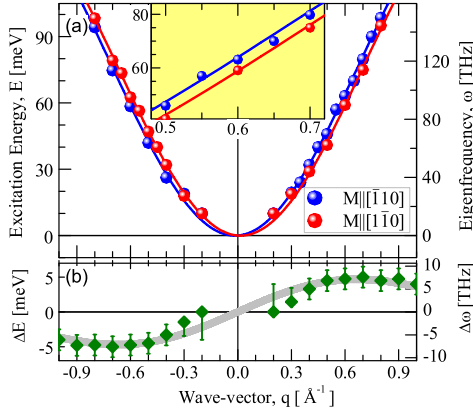


FIG. 1 (color online). (a) Magnon dispersion relation measured on a 2 ML Fe on W(110) at room temperature and for two different magnetization directions. The inset shows a magnified part of the graph for a smaller energy and wave-vector window. (b) The energy splitting defined as  $\Delta E(q) = E_{M||[110]}(q) - E_{M||[110\bar{0}]}(q)$  obtained from (a). The symbols represent the experimental results, while the solid lines represent the fits based on the extended Heisenberg spin Hamiltonian.

time reversal and space inversion symmetry breaks the degeneracy of the magnon energy and leads to a splitting of the magnon band structure. The asymmetric dispersion relation can be understood in terms of the antisymmetric DMI, which is a consequence of the spin-orbit coupling [15,19]. In such cases, the extended Heisenberg spin Hamiltonian (HSH) may be used to obtain the DM vectors. The extended HSH reads as  $H = -\sum_{i \neq j} J_{ij} \mathbf{S}_i \cdot \mathbf{S}_j + \sum_{i \neq j} \mathbf{D}_{ij} \cdot \mathbf{S}_i \times \mathbf{S}_j - K \sum_i (\mathbf{S}_i \cdot \hat{z})^2$ . The first term represents the symmetric exchange interaction with the isotropic exchange coupling constant  $J_{ij}$  between spins  $\mathbf{S}_i$  and  $\mathbf{S}_j$ , the second term represents the antisymmetric DMI with the DM vectors  $\mathbf{D}_{ij}$ , and the last term accounts for the magnetic anisotropy energy in the system with an easy axis along  $\hat{z}$  ( $K$  denotes the effective magnetic anisotropy energy constant). The solid lines in Fig. 1 are the fits based on the extended HSH given above. The fit parameters are  $K = 0$ ,  $J_1 = 7.5(5)$  meV,  $J_2 = 4.5(3)$  meV,  $|2D_1^x + \dot{D}_1^x| = 0.9(3)$  meV, and  $|D_2^x| = 0.5(3)$  meV. The subscript 1(2) represents the nearest-neighbor (next-nearest-neighbor) interaction.  $D_1^x$  ( $\dot{D}_1^x$ ) is the longitudinal component of the DM vector of the nearest neighbors in the same atomic plane (in the neighboring atomic plane). A detailed discussion and a comparison to the literature can be found in Ref. [15].

The splitting of the magnon band structure shown in Fig. 1 is very similar to the well-known Rashba effect observed for electrons in a two-dimensional electron gas or at metal surfaces [7–9]. Therefore, the effect may be called the “*magnon Rashba effect*” [20]. More importantly, we observed that the magnons’ lifetimes are different when

they propagate along opposite (but crystallographically equivalent) directions. Our experimental results are in line with the recent theoretical calculations based on the multiband Hubbard model [20]. The difference in the lifetime when the magnons propagate along opposite directions is a consequence of the spin-orbit coupling. The spin-orbit-induced damping is a well-known damping mechanism for small wave-vector magnons, in particular, in the case of the uniform ferromagnetic resonance mode ( $q = 0$ ). As a simple model for the intrinsic ferromagnetic resonance damping, one may imagine the precession of the spin that is coupled to its orbital motion via the spin-orbit coupling. The orbital motion is perturbed by the lattice simultaneously and hence cannot follow the same phase anymore and it results in a damping. For high wave-vector magnons, the damping is mainly governed by dissipation into the Stoner states (known as *Landau damping*) [21]. In the case of Fe films on W(110), magnons are subjected to a large spin-orbit coupling coming mainly from the hybridization with the tungsten substrate. In such a case, a spin-orbit-induced damping is superimposed to the Landau type of damping. Since the time reversal inverts the angular and linear momentum, it inverts the spin-orbit contribution to the lifetime (the lifetime of magnons with  $+M$ ,  $+q$  is identical to the one of magnons with  $-M$ ,  $-q$ ). This is exactly what we observe in our experiment.

The spin Hamiltonian discussed above does not account for the magnons’ lifetimes. In order to obtain detailed information on the magnons’ lifetimes and amplitudes, one needs to perform a full intensity and broadening analysis of the excitations. For that, the SPEEL spectra are measured at a fixed scattering geometry and with exactly the same parameters (like incidence energy, beam current, and energy resolution) and only the sample magnetization is switched to the opposite direction. The experiment is designed such that the magnons propagate in the mirror symmetry plane of the magnetization. Since the magnon intensity depends on the scattering matrix elements, keeping the scattering geometry and experimental parameters unchanged during the experiment would avoid the effects caused by geometry on the electron scattering processes and thereby on the magnon intensity. Reversing the magnetization is equivalent to time inversion; therefore, one can reverse the magnon propagation direction only by reversing the direction of the magnetization. This approach opens a possibility to measure the magnons with positive and negative wave vectors without changing the scattering geometry. The SPEELS intensity spectra are recorded for different wave vectors. The difference spectra are obtained according to  $I_{\text{Diff.}} = I_{\downarrow} - I_{\uparrow}$  ( $I_{\downarrow}$  and  $I_{\uparrow}$  represent the intensity of the scattered electrons for the incidence of spin-down and spin-up electrons, respectively). The obtained SPEELS difference spectra are fitted with Voigt profiles [22], which then are plotted in Fig. 2 as a contour map (the

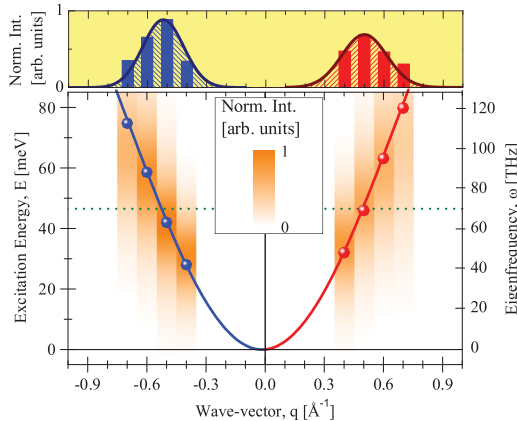


FIG. 2 (color). Magnon dispersion relation together with the intensity map. The negative branch is measured by reversing the magnetization. The SPEELS difference spectra are obtained based on  $I_{\text{Diff.}} = I_{\uparrow} - I_{\downarrow}$  after recording  $I_{\uparrow}$  and  $I_{\downarrow}$  spectra and are fitted with Voigt functions. The resulting curves are plotted as a contour map. The peak position is represented as solid circles. The solid line is a fit based on the extended Heisenberg spin Hamiltonian. The upper panel shows the intensity profile along the dotted line at  $E = 46.5$  meV.

intensity is represented in the color scale). The excitation energies are shown as filled circles.

Now, we attempt to provide a real time and space representation of the magnons from our experimental data. This is essential because only then can we clearly see the consequences of the differences in the lifetime, amplitude, group, and phase velocity on the behavior of the magnon wave packets. An example is given for the magnons with an excitation energy of  $E = 46.5$  meV. The distribution of magnon intensity in momentum space is obtained from the line profile at  $E = 46.5$  meV. The profiles are shown in the upper panel of Fig. 2. We assume that the momentum distribution is a Gaussian distribution. Using the Fourier transform, one can have direct access to the real space representation of the magnons. For the magnons with an energy of  $E = 46.5$  meV, the wave vectors are  $+0.50 \text{ \AA}^{-1}$  and  $-0.52 \text{ \AA}^{-1}$ . The corresponding wavelengths are about  $12.6 \text{ \AA}$  and  $12.1 \text{ \AA}$ , respectively. Note that, in the absence of relativistic effects, the absolute values of the wave vectors (wavelengths) for the positive and negative branches have to be exactly the same. The difference in the absolute value of the wave vectors (wavelengths) is a direct consequence of the spin-orbit coupling. The real time and space representation of the magnons is presented in Fig. 3 (see the animated movie in the Supplemental Material [23]). The magnon wave packet starts to propagate at  $t = 0$ , with the maximum amplitude at  $x = 0$ . The lifetime of the magnons in itinerant ferromagnets is usually very short. It is defined as the time in which the amplitude of the magnon wave packet is reduced

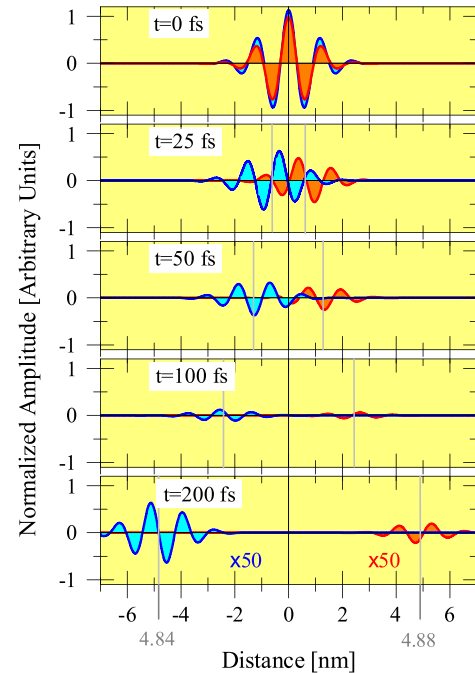


FIG. 3 (color online). A real time and space representation of the magnon wave packets. The wave packets start to propagate at  $t = 0$ , with the maximum amplitude at  $x = 0$ . The wave packet with smaller amplitude propagates along the  $[001]$  direction, and the one with larger amplitude propagates along the  $[00\bar{1}]$  direction. The vertical gray lines indicate the center of the mass of the wave packets.

by a factor of  $1/e$ . The values obtained at  $E = 46.5$  meV for positive and negative wave vectors are  $\tau_+ \approx 37 \pm 5$  fs and  $\tau_- \approx 45 \pm 5$  fs, respectively. The short wavelength together with the short lifetime compress the magnon's wave packet such that it contains only a few oscillations in space (see Fig. 3). The group velocity,  $v_g = \partial\omega/\partial q$  ( $\omega = E/\hbar$  is the eigenfrequency and  $q$  is the wave vector), is obtained from the slope of the dispersion curve at the given energy ( $E = 46.5$  meV) and wave vectors ( $q = +0.50 \text{ \AA}^{-1}$  and  $-0.52 \text{ \AA}^{-1}$ ). Since the dispersion relation is asymmetric, the group velocity is different for the magnons propagating along two opposite directions. For the ones that are propagating along the  $[001]$  direction (the ones with  $q = +0.50 \text{ \AA}^{-1}$ ), it is  $v_g = 24.4$  km/s, and, for the ones propagating along the  $[00\bar{1}]$  direction (the ones with  $q = -0.52 \text{ \AA}^{-1}$ ), it is about  $v_g = -24.2$  km/s. The differences in the group velocity, lifetime, and amplitude lead to a different propagation behavior for the magnons along two opposite directions. Figure 3 demonstrates that after 200 fs the magnon's wave packet, which is propagating along the  $[001]$  direction, propagates  $48.8 \text{ \AA}$  and is strongly damped but the one which is propagating along the  $[00\bar{1}]$  direction propagates  $48.4 \text{ \AA}$ . The extrapolation of

our results to  $q = 0$  reveals that the uniform mode with zero wave vector possesses a finite group velocity of about  $v_g(q = 0) \approx 1$  km/s. The phase velocity can be obtained using the simple expression  $v_p = E/q$ , which results in  $v_p = 14.4$  km/s for the magnons with an energy of 46.5 meV and  $q = 0.50 \text{ \AA}^{-1}$ . It is about  $-13.4$  km/s for the magnons with an energy of 46.5 meV and  $q = -0.52 \text{ \AA}^{-1}$ . The phase velocity is smaller than the group velocity, meaning that the magnon wave packets disperse during the propagation (see Fig. 3 and [23]).

Now, we comment on the temperature effects. The experiments performed at 10 K reveal that the splitting of the magnon band structure and the spin-orbit-induced modifications of the lifetime and amplitude, discussed above, do not depend strongly on temperature. The splitting in the energy observed for the wave vector of  $\pm 0.5 \text{ \AA}^{-1}$  is about  $\Delta E = 6 \pm 2$  meV at 10 K, which is very close to the value measured at 300 K. The absolute values of magnon energies measured at low temperatures are found to be slightly larger than the ones measured at 300 K. This reflects mainly the temperature dependence of the effective exchange coupling (or exchange stiffness). The negligible temperature dependence of this effect might be due to the fact that the Curie temperature of the system is far above the measured temperature window [17].

The effect discussed above may be used to propose spintronic devices, since it is not restricted to the Fe/W (110) system. The basic functionality of such a device would be somehow similar to the ones that are proposed based on the conventional Rashba effect [1,11–14], but with considering the fact that magnons are basically different from electrons. The simplest device, based on this principle, can be imagined as follows: One excites the transversal surface magnons (those that are propagating perpendicular to the magnetization) on a ferromagnetic surface. Simultaneously, two wave packets will propagate to opposite directions. Because of the spin-orbit-induced effects, the wave packet which is propagating towards the left gate possesses a larger amplitude and lifetime, while the one that is propagating towards the right gate will die out quickly. When the magnon wave packet arrives at the left gate, it can be detected. At the same time, no magnon signal can be detected by the other gate. The switching of this state to a state in which the right gate detects a signal and no signal arrives at the left gate can be realized just by reversing the magnetization of the ferromagnet (see the text in the Supplemental Material [23]). Since the magnons discussed here have wavelengths of a few nanometers, they would allow signal processing at the nanometer scale, which is essential for such small devices. However, the suggestion and realization of such devices require detailed knowledge of the basic concepts of the effect.

In conclusion, we showed that, in addition to the magnons' energy, their lifetime and amplitude are also modified by spin-orbit coupling, when they propagate along

two opposite directions perpendicular to the magnetization. The differences in the lifetime, amplitude, and group velocity lead to a substantial difference in the magnon propagation behavior along two opposite (but crystallographically equivalent) directions. The spin-orbit-induced effects on magnon band structure, lifetime, and amplitude are found to be nearly temperature-independent within the temperature range of 10–300 K. In addition to the fact that our results manifest the relativistic spin-orbit effects on spin excitations, which will provide a deeper understanding of magnetism on the nanoscale, they may inspire new ideas for designing new spintronic devices based on these effects.

\*Corresponding author  
zakeri@mpi-halle.de

- [1] S. A. Wolf, D. D. Awschalom, R. A. Buhrman, J. M. Daughton, S. von Molnár, M. L. Roukes, A. Y. Chtchelkanova, and D. M. Treger, *Science* **294**, 1488 (2001).
- [2] E. I. Rashba, *Sov. Phys. Solid State* **2**, 1109 (1960).
- [3] Yu. A. Bychkov and E. I. Rashba, *JETP Lett.* **39**, 78 (1984).
- [4] H. Chapman and C. A. R. Sa de Melo, *Nature (London)* **471**, 41 (2011).
- [5] R. Winkler, *Spin-Orbit Coupling Effects in Two-Dimensional Electron and Hole Systems* (Springer, New York, 2003).
- [6] S. LaShell, B. A. McDougall, and E. Jensen, *Phys. Rev. Lett.* **77**, 3419 (1996).
- [7] J. Henk, A. Ernst, and P. Bruno, *Phys. Rev. B* **68**, 165416 (2003).
- [8] O. Krupin, G. Bihlmayer, K. Starke, S. Gorovikov, J. E. Prieto, K. Döbrich, S. Blügel, and G. Kaindl, *Phys. Rev. B* **71**, 201403(R) (2005).
- [9] G. Bihlmayer, Yu. M. Koroteev, P. M. Echenique, E. V. Chulkov, and S. Blügel, *Surf. Sci.* **600**, 3888 (2006).
- [10] C. R. Ast, J. Henk, A. Ernst, L. Moreschini, M. C. Falub, D. Pacile, P. Bruno, K. Kern, and M. Grioni, *Phys. Rev. Lett.* **98**, 186807 (2007).
- [11] S. Datta and B. Das, *Appl. Phys. Lett.* **56**, 665 (1990).
- [12] T. Koga, J. Nitta, H. Takayanagi, and S. Datta, *Phys. Rev. Lett.* **88**, 126601 (2002).
- [13] H. C. Koo, J. H. Kwon, J. Eom, J. Chang, S. H. Han, and M. Johnson, *Science* **325**, 1515 (2009).
- [14] I. M. Miron, G. Gaudin, S. Auffret, B. Rodmacq, A. Schuhl, S. Pizzini, J. Vogel, and P. Gambardella, *Nature Mater.* **9**, 230 (2010).
- [15] Kh. Zakeri, Y. Zhang, J. Prokop, T.-H. Chuang, N. Sakr, W. X. Tang, and J. Kirschner, *Phys. Rev. Lett.* **104**, 137203 (2010).
- [16] H. Ibach, D. Bruchmann, R. Vollmer, M. Etzkorn, P. S. Anil Kumar, and J. Kirschner, *Rev. Sci. Instrum.* **74**, 4089 (2003).
- [17] H. J. Elmers, *Int. J. Mod. Phys. B* **9**, 3115 (1995).
- [18] W. X. Tang, Y. Zhang, I. Tudosa, J. Prokop, M. Etzkorn, and J. Kirschner, *Phys. Rev. Lett.* **99**, 087202 (2007).

- [19] L. Udvardi and L. Szunyogh, *Phys. Rev. Lett.* **102**, 207204 (2009).
- [20] A. T. Costa, R. B. Muniz, S. Lounis, A. B. Klautau, and D. L. Mills, *Phys. Rev. B* **82**, 014428 (2010).
- [21] P. Buczek, A. Ernst, and L. M. Sandratskii, *Phys. Rev. Lett.* **106**, 157204 (2011).
- [22] The choice of the Voigt function is based on the fact that the measured SPEELS spectra are a convolution of a Lorentzian line shape with a Gaussian distribution, caused by instrumental broadenings.
- [23] See Supplemental Material at <http://link.aps.org/supplemental/10.1103/PhysRevLett.108.197205> for detailed information.



# Direct probing of the exchange interaction at buried interfaces

Kh. Zakeri<sup>1\*</sup>, T.-H. Chuang<sup>1</sup>, A. Ernst<sup>1,2</sup>, L. M. Sandratskii<sup>1</sup>, P. Buczek<sup>1</sup>, H. J. Qin<sup>1</sup>, Y. Zhang<sup>1,3</sup>  
and J. Kirschner<sup>1,4</sup>

**The fundamental interactions between magnetic moments at interfaces have an important impact on the properties of layered magnetic structures. Hence, a direct probing of these interactions is highly desirable for understanding a wide range of phenomena in low-dimensional solids. Here we propose a method for probing the magnetic exchange interaction at buried interfaces using spin-polarized electrons and taking advantage of the collective nature of elementary magnetic excitations (magnons). We demonstrate that, for the case of weak coupling at the interface, the low-energy magnon mode is mainly localized at the interface. Because this mode has the longest lifetime of the modes and has a finite spectral weight across the layers on top, it can be probed by electrons. A comparison of experimental data and first-principles calculations leads to the determination of the interface exchange parameters. This method may help the development of spectroscopy of buried magnetic interfaces.**

Magnons are the elementary magnetic excitations in a magnetically ordered solid. Generally, each magnon corresponds to the reduction in the total magnetization of the system by two Bohr magnetons ( $2\mu_B$ ), which is manifested as the deviation of the atomic moments from the equilibrium direction. There are a few important differences between magnon excitations in thin films grown on a substrate and those in bulk crystals. In single-element bulk crystals all atoms are equivalent and contribute equally to different magnon modes. This means that a magnon can be visualized as the deviation of all atomic moments by the same angle  $\theta$  from the equilibrium direction, whereas the variation of the azimuth angle  $\phi$  is defined by the wavevector of the magnon. All moments precess with the same eigenfrequency about the equilibrium direction. The eigenfrequency  $\omega$  of the precession determines the energy of the magnons ( $E = \hbar\omega$ , where  $\hbar$  is the reduced Planck's constant).

However, in thin films, the atoms become inequivalent due to the absence of translational invariance in the direction orthogonal to the surface. Consequently, the atoms located in the surface and interface atomic layers have a smaller effective interatomic exchange coupling than the atoms located in the inner part of the film. Of particular interest is the strength of the coupling at the interface, because it has a direct impact on the properties of the system<sup>1</sup>. For atoms located in the surface atomic layer, the important factor influencing the interatomic exchange interaction is the reduced atomic coordination. For atoms located in the interface atomic layer an additional strong influence comes from the hybridization of the electronic states of the atoms with those of the substrate atoms. A natural consequence of the inequivalence of the atomic layers is that the deviations of the moments  $\theta$  characterizing a given magnon mode can differ for atoms located at different places in the structure<sup>2,3</sup>. Hence, one can anticipate the existence of at least three different types of magnon: surface, bulk and interface magnons. In this nomenclature each magnon mode is named according to the part of the film whose atomic moments contribute most to that particular magnon mode. How different the surface and

interface magnons are in a given system depends strongly on the relative values of the interatomic exchange parameters at the surface, interface and bulk.

Generally, magnons can be excited and probed by different means, for example, neutrons, electrons and photons. Of these, electrons are the best for exciting magnons in small-sized structures, such as ultrathin films and nanostructures<sup>4–14</sup>, because the interaction of electrons with the matter is much stronger than that with neutrons and photons. As a consequence, the spin-dependent inelastic mean free path in metallic ferromagnets is short<sup>15,16</sup>. However, one has to take into account the most important feature of magnons in metallic systems. Different magnon modes have different spatial distributions across the film. Even those that are carrying the interface information have a finite spectral weight in the atomic layers on top. Moreover, the lifetime of different magnon modes is different. A competition between the spectral weight and the lifetime determines the experimental spectra. We will show that the low-energy magnon mode, localized mainly at the interface, has the longest lifetime of the modes, so a small spectral weight at the surface is sufficient to excite and probe this mode and thereby probe the interface exchange parameters.

## Probing low-energy magnons in Fe(001) films on Ir(001)

As an example, we study the magnetic coupling at the interface of epitaxial thin Fe(001) films, six to nine atomic layers thick, grown on Ir(001). We use spin-polarized electron energy loss spectroscopy (SPEELS) to excite and probe the magnons. A schematic representation of the excitation and detection scheme in our experiment is presented in Fig. 1a. The Fe films investigated here are ferromagnetic at room temperature, as can be seen from the magnetic hysteresis loop presented in Fig. 1b. In SPEELS a well-defined spin-polarized electron beam is shot onto the sample surface, and the energy distribution of the scattered electrons is measured for two different spin polarizations of the incoming beam (parallel or antiparallel to the macroscopic magnetization). The difference spectrum is defined as  $I_{\downarrow} - I_{\uparrow}$ , where  $I_{\downarrow}$  and  $I_{\uparrow}$  are the recorded intensities of

<sup>1</sup>Max-Planck-Institut für Mikrostrukturphysik, Weinberg 2, 06120 Halle, Germany, <sup>2</sup>Wilhelm Ostwald Institut für Physikalische und Theoretische Chemie, Universität Leipzig, Linnéstrasse 2, 04103 Leipzig, Germany, <sup>3</sup>Department of Chemistry, University College London, 20 Gordon Street, London WC1H 0AJ, UK, <sup>4</sup>Institut für Physik, Martin-Luther-Universität Halle-Wittenberg, 06120 Halle, Germany. \*e-mail: zakeri@mpi-halle.de

## ARTICLES

## NATURE NANOTECHNOLOGY DOI: 10.1038/NNANO.2013.188

were obtained by using the magnetic force theorem, implemented within the Green function method<sup>26</sup>.

The second set of calculations were performed based on linear-response, time-dependent density functional theory<sup>21</sup>. This type of calculation provides information on the lifetime of excitations.

Received 18 March 2013; accepted 20 August 2013;  
published online 22 September 2013

## References

- Nolting, F. *et al.* Direct observation of the alignment of ferromagnetic spins by antiferromagnetic spins. *Nature* **405**, 767–769 (2000).
- Mills, D. L. Surface corrections to the specific heat of ferromagnetic films. *Phys. Rev. B* **1**, 264–274 (1970).
- Costa, A. T., Muniz, R. B. & Mills, D. L. Spin waves and their damping in itinerant ultrathin ferromagnets: intermediate wave vectors. *Phys. Rev. B* **74**, 214403 (2006).
- Ibach, H. *et al.* A novel spectrometer for spin-polarized electron energy-loss spectroscopy. *Rev. Sci. Instrum.* **74**, 4089–4095 (2003).
- Ibach, H., Rajeswari, J. & Schneider, C. M. An electron energy loss spectrometer designed for studies of electronic energy losses and spin waves in the large momentum regime. *Rev. Sci. Instrum.* **82**, 123904 (2011).
- Vollmer, R., Etkorn, M., Kumar, P. S. A., Ibach, H. & Kirschner, J. Spin-polarized electron energy loss spectroscopy of high energy, large wave vector spin waves in ultrathin fcc Co films on Cu(001). *Phys. Rev. Lett.* **91**, 147201 (2003).
- Heinrich, A. J., Gupta, J. A., Lutz, C. P. & Eigler, D. M. Single-atom spin-flip spectroscopy. *Science* **306**, 466–469 (2004).
- Balashov, T., Takács, A. F., Wulfhekel, W. & Kirschner, J. Magnon excitation with spin-polarized scanning tunneling microscopy. *Phys. Rev. Lett.* **97**, 187201 (2006).
- Tang, W. X. *et al.* Large wave vector spin waves and dispersion in two monolayer Fe on *w*(110). *Phys. Rev. Lett.* **99**, 087202 (2007).
- Gao, C. L. *et al.* Spin wave dispersion on the nanometer scale. *Phys. Rev. Lett.* **101**, 167201 (2008).
- Prokop, J. *et al.* Magnons in a ferromagnetic monolayer. *Phys. Rev. Lett.* **102**, 177206 (2009).
- Zhang, Y. *et al.* Nonmonotonic thickness dependence of spin wave energy in ultrathin Fe films: experiment and theory. *Phys. Rev. B* **81**, 094438 (2010).
- Zakeri, K. *et al.* Asymmetric spin-wave dispersion on Fe(110): direct evidence of the Dzyaloshinskii–Moriya interaction. *Phys. Rev. Lett.* **104**, 137203 (2010).
- Zakeri, K., Zhang, Y., Chuang, T.-H. & Kirschner, J. Magnon lifetimes on the Fe(110) surface: the role of spin–orbit coupling. *Phys. Rev. Lett.* **108**, 197205 (2012).
- Hong, J. & Mills, D. L. Theory of the spin dependence of the inelastic mean free path of electrons in ferromagnetic metals: a model study. *Phys. Rev. B* **59**, 13840–13848 (1999).
- Hong, J. & Mills, D. L. Spin dependence of the inelastic electron mean free path in Fe and Ni: explicit calculations and implications. *Phys. Rev. B* **62**, 5589–5600 (2000).
- Zakeri, K. & Kirschner, J. in *Probing Magnons by Spin-Polarized Electrons* Ch. 7, 84–99 (Topics in Applied Physics Magnonics From Fundamentals to Applications 125, Springer, 2013).
- Zhang, Y., Chuang, T.-H., Zakeri, K. & Kirschner, J. Relaxation time of terahertz magnons excited at ferromagnetic surfaces. *Phys. Rev. Lett.* **109**, 087203 (2012).
- Martin, V. *et al.* Pseudomorphic growth of Fe monolayers on Ir(001)(1×1): from a fct precursor to a bct film. *Phys. Rev. B* **76**, 205418 (2007).
- Zakeri, K., Zhang, Y. & Kirschner, J. Surface magnons probed by spin-polarized electron energy loss spectroscopy. *J. Electron Spectrosc. Rel. Phenom.* <http://dx.doi.org/10.1016/j.elspec.2012.06.009> (in the press).
- Buczek, P., Ernst, A. & Sandratskii, L. M. Different dimensionality trends in the Landau damping of magnons in iron, cobalt, and nickel: time-dependent density functional study. *Phys. Rev. B* **84**, 174418 (2011).
- Zakeri, K., Peixoto, T., Zhang, Y., Prokop, J. & Kirschner, J. On the preparation of clean tungsten single crystals. *Surf. Sci.* **604**, L1–L3 (2010).
- Deák, A., Szunyogh, L. & Ujfalussy, B. Thickness-dependent magnetic structure of ultrathin Fe/Ir(001) films: from spin-spiral states toward ferromagnetic order. *Phys. Rev. B* **84**, 224413 (2011).
- Perdew, J. P., Burke, K. & Ernzerhof, M. Generalized gradient approximation made simple. *Phys. Rev. Lett.* **77**, 3865–3868 (1996).
- Lüders, M., Ernst, A., Temmerman, W. M., Szotek, Z. & Durham, P. J. *Ab initio* angle-resolved photoemission in multiple-scattering formulation. *J. Phys.* **13**, 8587–8606 (2001).
- Lichtenstein, A. I., Katsnelson, M. I., Antropov, V. P. & Gubanov, V. A. Local spin density functional approach to the theory of exchange interactions in ferromagnetic metals and alloys. *J. Magn. Magn. Mater.* **67**, 65–74 (1987).

## Acknowledgements

A.E. acknowledges funding from the Deutsche Forschungsgemeinschaft (DFG priority programme SPP 1538 ‘Spin Caloric Transport’). The calculations were performed at the Rechenzentrum Garching of the Max Planck Society.

## Author contributions

Kh.Z. supervised the project, conceived and planned the experiments, participated in the analysis of the experimental data and wrote the paper. T.-H.C. carried out the experiments and analysed the experimental data. A.E. and P.B. performed the theoretical calculations. A.E. analysed the theoretical results. L.M.S. participated in the analysis of the theoretical results, the development of the structure of the paper and in writing the paper. H.J.Q. performed one part of the experiments and analysed the experimental data. Y.Z. contributed to the experiments. J.K. supervised the project. All authors contributed to the discussion of the results and improving the manuscript.

## Additional information

Supplementary information is available in the [online version](#) of the paper. Reprints and permissions information is available online at [www.nature.com/reprints](http://www.nature.com/reprints). Correspondence and requests for materials should be addressed to Kh.Z.

## Competing financial interests

The authors declare no competing financial interests.



## Magnons in ultrathin ferromagnetic films with a large perpendicular magnetic anisotropy

H. J. Qin,<sup>1</sup> Kh. Zakeri,<sup>1,\*</sup> A. Ernst,<sup>1,2</sup> T.-H. Chuang,<sup>1</sup> Y.-J. Chen,<sup>1</sup> Y. Meng,<sup>1</sup> and J. Kirschner<sup>1,3</sup>

<sup>1</sup>Max-Planck-Institut für Mikrostrukturphysik, Weinberg 2, 06120 Halle, Germany

<sup>2</sup>Wilhelm Ostwald Institut für Physikalische und Theoretische Chemie, Universität Leipzig, Linnéstraße 2, 04103 Leipzig, Germany

<sup>3</sup>Institut für Physik, Martin-Luther-Universität Halle-Wittenberg, 06120 Halle, Germany

(Received 15 April 2013; published 15 July 2013)

We report on an experimental observation of high-energy magnon excitations in ultrathin ferromagnetic films with a perpendicular easy axis. We demonstrate that a transversally spin-polarized beam can be used to excite and probe the high-energy magnons within spin-polarized electron energy-loss spectroscopy experiments. The magnon dispersion relation and lifetime are probed over the entire surface Brillouin zone for a set of body-centered tetragonal FeCo films with a large perpendicular magnetic anisotropy. First-principles calculations reveal that in addition to the tetragonal distortion, which is the origin of the large perpendicular magnetic anisotropy, the interfacial electronic hybridization also has a considerable impact on the properties of magnons.

DOI: 10.1103/PhysRevB.88.020404

PACS number(s): 75.30.Ds, 75.50.Bb, 75.70.Ak, 75.70.Rf

Ultrathin magnetic films with large perpendicular magnetic anisotropy (PMA) have attracted much attention due to their interesting fundamental properties and also their promising technological applications in ultrahigh-density magnetic recording,<sup>1,2</sup> magnetic tunneling junctions (MTJs),<sup>3</sup> and spin-transfer torque (STT) devices.<sup>4,5</sup> Because of their large PMA, these materials allow development of smaller magnetic elements with a high thermal stability. The STT devices fabricated by layers with PMA require a smaller switching current.

Many observed phenomena in the above-mentioned devices are attributed to the emission or absorption of interface magnons while performing transport experiments. For instance, the bias and temperature dependence of tunneling magnetoresistance in MTJs are attributed to the magnon emission and absorption by the tunneling hot electrons at the ferromagnet/insulator interface.<sup>6–8</sup> Although the magnon excitations are lying in the central point of explanation of all these phenomena, the full magnon spectrum of these materials is not known experimentally. Certainly, the knowledge on terahertz magnons would have a large impact on the understanding of many observed phenomena in the transport experiments as well as the ultrafast spin dynamics in these materials.

The experimental techniques enabling magnon investigation either do not have enough sensitivity, as in inelastic neutron scattering, or probe only a very narrow region of the momentum space close to the Brillouin zone center, as in Brillouin light scattering, and ferromagnetic resonance experiments. Recently, new experimental methods have been successfully applied to study magnetic excitations in low-dimensional magnets. They are based either on inelastic tunneling spectroscopy<sup>9</sup> or on spin-polarized electron energy loss spectroscopy (SPEELS).<sup>10,11</sup> Until now SPEELS has been used to study terahertz magnons in ultrathin films *with an in-plane easy axis*.<sup>10–20</sup> As the films with PMA possess an out-of-plane magnetic stray field, there has been a long-standing question concerning the possibility of probing magnons in these materials using SPEELS.

Here we report on an experimental observation of magnon excitations in a prototype PMA system, e.g., an ultrathin FeCo film (in the form of alloy as well as alternating Fe

and Co atomic layers). We will show how a transversally spin-polarized electron beam can be used to excite the magnons in an ultrathin film with a perpendicular easy axis. We demonstrate that the excitation probability (cross section) is rather strong such that one can easily excite and probe the magnons up to the surface Brillouin zone boundary and beyond. The dispersion relation and the lifetime of terahertz magnons in these materials are probed over the whole surface Brillouin zone. We show that the magnons' energies are rather low and their lifetimes are relatively short. Our first-principles calculations in the framework of density functional theory account for the explanation of the observed effects and provide us with information on the magnetic exchange parameters. We will also comment on the role of tetragonal distortion, which is the origin of large PMA in these materials, on the magnon dispersion relation.

The first main question to answer is: How might a transversally spin-polarized beam be used to excite the magnons? Let us assume a spin-polarized beam with an arbitrary polarization vector  $\mathbf{P} = |P|\mathbf{e}$ , where  $\mathbf{e} = \sin \vartheta \cos \varphi \hat{i} + \sin \vartheta \sin \varphi \hat{j} + \cos \vartheta \hat{k}$  is the unit vector in space indicating the direction of the spin-polarization vector [ $\vartheta$  and  $\varphi$  are the polar and azimuthal angles, respectively, and are defined with respect to the quantization axis; see Fig. 1(a)] and  $|P|$  is the norm of the polarization vector. The polarization vector of a given spin-polarized beam can be expressed in terms of Dirac spinors defining the spin-up and spin-down states.<sup>21</sup> This can be simply done by finding the eigenstates of

$$(\boldsymbol{\sigma} \cdot \mathbf{e})\chi = \lambda\chi, \quad (1)$$

where  $\boldsymbol{\sigma}$  represents the Pauli spin matrices and  $\boldsymbol{\sigma} \cdot \mathbf{e}$  is the projection of the spin operator in a polarization direction.  $\lambda$  and  $\chi$  represent the eigenvalue and the eigenstate of  $\boldsymbol{\sigma} \cdot \mathbf{e}$ , respectively. The solution of Eq. (1) is

$$\chi = \begin{pmatrix} \cos \frac{\vartheta}{2} \\ \sin \frac{\vartheta}{2} e^{i\varphi} \end{pmatrix} \quad \text{for } \lambda = +1, \quad (2)$$

$$\chi = \begin{pmatrix} \sin \frac{\vartheta}{2} \\ -\cos \frac{\vartheta}{2} e^{i\varphi} \end{pmatrix} \quad \text{for } \lambda = -1.$$

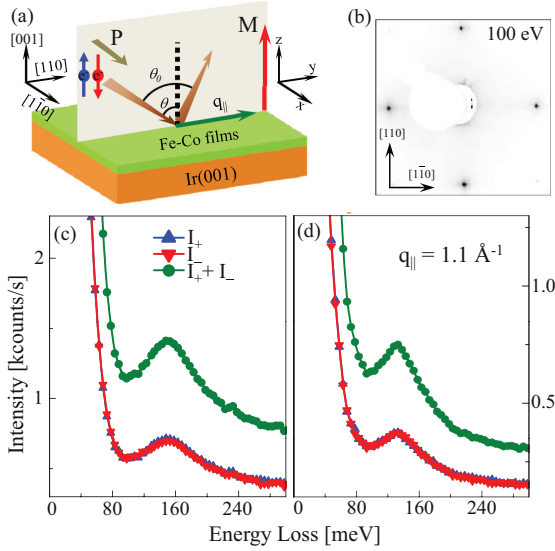
H. J. QIN *et al.*PHYSICAL REVIEW B **88**, 020404(R) (2013)

FIG. 1. (Color online) (a) A schematic representation of the scattering geometry. The beam polarization is either parallel or antiparallel to the  $[1\bar{1}0]$  direction (it is perpendicular to the quantization axis being the  $[001]$  direction). (b) A typical LEED pattern recorded on an ultrathin Fe<sub>0.5</sub>Co<sub>0.5</sub> alloy film with a thickness of 4 ML. SPEELS spectra recorded on the surfaces of a 4 ML Fe<sub>0.5</sub>Co<sub>0.5</sub> alloy film (c) and a 4 ML Fe/Co multilayer film (d) at a wave vector of  $q_{\parallel} = 1.1 \text{ \AA}^{-1}$ .  $I_{-}$  ( $I_{+}$ ) indicates the intensity of the scattered electrons for the polarization vector of incident beam parallel (antiparallel) to the  $[1\bar{1}0]$  direction. The total spectrum is shown by  $I_{+} + I_{-}$ . All the crystallographic directions depicted here are the ones of Ir(001).

For the case where  $\mathbf{P}$  is parallel or antiparallel to the the magnetization (the quantization axis) one has  $\vartheta = 0, \varphi = 0$  [see Fig. 1(a)] and hence Eq. (1) yields the expected eigenstate of  $\sigma_z$ ,  $\begin{pmatrix} 1 \\ 0 \end{pmatrix}$  or  $\begin{pmatrix} 0 \\ 1 \end{pmatrix}$ .

For the case where  $\mathbf{P}$  is parallel or antiparallel to the  $x$  direction and the magnetization (the quantization axis) is along the  $z$  direction one has  $\vartheta = \pi/2, \varphi = 0$  and hence Eq. (1) yields the eigenstate  $\chi = \frac{1/\sqrt{2}}{1/\sqrt{2}} = \frac{1}{\sqrt{2}}\begin{pmatrix} 1 \\ 0 \end{pmatrix} + \frac{1}{\sqrt{2}}\begin{pmatrix} 0 \\ 1 \end{pmatrix}$ , where,  $\begin{pmatrix} 1 \\ 0 \end{pmatrix}$  and  $\begin{pmatrix} 0 \\ 1 \end{pmatrix}$  are the Dirac spinors and can be regarded as majority and minority spin states of the sample, respectively. Note that in both examples the quantization axis is defined as the direction of the easy axis.

In our previous experiments, where  $\mathbf{P}$  was parallel or antiparallel to the quantization axis, the beam is composed of either majority or minority spins (assuming a polarization of 100%,  $|P| = 1$ ). In this case it is easy to think of an exchange process. An electron of minority character occupies a state above the Fermi level and another electron of majority character leaves the sample from a state below the Fermi level. Since the magnons carry a total angular momentum of  $\hbar$ , they can only be excited by incident electrons of minority character via an exchange process. Hence one sees only the magnon excitation peak in minority spin spectra. Based on the discussion above, it is now rather straightforward to design

an experiment in which a transversally spin-polarized beam excites and probes magnons. In this case the beam can be regarded as a totally spin-unpolarized beam equally composed of both majority and minority spins. If the exchange process is valid here, only the incident electrons of minority character are allowed to excite magnons.<sup>20</sup> Since for both polarization directions (+ and -) the beam carries the same amount of majority and minority spins, one would expect exactly the same magnon peak intensity in  $I_{+}$  and  $I_{-}$  spectra. This would be another confirmation that the magnon excitation is caused by the exchange process, meaning that if one does the same experiment with positrons, one would not see the characteristic magnon energy losses.

To demonstrate that this idea works, we studied ultrathin magnetic FeCo-based films with large perpendicular magnetic anisotropy; systems which are of great fundamental as well as technological interest.<sup>3-5,22,23</sup> The experiments were carried out in an ultrahigh vacuum chamber with a base pressure of  $3 \times 10^{-11}$  mbar. The clean Ir(001) surface was obtained by cycles of low power flashes at 1200 K in oxygen atmosphere to remove the carbon contamination, followed by a single high power flash at 1800 K in ultrahigh vacuum, to remove the residual oxygen.<sup>24</sup> This preparation leads to a clean  $(1 \times 5)$ -Ir(001) surface as verified by low-energy electron diffraction (LEED) experiments. Two kinds of ultrathin films were grown following the procedure reported in Ref. 22: (i) an ultrathin Fe<sub>0.5</sub>Co<sub>0.5</sub> alloy film with a total thickness of four atomic layers (ML) prepared by codeposition of Fe and Co at room temperature and (ii) an ultrathin Fe/Co multilayer film composed of four alternating atomic layers of Co and Fe [starting with a Co layer; Fe/Co/Fe/Co/Ir(001)]. In both cases the films grow epitaxially with the epitaxial relationship  $[100]_{\text{film}} \parallel [110]_{\text{substrate}}$ . The sharp LEED patterns recorded on these surfaces indicate a high crystalline structure of the films [see, for example, Fig. 1(b)]. Both systems exhibit an out-of-plane easy axis due to the large PMA, originating from the tetragonal distortion of the epitaxial layers.<sup>22,23</sup> All measurements were carried out at room temperature. In the SPEELS measurements, the scattering plane was chosen to be parallel to the  $[110]$  direction of Ir(001) (the  $[010]$  direction of the films). The polarization vector of the beam  $\mathbf{P}$  is parallel (or antiparallel) to the  $[1\bar{1}0]$  direction of Ir(001). The degree of spin polarization of the incident electrons is  $|P| = 0.72 \pm 0.05$ . The energy of the incident electron beam was 8 eV. Different wave vectors were selected by changing the angle between incident and scattered beam, i.e., by rotating the sample about the symmetry axis  $[[1\bar{1}0]$  direction of Ir(001)]. In this configuration the effective beam polarization does not depend on the scattering geometry, since it is parallel to the symmetry axis. The wave vector of excited magnons parallel to the surface  $q_{\parallel}$  is given by the scattering geometry:  $q_{\parallel} = k_i \sin \theta - k_f \sin(\theta_0 - \theta)$ , where  $k_i$  ( $k_f$ ) is the magnitude of the wave vector of the incident (scattered) electrons and  $\theta$  ( $\theta_0$ ) is the angle between the incident beam and the sample normal (the scattered beam) [see Fig. 1(a)]. SPEELS spectra were recorded for the spin-polarization vector  $\mathbf{P}$  of the incident beam parallel and antiparallel to the  $[1\bar{1}0]$  direction of Ir(001), i.e., perpendicular to the quantization axis that is defined as the easy magnetization direction being normal to the sample plane (the  $[001]$  direction).

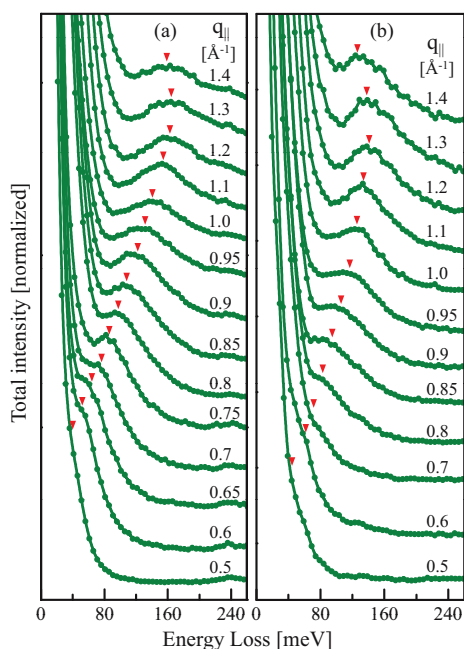


FIG. 2. (Color online) Series of normalized total spectra ( $I_+$  +  $I_-$ ) recorded at different wave vectors along the  $\bar{\Gamma}$ - $\bar{X}$  direction on the surfaces of a 4 ML Fe<sub>0.5</sub>Co<sub>0.5</sub> alloy film (a) and a 4 ML Fe/Co multilayer film (b). The spectra are shifted upwards for a better comparison. The small triangles denote the magnon excitation energies.

Figures 1(c) and 1(d) show the  $I_+$  and  $I_-$  SPEELS spectra measured at a wave vector of  $1.1 \text{ \AA}^{-1}$  on the surfaces of a 4 ML Fe<sub>0.5</sub>Co<sub>0.5</sub> alloy film and a 4 ML Fe/Co multilayer film, respectively.  $I_+$  ( $I_-$ ) denotes the intensity of the scattered beam when  $\mathbf{P}$  is parallel (antiparallel) to the  $[1\bar{1}0]$  direction. On both surfaces, a pronounced peak appears in both  $I_+$  and  $I_-$  spectra with the same intensity and peak position. As expected, the peak intensity shows no dependence on the direction of  $\mathbf{P}$ , different than those recorded on the ultrathin films with in-plane magnetization.<sup>11,12</sup> This is due to the fact that unlike the previous experiments, where the beam polarization vector  $\mathbf{P}$  was parallel or antiparallel to magnetization direction (quantization axis), in the present case it is perpendicular to that.

A series of SPEELS total spectra recorded at different wave vectors along the  $\bar{\Gamma}$ - $\bar{X}$  direction are shown in Fig. 2. On both surfaces, the peak moves towards higher energies as the wave vector increases up to the zone boundary (at about  $1.2 \text{ \AA}^{-1}$ ). It moves towards lower energies when further increasing the wave vector. This is the indication of reaching the second Brillouin zone. As expected, the magnon energy starts decreasing beyond the first Brillouin zone because of the translational symmetry in the two-dimensional Brillouin zone. To completely describe the measured spectra, we fit them with a function which includes three Gaussians and one Voigt function. The Gaussians describe the quasielastic peak and the Rayleigh surface phonons and the Voigt func-

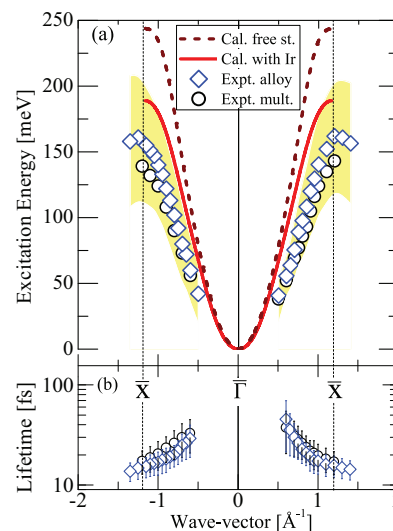


FIG. 3. (Color online) (a) The magnon dispersion relation probed along the  $\bar{\Gamma}$ - $\bar{X}$  direction on a 4 ML Fe<sub>0.5</sub>Co<sub>0.5</sub> alloy film ( $\diamond$ ) and a 4 ML Fe/Co multilayer film ( $\circ$ ). The intrinsic linewidth of the spectra is depicted as the background color. The solid line represents the theoretical calculation for a 4 ML body-centered tetragonal FeCo film on Ir(001) composed of alternating layers of Co and Fe. The layer next to Ir(001) is a Co layer (as in the experiment). The dashed line represents the results of the calculations for a freestanding film. (b) The magnon lifetime as a function of the wave vector.

tion describes the magnon peak.<sup>17,25</sup> In the Voigt function, the linewidth of the Gaussian contribution is chosen to be the same as the experimental resolution (the linewidth of the quasielastic peak). The peak position denotes the magnon energy and the intrinsic linewidth provides information on the magnon lifetime.<sup>26</sup> Due to the large contribution of the quasielastic peak in the spectra at the wave vectors smaller than  $0.5 \text{ \AA}^{-1}$  it is rather difficult to extract the magnon excitation energy. The only nonmagnetic excitations which are in the same energy range as magnons are the vibrational excitations of adsorbed atoms or molecules. For example, the narrow and very weak peak around 240 meV in Fig. 1(c) corresponds to the vibrational excitations of CO molecules. As the experiments are performed under ultrahigh vacuum conditions, the vibrational excitations are very weak so that their influence on the magnon peak can be neglected.

The magnon dispersion relation measured on both Fe<sub>0.5</sub>Co<sub>0.5</sub> alloy and Fe/Co multilayer films is presented in Fig. 3(a). At low wave vectors both systems possess almost identical magnon energies. Small differences in magnon energies appear at high wave vectors. For the Fe<sub>0.5</sub>Co<sub>0.5</sub> alloy film, the energy reaches a value of 160 meV at the  $\bar{X}$  point; for the Fe/Co multilayer film, the energy is about 140 meV. In both cases the magnon energies are much smaller than the one in bulk Fe and Co. They are even smaller than the one of 2 ML Fe(110)/W(110)<sup>12</sup> and 8 ML Co(001)/Cu(001).<sup>11</sup> Recent calculations of tetragonally distorted bulk FeCo compounds within the many-body perturbation theory predict a magnon softening.<sup>27</sup> Due to technical difficulties in those calculations

H. J. QIN *et al.*PHYSICAL REVIEW B **88**, 020404(R) (2013)

the effects of the substrate, which seem to be important, could not be taken into consideration.

We perform first-principles calculations within the generalized gradient approximation of the density functional theory. The structural parameters are taken from the available experimental data.<sup>28,29</sup> The electronic and magnetic properties are calculated using a self-consistent Green function method, specially designed for layered structures.<sup>30</sup> The interatomic exchange parameters were determined employing the magnetic force theorem, implemented within the Green function method.<sup>31</sup> The results of calculations are presented in Fig. 3(a) showing a rather good agreement with the experimental data. The small differences between the calculated dispersion relation and the experimental results might be due to different reasons. The intermixing of Fe and Co resulting in a chemically disordered alloy might be the first reason. The second reason might be a deviation from the perfect multilayer structure due to uncertainties in the thickness of Fe and Co layers and also a nonperfect (layer-by-layer) growth mode of Fe and Co layers on Ir(001). We also noticed that the calculations based on local spin density approximation results in magnon energies which are slightly smaller than the ones calculated within the generalized gradient approximation (they are very similar to the experimental results).

To see the impact of the Ir(001) substrate on the magnon dispersion relation we performed calculations for a freestanding film taking the interatomic distances the same as the film with substrate. The results, shown in Fig. 3(a) as a dashed line, indicate that the role of the substrate in determining the magnon energies is very important. The presence of the Ir(001) substrate reduces the magnon energies by 55 meV at the  $\bar{X}$  point. This fact is the consequence of the weakening of the interatomic exchange interaction and beautifully manifests the importance of electronic hybridization of the ultrathin film and the substrate. Detailed analysis of exchange coupling constants reveals that mainly the nearest-neighbor and next-nearest-neighbor coupling constants of Co atoms sitting next to Ir substrate are reduced by a factor of 2 in the presence of the substrate. This reduction is due to the reconstruction of the electronic structures of the film in contact with the substrate.

The background color in Fig. 3(a) denotes the intrinsic linewidth of the magnon peaks as observed in the experiments.

Since they are very similar in both systems we only show the results of the alloy film. The intrinsic linewidth increases from 40 to 100 meV when the wave vector increases from 0.5 to 1.2  $\text{\AA}^{-1}$ , similar to that of an 8 ML Co/Cu(100) and a 2 ML Fe/W(110).<sup>25</sup> The magnon lifetime is obtained using the procedure explained in Refs. 25 and 17 and is presented in Fig. 3(b). The damping of magnons in itinerant ferromagnets is mainly governed by the decay of collective excitations into single-particle Stoner excitations.<sup>25,32,33</sup> This damping mechanism which is usually referred to as Landau damping depends strongly on the available Stoner states near the Fermi level. Due to strong damping, terahertz magnons possess a very short lifetime being in the order of a few tens of femtoseconds.<sup>17,25</sup> The lifetime of FeCo with large PMA is very similar to that of the Fe and Co films meaning that the tetragonal distortion does not significantly influence the magnons lifetime. A large damping of magnons in the tetragonally distorted bulk FeCo compounds is also predicted theoretically.<sup>27</sup>

In conclusion, we demonstrate that the high-energy magnons in ultrathin ferromagnetic films with an out-of-plane easy axis can be probed by a transversally spin-polarized beam. The excitation cross section is rather large so that a pronounced peak in the spectra can be observed. Since ultrathin films with PMA are of great fundamental and technological interest, our experiments would open a way towards investigation of magnon excitations in this class of materials by SPEELS and also by inelastic tunneling spectroscopy.<sup>9</sup> The magnon dispersion relation and lifetime of tetragonally distorted ultrathin FeCo films with large PMA are probed. Our first-principles calculations reveal that in addition to the tetragonal distortion, the interfacial electronic hybridizations play an important role in determining the magnon energies in these compounds. We anticipate that our results would have an impact on the understanding of phenomena related to spin dynamics in these materials.

Funding from the Deutsche Forschungsgemeinschaft is acknowledged by A.E. (DFG priority program SPP 1538 “Spin Caloric Transport”). The calculations were performed at the Rechenzentrum Garching of the Max Planck Society (Germany).

\*zakeri@mpi-halle.de

<sup>1</sup>D. Weller, A. Moser, L. Folks, M. E. Best, W. Lee, M. F. Toney, M. Schwickert, J.-U. Thiele, and M. F. Doerner, *IEEE Trans. Magn.* **36**, 10 (2000).<sup>2</sup>A. Moser, K. Takano, D. T. Margulies, M. Albrecht, Y. Sonobe, Y. Ikeda, S. Sun, and E. E. Fullerton, *J. Phys. D: Appl. Phys.* **35**, R157 (2002).<sup>3</sup>S. Ikeda, K. Miura, H. Yamamoto, K. Mizunuma, H. D. Gan, M. Endo, S. Kanai, J. Hayakawa, F. Matsukura, and H. Ohno, *Nat. Mater.* **9**, 721 (2010).<sup>4</sup>L. Liu, C.-F. Pai, Y. Li, H. W. Tseng, D. C. Ralph, and R. A. Buhrman, *Science* **336**, 555 (2012).<sup>5</sup>L. Liu, O. J. Lee, T. J. Gudmundsen, D. C. Ralph, and R. A. Buhrman, *Phys. Rev. Lett.* **109**, 096602 (2012).<sup>6</sup>S. Zhang, P. M. Levy, A. C. Marley, and S. S. P. Parkin, *Phys. Rev. Lett.* **79**, 3744 (1997).<sup>7</sup>X.-F. Han, A. C. C. Yu, M. Oogane, J. Murai, T. Daibou, and T. Miyazaki, *Phys. Rev. B* **63**, 224404 (2001).<sup>8</sup>P. M. Levy and A. Fert, *Phys. Rev. Lett.* **97**, 097205 (2006).<sup>9</sup>T. Balashov, A. F. Takacs, W. Wulfhekel, and J. Kirschner, *Phys. Rev. Lett.* **97**, 187201 (2006).<sup>10</sup>H. Ibach, D. Bruchmann, R. Vollmer, M. Etzkorn, P. S. A. Kumar, and J. Kirschner, *Rev. Sci. Instrum.* **74**, 4089 (2003).<sup>11</sup>R. Vollmer, M. Etzkorn, P. S. Anil Kumar, H. Ibach, and J. Kirschner, *Phys. Rev. Lett.* **91**, 147201 (2003).<sup>12</sup>W. X. Tang, Y. Zhang, I. Tudosa, J. Prokop, M. Etzkorn, and J. Kirschner, *Phys. Rev. Lett.* **99**, 087202 (2007).

- <sup>13</sup>J. Prokop, W. X. Tang, Y. Zhang, I. Tudosa, T. R. F. Peixoto, K. Zakeri, and J. Kirschner, *Phys. Rev. Lett.* **102**, 177206 (2009).
- <sup>14</sup>K. Zakeri, Y. Zhang, J. Prokop, T.-H. Chuang, N. Sakr, W. X. Tang, and J. Kirschner, *Phys. Rev. Lett.* **104**, 137203 (2010).
- <sup>15</sup>Y. Zhang, P. A. Ignatiev, J. Prokop, I. Tudosa, K. Zakeri, V. S. Stepanyuk, J. Kirschner, T. R. F. Peixoto, and W. X. Tang, *Phys. Rev. Lett.* **106**, 127201 (2011).
- <sup>16</sup>H. Ibach, J. Rajeswari, and C. M. Schneider, *Rev. Sci. Instrum.* **82**, 123904 (2011).
- <sup>17</sup>K. Zakeri, Y. Zhang, T.-H. Chuang, and J. Kirschner, *Phys. Rev. Lett.* **108**, 197205 (2012).
- <sup>18</sup>T.-H. Chuang, K. Zakeri, A. Ernst, L. M. Sandratskii, P. Buczek, Y. Zhang, H. J. Qin, W. Adeagbo, W. Hergert, and J. Kirschner, *Phys. Rev. Lett.* **109**, 207201 (2012).
- <sup>19</sup>J. Rajeswari, H. Ibach, C. M. Schneider, A. T. Costa, D. L. R. Santos, and D. L. Mills, *Phys. Rev. B* **86**, 165436 (2012).
- <sup>20</sup>K. Zakeri and J. Kirschner, in *Probing Magnons by Spin-Polarized Electrons*, Topics in Applied Physics Magnonics from Fundamentals to Applications, Vol. 125 (Springer, Berlin, Heidelberg, 2013), Chap. 7, pp. 84–99.
- <sup>21</sup>J. Kessler, *Polarized Electrons* (Springer, Berlin, 1985).
- <sup>22</sup>F. Yildiz, M. Przybylski, X.-D. Ma, and J. Kirschner, *Phys. Rev. B* **80**, 064415 (2009).
- <sup>23</sup>T. Burkert, L. Nordström, O. Eriksson, and O. Heinonen, *Phys. Rev. Lett.* **93**, 027203 (2004).
- <sup>24</sup>K. Zakeri, T. Peixoto, Y. Zhang, J. Prokop, and J. Kirschner, *Surf. Sci.* **604**, L1 (2010).
- <sup>25</sup>Y. Zhang, T.-H. Chuang, K. Zakeri, and J. Kirschner, *Phys. Rev. Lett.* **109**, 087203 (2012).
- <sup>26</sup>See Supplemental Material at <http://link.aps.org/supplemental/10.1103/PhysRevB.88.020404> for detailed information on the fitting procedure of the experimental data.
- <sup>27</sup>E. Sasioglu, C. Friedrich, and S. Blugel, *Phys. Rev. B* **87**, 020410 (2013).
- <sup>28</sup>V. Martin, W. Meyer, C. Giovanardi, L. Hammer, K. Heinz, Z. Tian, D. Sander, and J. Kirschner, *Phys. Rev. B* **76**, 205418 (2007).
- <sup>29</sup>K. Heinz and L. Hammer, *Prog. Surf. Sci.* **84**, 2 (2009).
- <sup>30</sup>M. Lüders, A. Ernst, W. M. Temmerman, Z. Szotek, and P. J. Durham, *J. Phys.: Condens. Matter* **13**, 8587 (2001).
- <sup>31</sup>A. I. Liechtenstein, M. I. Katsnelson, V. P. Antropov, and V. A. Gubanov, *J. Magn. Magn. Mater.* **67**, 65 (1987).
- <sup>32</sup>A. T. Costa, R. B. Muniz, and D. L. Mills, *Phys. Rev. B* **74**, 214403 (2006).
- <sup>33</sup>P. Buczek, A. Ernst, and L. M. Sandratskii, *Phys. Rev. Lett.* **106**, 157204 (2011).



# Acknowledgment

At this point, I would like to thank all of those who contributed in various ways in the realization of this work.

First of all, I'd like to gratefully thank Prof. J. Kirschner for many discussions, strong support and continuous encouragement. I had this opportunity to benefit a lot from his vast knowledge and experience on electron spectroscopy during our discussions. I very much enjoyed our Saturday meetings in which we intensively discussed the physics and ideas. It is a honor for me to express all my sincere gratitude to him.

I'd like to also thank all former and present members of SPEELS team who contributed to the experiments discussed here. I wish to thank Prof. W.X. Tang, Dr. J. Prokop, Dr. Y. Zhang, Dr. T. R. F. Peixoto, Dr. T.-H. Chuang, Dr. H. J. Qin, Dr. Y. Meng and Y.-J. Chen.

I would like to thank our collaborators from the theory department: Dr. V. S. Stepanyuk, Dr. P. A. Ignatiev, PD Dr. A. Ernst, PD Dr. L.M. Sandratskii and Dr. P. Buczek for their theoretical support and discussions. I would like to express my special thanks to PD Dr. A. Ernst who was always ready for discussion with a couple of pots of tea.

I'm thankful to all my colleagues at the institute for discussions on various subjects, specially PD Dr. A. Winkelmann, PD Dr. F. Schumann, PD Dr. D. Sander, PD Dr. H.L. Meyerheim, Dr. J. Barthel, Dr. C. Winkler, Prof. M. Przybylski, Prof. W. Keune and Prof. E.K.U. Gross.

I'd like to also thank my colleagues at the Martin-Luther-Universität Halle-Wittenberg: Prof. W. Widdra, Prof. J. Berakdar, Prof. W. Hergert and Prof. S. Trimper for various discussions. I would like to express my special thanks to Prof. W. Widdra for allowing me to actively take part in teaching.

I would like to acknowledge the technical support from H. Engelhard, H. Menge, F. Weiss and also the co-workers from the mechanical and electronics workshop. Likewise I'd like to thank the co-workers from the administration office for their help.

Last but not least I am very grateful to my family, my dear parents, my brothers and sisters for their emotional support and countless sacrifices. Their unconditional love has always been a source of hope and motivation in my life. I'm proud of having such a wonderful family.





Khalil Zakeri Lori

*Dr. rer. nat.*

Max-Planck-Institut für Mikrostrukturphysik  
Weinberg 2, D-06120 Halle, Germany

☎ +49(0)345 5582749

FAX +49(0)345 5511223

✉ [zakeri@mpi-halle.de](mailto:zakeri@mpi-halle.de)

🌐 [www.mpi-halle.de](http://www.mpi-halle.de)

## Lebenslauf

### — Persönliche Daten

Name **Zakeri Lori**  
Vorname **Khalil**  
Geburtsdatum **23.09.1979**  
Geburtsort **Sirjan – Iran**

### — Akademischer Werdegang

- Seit 10.2008 **Principal Investigator**, *Max-Planck-Institut für Mikrostrukturphysik*, Halle.  
Gruppenleiter und Verantwortlicher für Experimente zur spinpolarisierten Elektronenenergieverlustspektroskopie (SPEELS)
- 01.2008 – 10.2008 **Post-Doc**, *Max-Planck-Institut für Mikrostrukturphysik*, Halle.  
Thema: Spinpolarisierte Rastertunnelmikroskopie (Sp-STM) an magnetischen Nanostrukturen
- 06.2007 – 01.2008 **Post-Doc**, *Fachbereich Physik, Experimentalphysik, AG Farle und Center for Nanointegration, Universität Duisburg- Essen*, Duisburg.  
Thema: Ferromagnetische Resonanz (FMR) an magnetischen Heterostrukturen
- 12.2003 – 06.2007 **Doktorand**, *Fachbereich Physik, Experimentalphysik, AG Farle und Center for Nanointegration, Universität Duisburg- Essen*, Duisburg.  
Thema: In-situ Ferromagnetische Resonanz (FMR) an magnetischen Monolagen

### — Schul- und Hochschulbildung

10. 2007 **Promotion in Physik**, *Fachbereich Physik, Universität Duisburg- Essen*, Duisburg, Abschlussnote: mit Auszeichnung.
02. 2003 **Masterabschluss in Physik**, *Department of Physics, Sharif University of Technology*, Teheran, Iran, Abschlussnote: Sehr gut.
06. 2001 **Bachelorabschluss in Physik**, *Department of Physics, Shahid Bahonar University of Kerman*, Kerman, Iran, Abschlussnote: Sehr gut.
06. 1997 **Abitur**, Sirjan, Iran.



# **Erklärung an Eides statt**

Ich erkläre hiermit, die vorliegende Habilitationsschrift

## **Spin Excitations in Ultrathin Ferromagnets**

selbständig und ohne fremde Hilfe verfasst und keine anderen als die von mir angegebenen Quellen und Hilfsmittel benutzt zu haben. Die den benutzten Werken wörtlich oder inhaltlich entnommenen Stellen sind als solche kenntlich gemacht.

Khalil Zakeri Lori

Halle, den 11. Dezember 2013

